Volume 16, Number 1, 2022

Technical University of Cluj-Napoca
North University Centre of Baia Mare
Faculty of Engineering
Electrical, Electronic and Computer Engineering Department

Volume 16, Number 1, 2022

Carpathian Journal of Electrical Engineering

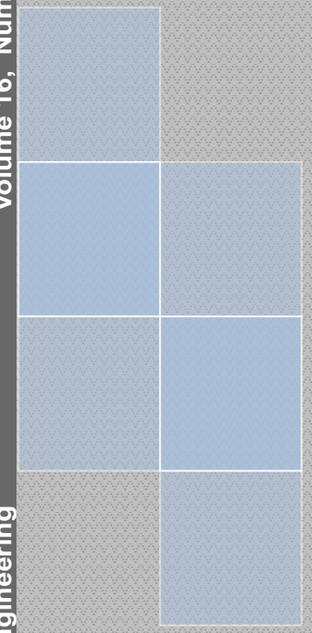

Carpathian Journal of Electrical Engineering

ISSN 1843 - 7583

UTPRESS PUBLISHER

TECHNICAL UNIVERSITY
OF CLUJ-NAPOCA

NORTH UNIVERSITY CENTRE OF BAIA MARE
FACULTY of ENGINEERING

ELECTRICAL, ELECTRONIC AND
COMPUTER ENGINEERING DEPARTMENT

Carpathian Journal of Electrical Engineering

Volume 16, Number 1, 2022

ISSN 1843 – 7583
http://cee.cunbm.utcluj.ro/cjee/

EDITOR-IN-CHIEF

Liviu NEAMȚ — Technical University of Cluj-Napoca, Romania

ASSOCIATE EDITOR

Mircea HORGOȘ — Technical University of Cluj-Napoca, Romania
Ovidiu COSMA — Technical University of Cluj-Napoca, Romania

EDITORIAL SECRETARY

Olivian CHIVER — Technical University of Cluj-Napoca, Romania

SCIENTIFIC BOARD

Gene APPERSON	Digilent Inc. SUA
Cristian BARZ	Technical University of Cluj-Napoca, Romania
Iulian BIROU	Technical University of Cluj-Napoca, Romania
Florin BREABĂN	Artois University, France
Vasilis CHATZIATHANASIOU	*Aristotle* University of Thessaloniki, Greece
Clint COLE	Washington State University, SUA
Iuliu DELESEGA	Polytechnic University of Timişoara, Romania
Luis Adriano DOMINGUES	Brazilian Electrical Energy Research Center, Brazil
Francis Boafo EFFAH	Kwame Nkrumah University of Science & Technology, Ghana
Zoltan ERDEI	Technical University of Cluj-Napoca, Romania
Patrick FAVIER	Artois University, France
Emmanuel Asuming FRIMPONG	Kwame Nkrumah University of Science & Technology, Ghana
Ştefan MARINCA	Analog Devices, Ireland
Andrei MARINESCU	Research and Testing Institute ICMET, Romania
Oliviu MATEI	Technical University of Cluj-Napoca, Romania
Tom O'DWYER	Analog Devices, Ireland
Ioan ORHA	Technical University of Cluj-Napoca, Romania
Sorin PAVEL	Technical University of Cluj-Napoca, Romania
Desire RASOLOMAMPIONONA	Warsaw University of Technology, Poland
Toufik SEBBAGH	University of 20 Août 1955 – Skikda, Algeria
Alexandru SIMION	*Gheorghe Asachi* Technical University of Iasi, Romania
Adam TIHMER	University of Miskolc, Hungary
Radu TÎRNOVAN	Technical University of Cluj-Napoca, Romania
Theodoros D. TSIBOUKIS	*Aristotle* University of Thessaloniki, Greece
Jan TURAN	Technical University of Kosice, Slovakia
Jozsef VASARHELYI	University of Miskolc, Hungary
Andrei VLADIMIRESCU	University of California, Berkeley, USA

CONTENTS

REGULAR PAPERS:

MULTI-OBJECTIVE CONGESTION MANAGEMENT OF TRANSMISSION LINES USING DEMAND RESPONSE AND STATIC VAR COMPENSATORS

Paul **OWUSU-AFRIYIE**, Emmanuel Kwaku **ANTO,** Francis Boafo **EFFAH**
Kwame Nkrumah University of Science and Technology, Kumasi, Ghana.
paulowusuafriyie@gmail.com, kwakuantoh@yahoo.com, fbeffah74@gmail.com.

Keywords: Congestion, Demand Response, Static Var Compensator, Particle Swarm Optimization

Abstract*: This paper presents multi-objective congestion management of transmission lines using time-of-use (TOU) based demand response (DR) program and static var compensator (SVC). Congestion of transmission lines is managed, while system parameters such as generation fuel cost and active power losses are reduced, in addition to enhancement of bus voltages. The SVC was modeled as a reactive power injector, while the TOU-based DR was modelled using the price elasticity of demand for responsive loads. Particle swarm optimization was used for the optimal placement and sizing of the SVCs, considering the rolled-out DR program in MATLAB/MATPOWER. The DR program was first tested separately on the IEEE-30 bus test system to show its effects on the afore-mentioned system parameters. Subsequently, the DR program was combined with the SVC, and again tested on the IEEE-30 bus test system. The results showed a significant improvement of 1.414% on the voltage profile, 44.65% reduction on the generation fuel cost, and much significant 71.13% reduction on the system losses with the proposed method, compared with the Base Case Scenario (the Peak Period) where there was congestion. This shows the effectiveness of the proposed hybridized DR-SVC method in congestion management of transmission lines.*

1. INTRODUCTION

Traditionally, electric grids were designed to operate as a vertical structure consisting of generation, transmission, and distribution, supported with controls and devices to maintain reliability, stability, and efficiency. Generation companies enjoyed monopoly by operating the whole vertical structure. Now, the increase in demand in the electric power systems has necessitated the restructuring of the power system, even as more generators are required,

resulting in a market-based competition by creating an open market environment which allows the power supply to function competitively, as well as allowing consumers to choose their own suppliers of electric energy [1].

The restructuring has moved the electric grid from a highly regulated, vertical structure to a fully unbundled structure referred to as power sector deregulation. The principal aim of deregulation is to create the avenue for more generation from independent power producers (IPPs), enhance the existing efficiency, reliability, and security, as well as reduce the cost of producing and using energy by introducing competition in the power industry [2].

Increased demand for energy in a deregulated power system has also resulted in an increase in the number of power producers, whilst consumers have the liberty to choose their own generating companies. Ordinarily, increase in demand with its associated increase in generation should result in an increase in the number of transmission lines. However, as a result of environmental concerns, right-of-way issues, and increased cost of construction of lines, amongst others, there is an increasing recognition of an absolute necessity to utilize the existing transmission systems' assets to the maximum extent as possible. But increasing energy demand creates constraints in the power transmission system, as more generators are added, and the existing lines are forced to carry power beyond their limits [3], [4]. This situation has resulted in congestion of the existing transmission lines and leads to violations of transmission constraints, leading to an increase in transmission losses and generation fuel cost. This is inimical to the transmission system and optimal power flow, and as a result, this congestion must be managed [3].

A number of measures have been adopted to address the issue of transmission congestion. Each of these methods has different effects on the generation fuel cost, system losses and the voltage profile. Some of these methods include demand response (DR), generator rescheduling, load shedding, distributed generations, nodal pricing schemes, operation of transformer taps, operation of Flexible Alternating Current Transmission System (FACTS) devices and so forth [5], [6], [7].

Singh and Kumar [8], modelled the Time-Of-Use (TOU) and the Emergency Demand Response Program (EDRP) using the responsive load model and price elasticity of demand in congestion management. The models of both DR programs were tested on the IEEE 24-bus reliability test system using MATLAB. The incentives considered for the EDRP were 10 $/MWh, 25 $/MWh, and 35 $/MWh. This work, however, does not consider the uncertainty nature of the load and the customers. The uncertainty nature of the DR responsive load, a demerit of the DRPs, has to do with the fact that customers can choose whether or not to participate in the DRP when used as the sole congestion management tool, leading to a jeopardy of the program at times (an effect of this uncertainty).

Also, Luo et al. [9] worked on minimizing this uncertainty nature associated with the DR responsive load in congestion management. The authors proposed a Consensus-based Nodal Pricing Mechanism for Automated Demand Response by using automated DR devices.

These automated DR devices are smart breakers and telemetry devices which trip off to cut the load on which they are placed when their preset times are reached. This method minimizes the uncertainty and its effect to some extent, because customers who decide to participate in the Automated DR program will not be able to leave the program along the way, as these timed-preset automatic tripping devices will be installed on their loads. However, customers can still decide from the beginning not to participate in the program and will have no automated device installed on their load. Secondly, the application is expensive, as these automated devices are costly. Thirdly, the application involves a two-way communication infrastructure in the grid, and so not all grids will be capable of implementing this approach. A relatively more inclusive and less expensive remedy to minimize this uncertainty and its effect, is the proposed combination of the DRP approach with another congestion management tool, say SVC FACTS device, to obtain a hybridized congestion management approach. With the application of the SVC, the voltage profile will still be enhanced, even if the customers decide no more to participate in the DRP or abandon the program along the way, thereby eliminating or reducing the effect of the uncertainty.

Nandini et al. [10] and Yousefi et al. [11] worked on congestion management using both demand response and FACTS devices. Their works considered the uncertainty nature of the responsive load by adding FACTS devices. The demerits are that these works failed to consider cross-elasticity (flexible load model) in the price elasticity of demand model. The non-inclusion of the flexible load (cross-elasticity) model in the DR responsive load modelling means that only fixed loads (like lights, television sets, etc.) were considered in the DR responsive load modelling. But this should not be the case, because the customer's load of a real-world power grid (real-world load) is a combination of both fixed loads (lights, TV sets etc.) and flexible loads (like heating, ventilation and air conditioning (HVAC) equipment, electric vehicle, etc.). Hence the non-inclusion of the flexible load model makes that modelling of the customer's load incomplete, and it does not represent the load of a real-world power grid. Therefore, in this paper, the flexible load model (cross-elasticity) has been factored in the modelling of a real-world DR responsive load, and its effects in congestion management analyzed. Additionally, when only the demand was optimized (single-objective function approach), without considering voltage and fuel cost**,** it resulted in voltage constraint issues at Bus 29. Hence two or more parameters must be optimized at the same time (the multi-objective functionality approach).

This paper therefore considers congestion management using a multi-objective approach, where some key grid parameters are optimized simultaneously, producing effects and results far better than the single-objective function approach. A combined application of demand response program (DRP) and static var compensator (SVC) FACTS devices was adopted, and the resulting effects on the generation fuel cost and system losses, as well as voltage profile of the system analyzed. The TOU demand response program was modeled based on price elasticity of demand (PED) for responsive loads including the flexible

load model, and used in conjunction with the SVC modelled as a reactive power injector operating as a variable susceptance. The effects of this hybridized DRP-SVC approach were explored on the IEEE 30-bus test system using the particle swarm optimization (PSO) tool to optimally size and place the SVC using the MATLAB/MATPOWER simulation environment.

2. THEORITICAL CONSIDERATIONS

2.1. Transmission congestion and its effects

Transmission congestion refers to situations when transmission constraints limit transmission flows or throughput below levels desired by market participants or government policy in order to comply with reliability rules. Transmission congestion occurs as a result of transmission constraints – a lack of transmission line capacity to deliver electricity without exceeding thermal, voltage and stability limits designed to ensure reliability [12]. Congestion arises when there is a desire to increase throughput across a transmission path, but such higher utilization is thwarted by one or more constraints. Congestion management in transmission system refers to any strategy or group of strategies focused on avoiding, reducing, or eliminating congestion in the transmission system as well as its consequences on the transmission grid. It is a process of performing the task of prioritizing the transactions and making such a schedule which solves the problem of overloading the network [13].

When thermal, voltage or stability limits are violated in a transmission network, congestion is said to have occurred and available electricity supply is not delivered at low cost to the load which, and as a result, defeats the intention of deregulation [14]. Congestion in power system makes the system unsecure with hikes in power prices due to avoidable losses, as it jeopardizes optimal power flow (OPF) [15]. Additionally, congestion maximizes the cost objective function by increasing the cost of generation and marginal costs at the buses. This situation increases the amount that the consumer pays as the cost of energy [16]. In [13], the relevance of congestion management is discussed in detail by identifying congestion management as one of the key issues to maintain security and reliability of transmission networks. Furthermore, congestion management balances the system and solves financial issues arising from the inability of the network to deliver the demanded power. The finding in [5] further stipulates that, lack of attention to congestion in the system may lead to widespread blackouts, and the associated negative social and economic consequences.

2.2. Demand response

According to the Federal Energy Regulatory Commission (FERC), demand response (DR) is defined as: “changes in electric energy usage by end-use customers from their normal

consumption patterns, in response to changes in the price of electricity over time, or incentive payments designed to induce lower electricity use at times of high wholesale market prices or when system reliability is likely to be jeopardized." [17]. Demand response is a wide range of actions which can be taken at the customer side of the electricity meter, in response to particular conditions within the electricity system (such as peak period network congestion or high prices). Demand response program furthermore plays a vital role in a smart grid environment, as it is an economical and flexible attempt towards the maintenance of system security and reliability, and also creates opportunities for customers to also be players in the market [14]. As a result, DR programs demand a two-way communication in the grid. However, DR has a limited capability, as it totally depends on the effective participation of customers from time to time. The consumer may fail to reduce their load due to some external factors, and this sometimes jeopardizes the effectiveness of the program in the congestion management. This kind of situation is referred to as the uncertainty nature of the responsive load or the consumers.

Demand response is able to change the amount and duration of electric energy usage, so that the best efficiency of consumption takes place in the peak interval [18]. Demand response programs are categorized as incentive-based (IB) or time-based (TB) programs. The IB programs are further divided into direct load control (DLC), interruptible/curtailable (I/C) service, demand bidding/buy back, emergency demand response program (EDRP), capacity market program (CMP) and ancillary service (A/S) markets. The TB programs, on the other hand, are further grouped as time-of-use (TOU), real time pricing (RTP) and critical peak pricing (CPP) programs [19], [20].

2.3. Economic model of responsive load

During the early years of deregulation of the power sector, consumers were fundamentally not participating effectively in the power markets [19]. As a result, consumers were isolated from any information of the markets, and did not enjoy the benefits either. This was basically as a result of the absence of knowledge, proper hardware, and infrastructure to aid the participation of the consumers in the power markets. The absence of consumer participation in the power markets resulted in price spikes, and also caused the transmission system to be congested [21].

The economic model of the responsive load is based on price elasticity of demand (PED). The demand for most commodities decreases as their prices increase. Price elasticity of demand or simply elasticity (E) is defined as the sensitivity of demand in respect of the price [22]. Mathematically, the elasticity E is expressed as [8], [14] and [22]:

$$E = \frac{\partial q}{\partial \rho} \tag{1}$$

where, E is elasticity of demand, q is demand value in respect to a period (MW), and ρ is electricity price in respect to a period ($/MWh).

As is the case for the TOU program, there are three prices periods with different prices variations. Also, the demand is one or both of the following:

1. *Fixed loads* – These are the loads that are not able to move or be shifted from one period to another. Examples are illuminating loads (lights), television sets, and so on. They could only be either 'on' or 'off', and so such loads have a *sensitivity* just in a *single period*, called *self-elasticity* [22] and it always has a *negative value*.
2. *Flexible loads* - These are the loads that could be shifted or transferred from one period to the other, say, from the peak period to the off-peak or to the flat period. Examples are heating, ventilation and air-conditioning (HVAC) equipment, electric vehicles (EV) and so on. Such loads have sensitivity in *multi periods* and evaluation is done by *cross-elasticity* [22]. This always denotes a *positive value*.

From (1), self-elasticities and cross-elasticities are suitably expressed according to [8], [14], [22] as:

$$E_{ii} = \frac{\Delta q_i}{\Delta \rho_i} \leq 0 \tag{2}$$

$$E_{ij} = \frac{\Delta q_i}{\Delta \rho_j} \geq \tag{3}$$

where Δq_i is the change in demand in *i*-th hour in a period, $\Delta \rho_i$ is the change in price in *i*-th hour in the same period and $\Delta \rho_j$ is the changes in price in *j*-th hour in another period. E_{ii} and E_{ij} are respectively self- and cross- elasticities. Both E_{ii} and E_{ij} for a 24-hour TOU program divided into 24 slots of one hour are 24x24 matrix called price elasticity matrix of demand (PEMD) with E_{ii} having only its diagonal values being non-zero (all other values of the matrix are zero) [23], [24].

The adopted TOU program is modelled using PED to show its effects on the electricity/power markets demands and prices, and also to show how beneficial this is to customers when they follow the program. This is done using both the single and multi periods models. Concerning the adopted model for the TOU program in this paper, the 24-hour day was divided into one-hour slots of twenty-four, i.e., 1, 2, 3, …, 24, and further grouped into three periods, namely; peak, flat and valley periods.

The Valley Period has comparatively the *lowest power (energy demand)*. In this period, congestion does not occur, and locational marginal prices (LMPs) are at their lowest. The utilities then set the energy prices at the lowest as a result of the afore-mentioned conditions [19], [25]. The Flat Period is the longest period by duration. A chunk of the power

(energy) demand in this period is a combination of industrial, commercial and residential. In most of the time, bulk customers install static capacitors and other FACTS devices to help boost their voltage and power factor. As a result, the energy demand during this period is not as high as the Peak Period, and not as low as the Valley Period with its matching tariff set by the utilities [19], [25]. The Peak Period is the period during which the energy demand is the highest. The demand in this period is mostly residential, when most of the consumers have closed from work, preparing for the next day activities, charging their battery-drained electric vehicles, operating their HVAC systems and so forth. However, some of the demand here could also be from the commercial and industrial customers who do shift operations. As a result, the lines become loaded, leading to congestion. The LMPs increase and utilities set their tariffs at the highest [19], [20], [25].

i. Single-Period Model (For Fixed Load. e.g., Lights, TV sets etc.)

Consider the following electricity market parameters for the customer:

d(i) = Customer's demand in *i*-th hour (MWh).

ρ(i) = Electricity price in *i*-th hour ($/MWh).

C(i) = Customer's income in *i*-th hour readily available to follow program ($).

Now, let us suppose that the customer changes their demand value from an initial value of $d_0(i)$ to a final value of *d(i)* due to the spot electricity price in the *i*-th hour (*i*) , then we can express the change in demand $\Delta d(i)$ as:

$$\Delta d(i) = d(i) - do(i) \tag{4}$$

Hence, the customer's balance *M($)* in the *i*-th hour for running the TOU program will be:

$$M(d(i)) = C(d(i)) - \Delta d(i).\rho(i) \ (\$) \tag{5}$$

$$M(d(i)) = C(d(i)) - \rho(i).[d(i) - do\ (i)] \ (\$) \tag{6}$$

$$M(d(i)) = C(d(i)) - \rho(i)d(i) + \rho(i)\ do\ (i) \ (\$) \tag{7}$$

In order to maximize the customer's benefit, the partial differential of *M* with respect to *d(i)*, that is, $\left(\frac{\partial M(d(i))}{\partial d(i)}\right)$ should be zero.

Hence:

$$\frac{\partial M(d(i))}{\partial d(i)} = \frac{\partial C(d(i))}{\partial d(i)} - \rho(i) + \frac{\partial \rho(i) d_o(i)}{\partial d(i)} = 0 \tag{8}$$

Therefore,

$$\frac{\partial C(d(i))}{\partial d(i)} = \rho(i) \tag{9}$$

According to [19], [26], and [27], the customer's benefit, being a function of the customer's income, which is more appropriate and most of the time used, is a quadratic function and can be expressed as:

$$C\big(d(i)\big) = C_o(i) + \rho_o(i).[d(i) - d_o(i)].\left\{1 + \frac{(d(i)-d_o(i)}{2E(i).d_o(i)}\right\} \tag{10}$$

where $C_o(i)$ is the benefit when the demand is at its nominal or initial value of $d_o(i)$, and $\rho_o(i)$ is the initial spot electricity price when the demand is still at its nominal value.

Taking the partial derivative of (10) results in;

$$\frac{\partial C(d(i))}{\partial d(i)} = \rho_o(i) + \rho_o(i).\left\{\frac{(d(i)-d_o(i)}{E(i).d_o(i)}\right\} \tag{11}$$

$$\frac{\partial C(d(i))}{\partial d(i)} = \rho_o(i).\left\{1 + \frac{(d(i)-d_o(i)}{E(i).d_o(i)}\right\} \tag{12}$$

Considering (9) and (12),

$$\rho(i) = \rho_o(i).\left\{1 + \frac{(d(i)-d_o(i)}{E(i).d_o(i)}\right\} \tag{13}$$

By rearranging;

$$\rho(i) - \rho_o(i) = \rho_o(i).\frac{d(i)-d_o(i)}{E(i).d_o(i)} \tag{14}$$

$$d(i) - d_o(i) = E(i).d_o(i)\ \frac{\rho(i)-\rho_o(i)}{\rho_o(i)} \tag{15}$$

$$d_s(i) = d_o(i).\left\{1 + E(i).\frac{\rho(i)-\rho_o(i)}{\rho_o(i)}\right\} \tag{16}$$

Therefore, by further rearranging (16), the customer's consumption for the single-period model will be as:

$$d_s(i) = d_o(i).\left\{1 + E(i).\frac{\rho(i)-\rho_o(i)}{\rho_o(i)}\right\} \tag{17}$$

where $E(i)$ is the self-elasticity of demand as described above. It can, however, be realized in

(17) that, if there is no prize change from one period to the other, and that the price of electricity remains constant throughout the day (24 hours). Then the term $\rho(i) - \rho_o(i)$ will be equal to zero ($\rho(i) - \rho_o(i) = 0$), rendering the elasticity *E(i)* zero, and as a result, *d(i)* will be equal to $d_o(i)$. Thus, there will be no change in demand in respect to a change in price, as there will be no change in price, resulting in zero elasticity.

ii. Multi-Period Model (For Flexible Load. e.g., HVAC, EV, etc.)

According to [19] and [28], the cross-elasticity between the demand in the *i*-th hour and the price in the *j*-th hour can be expressed as:

$$E(i,j) = \frac{\rho_o(j)}{d_o(i)} \; x \; \frac{\partial d(i)}{\partial \rho(j)} \tag{18}$$

such that $E(i,j) \leq 0 \; if \; i = j$ and $E(i,j) \geq 0 \; if \; i \neq j$.

From the basis that the demand's response to price variations can be expressed as a linear function [28], and considering (18), let us suppose that $\partial d(i)/\partial \rho(j)$ is constant. This means that, for every change in electricity price in *j*-th hour in a particular period, there will be a corresponding change in demand in the *i*-th hour in another period with its associated cross-elasticity. Hence from (14);

$$\rho(j) - \rho_o(j) \; = \rho_o(j).\frac{d(i) - d_o(i)}{E(i,j).d_o(i)} \tag{19}$$

In cross-elasticity, every single demand in the *i*-th hour over the 24-hour day is influenced by all the prices variations in the *j*-th hour over the 24-hour day. Therefore;

$$d(i) - d_o(i) = \sum_{j=1}^{24} E(i,j).d_o(i) \left\{\frac{\rho(j) - \rho_o(j)}{\rho_o(j)}\right\} \tag{20}$$
$$i = 1, 2, 3, \ldots \ldots 24 \text{ and } j = 1, 2, 3, \ldots \ldots 24$$

Hence, the customer's demand function considering the multi-period model is:

$$d_m(i) = d_o(i) + \sum_{j=1}^{24} E(i,j).d_o(i) \left\{\frac{\rho(j) - \rho_o(j)}{\rho_o(j)}\right\} \tag{21}$$
$$i = 1, 2, 3, \ldots \ldots 24 \text{ and } j = 1, 2, 3, \ldots \ldots 24$$

iii. Final Demand Model (For both Fixed and Flexible Loads)

According to [19], [26], [27], and [29], the final demand model will be a combination of the single period and multi-period demand, (17) and (21), respectively. As already mentioned, the day is grouped into three periods under the TOU program in this work. The advantage of the TOU program over the RTP program is that, the former offers simple computations compared to the latter where the day is divided into many slots, usually 24 one-hour slots. This means that within the same period in a TOU program, irrespective of the duration of the period, the price remains the same. As a result, the customer's Final Demand equation $d_f(i)$ is expressed as:

$$d_f(i) = d_m(i) \,.\frac{d_s(i)}{d_o(i)} \tag{22}$$

Since there is self-elasticity in the same period and there is no change in price, there is no change in demand and so the term $d_s(i)/d_o(i)$ is always equal to unity ($d_s(i) = d_o(i)$) in the same period. This means that in the same period, $d_f(i) = d_s(i) = d_m(i)$ and therefore the expression for $d_f(i)$ is justifiably valid. Hence:

$$d_f(i) = \{d_o(i) + \sum_{j=1}^{24} E(i,j).\, d_o(i)[\frac{\rho(j)-\rho_o(j)}{\rho_o(j)}]\} \,.\{1 + E(i).\,[\frac{\rho(i)-\rho_o(i)}{\rho_o(i)}]\} \tag{23}$$

This is the customer's final demand or consumption for each hour of the day (24 hours). Equation (23) is seen to take into consideration both self-elasticities and cross-elasticities, that is, it factors both fixed and flexible loads (loads of a real-world system).

2.4. Model of the static var compensator

The SVC is a shunt static VAR generator or load whose output is arranged to switch and inject or consume either a capacitive or inductive current depending on the nature of the system's load, so as to vary power system parameters, in particular bus voltage and power factor [30], [31], [32]. When the bus at which the SVC is connected has a low voltage level, SVC injects reactive power (capacitive) to the bus. On the other hand, when the bus voltage level is high, SVC absorbs reactive power (inductive) from the bus. Typically, an SVC comprises one or more banks of fixed or switched shunt capacitors or reactors, of which at least one bank is switched by thyristors. Elements which may be used to make an SVC typically include:

- Thyristor controlled reactor (TCR), where the reactor may be air-cored or iron-cored.
- Thyristor switched capacitor (TSC).
- Harmonic filter(s).

- Mechanically switched capacitors or reactors (switched by a circuit breaker).

Figure 1 shows a schematic representation of an SVC.

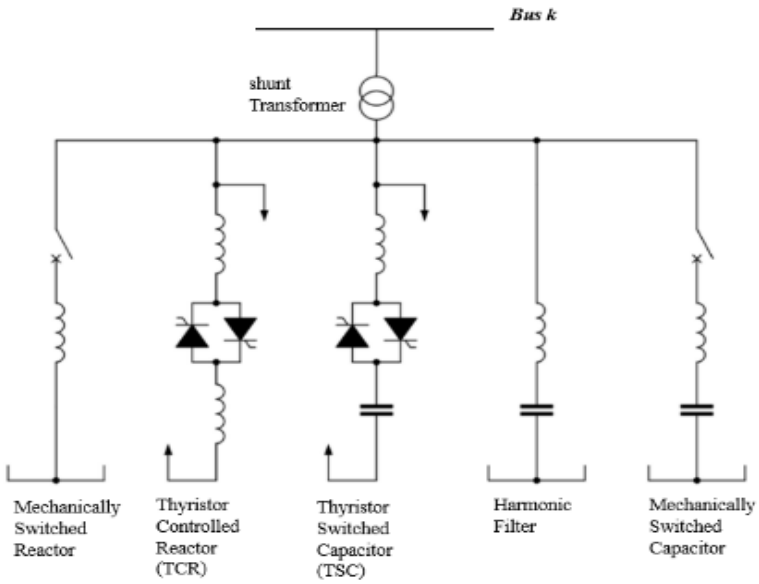

Fig. 1. Schematic diagram of an SVC [31], [33]

The structure of the static model of the SVC is a combination of a capacitor bank, shunted by a thyristor-controlled reactor with the whole connected in shunt to bus *k* as represented in *Fig. 2* where I_{SVC} and V_k are the injected current by the SVC and the bus voltage at bus *k*, respectively.

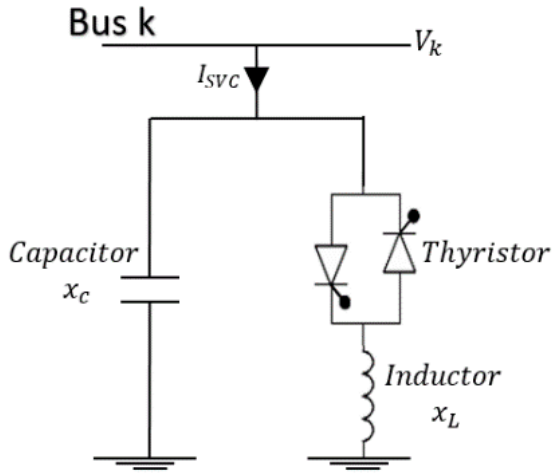

Fig. 2. Structure of the static model of the SVC [33], [34]

This static model is summarized and represented as a variable shunt susceptance B_{SVC}, shown in *Fig.3*.

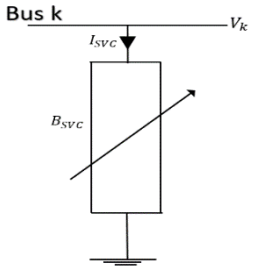

Fig. 3: Variable shunt susceptance model of the SVC [31], [34]

The injected reactive power Q_{SVC} at bus *k* by the SVC is expressed as:

$$Q_{SVC} = -V_k^2 * B_{SVC} \tag{24}$$

The linearized power flow models make use of (24) to make modifications in the corresponding Jacobian elements at the SVC bus. By considering the SVC's susceptance as a control variable, the load flow model of the SVC can always be developed.

2.5. Problem formulation

In this section, the mathematical concepts of the multi-objective approach are presented. The two objective functions to be considered here are generation (fuel) cost minimization and line active power losses minimization.

- *Generation fuel cost minimization*

This objective seeks to dispatch the generation such that priority is given to generators with very affordable fuel cost, and also to optimize the active power outputs of the generators. The optimization problem can therefore be formulated as [35]:

$$\text{Min } \sum_{i=1}^{nG} CPG_i \quad (\$/hr) \tag{25}$$

where *nG* is the number of generators, *CPG* is the cost of active power generation. *CPG* is often a polynomial function and can be expressed mathematically as [35]:

$$CPG_i = a_i PG_i^2 + b_i PG_i + c \ \ (\$/hr) \tag{26}$$

with a_i, b_i, c_i and PG_i being the generation coefficients of the i-th generator and the active power generated by the i-th generator, respectively.

- *Line active power losses minimization*

This objective seeks to achieve an optimal match of the active power generation with the active power demand (load) in the system. It optimizes the active power output of the slack bus and seeks to reduce the difference between generation and demand as far as active power is concerned, thus, minimizing the line losses. The optimization problem can be formulated as [35]:

$$\text{Min} \quad \left(\sum_{i=1}^{nG} PG_i - \sum_{k=1}^{nD} PD_k\right) \tag{27}$$

where PG_i and PD_k are the active power generated by the *i*-th generator and the active power demanded at the *k*-th bus respectively, nG and nD are the number of generators and the number of active power demand buses, respectively.

- *Optimization problem constraints*

The above problems that have been formulated are all subject to load flow equality and inequality constraints expressed below. The equality constraints are both the balanced active and reactive power flow equations of the system. The various equations can be expressed as:

Load flow equations without FACTS devices.

$$PG_i - PD_i = |V_i| \sum_{j=1}^{nBUS} \left|V_j\right| \left|Y_{ij}\right| \cos\left(\theta_{ij} + \delta_j - \delta_i\right) \tag{28}$$

$$QG_i - QD_i = -|V_i| \sum_{j=1}^{nBUS} \left|V_j\right| \left|Y_{ij}\right| \sin\left(\theta_{ij} + \delta_j - \delta_i\right) \tag{29}$$

where PG_i, PD_i, QG_i, and QD_i are the active power generated, active power demanded, reactive power generated, and reactive power demanded at bus i, respectively. V_i, V_j, Y_{ij}, θ_{ij}, δ_i, and δ_j are respectively the *i*-th bus voltage magnitude, the *j*-th bus voltage magnitude, the branch admittance magnitude between the *i*-th bus and the *j*-th bus, the branch admittance phase angle between the *i*-th and the *j*-th bus, the voltage angle of the *i*-th bus and the voltage angle of the *j*-th bus. $nBUS$ is the number of buses.

Load flow equation with SVC placed at bus k.

$$QG_k - QD_k = -(|V_k| \sum_{j=1}^{nBUS} |V_j|\,|Y_{ij}| \sin(\theta_{ij} + \delta_j - \delta_i) + V_k^2 B_{SVC}) \quad (30)$$

The inequality constraints are the system operating limits. They are expressed as follows:

A*ctive and reactive power generation limits:*

$$PG_i^{min} \le PG_i \le PG_i^{max} \qquad for\ i = 1, \dots\dots, nG \quad (31)$$

$$QG_i^{min} \le QG_i \le QG_i^{max} \qquad for\ i = 1, \dots\dots, nG \quad (32)$$

The MVA flow limits in the branches denoted by:

$$|S_i(\theta, V)| \le S_i^{max} \qquad for\ i = 1, \dots\dots, nBr \quad (33)$$

Bus voltage limits:

$$V_i^{min} \le V_i \le V_i^{max} \qquad for\ i = 1, \dots\dots, nBUS \quad (34)$$

SVC susceptance limit:

$$B_{SVC}^{mim} \le B_{SVC} \le B_{SVC}^{max} \quad (35)$$

2.6. Particle swarm optimization (PSO)

Particle swarm optimization (PSO) is a heuristic method that optimizes a problem by trying to improve a candidate's solution iteratively. It is a population-based search algorithm in which individuals, referred to as particles, change their positions in a seacrh-space in serach for a global best position called G_{best} [31], [34]. Each particle moves by its own experience and cognitive, taking cognizance of its environment/neighborhood, using its velocity. This particle's movement in the search-space is therefore influenced by its local best-known position called P_{best}, while it is also guided toward the best-known positions in the search-space which are updated as other particles find better positions. The P_{best} is an evaluted fitness value of the particle. The particle's velocity and position are updated at every iteration, until the maximum number of iterations T_{max} which is a major stopping criterion that is reached

by (36) and (37) below. These are the main equations of the PSO algorithm.

$$v_{id}(t+1) = wv_{id}(t) + c_1 r_1\left(p_{id} - x_{id}(t)\right) + c_2 r_2\left(p_{gd} - x_{id}(t)\right) \quad (36)$$

$$x_{id}(t+1) = x_{id}(t) + v_{id}(t+1) \quad (37)$$

where $x_{id}(t)$ is the current position of the particle i, p_{id} is a better position of particle i, p_{gd} is the entire swarm's better-known position, w is the inertia factor (positive constant), c_1 and c_2 are also positive constants called cognitive learning rate, r_1 and r_2 are randomly generated numbers ranging between 0 and 1, and v_{id} is the velocity of the particle belonging to the range of minimum and maximum velocities V_{min} and V_{max}.

3. PROPOSED METHOD

Towards the execution of the research work, the following methodological steps were followed:

1. The TOU demand response program was modeled based on price elasticity of demand (PED) for responsive loads including the flexible load model.
2. The SVC was modelled as a reactive power injector operating as a variable susceptance.
3. The standard IEEE 30-bus test system was selected as the case-study system, and simulated using the MATLAB/MATPOWER.
4. The DR (TOU) program was applied solely on the case-study system, and the multi-objective effects on congestion noted.
5. The DRP was then used in conjunction with the SVC, which was optimally sized and placed using the particle swarm optimization (PSO) tool, and again applied to the case-study system.
6. The multi-objective effects of this hybridized DRP-SVC approach on the IEEE 30-bus test system were also noted, and then compared with those of the DRP (TOU) approach.

3.1. Study system

The case study system is the standard IEEE 30-bus test system, which is represented in *Fig. 4*.

The generators' data for this standard test system above is shown in Table 1 [37].

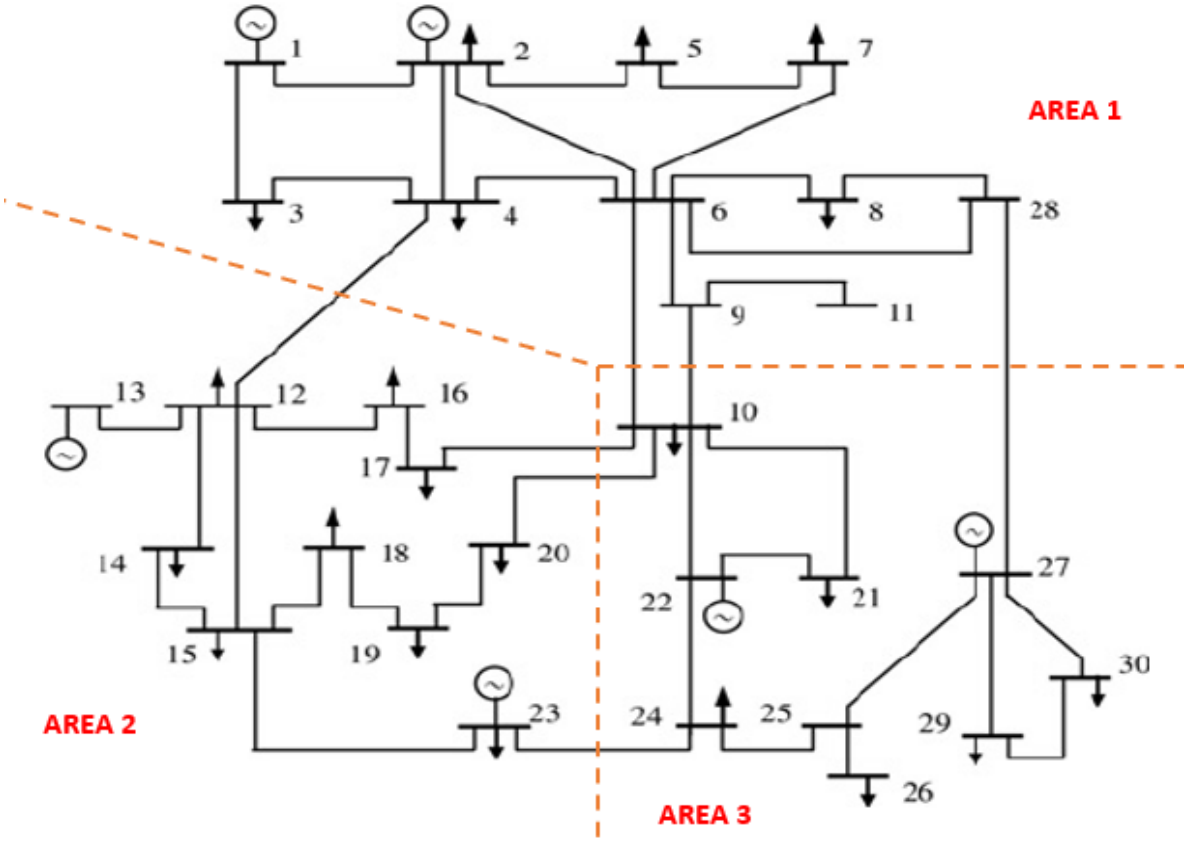

Figure 4: IEEE 30-bus test system [36]

Table 1. Generator data – IEEE 30-bus test system

Gen. no.	***Bus no.***	***Pmin (MW)***	***Pmax (MW)***	***ai ($/MW^{2}hr)***	***bi ($/MWhr)***	***ci ($/hr)***
1	*1*	*0.00*	*80.00*	*0.02000*	*2.00*	*0.00*
2	*2*	*0.00*	*80.00*	*0.01750*	*1.75*	*0.00*
3	*22*	*0.00*	*50.00*	*0.06250*	*1.00*	*0.00*
4	*27*	*0.00*	*55.00*	*0.00834*	*3.25*	*0.00*
5	*23*	*0.00*	*30.00*	*0.02500*	*3.00*	*0.00*
6	*13*	*0.00*	*40.00*	*0.02500*	*3.00*	*0.01*

3.2. Implementation of the PSO

The PSO was used to resize and locate the already sized (with the presence of DRP) SVC in the IEEE 30-bus test system considering the objective functions of voltage profile, generator fuel cost, system losses and demand. The algorithm was used to combine the DRP and the SVC FACTS device as a single hybridized congestion relieving program. In this application, three cases were considered. These are:

- Case 1 ('the Base Case or Reference Scenario') represents the Peak Period conditions.
- Case 2 ('with DRP only') represents the sole application of the DRP on the same case study system, and
- Case 3 ('with both DRP and SVC') represents the combination of the DRP and SVC FACTS device.

The implementation of the PSO was done according to the following steps:

- *Step 1-Setting of Network Parameters:* The IEEE 30-bus network data including the reactive power and voltage constraints were read and set. The bus data was replaced with bus data obtained from the results of the application of the DRP on the IEEE 30 bus system. This afore-mentioned data was used to compose the power flow algorithm where the locations, sizes, and limits of SVC were randomly picked, arranged, and set.
- *Step 2-Particle Parameters and Initialization*: The number of particles *NP*, accelerate constants C_1 and C_2, the minimum and maximum inertia weights W_{min} and W_{max}, as well as the maximum iteration number T_{max} were set. Subsequently, the position and velocity of the particle were randomly initialized.
- *Step 3-Fitness Evaluation*: The fitness of the particles of the swarm was evaluated according to the fitness function to obtain the P_{best} and the G_{best} and the particle's velocity was set at zero.
- *Step 4-Weight Inertia Determination and Velocity Updates*: While the maximum number of iterations T_{max} has not been reached by the iteration counter (t) and the counter variable (i) not exceeding the number of particles *NP*, determine the particle's weight inertia using equation

$$w = w_{max} - (\frac{w_{max} - w_{min}}{T_{max}}) * \mathrm{t} \tag{38}$$

  and subsequently update the particle's velocity using (36).
- *Step 5-Position Updates*: In accordance with the new velocity, the particle's new position is also updated using (37). If any particle violates its position limit, the position is reset at the violating limit.
- *Step 6-Update P_{best} and G_{best}*: The fitness of all the particles in the swarm is re-evaluated with the new positions to obtain the new P_{best} and G_{best}. The location of the SVC is indicated by the particle's position with an appropriate size considering the voltage of that position.
- *Step 7-Termination:* The termination criterion was based on the preset maximum number of iterations T_{max}.

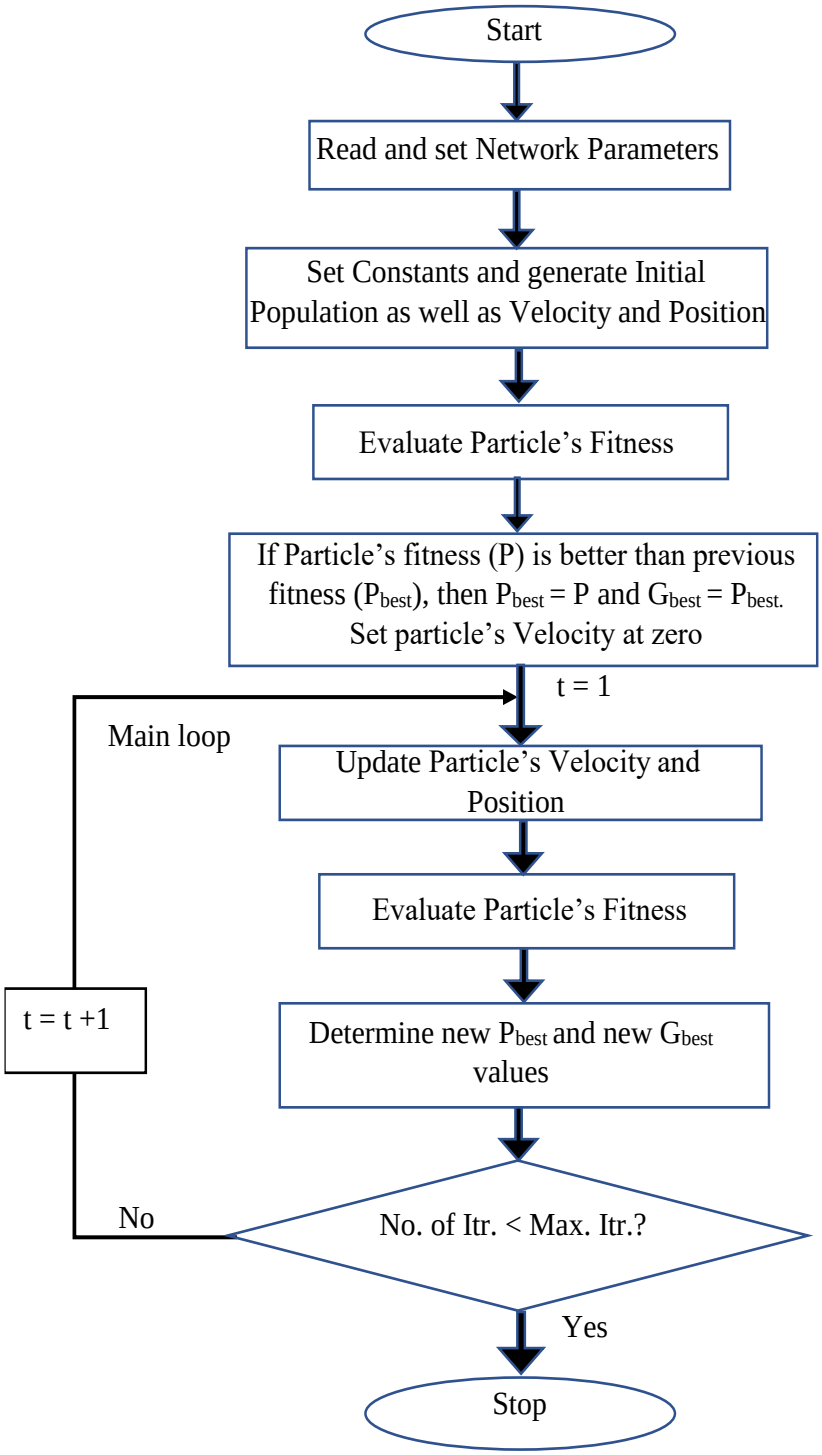

Fig.5. Flowchart of used PSO Algorithm

The flowchart is shown in *Fig. 5*.

4. RESULTS AND ANALYSIS

The PSO control variables or parameters used are:

Number of Particles (*NP*) = 50

Maximum number of iterations T_{max} = 100

Minimum inertia weight W_{min} = 0.4

Maximum inertia weight W_{max} = 0.9

Accelerate constants $C_1 = C_2 = 2$.

The PSO algorithm optimally placed two SVCs of sizes 15.33 MVar and 10.71 MVar at buses 8 and 21, respectively. Table 2 is a snapshot from the MATLAB command window showing the placed and sized SVCs by the PSO.

Table 2. Snapshot from the results of the PSO-based sizing and placing of the SVCs

```
t = 95 BEST = 46247.5268
t = 96 BEST = 46247.5268
t = 97 BEST = 46247.5268
t = 98 BEST = 46247.5267
t = 99 BEST = 46247.5266
t = 100 BEST = 46247.5265
=====================================================
Buses are   4   5   2  19  17  22  24  23  20  18  21  25  26   9   8  11  27
sizes are   0   0   0   0   0   0   0   0   0   0   10.71   0    0   0  15.33  0  0

          Buses     Size(MVAr)
            8         15.33

           21         10.71

=====================================================
```

The results have been presented for the three cases, namely: Case 1 - the Base Case Scenario, Case 2 - with DRP only, and Case 3 - with both DRP and SVC, as follows.

4.1 Effects on the Voltage Profile

Table 3 and *Fig. 6* present the 30 voltage profiles for all the three cases.

Table 3. Voltage profiles for all the three cases

	Voltage Profile				
Bus Number	***Case 1 (Base Case Scenario)***	***Case 2 (With DRP Only)***		***Case 3 (With DRP and SVC)***	
		In p.u.	***% Increase***	***In p.u.***	***% Increase***
1	*1.050*	*1.050*	*0.000*	*1.050*	*0.000*
2	*1.013*	*1.017*	*0.395*	*1.024*	*1.086*
3	*1.000*	*1.011*	*1.100*	*1.027*	*2.700*
4	*0.981*	*1.001*	*2.039*	*1.012*	*3.160*
5	*0.979*	*0.985*	*0.613*	*0.992*	*1.328*
6	*0.972*	*0.981*	*0.926*	*0.988*	*1.646*
7	*0.976*	*0.984*	*0.820*	*0.990*	*1.434*
8	*0.979*	*0.985*	*0.922*	*1.008*	*3.279*
9	*1.015*	*1.022*	*0.690*	*1.031*	*1.576*
10	*1.012*	*1.019*	*0.692*	*1.025*	*1.285*
11	*1.071*	*1.071*	*0.000*	*1.071*	*0.000*
12	*1.038*	*1.041*	*0.289*	*1.048*	*0.963*
13	*1.062*	*1.069*	*0.564*	*1.069*	*0.564*
14	*1.019*	*1.024*	*0.491*	*1.027*	*0.785*
15	*1.011*	*1.019*	*0.791*	*1.025*	*1.385*
16	*1.019*	*1.027*	*0.785*	*1.028*	*0.883*
17	*1.000*	*1.012*	*1.200*	*1.024*	*2.400*
18	*0.998*	*1.004*	*0.601*	*1.013*	*1.503*
19	*0.994*	*0.999*	*0.503*	*1.006*	*1.207*
20	*0.999*	*1.004*	*0.501*	*1.014*	*1.501*
21	*1.001*	*1.010*	*0.899*	*1.019*	*1.798*
22	*1.001*	*1.010*	*0.899*	*1.016*	*1.499*
23	*0.997*	*1.000*	*0.301*	*1.011*	*1.404*
24	*0.986*	*0.993*	*0.710*	*0.995*	*0.913*
25	*0.980*	*0.985*	*0.510*	*0.989*	*0.918*
26	*0.955*	*0.966*	*1.152*	*0.980*	*2.618*
27	*0.987*	*0.991*	*0.405*	*0.997*	*1.013*
28	*0.983*	*0.989*	*0.610*	*0.992*	*0.916*
29	*0.976*	*0.981*	*0.512*	*0.987*	*1.127*
30	*0.966*	*0.978*	*1.242*	*0.981*	*1.553*
Average % Increase		*0.705*		*1.414*	

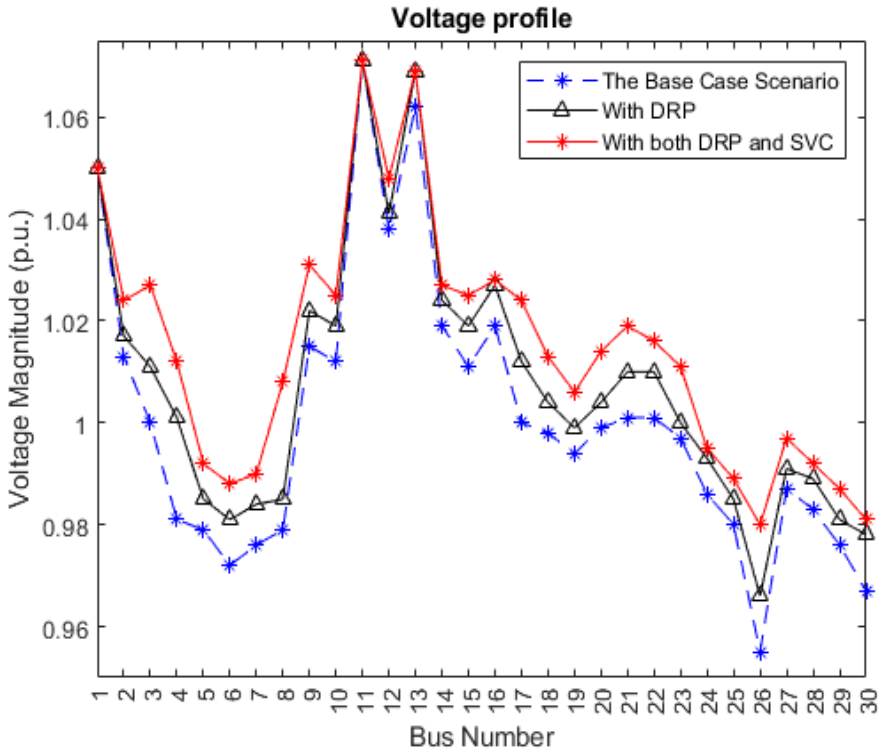

Fig.6. Voltage profiles for all the three Cases

Discussions

It can be seen from Table 3 and *Fig. 6* that:

i. There has been an average of 0.705% improvement in the bus voltage profile from Case 1 (the Base Case Scenario) where there was congestion, to Case 2 where the TOU program (DRP) was solely applied to relieve the congestion. The addition of the SVCs in Case 3 further improved the voltage profile of Case 2 by an average of 0.709%.

ii. The three voltage profiles show clearly that when there is congestion (Case 1), the bus voltage levels decrease, resulting in greater voltage deviations. This base case scenario does not only increase the system losses, but also creates voltage regulation problems for the customers.

iii. The application of TOU program (DRP) in Case 2 raised the bus voltages to very appreciable levels (average of 0.705% increase, and as a result, decreased the margin of deviation. However, when the SVCs were added to the DRP (Case 3), the bus voltage levels were further improved by 0.709% on the average, resulting in a total improvement of averagely 1.414% from Case 1.

iv. This really shows that even though DRPs single-handedly are effective in congestion management by enhancing system voltage profiles, adding SVC further enhances the

system voltage profiles and thus reduces losses. Therefore, the combination of DRP and FACTS devices leads to better congestion management than DRPs only, by having a greater effect on system voltage profiles.

4.2 Effects on Generation Fuel Cost, Demand and System Losses

Figure 7 and Table 4 present a comparison of the total average demands, the total average fuel costs, and the total average losses for all the three cases.

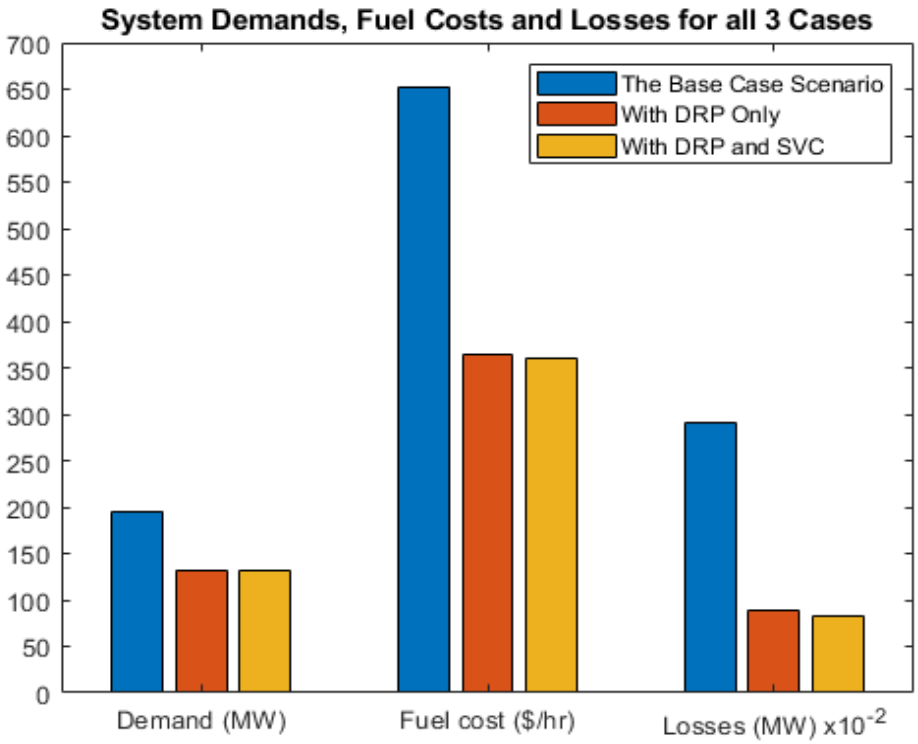

Fig. 7. Comparison of demands, fuel costs and losses for all the three cases

Table 4. Summary of results for the three (3) Cases in *Fig. 7*

Parameter	***Case 1 (Base case scenario)***	***Case 2 (With DRP only)***		***Case 3 (With both DRP and SVC)***	
			% Reduction		***% Reduction***
Demand (MW)	*195.6*	*132.50*	*32.25*	*132.50*	*32.25*
Generation Fuel Cost ($/hr)	*652.66*	*363.51*	*44.3*	*361.22*	*44.65*
System Losses (MW)	*2.91*	*0.89*	*69.42*	*0.84*	*71.13*

Discussions

The following analyses can be made from *Fig. 7* and Table 4:

On Fuel Cost:

i. The fuel cost in Case 1 is greater by 79.54% (652.66 $/hr compared to 363.51 $/hr) than that of Case 2, whilst that of Case 2 also being greater by 0.7% (363.52 $/hr compared to 361 $/hr) than that of Case 3. The high fuel cost in the Peak Period for Case 1 points to the fact that congestion presents some costs to both utilities and customers.
ii. However, with the application of the TOU program in Case 2, even though only 32% of the load responded to the TOU program, the fuel cost reduced drastically by 44.3% (as shown in *Fig.7*).
iii. The good results of Case 2 were slightly improved in Case 3, when both the DRP and the SVC were combined. As can be seen, the fuel cost further decreased slightly in Case 3. The fuel cost decreased from 363.51 $/hr to 361.22 $/hr, representing 0.63% (from 652.66 $/hr in Case 1 to 361.22 $/hr in Case 3, thus by 44.65% - compared with 44.3% for Case 2). This is attributed to the presence of the SVC.

On System Losses:

i. The system losses in Case 1 is greater by 226.97% (2.91 MW compared to 0.89 MW) than that of Case 2, whilst that of Case 2 also being greater by 5.95% (0.89 MW compared to 0.84 MW) than that of Case 3.
ii. Again, with the application of the TOU program in Case 2, with only 32% load participation in the TOU program, the losses reduced by 69.4%. The losses further reduced slightly in Case 3 by 5.62%, decreasing from 0.89 MW in Case 2 to 0.84 MW in Case 3.

On Demand:

i. Both the DRP only (Case 2) and the hybridized approach (Case 3) reduced the demand from 195.6 MW to 132.5 MW representing a reduction of 32.25%.
ii. The application of the SVC in Case 3 has no effect on the demand.

4.3 Effects on MVA flows on Congestion-Prone Lines

Figure 8 and Table 5 present results comparing the MVA flows in the congestion-prone lines for all the three cases.

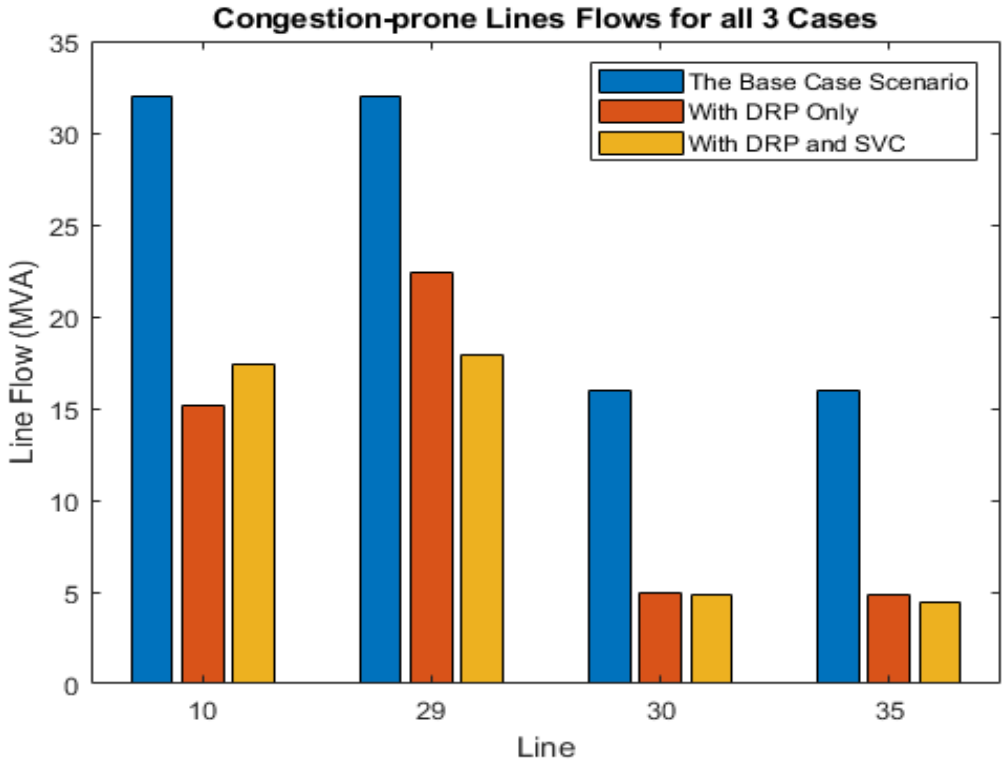

Fig.8. Comparison of MVA flows in congestion-prone lines for all three cases

Table 5. Comparison of MVA flows in congestion-prone lines for all three cases

Line	***MVA Flows (Limit)***	***MVA Flows (Case 1)***	***MVA Flows (Case 2)***	***MVA Flows (Case 3)***
10	*32.00*	*32.00*	*15.16*	*17.38*
29	*32.00*	*32.00*	*22.44*	*17.93*
30	*16.00*	*16.00*	*4.98*	*4.48*
35	*16.00*	*16.00*	*4.89*	*4.45*

Discussions

i. The flows (in MVA) in lines 10, 29, 30, and 35 are higher in the base case scenario (Case 1) than those in the same lines for Case 2 (DRP Only) and Case 3 (DRP and SVC). This is because, before the application of the TOU program, it can be seen in Table 5 that these lines were congested as the MVA flows in them reached their respective ratings. This means that the operating limits of these lines were reached.

ii. However, after the application of the TOU program (Case 2), it can clearly be seen from *Fig. 8* and Table 5 that the flows in these lines have reduced significantly, relieving the congestion in the lines.

iii. Case 3 also has the flows in lines 29, 30 and 35 being lower than the same lines for

Case 2. Again, these good results from the application of the TOU program (DRP) were further enhanced by the addition of the SVC, as can be seen in Case 3, where the flows in lines 29, 30 and 35 further reduced by 20.1% (from 22.44 MVA to 17.93 MVA), 10.04% (from 4.98 MVA to 4.48 MVA), and 9.0% (from 4.89 MVA to 4.45 MVA) respectively, compared to the flows in the same lines in Case 2.

8. CONCLUSION

In this paper, the effects of a combination of DRP and SVC FACTS device as a multi-objective approach for congestion management in transmission lines have been studied. The results show that, in comparison with the Base Case Scenario, the proposed method (employing both DR and SVC) reduced the Peak Period fuel cost from 652.66$/hr to 361.22$/hr, signifying a significant 44.65% reduction, as well as the losses in this same Peak Period from 2.913MW to 0.84MW, resulting in another significant 71.13% reduction. The voltage profile was also significantly enhanced by an average of 1.414% increase from the Base Case Scenario.

The high losses (2.913MW) and high generation fuel cost (652.66$/hr) in the Peak Period (represented by Case 1) again point to the fact that congestion presents some costs to both utilities and customers. Also, the proposed hybridized DRP-SVC method (represented by Case 3) further reduced VAR flows in the lines from 111.18MVAr in the Peak Period (Case 1) to 37.44MVAr, resulting in a significant 66.34% decrease in VAR flows (and hence losses), thus further decongesting the lines of reactive power and leading to an increased or higher line utilization factor (LUF) for the active power. The effectiveness of the proposed hybridized DR-SVC, multi-objective method in congestion management of transmission lines has thus been underscored.

REFERENCES

[1] M. Bavafa, N. Navidi, S. Hesami, and B. A. Parsa, "A new approach for security constrained congestion management using sssc with ant colony search algorithm," *Asia-Pacific Power and Energy Engineering Conference, APPEEC*, pp. 1–5, 2010, doi: 10.1109/APPEEC.2010.5448807.

[2] G. Srinivasulu and P. Balakrishna, "A case study on analysis of congestion management methods in smart grid scenario," *2018 International Conference on Computing, Power and Communication Technologies, GUCON 2018*, pp. 242–247, 2019, doi: 10.1109/GUCON.2018.8675125.

[3] N. Hosseinipoor and S. M. H. Nabavi, "Optimal locating and sizing of TCSC using genetic Algorithm for congestion management in deregualted power markets," *2010 9th Conference on Environment and Electrical Engineering, EEEIC 2010*, vol. 1, pp. 136–139, 2010, doi: 10.1109/EEEIC.2010.5489968.

[4] A. Gautam, P. Sahrma, and Y. Kumar, "Congestion Management by Sensitivity based approach for optimal allocation and parameter setting of TCSC using Grey Wolf Optimisation," 2020.

[5] S. Riyaz, R. Upputuri, and N. Kumar, "Congestion Management in Power System—A Review," *Lecture Notes in Electrical Engineering*, vol. 699, pp. 425–433, 2021, doi: 10.1007/978-981-15-7994-3_39.

[6] N. I. Yusoff, A. A. M. Zin, and A. Bin Khairuddin, "Congestion management in power system: A review," *3rd International Conference on Power Generation Systems and Renewable Energy Technologies, PGSRET 2017*, vol. 2018-Janua, no. March 2018, pp. 22–27, 2017, doi: 10.1109/PGSRET.2017.8251795.

[7] G. Sophia Jasmine and P. Vijaya Kumar, "Congestion management in competitive power market using TCSC," *ARPN Journal of Engineering and Applied Sciences*, vol. 10, no. 9, pp. 4271–4274, 2015.

[8] S. Singh and A. Kumar, "Congestion management using demand response program," *International Conference on Power and Embedded Drive Control, ICPEDC 2017*, pp. 83–88, 2017, doi: 10.1109/ICPEDC.2017.8081064.

[9] G. Luo, Y. Chen, Y. Zhao, Y. He, C. Gong, and C. Zhao, "Consensus-based Nodal Pricing Mechanism for Automated Demand Response Considering Congestion Management on Distribution Networks," *2020 IEEE/IAS Industrial and Commercial Power System Asia, I and CPS Asia 2020*, no. 036000, pp. 575–580, 2020, doi: 10.1109/ICPSAsia48933.2020.9208438.

[10] S. Nandini, P. Suganya, and K. M. Lakshmi, "Congestion Management in Transmission Lines Considering Demand Response and FACTS Devices," *International Journal of Innovative Research in Science, Engineering and Technology*, vol. 3, no. 1, pp. 682–688, 2014.

[11] A. Yousefi, T. T. Nguyen, H. Zareipour, and O. P. Malik, "Congestion management using demand response and FACTS devices," *International Journal of Electrical Power and Energy Systems*, vol. 37, no. 1, pp. 78–85, 2012, doi: 10.1016/j.ijepes.2011.12.008.

[12] "Welcome to NRG | NRG Energy." https://www.nrg.com/insights/energy-education/transmission-congestion---constraints.html (accessed Aug. 11, 2020).

[13] K. Saurabh and S. Gupta, "Transmission line congestion management in liberalized environment," *2016 IEEE 7th Power India International Conference, PIICON 2016*, pp. 0–5, 2017, doi: 10.1109/POWERI.2016.8077286.

[14] S. Singh and A. Kumar, "Demand response program solution to manage congestion in transmission network considering uncertainty of load," *8th International Conference on Computing, Communications and Networking Technologies, ICCCNT 2017*, 2017, doi: 10.1109/ICCCNT.2017.8203983.

[15] Y. Niu, Y. L. Cong, and T. Niimura, "Transmission congestion relief solutions by load management," *Canadian Conference on Electrical and Computer Engineering*, vol. 1, pp. 18–23, 2002, doi: 10.1109/ccece.2002.1015168.

[16] M. D. Ilić, K. D. Bachovchin, and A. S. Lewis, "Costs and benefits of transmission congestion management," *2011 IEEE/PES Power Systems Conference and Exposition, PSCE 2011*, no. March, 2011, doi: 10.1109/PSCE.2011.5772585.

[17] M. Holt and C. Glover, "Energy Policy Act of 2005: Summary and Analysis of Enacted Provisions," *Congressional Research Service. Resources, Science, and Industry Division*, pp. 67–107, 2006.

[18] J. Wellinghoff, "Collaborative dialog on demand response," *FERC 12 Nov. 2006, www.FERC.gov*, 2006, [Online]. Available: http://www.ferc.gov/legal/staff-reports/09-07-demand-response.pdf

[19] H. Aalami, G. R. Yousefi, and M. Parsa Moghadam, "Demand response model considering EDRP and TOU programs," 2008. doi: 10.1109/TDC.2008.4517059.

[20] N. Nikmehr, L. Wang, S. Najafi-Ravadanegh, and S. Moradi-Moghadam, *Demand Response Enabled Optimal Energy Management of Networked Microgrids for Resilience Enhancement*. Elsevier Inc., 2018. doi: 10.1016/B978-0-12-814891-4.00003-5.

[21] D. S. Kirschen, "Demand-Side View of Electricity Markets - Invited Paper," *IEEE Transactions on Power Systems*, vol. 18, no. 2, pp. 520–527, 2003.

[22] E. Shayesteh, M. P. Moghaddam, S. Taherynejhad, and M. K. Sheikh-El-Eslami, "Congestion Management using Response Programs in Power Market," *IEEE Transactions on Power Systems*, no. Cm, 2008.

[23] X. Qu, H. Hui, S. Yang, Y. Li, and Y. Ding, "Price elasticity matrix of demand in power system considering demand response programs," in *IOP Conference Series: Earth and Environmental Science*, Mar. 2018, vol. 121, no. 5. doi: 10.1088/1755-1315/121/5/052081.

[24] S. Zhao and Z. Ming, "Modeling demand response under time-of-use pricing," in *POWERCON 2014 - 2014 International Conference on Power System Technology: Towards Green, Efficient and Smart Power System, Proceedings*, Dec. 2014, pp. 1948–1955. doi: 10.1109/POWERCON.2014.6993842.

[25] V. Mounika and K. Narasimharao, "Congestion Management in Deregulated Power System using Price based Programs," *International Journal of Engineering Research and Technology*, vol. V5, no. 08, pp. 169–174, 2016, doi: 10.17577/ijertv5is080159.

[26] F. C. Schweppe, M. C. Caramanis, R. D. Tabors, and R. E. Bohn, "Energy Marketplace Transactions," in *Spot Pricing of Electricity*, Springer US, 1988, pp. 55–80. doi: 10.1007/978-1-4613-1683-1_3.

[27] J. G. Roos, "Industrial power demand response analysis for one-part real-time pricing," *IEEE Transactions on Power Systems*, vol. 13, no. 1, pp. 159–164, 1998, doi: 10.1109/59.651628.

[28] N. Yu and J.-L. Yu, "Optimal TOU Decision Considering Demand Response Model," Power System Technology, 2006.

[29] Y. Hongming, Z. Yeping, and L. Xiaojiao, "System dynamics model for demand side management," *2006 3rd International Conference on Electrical and Electronics Engineering*, no. 05, 2006, doi: 10.1109/ICEEE.2006.251854.

[30] S. S. Reddy, M. S. Kumari, and M. Sydulu, "Congestion management in deregulated power system by optimal choice and allocation of FACTS controllers using multi-objective genetic algorithm," *Journal of Electrical Engineering and Technology*, vol. 4, no. 4, pp. 467–475, 2009, doi: 10.5370/JEET.2009.4.4.467.

[31] M. S. Iqbal and B. Sujatha, "Multiple Contingency Analysis for optimal placement and estimate the value of SVC for power loss reduction employing Particle Swarm Optimization," *4th International Conference on Electrical, Electronics, Communication, Computer Technologies and Optimization Techniques, ICEECCOT 2019*, pp. 129–133, 2019, doi: 10.1109/ICEECCOT46775.2019.9114569.

[32] D. Thukaram and A. Lomi, "Selection of static VAR compensator location and size for system voltage stability improvement," *Electric Power Systems Research*, vol. 54, no. 2, pp. 139–150, 2000, doi: 10.1016/S0378-7796(99)00082-6.

[33] S. Gerbex, R. Cherkaoui, and A. J. Germond, "Optimal location of multi-type FACTS devices in a power system by means of genetic algorithms," *IEEE Transactions on Power Systems*, vol. 16, no. 3, pp. 537–544, 2001, doi: 10.1109/59.932292.

[34] S. A. Jumaat, I. Musirin, M. M. Othman, and H. Mokhlis, "Optimal placement and sizing of multiple FACTS devices installation," *PECon 2012 - 2012 IEEE International Conference on Power and Energy*, no. June 2014, pp. 145–150, 2012, doi: 10.1109/PECon.2012.6450195.

[35] M. Esmaili, H. A. Shayanfar, and R. Moslemi, "Locating series FACTS devices for multi-objective congestion management improving voltage and transient stability," *European Journal of Operational Research*, vol. 236, pp. 763–773, 2014.

[36] P. Kachore and M. v. Palandurkar, "TTC and CBM calculation of IEEE-30 bus system," *2009 2nd International Conference on Emerging Trends in Engineering and Technology, ICETET 2009*, pp. 539–542, 2009, doi: 10.1109/ICETET.2009.227.

[37] "MATPOWER – Free, open-source tools for electric power system simulation and optimization." https://matpower.org/ (accessed May 26, 2021).

DYNAMICS MODELING AND CONTROL SYSTEM DEFINITION FOR VIBRATION ATTENUATION OF A THIN TITANIUM PLATE WITH MATLAB AND ANSYS

Vlad Mihai **PANAINTE**, Horia **BĂLAN**
Technical University of Cluj-Napoca
vlad_panainte@yahoo.com, horia.balan@enm.utcluj.ro

Keywords: software fault diagnosis, feedback, control systems, proportional control

Abstract*: Vibration artefacts that appear at small dimension components are frequently encountered in multiple domains such electronic equipment production, surgical and high precision medical applications, optical applications high quality photo/video equipment. The main objective of this work is to develop a reduced model that accurately represents the dynamics of a small dimension titanium plate and define a suitable vibration control system. With the aid of powerful engineering software instruments, the mathematical model of the studied object is defined with MATLAB after it was modeled and analyzed with ANSYS (mode shape analysis). The mathematical model is developed based on the eigenvectors and eigenvalues extracted from ANSYS and it is called the state space model which is than transformed into a transfer function for simplicity reasons. The mathematical model is than integrated in Simulink and the vibration velocity is evaluated, followed by the definition of a control system comprised of a piezoelectric actuator and PID controller. The evaluation of the system was performed by applying a step signal at the input of the plant and the velocity response is observed comparatively in three configurations as listed: small dimension plate response, plate and piezoelectric actuator and full plant (titanium plate, actuator and PID controller).*

1. INTRODUCTION

The vibration artefacts that appear at small dimension components are frequently encountered in multiple domains such electronic equipment production, surgical and high precision medical applications, optical applications high quality photo/video equipment. In general terms, the vibration that can be detected at different components is harmful to the

equipment and can lead to irremediable defects or they can decrease the performance of the equipment. Considering the previous mentions, the study of the vibration reduction technique is of a major importance and took the attention of numerous researchers becoming a subject of interest at a global level. The work of [1], [2], [3], [4] stood at the base of this paper as they are focusing on developing active vibration attenuation techniques with piezoelectric actuators.

The vibration reduction can be obtained by using two different techniques such as passive and active. The first mentioned technique can't be implemented in small scale applications due to different factors hence for reduced dimension applications the only applicable techniques are the ones which are using active components such as piezoelectric actuators. Beside the actuators which are operating based on the piezoelectric effect, in vibration control systems can also be used electro-mechanical, electrical, electrodynamic hydraulic and pneumatic actuators, but all the listed types are of large dimensions and are only suitable for large scale applications.

The main objective of this work is to develop an active vibration control system for small scale applications. Considering the fact that the modeling and analysis techniques do often induce errors in the results, for simplicity purposes in this paper it is presented a titanium thin plate with a length of 15 mm, width of 7 mm and a thickness of 0.5 mm.

The mathematical model of the titanium plate with the previously listed dimensions is obtained with the help of MATLAB software from the eigenvectors and eigenvalues extracted from ANSYS Mode Shape Analysis tool with the Block Lanczos method.

This paper is organized in six sections. The first part, the introduction with the objective and motivation description, the second section, with the physical description of the studied object and the third is presenting the mode shape analysis results. In the fourth part, the mathematical model extraction technique is described and in the fifth and sixth part, the MATLAB/SIMULINK project is presented, followed by the discussion of the results in the sixth part and conclusions in the end.

2. PHYSICAL MODEL DESCRIPTION

For this study, the research team has reached the conclusion that a small, simple object can be used for analysis. The physical characteristics of the thin titanium plate can be seen in *figure 1* and the mechanical properties in Table 1.

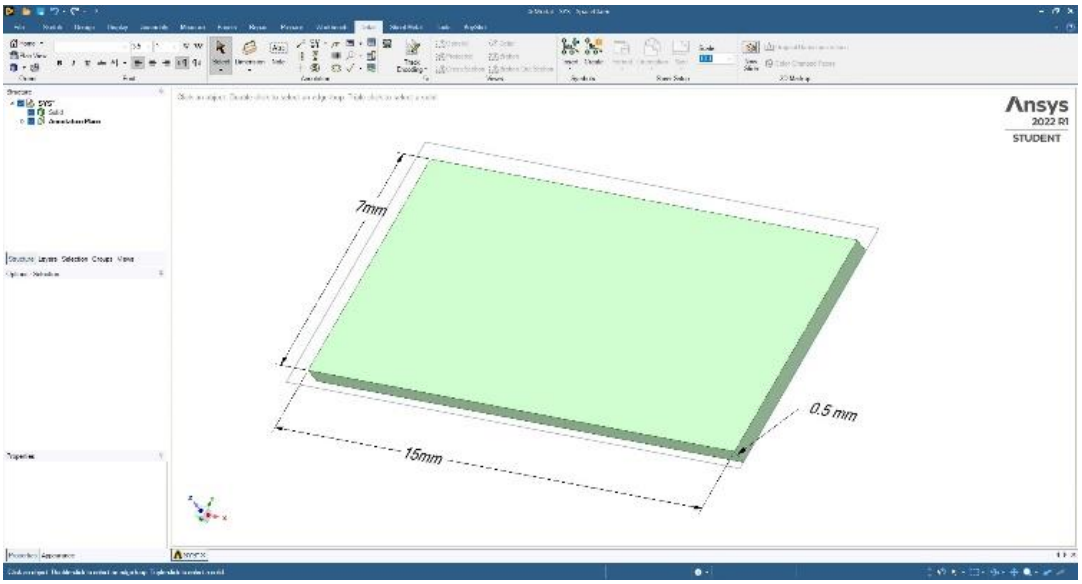

Fig. 1 Physical dimensions of the studied object

Table 1. Mechanical properties of the titanium alloy, selected as material of the thin plate.

Property	Value	Unit
Density	4620	Kg/m^3
Coefficient of thermal expansion	9.4E-06	$^oC^{-1}$
Young's Modulus	9.6E+10	Pa
Poisson's ratio	0.36	

3. MODE SHAPE ANALYSIS

As described in the introduction, an important step in finding the mathematical model of the studied object is to extract the eigenvalues and eigenvectors in order to be further processed. The eigenvalues and eigenvectors are extracted from ANSYS after the modal analysis is performed with specific instruments which are at the user's disposal in ANSYS. The eigenvalues and eigenvectors are extracted using the Block Lanczos method, as a standard technique. After extracting the necessary values by software specific means, the information corresponding to the X and Y displacement are isolated and only the Z component is used in the analysis. The natural frequencies for the first six modes of vibration were extracted and the corresponding eigenvalues for the Z displacement component were used. The natural frequencies (eigenvalues) are presented in table 2 but the eigenvectors can't be presented due to the high volume of extracted values. The studied component was split into 1340 nodes and 171 elements. For each natural frequency was extracted a number of 1340 values to form the eigenvector.

Table 2. Modes of vibration and natural frequencies.

Mode	1	2	3	4	5	6
Frequency [Hz]	1705.1	7383.5	10560	19965	23888	29425

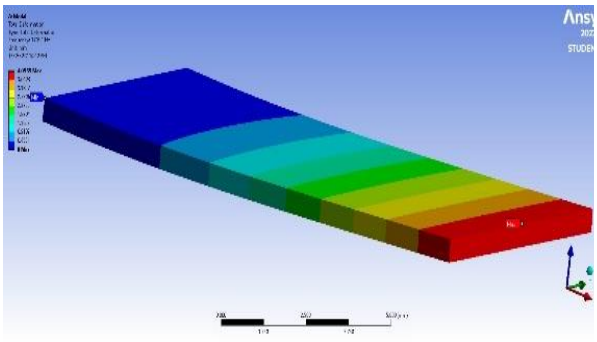

Fig. 2.1

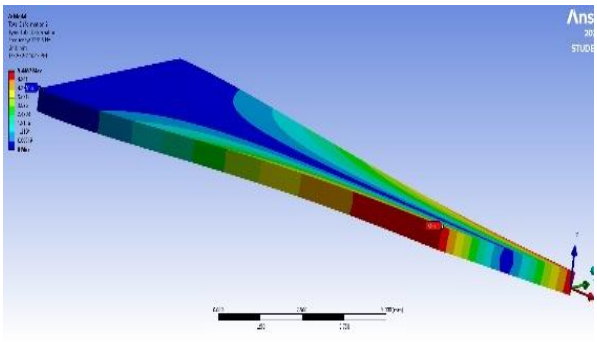

Fig. 2.2

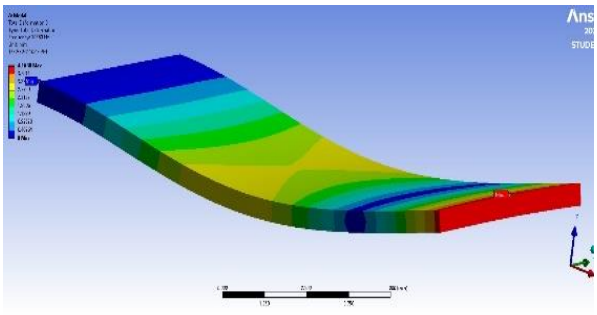

Fig. 2.3

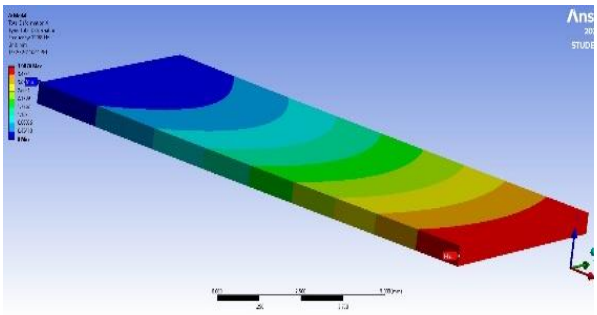

Fig. 2.4

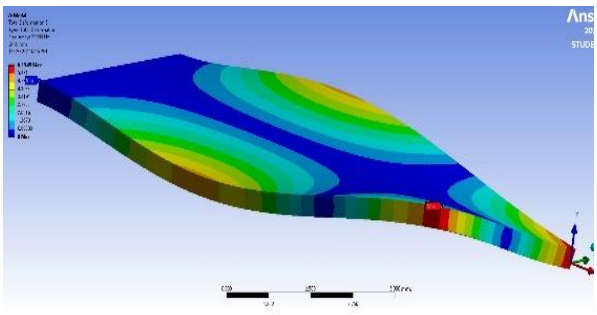

Fig. 2.5

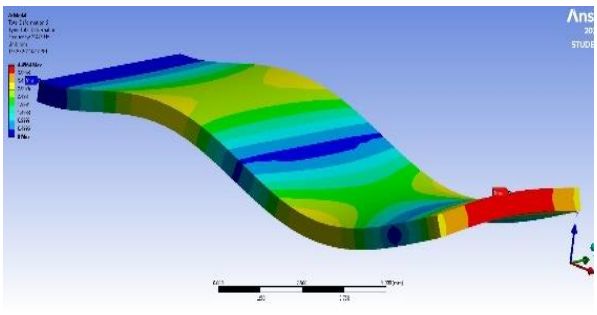

Fig. 2.6

Fig. 2.1 … 2.6 Mode shape vibration pattern (all six modes). Index = number of the vibration mode

The general theory for the mode shape analysis is presented in [5]. The equation of motion of a multi DOF system under external forces is given by:

$$[m]\ddot{x} + [c]\dot{x} + [k]x = F \tag{1}$$

Considering that the mass, damping and stiffness matrices are non-diagonal, equation 1 is leading to n coupled second order differential equations. The eigenvalue problem for equation 1 is solved to uncouple the coupled equation set and the eigenvectors are obtained as *x(1), x(2) … x(n)* which leads to the modal matrix of the system:

$$x_n = \left\lfloor x_{(1)} x_{(2)} \cdots x_{(n)} \right\rfloor \tag{2}$$

For a system with multiple degree of freedom, taking as general assumption a proportional damping, the solution of the first equation can be expressed as:

$$x(t) = [x_n] \cdot x_p(t) \tag{3}$$

Having $x_p(t)$ the displacement in principal coordinates. As ANSYS is normalizing the normal modes to mass, the equation of motion in the principal coordinates will be of the form [4]:

$$\ddot{x}_{pi}(t) + 2 \cdot \xi_i \cdot \omega_i \cdot \dot{x}_{pi} + \omega_i^2 \cdot x_{pi}(t) = F_{pi}(t) \tag{4}$$

With i=1, 2, ,n and

$$F_p(t) = [x_n]^T \cdot F(t) \tag{5}$$

being the vector of forces in principal coordinates system. As it follows, a set of n uncoupled differential equations of the second order is obtained from the set of n coupled differential equations of the second order. The resulting equations are converted into a state space form as first order differential equations. A general algorithm used for vibration analysis with ANSYS and MATLAB is summarized below and it was developed in [6].

4. MATHEMATICAL MODEL EXTRACTION TECHNIQUE

The state space model of the studied object can be constructed from the eigenvectors and eigenvalues normalized with respect to mass.

$$\begin{aligned} \dot{x} &= A \cdot x + B \cdot u \\ y &= C \cdot x + D \cdot u \end{aligned} \tag{6}$$

where $\dot{x}$it is state vector, and y it is output vector.

The system matrix A, input matrix B, output matrix C and direct transmission matrix D of the state space model for a dynamic system with n modes can be written as below [6]:

$$A=\begin{bmatrix} 0 & 1 & \cdots & \cdots & \cdots \\ -\omega_1^2 & -2\cdot\xi_1\cdot\omega_1 & \cdots & \cdots & \cdots \\ \cdots & \cdots & \cdots & \cdots & \cdots \\ \cdots & \cdots & \cdots & \cdots & \cdots \\ \cdots & \cdots & \cdots & -\omega_1^2 & -2\xi_n\cdot\omega_n \end{bmatrix} \tag{7}$$

$$\mathrm{B}=\begin{bmatrix} 0 \\ F_{p1} \\ 0 \\ F_{p2} \\ \cdots \\ F_{pn} \end{bmatrix} \tag{8}$$

Here F_p is the vector of forces in principal coordinates. Value of C depends upon the output of interest so that for velocity output, C is given by:

$$\mathrm{C}=\begin{bmatrix} 0 & 0 & 0 & 0 & \cdots \\ 0 & x_{n11} & 0 & x_{n12} & \cdots \\ 0 & 0 & 0 & 0 & \cdots \\ 0 & x_{n21} & 0 & x_{n22} & \cdots \\ \cdots & \cdots & \cdots & \cdots & \cdots \end{bmatrix} \tag{9}$$

Having x_{n11}, x_{n12} the elements of the modal matrix normalized to mass.

For this analysis, no direct transmission to the output is considered hence:

$$D=[0] \tag{10}$$

Considering the above definitions of the state space matrices, having the eigenvectors and eigenvalues from ANSYS the state space system was constructed.

5. SIMULINK MODEL DEFINITION

Since the matrices representing the state space system are large for simplicity purposes, the state space system was converted to a transfer function with the aid of MATLAB.

The vibration simulations were performed considering an input force at the middle of the thin plate, node 497 and measured at node 1317 at the tip (the position of both nodes is indicated in *figure 3*). It is worth noting the fixed support position which was considered the far left edge of the plate, indicated in *figure 3* with 2 red arrows.

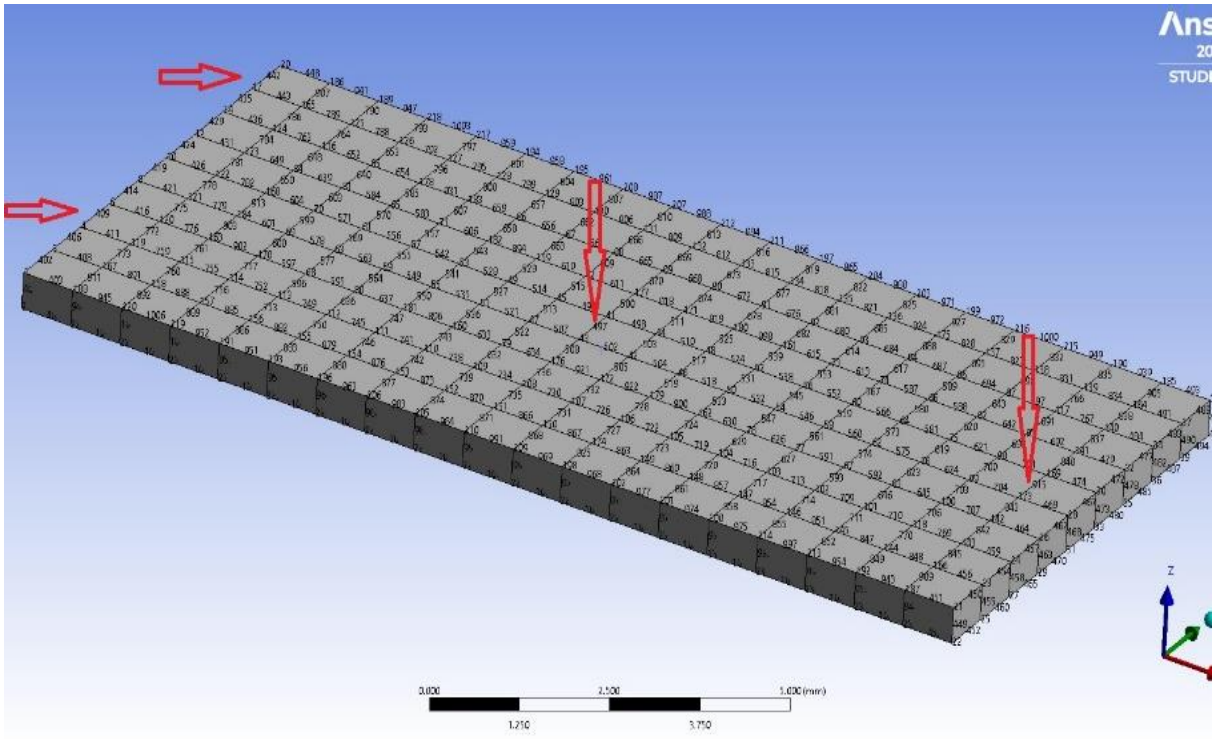

Fig. 3. Fixed support, input and output node position indication

The actuator model used in the SIMULINK system is a piezoelectric actuator defined and developed by another researcher in [1] and it is represented by the below transfer function.

$$TF_{act} = \frac{0.07962 \cdot s + 0.1521}{s^4 + 2.201 \cdot s^3 + 7.816 \cdot s^2 + s + 6.93} \tag{11}$$

The parameters used for the PID controller are listed in Table 3.

Table 3. PID controller parameters

Parameter	P	I	D	N
Value	49811618.8789	69870496.6521	8709427.0764	154.4799

The above defined components were integrated into a full SIMULINK model which is presented in *figure 4* below:

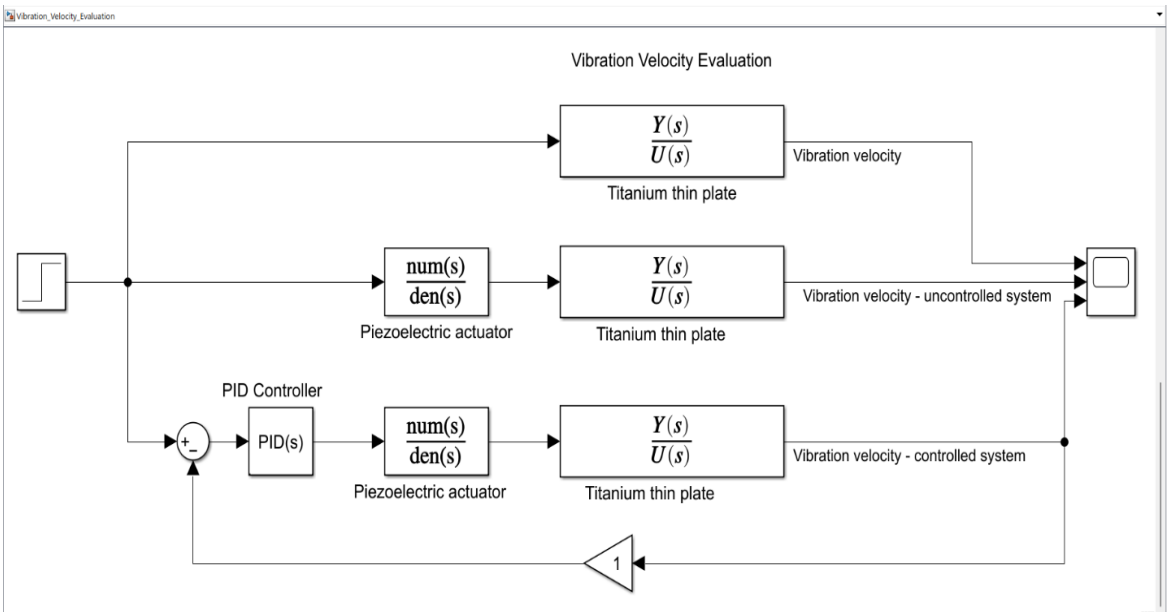

Fig. 4 The block diagram of the control system

6. RESULTS AND DISCUSSIONS

The uncontrolled system response to a unit force can be seen in *figure 5* below, over an interval of 0.5 seconds. The vibration velocity in this situation is osculating between -0.6 to 0.6 m/s and it is never stabilizing over 0, oscillating continuously between -0.05 and 0.05 m/s. The system reason for which the system is never stabilizing is that it is considered an undamped system having the damping coefficient is 0.001.

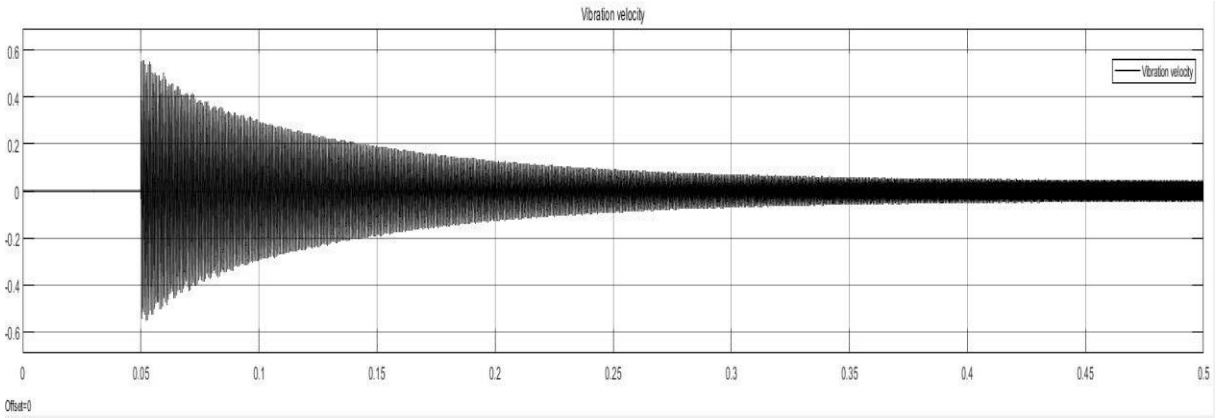

Fig. 5. Uncontrolled system vibration velocity

After introducing the piezoelectric actuator in the system, it can be observed a significant decrease in the vibration velocity (*fig 6*), however the introduction of a control system is needed. The system observation in this case was performed over a time interval of 10 seconds.

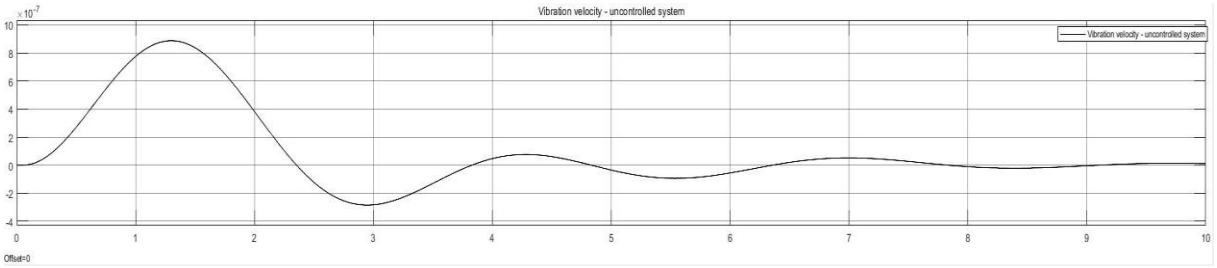

Fig. 6 The velocity of vibration after the introduction of the piezoelectric actuator

The 7th figure of this paper is presenting the system response after the introduction of the previously defined PID controller. The observation period is of 1 sec. As it can be observed, the system is stable, having the control curve parameters defined by a rise time of 0.0468 seconds, setting after 0.916 seconds with a peak amplitude of 1.12 and overshoot 12.1%.

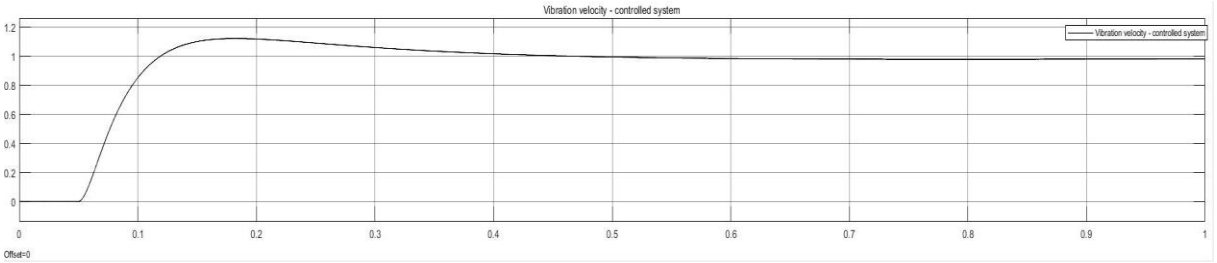

Fig. 7 Complete system response to step signal

The 8th figure is presented with the intent to show that the system is stabilizing in the proposed configuration after applying a fixed pulse signal at the input.

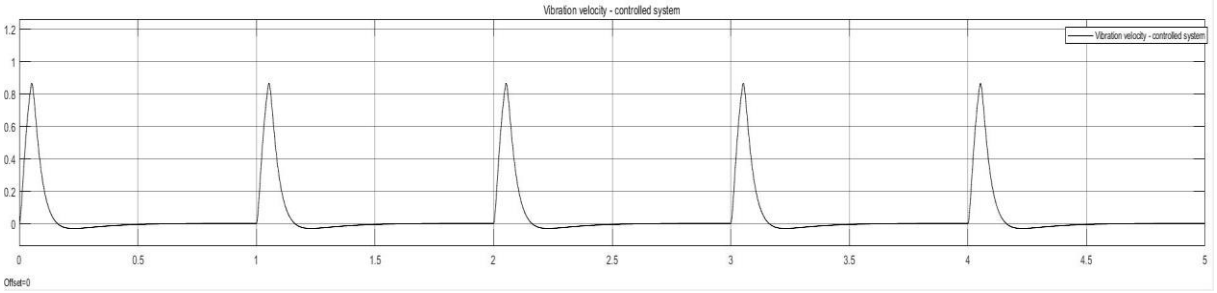

Figure 8. Complete system response to impulse signal

From what can be observed in *figure 9*, the controller is settling at the value of 0.9837 with an error of 0.0163 and as detailed in the description of the 7th figure, we can also mention that an efficient controller design was defined for this specific application.

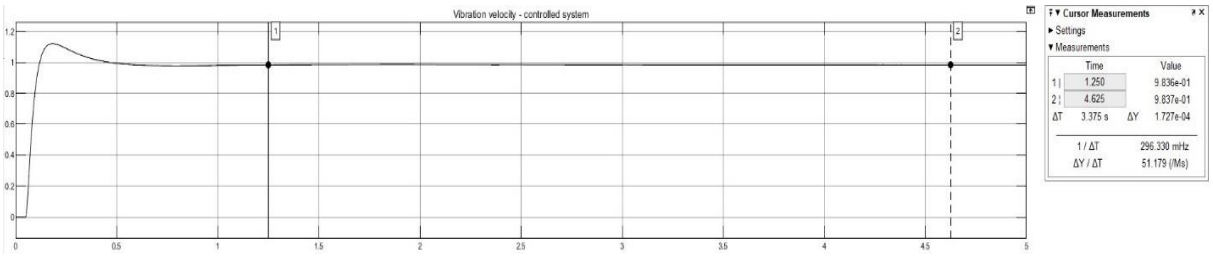

Fig. 9. Controller error definition

7. CONCLUSIONS

This paper presents the results of multiple simulations performed with ANSYS and MATLAB/SIMULINK software in order to evaluate the vibration of a thin titanium plate and the efficiency of a control system comprised of a piezoelectric actuator and PID controller.

In the images presented in *figures 2.1 – 2.6* the dynamics of the studied object can be observed and can be concluded that all the extracted modes of vibration can have a correspondent in reality as the shapes of vibration have understandable dynamic behavior.

In chapter 6, various SIMULINK simulation results are presented, and the efficiency of the control system can be observed. The vibration reduction is significantly reduced, and the controller output characteristics are showing good performances.

After analyzing the results of the simulations, we can conclude that the algorithm used to define the mathematical model of the mechanical object is found to be reliable and effective in performing an initial selection of a control system plant model. The results are inspiring and encouraging to apply the presented technique also for other type of applications.

ACKNOWLEDGEMENT

This paper was financially supported by the Project “Entrepreneurial competences and excellence research in doctoral and postdoctoral programs - ANTREDOC”, project co-founded by the European Social financing agreement no 56437/24.07.2019.

REFERENCES

[1] B. B. Muhammad, M. H. Rahman and M. R. bin Ahmad, "Modelling and simulation of piezoelectric actuator for vibration control" 2015 10th Asian Control Conference (ASCC), 2015, pp. 1-6, doi: 10.1109/ASCC.2015.7244627;

[2] L. Sui, X. Xiong, G. Shi, "Piezoelectric Actuator Design and Application on Active Vibration Control", Physics Procedia, Volume 25, 2012, Pages 1388-1396, ISSN 1875-3892,

https://doi.org/10.1016/j.phpro.2012.03.251;

[3] H. Shen, C. Wang, L. Li, L. Chen "Prototyping a compact system for active vibration isolation using piezoelectric sensors and actuators ", Rev. Sci. Instrum. 84, 055002 (2013), http://dx.doi.org/10.1063/1.4804651;

[4] M. Berardengo, A. Cigada, S. Manzoni, M. Vanali "Vibration Control by Means of Piezoelectric Actuators Shunted with LR Impedances: Performance and Robustness Analysis", Hindawi Publishing Corporation, Shock and Vibration, Volume 2015, Article ID 704265, 30 pages, http://dx.doi.org/10.1155/2015/704265;

[5] F. Klimenda, J. Soukup, "Modal analysis of thin aluminium plate", Procedia Engineering, Volume 177, 2017, Pages 11-16, ISSN 1877-7058, https://doi.org/10.1016/j.proeng.2017.02.176;

[6] Hatch MR, Vibration Simulation Using MATLAB and ANSYS, 1st ed. Boca Raton, Florida: Chapman & Hall/CRC, 2001.

AN ENHANCED JUMPING SPIDER OPTIMIZATION ALGORITHM

Betrand Ngwa **ATANGA**, Francis Boafo **EFFAH,** Philip Yaw **OKYERE**
Kwame Nkrumah University of Science and Technology, Kumasi, Ghana
atangabertrand@gmail.com, fbeffah74@gmail.com, okyerepy@yahoo.com

Keywords: Jumping spider optimization, bio-inspired algorithm, meta-heuristics, levy flight.

Abstract*: Jumping Spider Optimization (JSO) algorithm is a more recent meta-heuristic algorithm shown to outperform recent algorithms in the literature. This paper presents a JSO variant that modifies standard JSO in its global search and jumping on prey phases to improve further its global search capability. The proposed algorithm employs levy flight to update the position of global search agent for better performance. It also introduces a random number generator in the equation for the trajectory of the spider when jumping on prey to provide the updated agent with flexibility to attack prey. The enhanced jumping spider optimization algorithm (EJSO) is tested on 17 well-known benchmark functions and its performance compared with the standard JSO and five other well-known algorithms. The EJSO is also verified on a welded beam design problem to validate our algorithm. The results of statistical analyses conducted show the superiority of EJSO over the standard JSO and the other state-of-arts algorithms*.

1. INTRODUCTION

Several meta-heuristic algorithms have been developed to solve a variety of complex problems in a variety of domains, including data mining, engineering applications, energy, networks, medical, and other fields [1]. Meta-heuristics algorithms are flexible and straightforward because they mimic biological or physical phenomena by focusing solely on inputs and outputs [1]. Furthermore, because meta-heuristics are a type of stochastic optimization technique, they can effectively circumvent local optimum, usually encountered in real-world problems [2]. Meta-heuristic optimization algorithms outperform heuristic algorithms in various sophisticated and tricky optimization real-world problems due to the benefits of simplicity, flexibility, and the ability to avoid local optima [3]. The recent meta-

heuristic algorithms include Coot Bird Algorithm (COOT) [4], Mexican Axolotl Optimization (MAO) [5], Gradient-base Optimizer (GBO) [6], Hunger Game Search (HGS) [7], and Harris Hawks Optimization (HHO) [8].

Researchers continue to develop new meta-heuristic algorithms because one algorithm is unable to obtain suitable results in all fields [9]. The jumping spider optimization algorithm (JSO), stirred by the tracking style of a jumping spider, is one of the recent additions to the existing meta-heuristic algorithms. It is shown to have the capability to solve real-world problems such as selective harmonics elimination problem and ideal tuning of parameters of a proportional integral derivative (PID) controller [10].

The optimization method presented in this paper aims at improving further the performance of the JSO. The modified version, named Enhanced Jumping Spider Optimization (EJSO) Algorithm, proves to improve the convergence rate, the efficiency in finding optimal solutions, stability and robustness of the standard JSO. The modification targets the global search and the jumping on prey phases of the JSO. The modified version introduces randomness (stochastics) into the algorithm to enable the spider agent to move in the search space efficiently and effectively to reach a good global optimization.

The remaining of the paper is organised as follows: Section 2 explains the original JSO. Section 3 presents the modified JSO. Section 4 presents the various tests done to validate the performance of the algorithm. Results and discussion are presented in section 5. Section 6 presents the conclusion.

2. ORIGINAL JSO [8]

The JSO mimics the foraging characteristics of jumping spiders. The jumping spider mathematical modelling is presented in 3 stages: searching, persecution and jumping on its prey. A model is also given for the pheromone rate of the spider.

2.1. Searching for prey

At start, the search agents are randomly generated to search for prey. In the searching for prey phase, the jumping spider undergoes a random search in the search space to find the exact position of a prey. The search is mathematically modelled in both local and global searches as depicted in *Fig. 1*.

The local search is represented by (1):

$$\vec{x}_i(k+1) = \vec{x}_{best}(k) + walk\left(\frac{1}{2} - \varepsilon\right) \quad (1)$$
$$i = 1, 2, 3, \dots, n.$$

where $\vec{x}_i(k+1)$ is the updated location of the *i*th search agent, $\vec{x}_{best}(k)$ is previous iteration best agent, $walk$ is a uniformly distributed pseudo-random number in the range [-2, 2] and ε is a normally distributed pseudo-random number in the range [0,1].

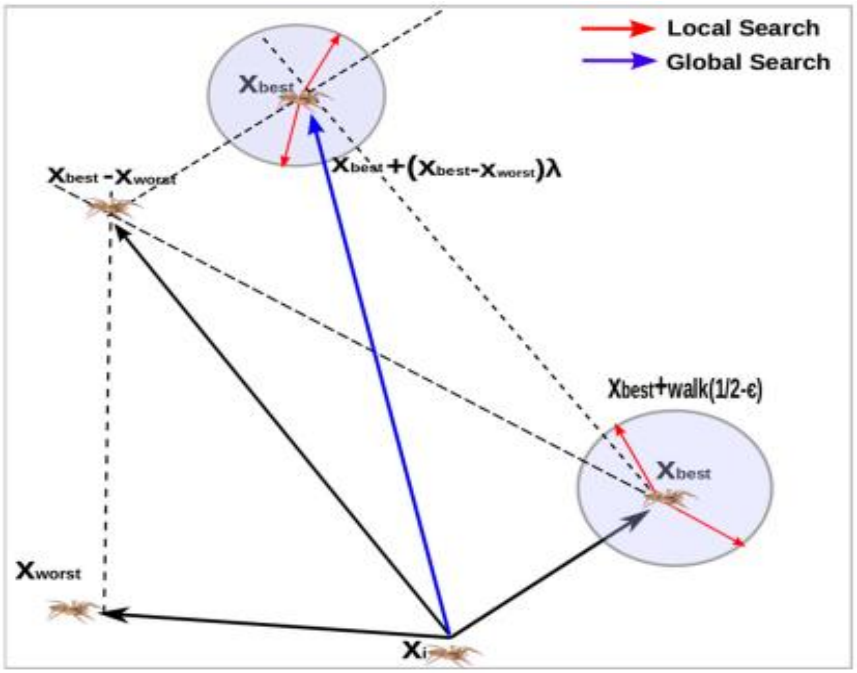

Fig. 1. Search phase

The global search is described by (2):

$$\vec{x}_i(k+1) = \vec{x}_{best}(k) + \left(\vec{x}_{best}(k) - \vec{x}_{worst}(k)\right)\lambda \qquad (2)$$
$$i = 1,2,3 \ldots \ldots . n.$$

where $\vec{x}_i(k+1)$ is updated location of *i*th search agent, $\vec{x}_{best}(k)$ and $\vec{x}_{worst}(k)$ indicate best and worst search agents from previous iteration, λ is a Cauchy arbitrary figure with μ=0 and θ=1.

2.2. Persecution

During hunting, the spider may find itself not within a reachable distance to capture a prey. It will creep closer until it is within a good range to jump and capture the prey. The movement is represented by uniformly accelerated rectilinear motion given by (3).

$$x_i = \frac{1}{2}at^2 + v_o t \qquad (3)$$

where x_i is the position of the *i*th spider chasing a prey, t is time, and v_o is the starting speed. Acceleration *a* can be expressed as $a = \frac{v}{t}$, where $v = x - x_0$. Each iteration is taken to be time with the difference from one iteration to the next being 1. The starting speed is usually made zero and (3) redefined as in (4):

$$\vec{x}_i(k+1) = \frac{1}{2}\left(\vec{x}_i(k) - \vec{x}_r(k)\right) \tag{4}$$

where $\vec{x}_i(k+1)$ is the updated location of *i*th search agent, $\vec{x}_i(k)$ being the *i*th search agent in the previous iteration, with $\vec{x}_r(k)$ being the *r*th search agent arbitrarily picked from the previous iteration. The integer r lies in the interval [1, *n*] where *n* is maximum number of search agents and it must not be equal to *i*. The persecution is depicted as shown in *Fig. 2*.

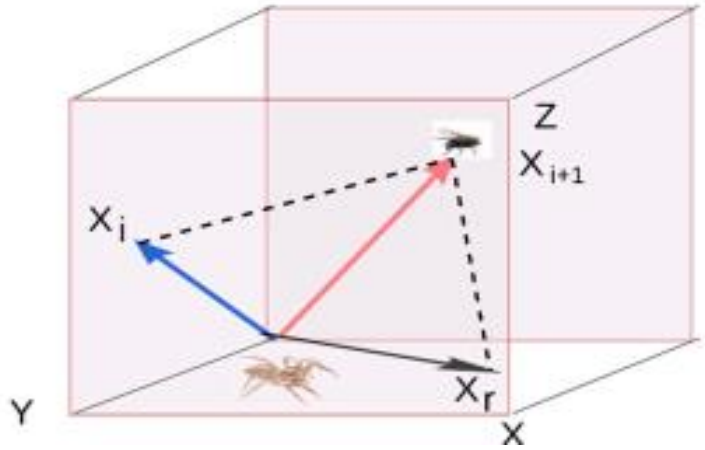

Fig. 2. Representation of persecution

2.3. Jumping on the prey

When the spider is within a jumping distance of the prey, it jumps on it. The jumping motion is considered to be a projectile motion shown in *Fig. 3*.

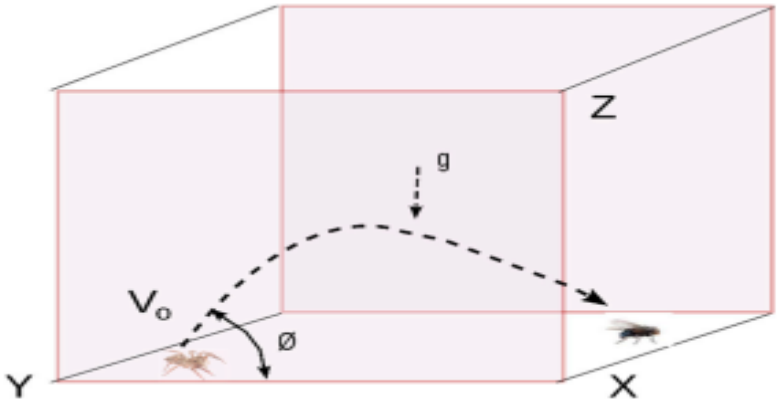

Fig. 3. Jumping on prey

The equation of projectile motion can be expressed in terms of the vertical (Y-axis) and horizontal (X-axis) displacements of the particle. The displacement along the X-axis has uniform rectilinear motion, and the Y-axis has uniformly accelerated motion. Equations (5) and (6) represent X-axis and Y-axis displacements respectively.

$$\vec{x}_i = v_o \cos(\alpha) t\vec{i} \tag{5}$$

$$\vec{y}_{\,i} = \left(v_0 \sin(\alpha) t - \frac{1}{2} g t^2\right)\overrightarrow{J} \tag{6}$$

Eliminating the time *t* from (5) and (6), the equation of the trajectory of the projectile becomes

$$y = x \tan(\alpha) - \frac{g x^2}{2V_0^2 cos^2(\alpha)} \tag{7}$$

The trajectory in its final form is expressed as follows:

$$\vec{x}_i(k+1) = \vec{x}_i(k) \tan(\alpha) - \frac{g\vec{x}_i^2(k)}{2V_0^2 cos^2(\alpha)} \tag{8}$$

$$\alpha = \frac{\varphi\pi}{180}$$

where $\vec{x}_i(k+1)$ is the new location of *i*th search agent, with $\vec{x}_i(k)$ being the current location of *i*th search agent. The projection speed v_o is fixed as 100 mm/sec, g (acceleration due to gravity) = 9.80665 m/s^2 and φ in degrees is randomly generated between 0 and 1.

2.4. Pheromone Rates

Jumping spiders produce pheromones. Pheromones are olfactorily noticed by other members of the same species and they cause behavioural changes. The rate of pheromones is modelled as follows:

$$pheromone(i) = \frac{Fitness_{max} - Fitness(i)}{Fitness_{max} - Fitness_{min}} \tag{9}$$

Fitness(*i*) defines the present fitness value of the *i*th search agent, and $Fitness_{max}$ and $Fitness_{min}$ are the worst and the best fitness value in the current generation, respectively. The fitness value is normalized in the interval (0, 1) with 0 being the worst and 1 the best pheromone rate, respectively.

An unfit agent with low pheromone rate, less or equal to 0.3 is updated by a better fitted agent as follows:

$$\vec{x}_i(k) = \vec{x}_{best}(k) + \frac{1}{2}\left(\vec{x}_{r1}(k) - (-1)^{\sigma} * \vec{x}_{r2}(k)\right) \quad (10)$$
$$r_1 \neq r_2$$

where $\vec{x}_i(k)$ is the weak jumping spider search agent with low pheromone to be updated, r_1 and r_2 are randomly generated integers in the interval [1, *n*], *n* is the maximum number of search agents, $\vec{x}_{r1}(k)$ and $\vec{x}_{r2}$ are the $r_1 th$ and $r_2 th$ search agents selected, $\vec{x}_{best}(k)$ is the best search agent found from the previous iteration and σ is a randomly generated binary number in the interval [0,1].

3. THE PROPOSED JSO VARIANT

The JSO variant is achieved by modifying the searching for prey and jumping on prey equations of the original JSO.

3.1. Modification of Searching for Prey Phase

The global search of the standard JSO is represented mathematically by (2). The second term generates new solutions around the best solution using the difference between the best solution and worst solution times the Cauchy random variable with μ= 0 and θ=1. The modified JSO replaces this term with Lévy flight which has been successfully applied for global search in many metaheuristic algorithms [9]. The new equation is given by:

$$\vec{x}_i(k+1) = \vec{x}_{best}(k) + \gamma . L_{\alpha}(S) \quad (11)$$

where $\vec{x}_i(k+1)$ is the new location of *i*th search agent, $\gamma > 0$ is the step size which relates to the scales of the problem and $L_{\alpha}(S)$ provides a random walk whose random step length *S* is drawn from a Lévy distribution. The subscript α determines the probability of obtaining Lévy random numbers in the tail of the Lévy distribution. The choice of α significantly affects the search ability [11][12]. Its recommended value of 1.5 is used [12].

3.2. Jumping on Prey

The path followed by the spider as it jumps on prey is represented by a projectile path. In the standard JSO, the path is varied by randomly varying the projection angle φ in degrees in the interval (0, 1). For small values of α, (7) can be rewritten as

$$y = x\,\alpha - \frac{gx^2}{2V_0^2} \quad (12)$$

From (12), the variation of φ in this narrow range produces very little effect on the first term and negligible effect on the second term. Hence not enough randomness is provided for efficient local search. The modified JSO applies another random generator to each of the two terms for more efficient exploitation. The new update equation for jumping on prey is given by:

$$\vec{x}_i(k+1) = \left(\vec{x}_i(k)\, tan(\alpha) - \frac{g\vec{x}_i^2(k)}{2V_0^2 cos^2(\alpha)}\right) * \mu \tag{13}$$

$$\alpha = \frac{\varphi\pi}{180}$$

where $\vec{x}_i(k+1)$ is the new position of *i*th search agent, $\vec{x}_i(k)$ is the current position of *i*th search agent and both φ and μ are randomly generated numbers in range (0, 1).

The solution procedure of the EJSO is similar to the standard JSO except for the modified equations for the global search and the jumping trajectory. The steps taken are given in the flowchart shown in *Fig. 4* [13].

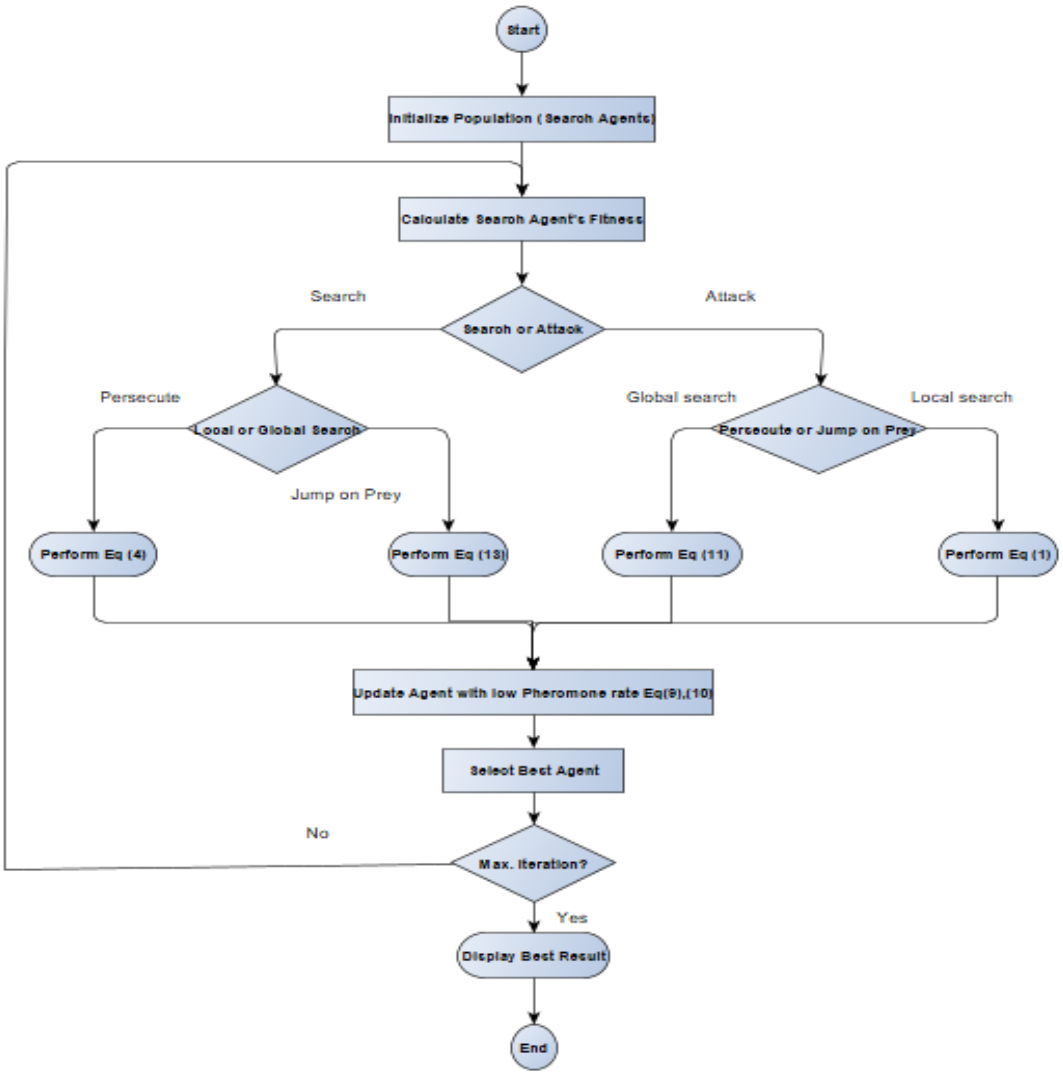

Fig. 4. Flow chart of EJOA

4. TESTING

This section presents the various computational experiments used to evaluate the performance of the proposed EJSO. The EJSO was tested on 17 standard benchmark optimization functions and welded beam design problem as an example of a real-world single objective bound constrained numerical optimization problem [8]. The results obtained were compared with the results of the standard JSO and five other recent state-of-the-art bioinspired algorithms from the literature.

4.1. Benchmark Optimization Functions

Details of the benchmark functions with varying levels of complexity are listed in Table 1. Dim indicates the dimension of the function.

Table 1. Benchmark functions

FCN	Function Name	Search Range	Dim	Optimum Value
F1	Sphere	[-100, 100]	10	0
F2	Schwefel 2.21	[-100, 100]	30	0
F3	Rotated Hyper-Ellipsoid	[65.536,65.536]	2	0
F4	Schwefel 2.22	[-100, 100]	30	0
F5	Rosenbrock	[-5, 10]	30	0
F6	Step Function	[-5.12, 5.12]	30	0
F7	Ackley	[-1,1]	30	0
F8	Beale	[-4.5,4.5]	2	0
F9	Happy cat	[-2,2]	30	0
F10	Matyas	[-10, 10]	2	0
F11	Powel	[-1,1]	50	0
F12	Salomon	[-100, 100]	50	0
F13	Colville	[-10,10]	4	0
F14	Griewank	[-600,600]	30	0
F15	Easom function	[-5,10]	30	0
F16	Sum of difference	[-1,1]	2	0
F17	Sum Square	[-10,10]	50	0

The following parameters were used for all algorithms:

Number of runs = 100

Population of search agents = 100

Maximum number of iterations = 500

Three of the algorithms require additional parameters. The algorithms and their extra parameters are given in Table 2.

Table 2. Additional parameter settings for MAO, GBO & HHO

Algorithms	**Parameters**	**Value**
	Crossover probability (*cop*)	0.5
MAO	Damage probability (*dp*)	0.5
	Regeneration probability (*rp*)	0.1
	Tournament size (*k*) Lamba value (*l*)	2, 0.5
GBO	βmin, βmax	0.2, 0.6
	pr	0.5
HHO	Harris Hawk Number	30
	E0 variable changes from -1 to 1 (Default)	

For each benchmark function, the optimum solution value, standard deviation, mean value and convergence curve were obtained for each of the seven algorithms.

The quality of the mean values obtained by each algorithm in all the 17 functions was further statistically determined using the Mean Absolute Error (MAE) given by:

$$MAE = \sum_{i=1}^{n} \frac{|O_i - P_i|}{n} \tag{14}$$

where O_i is the mean of the optimal values yielded by an algorithm for a test function *Fi*, P_i is the function optimal value and *n* is the number of the test functions.

4.2.Welded Beam Design Problem.

The main objective of this problem is to minimize the cost of manufacturing and to obtain best possible construction cost for the following constraint variables [13]: thickness of weld (x_1), height (x_2), length (x_3) and bar thickness (x_4). The mathematical formulation is as follows:

$\vec{x} = [x_1\ x_2\ x_3\ x_4]$

Minimize $f(\vec{x}) = 1.10471x_1^2x_2 + 0.04811x_3x_4(14.0 + x_2)$,

Subject to

$g_1(\vec{x}) = x_1 - x_4 \leq 0$
$g_2(\vec{x}) = \delta(\vec{x}) - \delta_{\max} \leq 0$
$g_3(\vec{x}) = P \leq P_c(\vec{x})$
$g_4(\vec{x}) = \tau_{max} \geq \tau(\vec{x})$
$g_5(\vec{x}) = \sigma(\vec{x}) - \sigma_{max} \leq 0$
Having bounds:
$0.125 \leq x_1 \leq 2$
$0.1 \leq x_2 x_3 \leq 10$
$0.1 \leq x_1, x_4 \leq 2$
Where,

$$\tau(\vec{x}) = \sqrt{(\tau')^2 + (\tau'')^2 + 2\tau'\tau''\frac{x_2}{2R}}$$

$$\tau' = \frac{P}{\sqrt{2}x_1x_2}, \tau'' = \frac{MR}{J}, M = P(L + \frac{x_2}{2})$$

$$R = \sqrt{\frac{x_2^2}{4} + \left(\frac{x_1 + x_3}{2}\right)^2}$$

$$J = 2\left\{\sqrt{2}x_1x_2\left[\frac{x_2^2}{12} + \frac{x_1 + x_3}{2}\right]\right\}$$

$$\sigma(\vec{x}) = \frac{6PL}{x_4x_3^3}$$

$L = 14in$, P=6000lb, E=30.10^6 psi, $\sigma_{max} = 30{,}000\ psi$,
$\tau_{max} = 13{,}600\ psi$, $\delta_{\max} = 0.25in$.

All experiments were carried out in MATLAB 2019a on a PC with Intel (R) Celeron (R) CPU N3050 @1.60GHz and a 4GB RAM memory on windows 10 OS.

5. RESULTS AND DISCUSSION

5.1. Results for Benchmark Functions

Comparison test results for the benchmark functions are presented in Tables 3 - 6. The convergence curves of the seven algorithms are compared for each test function in *Fig. 5*.

Table 3. Optimal Values.

FCN	EJSO	JSO	COOT	GBO	HGS	HHO	MAO
F1	**0.00x10^{00}**	3.96x10^{-152}	1.57x10^{-64}	8.17x10^{-199}	**0.00x10^{00}**	2.93x10^{-141}	3.87x10^{-01}
F2	1.78x10^{-181}	2.62x10^{-93}	1.39x10^{-29}	1.73x10^{-100}	**0.00x10^{00}**	3.44x10^{-72}	7.06x10^{-02}
F3	**0.00x10^{00}**	2.62x10^{-151}	9.78x10^{-30}	2.13x10^{-190}	**0.00x10^{00}**	2.77x10^{-118}	1.33x10^{+00}
F4	8.87x10^{-179}	5.57x10^{-94}	5.46x10^{-29}	2.68x10^{-99}	**0.00x10^{00}**	2.05x10^{-65}	6.27x10^{-02}

FCN	EJSO	JSO	COOT	GBO	HGS	HHO	MAO
F5	**0.00x10^{00}**	1.97x10^{-31}	1.76x10^{-14}	**0.00x10^{00}**	6.44x10^{-22}	**0.00x10^{00}**	4.34x10^{-01}
F6	**0.00x10^{00}**	**0.00x10^{00}**	5.91x10^{-27}	**0.00x10^{00}**	**0.00x10^{00}**	1.18x10^{-10}	3.93x10^{-01}
F7	**-8.88x10^{-16}**	-8.88x10^{-16}	6.22x10^{-15}	**-8.88x10^{-16}**	**-8.88x10^{-16}**	**-8.88x10^{-16}**	1.35x10^{+00}
F8	**0.00x10^{00}**	**0.00x10^{00}**	1.12x10^{-20}	0.00x10^{+00}	**0.00x10^{00}**	**0.00x10^{00}**	9.73x10^{-03}
F9	2.85x10^{-02}	2.50x10^{-01}	1.02x10^{-02}	6.58x10^{-03}	1.61x10^{-03}	**2.05x10^{-04}**	3.05x10^{-01}
F10	**0.00x10^{00}**	2.05x10^{-150}	8.26x10^{-67}	1.96x10^{-176}	**0.00x10^{00}**	8.88x10^{-155}	1.10x10^{-05}
F11	**0.00x10^{00}**	**0.00x10^{00}**	**0.00x10^{00}**	**0.00x10^{00}**	**0.00x10^{00}**	**0.00x10^{00}**	1.53x10^{-207}
F12	9.99x10^{-02}	1.20x10^{-90}	9.56x10^{-11}	6.77x10^{-59}	**0.00x10^{00}**	3.00x10^{-54}	1.50x10^{+01}
F13	**0.00x10^{00}**	1.09x10^{-11}	5.73x10^{-09}	**0.00x10^{00}**	3.62x10^{-06}	1.69x10^{-07}	1.49x10^{+01}
F14	**0.00x10^{00}**	**0.00x10^{00}**	**0.00x10^{00}**	**0.00x10^{00}**	**0.00x10^{00}**	**0.00x10^{00}**	1.83x10^{+00}
F15	6.46x10^{-191}	2.19x10^{-144}	6.73x10^{-48}	3.24x10^{-156}	**0.00x10^{00}**	8.36x10^{-121}	1.08x10^{+00}
F16	**0.00x10^{00}**	3.86x10^{-164}	1.09x10^{-43}	2.95x10^{-226}	6.07x10^{-260}	1.20x10^{-140}	4.20x10^{-05}
F17	6.46x10^{-191}	2.74x10^{-148}	2.49x10^{-45}	3.48x10^{-151}	**0.00x10^{00}**	1.28x10^{-118}	3.98x10^{+02}

Table 4. Mean Values.

FNC NO.	EJSO	JSO	COOT	GBO	HGS	HHO	MAO
F1	**8.42x10^{-06}**	1.07x10^{-02}	1.58x10^{-01}	1.15x10^{-02}	2.34x10^{-02}	9.48x10^{-03}	1.79x10^{+02}
F2	**2.81x10^{-04}**	7.32x10^{-04}	4.62x10^{-03}	1.22x10^{-03}	1.71x10^{-03}	5.80x10^{-04}	1.39x10^{+00}
F3	**1.62x10^{-05}**	1.42x10^{-02}	9.96x10^{-02}	1.87x10^{-02}	2.82x10^{-02}	1.39x10^{-02}	2.15x10^{+02}
F4	**1.78x10^{-04}**	7.28x10^{-03}	1.57x10^{-02}	9.88x10^{-03}	1.41x10^{-02}	4.90x10^{-03}	5.25x10^{+00}
F5	**2.52x10^{-03}**	1.30x10^{-01}	2.94x10^{-01}	1.00x10^{+00}	1.74x10^{-01}	9.29x10^{-02}	5.34x10^{+04}
F6	**8.95x10^{-06}**	6.47x10^{-03}	1.34x10^{-01}	1.10x10^{-02}	1.37x10^{-02}	6.81x10^{-03}	1.76x10^{+02}
F7	**7.74x10^{-04}**	2.03x10^{-02}	4.66x10^{-02}	1.49x10^{-02}	2.57x10^{-02}	1.09x10^{-02}	5.45x10^{+00}
F8	2.93x10^{-02}	1.75x10^{-03}	**1.50x10^{-03}**	5.35x10^{-04}	1.78x10^{-03}	1.75x10^{-03}	9.00x10^{+01}
F9	4.34x10^{-02}	2.91x10^{-01}	1.47x10^{-01}	4.46x10^{-02}	2.87x10^{-02}	**1.28x10^{-02}**	5.67x10^{-01}
F10	**3.39x10^{-07}**	3.44x10^{-05}	3.35x10^{-04}	2.09x10^{-05}	3.68x10^{-05}	1.78x10^{-05}	1.26x10^{-01}
F11	3.03x10^{-154}	8.39x10^{-135}	2.49x10^{-160}	**3.80x10^{-202}**	3.37x10^{-135}	3.36x10^{-135}	2.24x10^{-18}
F12	1.04x10^{-01}	**7.28x10^{-02}**	4.94x10^{-01}	1.08x10^{-01}	1.40x10^{-01}	1.25x10^{-01}	2.32x10^{+01}
F13	**4.24x10^{-01}**	1.77x10^{+00}	1.58x10^{+00}	6.02x10^{-01}	2.13x10^{+00}	1.57x10^{+00}	2.73x10^{+03}
F14	**9.99x10^{-05}**	3.66x10^{-02}	7.18x10^{-02}	3.01x10^{-02}	5.15x10^{-02}	4.44x10^{-02}	1.05x10^{+01}
F15	**3.46x10^{-03}**	4.78x10^{-02}	1.07x10^{-01}	2.10x10^{-02}	1.58x10^{-01}	6.44x10^{-02}	1.45x10^{+01}
F16	5.20x10^{-06}	1.46x10^{-07}	2.51x10^{-06}	1.15x10^{-07}	2.40x10-^{07}	**4.24x10^{-08}**	1.44x10^{-02}
F17	**3.46x10^{-03}**	1.77x10^{+01}	3.95x10^{+01}	7.80x10^{+00}	5.79x10^{+01}	2.38x10^{+01}	5.34x10^{+03}

Table 5. Standard Deviation

FNC N.	EJSO	JSO	COOT	GBO	HGS	HHO	MAO
F1	**1.32x10^{-04}**	2.13x10^{-01}	2.00x10^{+00}	2.12x10^{-01}	3.02x10^{-01}	2.11x10^{-01}	8.28x10^{+02}
F2	**3.98x10^{-03}**	1.22x10^{-02}	5.36x10^{-02}	1.39x10^{-02}	1.76x10^{-02}	1.14x10^{-02}	4.75x10^{+00}
F3	**2.96x10^{-04}**	2.80x10^{-01}	1.15x10^{+00}	2.99x10^{-01}	4.00x10^{-01}	2.80x10^{-01}	1.25x10^{+03}
F4	**2.31x10^{-03}**	1.13x10^{-01}	2.59x10^{-01}	1.35x10^{-01}	1.45x10^{-01}	9.62x10^{-02}	1.09x10^{+01}
F5	**5.33x10^{-02}**	2.17x10^{+00}	4.19x10^{+00}	1.13x10^{+00}	2.51x10^{+00}	1.97x10^{+00}	7.02x10^{+05}
F6	**1.16x10^{-04}**	1.25x10^{-01}	2.13x10^{+00}	1.45x10^{-01}	1.77x10^{-01}	1.24x10^{-01}	8.32x10^{+02}
F7	**1.14x10^{-02}**	2.54x10^{-01}	4.13x10^{-01}	1.71x10^{-01}	2.64x10^{-01}	1.60x10^{-01}	4.16x10^{+00}
F8	6.52x10^{-01}	3.76x10^{-02}	1.87x10^{-02}	**1.19x10^{-02}**	3.77x10^{-02}	3.77x10^{-02}	1.30x10^{+03}

FNC N.	EJSO	JSO	COOT	GBO	HGS	HHO	MAO
F9	$1.95x10^{-01}$	$6.63x10^{-02}$	$2.42x10^{-01}$	$8.22x10^{-02}$	$9.16x10^{-02}$	**$5.96x10^{-02}$**	$8.41x10^{-01}$
F10	**$4.05x10^{-06}$**	$5.44x10^{-04}$	$4.64x10^{-03}$	$4.04x10^{-04}$	$5.63x10^{-04}$	$3.99x10^{-04}$	$4.79x10^{-01}$
F11	$4.80x10^{-153}$	$1.19x10^{-133}$	**$0.00x10^{+00}$**	**$0.00x10^{+00}$**	$7.52x10^{-134}$	$7.50x10^{-134}$	$5.07x10^{-17}$
F12	**$2.73x10^{-02}$**	$1.49x10^{+00}$	$2.36x10^{+00}$	$5.50x10^{-01}$	$1.66x10^{+00}$	$1.68x10^{+00}$	$7.48x10^{+00}$
F13	**$3.46x10^{+00}$**	$3.32x10^{+01}$	$2.01x10^{+01}$	$7.55x10^{+00}$	$3.40x10^{+01}$	$3.31x10^{+01}$	$1.63x10^{+04}$
F14	**$2.05x10^{-03}$**	$7.47x10^{-01}$	$2.17x10^{-01}$	$1.81x10^{-01}$	$7.65x10^{-01}$	$7.61x10^{-01}$	$1.69x10^{+01}$
F15	**$6.46x10^{-02}$**	$1.07x10^{+00}$	$1.24x10^{+00}$	$3.95x10^{-01}$	$1.78x10^{+00}$	$1.12x10^{+00}$	$1.68x10^{+01}$
F16	$7.92x10^{-05}$	$1.67x10^{-06}$	$4.68x10^{-05}$	$1.38x10^{-06}$	$2.13x10^{-06}$	**$9.23x10^{-07}$**	$7.32x10^{-02}$
F17	**$6.46x10^{-02}$**	$3.95x10^{+02}$	$4.60x10^{+02}$	$1.18x10^{+02}$	$6.55x10^{+02}$	$4.13x10^{+02}$	$6.22x10^{+03}$

Table 6. Ranking of algorithms using MAE values

Algorithms	MAE	Rank
EJSO	$3.57x10^{-02}$	1
GBO	0.515906	2
JSO	1.187415	3
HHO	1.515363	4
COOT	2.508066854	5
HGS	3.482911	6
MAO	3655	7

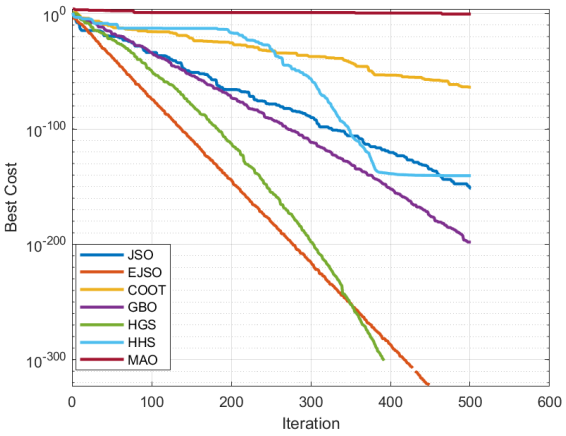

F1

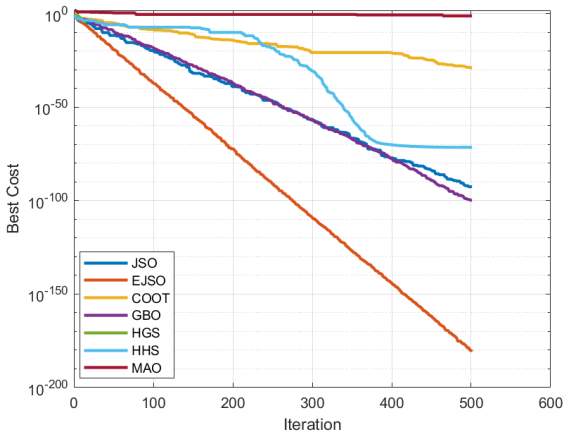

F2

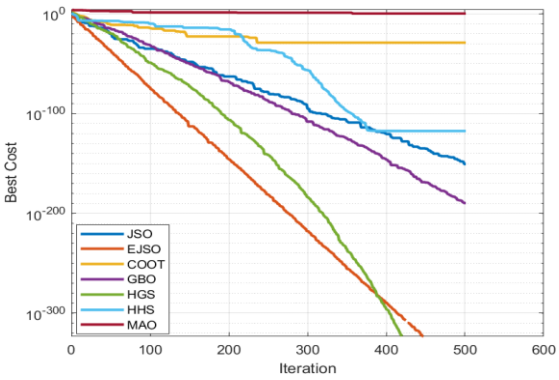

F3

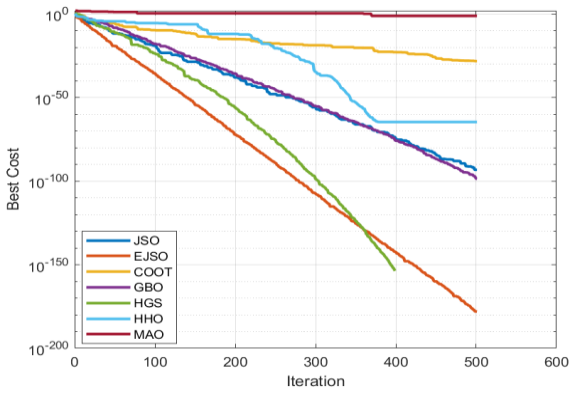

F4

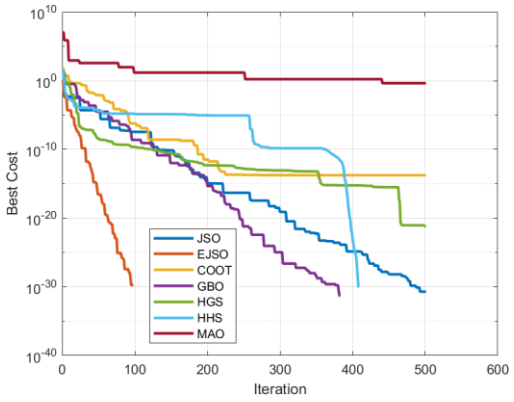

F5

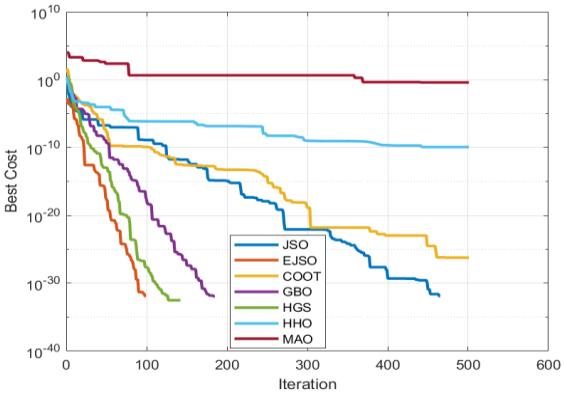

F6

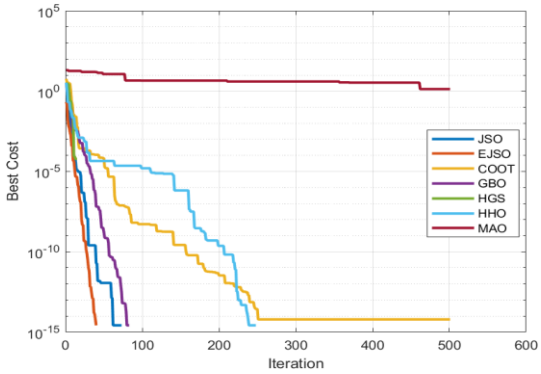

F7

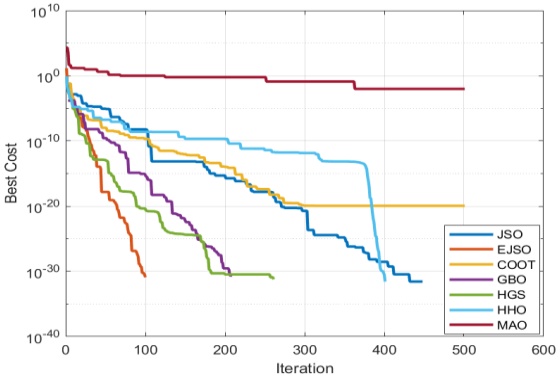

F8

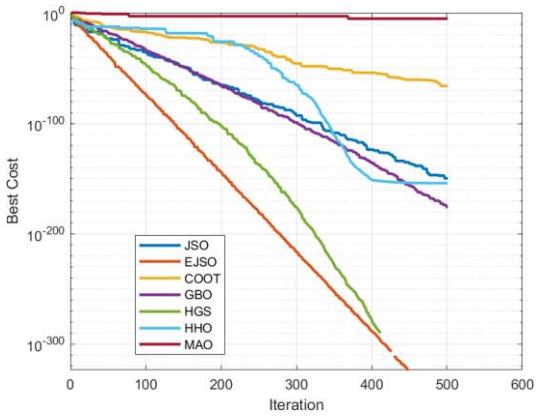

F9

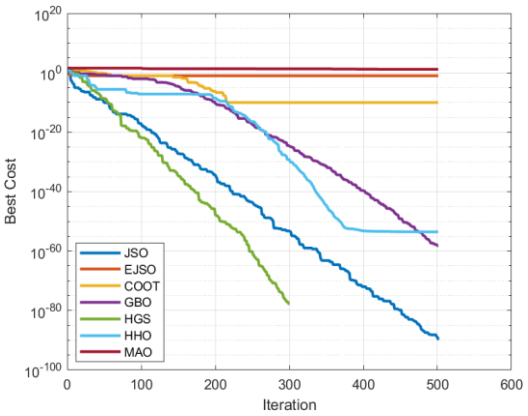

F10

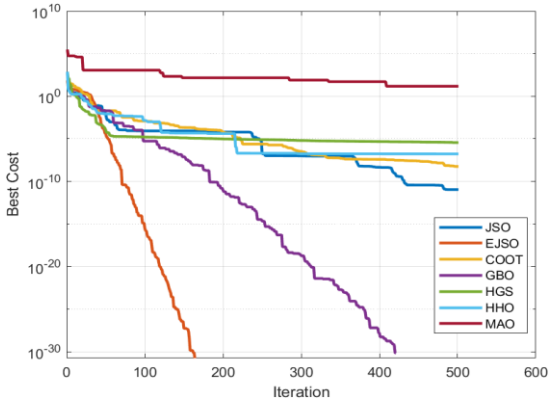

F11

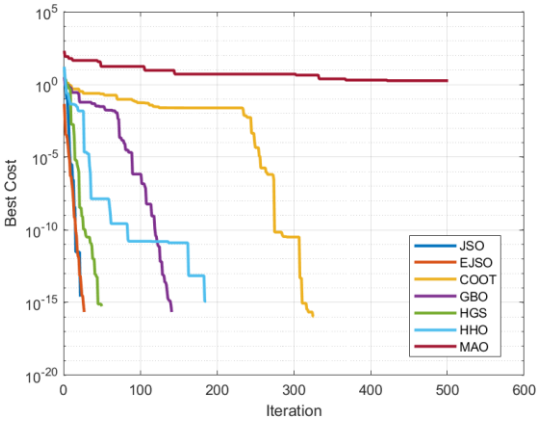

F12

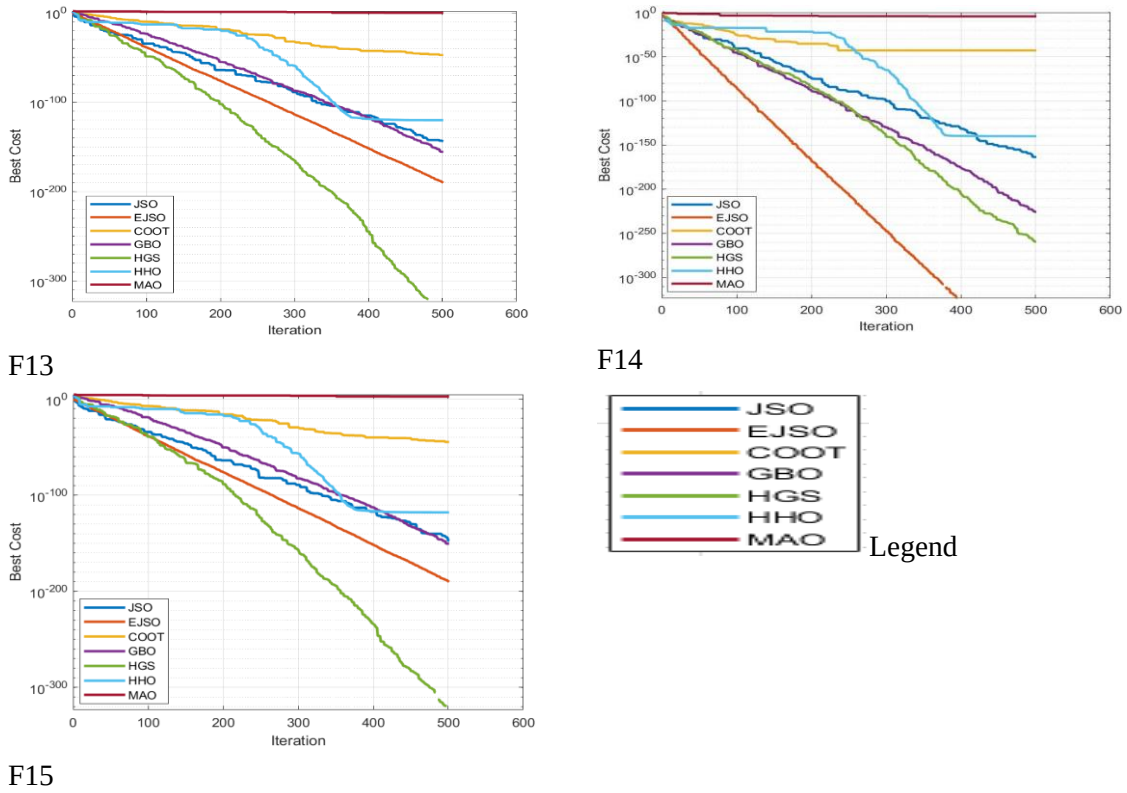

Fig. 5. Convergence Curves.

The results in Table 3 show that the EJSO and the standard JOA were equally efficient in finding five optimal or near optimal solutions (F6, F7, F8, F11, F14) and EJSO was more efficient in finding eleven optimal or near optimal solutions (F1- F5, F9, F10, F13, F15 – F17). EJSO was less efficient only in F12. Compared to all other algorithms, it produced superior or equivalent results in eleven functions. It ranked second to only HGS which yielded superior or equivalent results in fourteen functions.

The results in Tables 4 and 5 reveal that the average optimal or near optimal solutions and standard deviations yielded by the EJSO were better in fourteen functions compared to those of the standard JSO. Compared to all other algorithms, it produced the best average optimal or near optimal solutions in twelve of the benchmark functions and the least standard deviation in thirteen of them. Compared to the competitive HGS algorithm, the EJSO yielded better mean and standard deviations in fourteen functions. The results of the statistical analyses thus show the superiority of the EJSO over all the other algorithms.

In the performance evaluation based on MAE, the EJSO ranked first as shown in Table 6. This again confirms its superiority in terms of efficiency.

From the convergence curves in *Figure 6*, EJSO is seen to converge better and faster in nine functions, namely F2, F5-F9, F11, F12, and F14, and second better in functions F1, F3, F4, F13, F15. However, its convergence in F10 was very poor. It is also noticed that the HGO presented a competitive convergence against the EJSO. Overall, the EJSO converged better than the other algorithms.

5.2. Results for Welded Beam Design

Table 7 presents results obtained from solving the welded beam problem with EJSO and the six other algorithms. From the table, EJSO outperforms all the other six algorithms. However, the result produced by the standard JSO was very competitive.

Table 8. Best cost for welded Beam

Algorithm	Optimal Values for constraint Variables				Optimal Cost
	x_1	x_2	x_3	x_4	
EJSO	0.205729	3.470418	9.036613	0.205729	1.672485
JSO	0.168168	4.514591	9.036623	0.205729	1.677014
COOT	0.198085	3.484521	9.173125	0.399772	1.879285
GBO	0.205729	3.470488	9.036623	0.205729	1.724852
HGS	0.205721	3.470666	9.036627	0.205729	1.724863
HHO	0.177143	4.309538	9.036930	0.205728	1.787066
MAO	1.036525	4.075623	6.191996	1.164902	8.041845

6. CONCLUSION

This paper has presented an enhanced Jumping Spider algorithm. The modification was done on the Global search and the Jumping on prey phases of the standard algorithm. The algorithm was tested on 17 well-known benchmark functions and a real-world optimization problem and its performance compared with the standard JSO and five other well-known algorithms in the literature. The results showed an improved performance of the algorithm in terms of convergence rate, optimal solution values, stability and robustness over the standard JSO. It also provided superior statistical results when compared to the five other state-of-the-art algorithms (COOT, GBO, HGS, HHO and MAO) from the literature.

REFERENCES

[1] S. Bandaru and K. Deb, "Metaheuristic techniques," *Decis. Sci. Theory Pract.*, pp. 693–749, 2016, doi: 10.1201/9781315183176.

[2] K. Hussain, M. N. Mohd Salleh, S. Cheng, and Y. Shi, "Metaheuristic research: a comprehensive survey," *Artif. Intell. Rev.*, vol. 52, no. 4, pp. 2191–2233, 2019, doi: 10.1007/s10462-017-9605-z.

[3] L. Abualigah and A. Diabat, "A comprehensive survey of the Grasshopper optimization

algorithm: results, variants, and applications," *Neural Comput. Appl.*, vol. 32, no. 19, pp. 15533–15556, 2020, doi: 10.1007/s00521-020-04789-8.

[4] I. Naruei and F. Keynia, "A new optimization method based on COOT bird natural life model," *Expert Syst. Appl.*, vol. 183, no. February 2020, p. 115352, 2021, doi: 10.1016/j.eswa.2021.115352.

[5] Y. Villuendas-Rey, J. L. Velázquez-Rodríguez, M. D. Alanis-Tamez, M. A. Moreno-Ibarra, and C. Yáñez-Márquez, "Mexican axolotl optimization: A novel bioinspired heuristic," *Mathematics*, vol. 9, no. 7, pp. 1–20, 2021, doi: 10.3390/math9070781.

[6] I. Ahmadianfar, O. Bozorg-Haddad, and X. Chu, "Gradient-based optimizer: A new metaheuristic optimization algorithm," *Inf. Sci. (Ny).*, vol. 540, pp. 131–159, 2020, doi: 10.1016/j.ins.2020.06.037.

[7] Y. Yang, H. Chen, A. A. Heidari, and A. H. Gandomi, "Hunger games search: Visions, conception, implementation, deep analysis, perspectives, and towards performance shifts," *Expert Syst. Appl.*, vol. 177, no. March, p. 114864, 2021, doi: 10.1016/j.eswa.2021.114864.

[8] A. A. Heidari, S. Mirjalili, H. Faris, I. Aljarah, M. Mafarja, and H. Chen, "Harris hawks optimization: Algorithm and applications," *Futur. Gener. Comput. Syst.*, vol. 97, pp. 849–872, 2019, doi: 10.1016/j.future.2019.02.028.

[9] S. Mirjalili, J. Song Dong, A. Lewis, and A. S. Sadiq, *Particle swarm optimization: Theory, literature review, and application in airfoil design*, vol. 811. Springer International Publishing, 2020.

[10] H. Peraza-Vázquez, A. F. Peña-Delgado, G. Echavarría-Castillo, A. B. Morales-Cepeda, J. Velasco-Álvarez, and F. Ruiz-Perez, "A Bio-Inspired Method for Engineering Design Optimization Inspired by Dingoes Hunting Strategies," *Math. Probl. Eng.*, vol. 2021, 2021, doi: 10.1155/2021/9107547.

[11] M. Jamil and H. J. Zepernick, "Lévy Flights and Global Optimization," *Swarm Intell. Bio-Inspired Comput.*, pp. 49–72, 2013, doi: 10.1016/B978-0-12-405163-8.00003-X.

[12] X. Yang, S. Deb, and A. C. B. Behaviour, "Cuckoo Search via L ´ evy Flights," *Ieee*, pp. 210–214, 2009.

[13] H. Peraza-Vázquez, A. Peña-Delgado, P. Ranjan, C. Barde, A. Choubey, and A. B. Morales-Cepeda, "A bio-inspired method for mathematical optimization inspired by arachnida salticidade," *Mathematics*, vol. 10, no. 1, 2022, doi: 10.3390/math10010102.

MODIFIED INDIVIDUAL EXPERIENCE MAYFLY ALGORITHM

Nicholas Kwesi **PRAH II**, Emmanuel Assuming **FRIMPONG,** Elvis **TWUMASI**
Department of Electrical and Electronic Engineering, College of Engineering, Kwame Nkrumah University of Science and Technology, Kumasi, Ghana.
bravokwesi@gmail.com, eafrimpong.soe@knust.edu.gh, etwumasi.coe@knust.edu.gh.

Keywords: Optimization, Metaheuristics, Swarm Intelligence.

Abstract*: An algorithm that modifies the individual experience of mayflies in the mayfly algorithm (MA) to enhance its performance, is proposed. The proposed algorithm called the Modified Individual Experience Mayfly Algorithm (MIE-MA) calculates the experience of a mayfly by finding an average of the positions the mayfly has been to instead of just using the best position. A chaotic decreasing gravity coefficient is also employed to enhance the balance between the exploitation and exploration of the algorithm. The proposed algorithm was compared to the original MA, and two recent variants named, PGB-IMA and ModMA, on eight benchmark functions. The parameters used for comparison were Mean Absolute Error, Standard Deviation, and convergence rate. The results validate the superior performance of the MIE-MA over the other three algorithms. The MIE-MA yields better optimal values with minimal iterations.*

1. INTRODUCTION

Metaheuristic algorithms are a paradigm of computational intelligence helpful in solving complex problems. They offer advantages such as easy application to continuous and discrete problems, less complex mathematical computations, and efficient search for global optimum solutions [1]. Metaheuristic Algorithms are classified into single-solution and population-based algorithms [1, 2]. In single solution-based methods, a generated solution is improved continuously until a stopping criterion is met [2]. In population-based methods, a group of solutions is generated within a search space and is updated at each iteration to find an optimal solution [3]. The population-based techniques are divided into evolutionary algorithms and Swarm Intelligence optimization algorithms. Evolutionary Algorithms are

hinged on natural genetic evolution. Examples are differential evolution and genetic algorithm [3, 4]. Swarm Intelligence optimization algorithms (SIOA) are based on the social behavior of animal groups. SIOAs are flexible and adaptive to various problems and have strong global search ability and robust performance [5]. Examples are the mayfly algorithm, particle swarm optimization, whale optimization algorithm, and crow search algorithm [6-8].

MA is one of the very recent SIOAs, inspired by the movement and mating process of mayflies [7]. It is a promising algorithm that exhibits enhanced exploration and exploitation abilities. Researchers have employed MA in solving complex problems [10-12]. In [8], MA was used to solve a 2D path planning problem of agricultural unmanned aerial vehicles (UAVs). In [9], MA was used to solve an optimal power flow problem in regulated electricity markets. The algorithm has also been used to improve the Maximum Power Point Tracking (MPPT) for photovoltaic systems [10].

Even though the MA is quite effective in solving complex problems, it has drawbacks such as premature convergence and stagnation. There is, therefore, a need for contributions to address these problems. In [7], an improved version of the MA called PGB-IMA was introduced. Here, the global best is selected from the whole mayfly population (both males and females) to enhance the exploration abilities of the MA. This improvement was effective on unimodal functions. However, it was found to converge slower or get stuck at local optima points on multimodal functions. In [11], levy flight was used to enhance the exploration abilities of the mayflies in the MA. This method, however, causes a mayfly to fly out of a search space in smaller search spaces. In [8], researchers adopted the exponent decreasing inertia weight, the adaptive Cauchy method, and an enhanced crossover operator to enhance the balance between exploitation and exploration of the MA. This variant was named ModMA. Although the ModMA improves the convergence rate, it does not eliminate trapping at the local optimum. Thus, there is still a need to improve the MA to holistically address the entrapment problem in local optimum and premature convergence to enhance its performance.

This work, therefore, aims at addressing the aforementioned deficiencies of the MA. A modified version of the MA is presented. The modification focuses on the individual experience of the mayflies and thus is called Modified Individual Experience Mayfly Algorithm (MIE-MA). The MIE-MA modifies the experience of the mayflies to enhance the movement of the mayflies to improve the convergence rate and move the mayflies out of local optima entrapment. This is done by replacing the personal best (*pbest*) in the MA with personal experience (*Pexp*). *Pexp* is the mean of all the positions a mayfly has been to. This allows all the positions a mayfly has visited to contribute equally to its experience. This allows the mayflies to exploit their search spaces well to avoid premature stagnation and skipping of the optimal solution in their search space. Consequently, the approach leads to optimal solutions with minimal iterations. Furthermore, a chaotic decreasing gravity coefficient is adopted to aid in the balance between the exploration and exploitation of the algorithm.

This paper is organized as follows: The original MA is described in Section 2, Section 3 provides the modified individual experience and the chaotic decreasing gravity coefficient. The benchmark functions and the test parameters used for testing the algorithms are presented in Section 4. Results are presented and analyzed in Section 5. Section 6 concludes the paper.

2. MAYFLY ALGORITHM

The MA takes inspiration from the way mayflies fly and mate. It combines the major advantages of PSO [3], FA [12], and GA [4]. The MA is comprised of six phases [8].

2.1. Initialization

In this phase, sets of both male and female mayflies are generated at random. The current velocity and position of the *i*th mayfly are assigned as $v_i = (v_{i1}, v_{i2} \ldots, v_{in})$ and $x_i = (x_{i1}, x_{i2} \ldots, x_{in})$, respectively. Positions of the mayflies are modified based on their best ever position (*pbest*) position and the best position in the whole population (*gbest*).

2.2. Movement of male mayflies

The positions of male mayflies are updated based on the positions of mayflies around them and its past positions. $\boldsymbol{x_i^t}$ denotes the present position of the *i*th male mayfly at iteration *t*. In order to update the position of a particular mayfly, the velocity $\boldsymbol{v_i^{t+1}}$ is added to its current position. i.e.

$$x_i^{t+1} = x_i^t + v_i^{t+1} \tag{1}$$

The male mayfly's velocity update is obtained from:

$$v_{ij}^{t+1} = v_{ij}^t + a_1 e^{-vd_p^2}\left(pbest_{ij} - x_{ij}^t\right) + a_2 e^{-vd_g^2}(gbest_j - x_{ij}^t) \tag{1.1}$$

where:

v = visibility coefficient.

a_1 and a_2 = positive attraction constants.

$pbest_{ij}$ = Mayfly ith best position in dimension j.

d_p and d_g = Euclidean distances between mayfly *i* and its best position and between mayfly *i* and the best position, respectively.

g = gravity coefficient, can be a fixed number between 0 and 1, or can be expressed as:

$$g = g_{max} - \frac{g_{max} - g_{min}}{iter_{max}} \times iter \tag{2}$$

where,

$g_{max}\ and\ g_{min}$ = maximum and minimum values of g.

$iter$ = current iteration.

$iter_{max}$ = maximum no. of iterations.

The best position of the mayfly in iteration *t+1* is determined as:

$$pbest_i = \begin{cases} x_i^{t+1},\ if\ f(x_i^{t+1}) < f(pbest_i). \\ kept\ the\ same,\ otherwise. \end{cases} \tag{3}$$

The top-performing male mayflies continue to execute oscillatory movements at varying velocities. These velocities are determined by:

$$v_{ij}^{t+1} = v_{ij}^{t} + d * r, \tag{4}$$

d = nuptial dance coefficient

r = a random value in the range [-1, 1]

2.3. Movement of female mayflies.

Female mayflies move towards male mayflies. Their positions are updated by the following formula:

$$y_i^{t+1} = y_i^t + v_i^{t+1} \tag{5}$$

where:

y_i^{t+1}= female mayfly i's position in iteration t+1.

y_i^t = female mayfly i's position in iteration t.

v_i^{t+1} = female mayfly i's velocity for iteration t+1.

For minimization problems, female mayflies' velocity updates are calculated as:

$$v_{ij}^{t+1} = \begin{cases} g * v_{ij}^t + a_2 e^{-\beta r_d^2}\left(x_{ij}^t - y_{ij}^t\right),\ if\ f(y_i) > f(x_i). \\ g * v_{ij}^t + w * n,\ iff(y_i) \le f(x_i). \end{cases} \tag{6}$$

where,

v_{ij}^t and y_{ij}^t = The velocity and position of female mayfly *i* in dimension *j* during iteration *t*.

a_2 and β = constants which represent attraction and visibility, respectively.

r_d = Euclidean distance between female mayfly *i* and male mayfly *i*.

w= coefficient for random walk. Used when no attraction between male and female.

n= random number between −1 to 1.

2.4. Mating Phase

The crossover operator is used to represent this phase. Each mayfly pair produces two offspring. This is expressed as:

$$off1 = R \cdot m + (1-R) \cdot f \tag{7}$$

$$off2 = R \cdot f + (1-R) \cdot m \tag{8}$$

R = random value.
f and m= female and male respectively.

2.5. Mutation phase

This phase aims to enhance the exploitation abilities of the MA. This is done by mutating chosen offspring. This is expressed as:

$$offspring_n = offspring_n + \sigma N_n(0,1) \tag{9}$$

where,
σ and Nn= standard deviation and the standard normal distribution, respectively.

2.6. Reduction of Nuptial Dance and Random Walk

The random walk and nuptial dance are reduced through a geometric progression over the iterations in this phase. This is to aid the balance between exploration and exploitation of the MA. This is expressed as:

$$d_t = d_o \delta^t,\ 0 < \delta < 1 \tag{10}$$

$$fl_t = fl_o \delta^t,\ 0 < \delta < 1 \tag{11}$$

where, t = iteration and δ= a value between 0 and 1.

2.7. The process is summarized in the pseudocode below:

Objective function $f(x), x = (x_1, \ldots, x_d)^T$
Initialize the positions and velocities of the male mayfly and female mayfly population

Evaluate the solutions and find *gbest*

Do while iteration < maximum iterations

Update the velocities and solutions of both male and female mayflies

Assess the solutions

Sort and rank the mayflies

Mate the mayflies

Evaluate the resulting offspring

Randomly assign offspring to male and female categories

Substitute inferior solutions with superior solutions

Update the individual best (*pbest*) and global best (*gbest*) solutions

End while

Display Results

3. PROPOSED MODIFIED INDIVIDUAL EXPERIENCE MA

In the original MA, the position of each mayfly is adjusted according to its individual experience and the experience of its neighbors. The individual experience is represented as pbest which is the best position the mayfly ever visited. The deficiency with this approach is that mayflies which are averagely moving at a better rate than the gbest might not be given adequate opportunities to contribute to the global best. This approach may lead to a situation where the gbest is provided by mayflies stuck in a local optimum and hence may cause stagnation of the whole MA.

In this modification, the experience of the mayfly is represented as the mean of the positions the mayfly has been to in the search space. This provides a better representation of the experience and also provides a better picture of how the mayflies are approaching the global optimum and consequently provide the optimum value in the search space. This is formulated as:

$$P_{exp,i}^{t} = \frac{\sum_{t=1}^{iter} x_i^t}{iter} \tag{12}$$

where;

$P_{exp,i}^{t}$ = The experience of mayfly *i* at step *t*.

iter = Current iteration.

x_i^t = Position of mayfly *i* at step *t*.

Also, a chaotic random decreasing gravity coefficient strategy is adopted to enhance the balance between the exploration and exploitation abilities of the MA. This is motivated by a study in [13], where different weight strategies were applied to PSO to determine their influence. This is due to its ability to rough search and minute search alternately in all its

evolutionary processes [14]. A slightly modified version is used in this work and is formulated as:

$$g = (gmax - gmin) * \left(\frac{MaxIt - iter}{MaxIt}\right) + \text{gmin} * \text{z} \tag{13}$$
$$z = 4 * z * (1 - z)$$

where*: gmax* & *gmin* are the maximum and minimum inertia weights respectively and z = random number between 0 and 1.

3.1. The pseudocode of the proposed modification is shown below:

Objective function $f(x), x = (x_1, \ldots, x_d)^T$
Initialize the positions and velocities of the male and female mayfly population
Evaluate solutions and find gbest
Do while iteration<maximum iterations
    Update the velocities and solutions of both male and female mayflies
    Sort and rank the mayflies
    Mate the mayflies
    Evaluate the resulting offspring
    Randomly assign offspring to male and female categories
    Substitute inferior solutions with superior solutions
    Update mayfly experience, update pbest using modified formula in equation 12
    Update gbest
    Apply chaotic decreasing gravity coefficient in equation 13
End while
Display Results

4. TESTING OF THE PROPOSED MODIFICATION

The modified MA (MIE-MA) was tested on eight benchmark functions. The benchmark functions were obtained from [7]. The test results were compared to the original MA [7], the PGB-IMA version [7], and a modified MA named ModMA[8]. The benchmark functions were picked from the various types of benchmark functions i.e unimodal (1&2), multimodal (3&4), and fixed dimensions (5 & 6- Multimodal, 7 & 8- Unimodal) and thus provide varied levels of difficulty.

The details of the functions are shown below:

Table 1. Benchmark Functions

No.	Name	Search Range	Optimal Value	Dimensions	Error Limit
1	Sphere	[-10,10]	0	30	1.0E-05
2	Zakharov	[-5,10]	0	30	1.0E-05
3	Rastrigin	[-5.12,5.12]	0	2	1.0E-05
4	Ackley	[-1,1]	0	30	1.0E-05
5	Leon	[0,10]	0	2	1.0E-05
6	Colville	[-10,10]	0	4	1.0E-05
7	Beale	[-4.5,4.5]	0	2	1.0E-05
8	Michalewicz	[0,∏]	-9.6602	10	1.0E-05

The parameters used to compare the algorithms are shown below. The same was used in [7].

Number of iterations = 2000.

Number of runs = 50.

Male Population = 20.

Female Population = 20.

gmax=0.9, *gmin*=0.2.

$a_1 = 1, a_2 = 1.5, \beta$ = 2, *d* = 0.1, *fl* = 0.1, *g* = 0.8, $\delta = 0.77$

All four algorithms were run on the same computer, an Intel® Core™ i7-7500U with CPU @ 2.70 GHz 2.90GHz and 12GB RAM.

The comparative analysis parameters used were the Mean Absolute Error (MAE) and the Standard Deviation (SD). These were calculated as.

$$MAE = \frac{1}{S}\sum_{i=1}^{S} |X_{oi} - X_i| \tag{13}$$

where: *S* is the number of cost samples, X_{oi} is the benchmark value of the test function and X_i is the computed optimum value.

$$SD = \sqrt{\frac{\sum(X_i - \mu)^2}{S}} \tag{14}$$

μ is the mean of the total number of cost samples.

5 RESULTS AND DISCUSSIONS

5.1. Mean absolute error and standard deviation

Table 1 below shows the MAEs and the Standard Deviations of the optimal values of the MA, PGB-IMA, ModMA, and MIE-MA on the eight test functions. The MIE-MA achieved

zero MAEs on five of eight test functions (Sphere, Rastrigin, Leon, Colville, and Beale), compared to ModMA's two, MA and PGB-IMA's one. Compared to the benchmark error limit of 1E-05, MIE-MA achieved lower values for 7 of eight test functions.

The MIE-MA achieved zero SDs in 7 of eight test functions compared to ModMA's two, MA and PGB-IMA's one. Hence, the MIE-MA had the overall best performance.

Table 2. MAEs and SDs of the algorithms on the test functions

Function	Algorithm	MAE	SD
Sphere	MA	4.87967E-20	1.08699E-19
	PGB-IMA	4.6517E-20	1.10929E-19
	ModMA	7.59804E-34	1.06227E-34
	MIE-MA	**0**	**0**
Zakharov	MA	0.08919371	0.636970303
	PGB-IMA	6.76556E-10	4.6853E-09
	ModMA	7.7838E-16	2.92148E-17
	MIE-MA	**4.0552E-223**	**0**
Rastrigin	MA	2.38967	1.61645
	PGB-IMA	2.45849	2.39099
	ModMA	1.19371E-12	3.80069E-14
	MIE-MA	**0**	**0**
Ackley	MA	6.06933E-11	1.20174E-10
	PGB-IMA	8.81819E-11	1.10305E-10
	ModMA	8.89955E-13	4.28014E-15
	MIE-MA	**8.70763E-16**	**0**
Leon	MA	0	0
	PGB-IMA	0	0
	ModMA	0	0
	MIE-MA	0	0
Colville	MA	2.46273E-30	4.2634E-30
	PGB-IMA	2.23259E-30	3.91469E-30
	ModMA	7.03319E-29	3.95904E-30
	MIE-MA	**0**	**0**
Beale	MA	2.989E-02	1.494E-01
	PGB-IMA	7.471E-02	2.289E-01
	ModMA	0	0
	MIE-MA	0	0
Michalewicz	MA	0.1390	1.567E-01
	PGB-IMA	0.1065	1.161E-01
	ModMA	0.5407	1.371E-01
	MIE-MA	**9.414E-02**	**1.115E-01**

5.2. Optimum Values

Table 2 compares the optimum values of the four algorithms to the benchmark optimum values on the test functions. The values in (brackets) indicate the iteration number on which zero was achieved. MIE-MA achieved benchmark optimum values in six of eight functions (Sphere, Rastrigin, Leon, Beale, Colville, and Michalewicz), compared to modMA's four, PGB-IMA and MA's two. This is a testament to the superior performance of the MIE-MA to the other three algorithms. MIE-MA also achieved better optimum values in five of eight functions (Sphere, Zakharov, Rastrigin, Ackley, and Michalewicz) compared to the other three algorithms. The table, therefore confirms the overall superior performance of the MIE-MA.

Table 3. Comparison of optimum values

No.	Function	Benchmark Value	MA	PGB-IMA	ModMA	MIE-MA
1	Sphere	0	1.93924E-23	7.01756E-25	2.62277E-37	**0**
2	Zakharov	0	2.81062E-11	6.66323E-17	2.7536E-18	**3.0885E-296**
3	Rastrigin	0	2.9849	1.9899	0(250)	**0(50)**
4	Ackley	0	3.39258E-11	3.09982E-10	2.22045E-14	**8.88178E-16**
5	Leon	0	0(98)	**0(92)**	0(255)	0(264)
6	Beale	0	0(58)	**0(55)**	0(225)	0(229)
7	Colville	0	1.91471E-29	4.43734E-30	**0(253)**	0(268)
8	Michalewicz	-9.6602	-8.9052	-9.4513	-9.4684	**-9.6602**

5.3. Convergence Rate

Figures 1 to *8* show the convergence curves of the four algorithms for the eight test functions. It can be observed that MIE-MA has better convergence rates for five of eight test functions (Sphere, Zakharov, Rastrigin & Ackley). For test functions Leon and Beale, PGB-IMA had the best convergence rate. ModMA had the best convergence rate for the Colville test

function. Even though MIE-MA did not achieve the best convergence rate for Leon, Beale, and Colville, optimum values were still achieved before the 300th iteration.

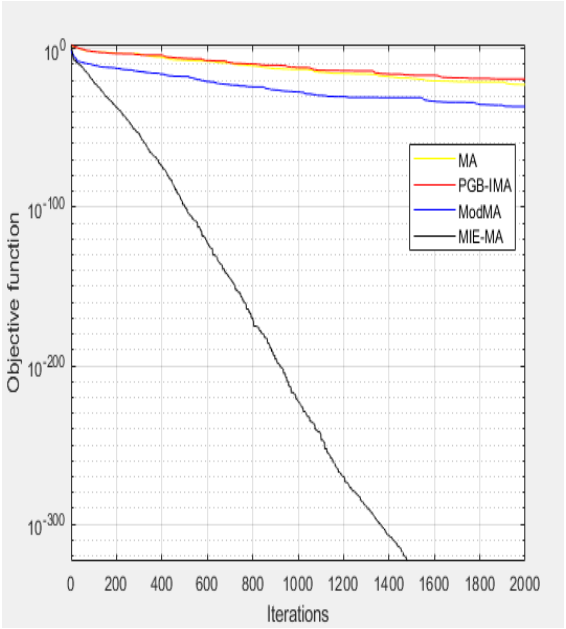

Fig. 1. Convergence Curve for Sphere

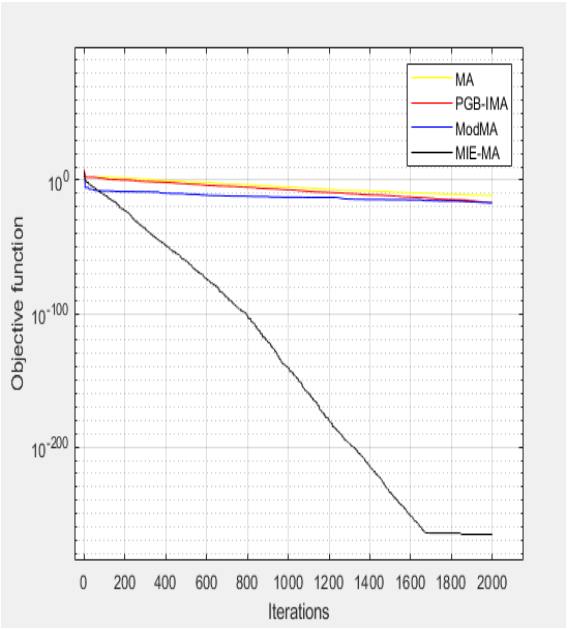

Fig. 2. Convergence Curve for Zakharov

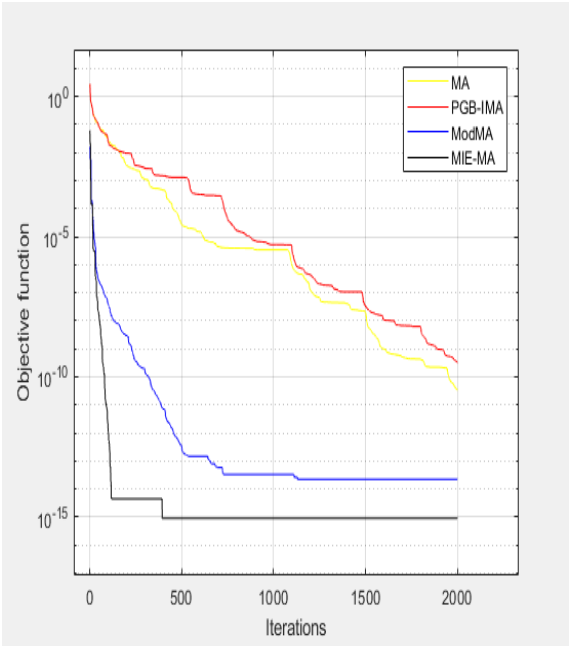

Fig. 3. Convergence Curve for Ackley

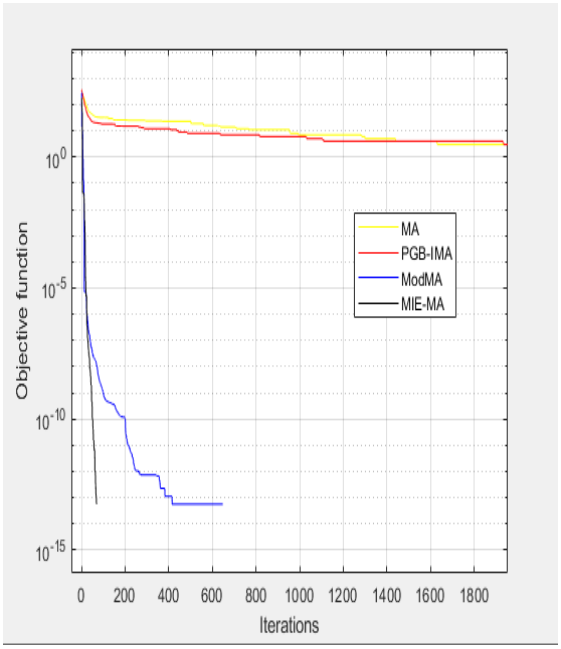

Fig. 4. Convergence Curve for Rastrigin

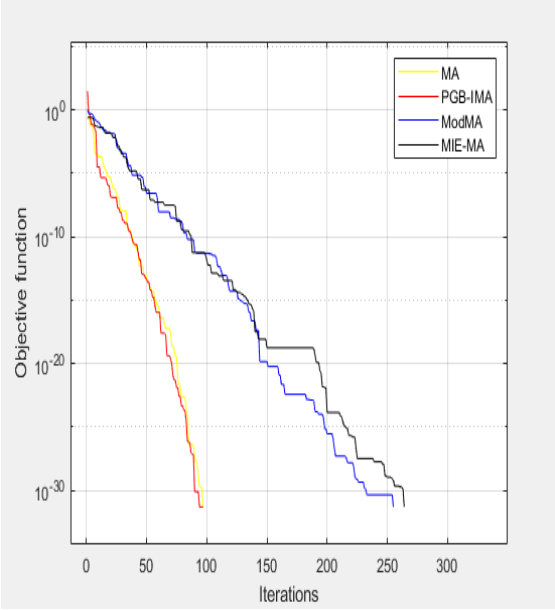

Fig.5. Convergence Curve for Leon

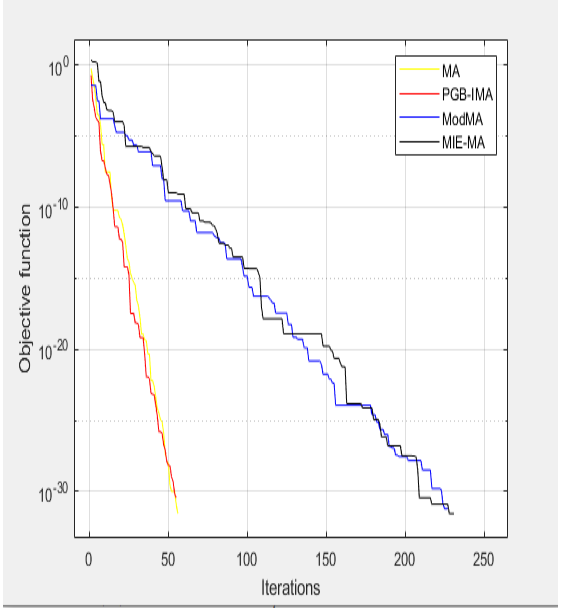

Fig. 6. Convergence Curve for Beale

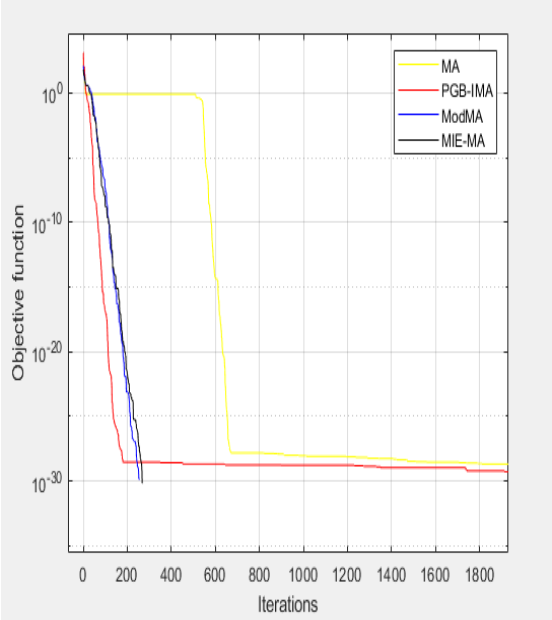

Fig. 7. Convergence Curve for Colville

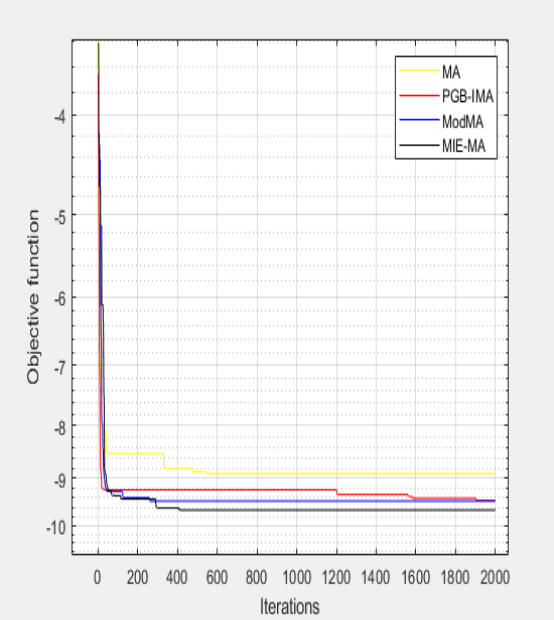

Fig. 8. Convergence Curve for Michalewicz

6. CONCLUSION

An improved mayfly algorithm called Modified Individual Experience Mayfly Algorithm (MIE-MA) has been made. This algorithm modifies the individual experience of each mayfly and also enhances the balance between exploitation and exploration. The MIE-MA achieved benchmark optimum values in six of eight test functions and also outperformed two other improvements in five out of eight functions in terms of convergence rate. The MIE-

MA also had the best MAE and SD in all eight test functions compared to the other two improvements. The results also indicated the ability of the MIE-MA to avoid local Stagnation.

REFERENCES

[1] Z. Beheshti and N. Branch, *A Review of Population-based Meta-Heuristic Algorithm*, International Journal of Advances in Soft Computing and its Applications, 5(1), pp. 1-35, 2013.

[2] J. Andres, M. Perez, N. Mladenovic, B. M. Batista, and I. J. Garcia, *Chapter 4 Variable Neighbourhood Search*, January, pp. 0–17, 2006, doi: 10.1007/0-387-33416-5.

[3] C. Wang and W. Song, *A modified particle swarm optimization algorithm based on velocity updating mechanism*, *Ain Shams Eng. J.*, vol. 10, no. 4, pp. 847–866, 2019, doi: 10.1016/j.asej.2019.02.006.

[4] D. J. Murray-Smith, *Experimental modelling: system identification, parameter estimation and model optimisation techniques*, *Model. Simul. Integr. Syst. Eng.*, pp. 165–214, 2012, doi: 10.1533/9780857096050.165.

[5] A. Banerjee, I. Nath, and B. Data, *Impacts of metaheuristic and swarm in- telligence approach in optimization Bio-Inspired Computation for Solving the Optimal Coverage Problem in Wireless Sensor Networks*, 2022.

[6] A. Askarzadeh, *A novel metaheuristic method for solving constrained engineering optimization problems: Crow search algorithm*, *Comput. Struct.*, vol. 169, pp. 1–12, 2016, doi: 10.1016/j.compstruc.2016.03.001.

[7] K. Zervoudakis and S. Tsafarakis, *A mayfly optimization algorithm*, *Comput. Ind. Eng.*, vol. 145, no. September 2019, p. 106559, 2020, doi: 10.1016/j.cie.2020.106559.

[8] X. Wang, J. Pan, Q. Yang, L. Kong, V. Snášel, and S. Chu, *Modified Mayfly Algorithm for UAV Path Planning*, pp. 1–21, 2022.

[9] V. B. K, S. Ramesh, P. Chandrasekar, K. Karunanithi, and A. Raja, *An improved mayfly algorithm based optimal power flow solution for regulated electric power network*, vol. 9, no. 92, pp. 979–995, 2022.

[10] S. Mo, Q. Ye, K. Jiang, X. Mo, and G. Shen, *An improved MPPT method for photovoltaic systems based on mayfly optimization algorithm*, *Energy Reports*, vol. 8, pp. 141–150, 2022, doi: 10.1016/j.egyr.2022.02.160.

[11] K. Nagarajan, A. Rajagopalan, S. Angalaeswari, L. Natrayan, and W. D. Mammo, *Combined Economic Emission Dispatch of Microgrid with the Incorporation of Renewable Energy Sources Using Improved Mayfly Optimization Algorithm*, vol. 2022, 2022.

[12] H. S. Chuah, L. P. Wong, and F. H. Hassan, *Swap-based discrete firefly algorithm for traveling salesman problem*, *Lect. Notes Comput. Sci. (including Subser. Lect. Notes Artif. Intell. Lect. Notes Bioinformatics)*, vol. 10607 LNAI, no. 2019, pp. 409–425, 2017.

[13] A. Rathore and H. Sharma, *Review on inertia weight strategies for particle swarm optimization*, *Adv. Intell. Syst. Comput.*, vol. 547, no. April, pp. 76–86, 2017.

[14] Y. Feng, G. F. Teng, A. X. Wang, and Y. M. Yao, *Chaotic inertia weight in particle swarm optimization*, *Second Int. Conf. Innov. Comput. Inf. Control. ICICIC 2007*, pp. 7–10, 2007.

OPTIMAL TUNING OF PI-CONTROLLER OF SHUNT ACTIVE POWER FILTER FOR HARMONICS MITIGATION USING ENHANCED JUMPING SPIDER ALGORITHM

Betrand N. **ATANGA**, Francis B. **EFFAH,** Daniel **KWEGYIR,** Philip Y. **OKYERE**
Kwame Nkrumah University of Science and Technology, Kumasi, Ghana
atangabertrand@gmail.com, fbeffah74@gmail.com

Keywords: shunt active power filter, PI-controller, harmonics mitigation, p-q theory

Abstract*: The increasing use of power electronic devices has resulted in harmonics that may cause in power systems overheating of equipment, poor power factor and voltage distortion. Shunt active power filter (SAPF) provides the most useful means for harmonics mitigation in power systems. In a certain number of SAPFs, the dc link capacitor voltage is regulated by means of a PI controller. This paper proposes a variant of a population based Jumping Spider Algorithm for optimal tuning of the PI controller to enhance the performance of the active filter. The SAPF considered in this paper uses the p-q theory to extract its reference current and the hysteresis current control to produce the triggering signals for the controlled switching devices of its inverter. The overall SAPF is developed and validated using MATLAB/Simulink tool under two different nonlinear loading conditions. The results obtained by simulation show that the SAPF with the proposed PI controller effectively controls the dc-link capacitor voltage and mitigates current harmonics.*

1. INTRODUCTION

Nowadays, there is an increased use of nonlinear loads such as computers, microwave oven, adjustable electric drives and arc furnaces in both domestic and industrial applications. These nonlinear loads give rise to current harmonics which cause power losses, overheating of equipment, and premature damage to motors, cables, transformers and sensitive equipment [1]. The Shunt Active Power Filter (SAPF) is preferred for reducing harmonics, compensating

for reactive power and improving power factor. The widely used SAPF consists of voltage fed or voltage source inverter (VSI) and its controller. The controller performs four main control actions [2], namely the extraction of harmonic currents or generation of reference current, control of dc link capacitor voltage, current control and synchronization. In some controllers, synchronization action is not explicitly required. The efficient performance of SAPF largely depends on the effectiveness of its control techniques [3].

The contribution of this paper is in the area of dc-link capacitor voltage control. The conduction and switching losses in the VSI cause a drop in the value of the capacitor voltage which then adversely affects the compensation performance of the active power filter [4]. Therefore, the capacitor voltage is regulated to keep it constant. The most common approach to regulate the capacitor voltage is the use of PI controller [5]. Conventional PI controller may not give optimum solution, because they require precise linear models. Again, the PI controller underperforms in the presence of non-linear loads, parameter variation, and disturbance [6]

Recently, researchers have used metaheuristic algorithms-based optimization techniques such as PSO [7], Ant Colony (ACO) [8], Genetic Algorithm (GA) [9], Bacteria Foraging [10], artificial bee colony (ABC) [11], to find the optimum gains of the PI controller of SAPF. None of these techniques seems to have yielded optimal parameters for the PI controller [12] and as one particular meta-heuristic algorithm is not capable of producing good results in all fields, researchers continue to try with new ones. This paper presents a new metaheuristic algorithm known as Enhanced Jumping Spider Algorithm (EJSA) for finding the optimum gains of the PI controller of the SAPF. The paper is organized as follows, section 2 – Theoretical background, section 3 – Implementation, section 4 – Results and discussions, and section 5 – Conclusion.

2. THEORITICAL BACKGROUND

2.1. SAPF Configuration and operation

A shunt active power filter has two main components, namely the power component and the control component. The power component consists of a VSI, an energy storage dc link capacitor, which maintains DC voltage at the VSI input, and an inductor which connects the VSI to the power system and acts as a filter. The function of the power component is to inject the needed mitigating current.

The SAPF works as follows. The power system's current in the absence of the filter at the point of common coupling (PCC) can be expressed as:

$$i_S = i_L = i_{1L} + i_H \tag{1}$$

where i_s = supply current, i_L = load current, and i_{1L} = fundamental component of the load current and i_H = harmonics present in the load current.

A SAPF connected to the PCC introduces these additional currents: the compensating current i_C injected by the SAPF which is equal and opposite in phase to i_H and then the dc link current i_{dc} drawn by the SAPF to account for the losses occurring in its switching devices and to keep the dc link capacitor voltage constant. The source current then becomes:

$$i_S = i_L = [i_{1L} + i_H] - i_C + i_{dc} \tag{2}$$

Harmonics mitigation current is obtained through the dc link capacitor voltage. By maintaining this voltage at a preset level, the compensation current becomes inversely identical to the harmonic component of the non-linear loads, thereby cancelling out each other. The source then supplies sinusoidal current having the fundamental frequency [2]. Equation (2) now becomes:

$$i_S = i_{1L} + i_{dc} \tag{3}$$

The SAPF controller continuously monitors the harmonics in the source current, which varies with time and then commands the power circuit to inject the necessary mitigating current.

2.2. Harmonic extraction algorithm

Harmonic extraction algorithm generates a reference current from the distorted load current. It is considered to be the most important control action [13]. The existing techniques that can be used to generate the reference current are many. The p-q theory, one of the most widely used time-domain techniques, is used in this work. These techniques require simple and less calculations and therefore, reduce the control process time. It does not require synchronization algorithm such as phase-lock loop technique, which involves complex calculations [2]. The p-q theory uses Clark transformation to convert currents and voltages from abc frame representation to 0αβ frame representation as follows:

$$\begin{bmatrix} i_0 \\ i_\alpha \\ i_\beta \end{bmatrix} = \sqrt{\frac{2}{3}} \cdot \begin{bmatrix} 1/\sqrt{2} & 1/\sqrt{2} & 1/\sqrt{2} \\ 1 & -1/2 & -1/2 \\ 0 & \sqrt{3}/2 & \sqrt{3}/2 \end{bmatrix} \cdot \begin{bmatrix} i_a \\ i_b \\ i_c \end{bmatrix} \tag{4}$$

$$\begin{bmatrix} v_0 \\ v_\alpha \\ v_\beta \end{bmatrix} = \sqrt{\frac{2}{3}} . \begin{bmatrix} \frac{1}{\sqrt{2}} & \frac{1}{\sqrt{2}} & \frac{1}{\sqrt{2}} \\ 1 & -\frac{1}{2} & -\frac{1}{2} \\ 0 & \frac{\sqrt{3}}{2} & \frac{\sqrt{3}}{2} \end{bmatrix} . \begin{bmatrix} v_a \\ v_b \\ v_c \end{bmatrix} \quad (5)$$

where i_a, i_b, and i_c are three-phase currents and v_a, v_b, and v_c are three-phase voltages in abc frame, and i_0, i_α and i_β are three-phase currents and v_0, v_α, and v_β are three-phase voltages in 0αβ frame.

For a three-phase, three-wire supply system considered in this paper, the zero-sequence component is absent. The instantaneous complex power *s* in the 0αβ frame is given by:

$$S = p + jq = v_{\alpha\beta} i^*_{\alpha\beta} = \left(v_\alpha - jv_\beta\right)\left(i_\alpha + ji_\beta\right) = \left(v_\alpha i_\alpha + v_\beta i_\beta\right) + j(v_\alpha i_\beta - v_\beta i_\alpha) \quad (6)$$

where p = instantaneous active power and q = instantaneous reactive power. The symbol "$*$ " denotes conjugate.

The p and q can be restated in the matrix form as follows:

$$\begin{bmatrix} p \\ q \end{bmatrix} = \begin{bmatrix} v_\alpha & v_\beta \\ -v_\beta & v_\alpha \end{bmatrix} . \begin{bmatrix} i_\alpha \\ i_\beta \end{bmatrix} \quad (7)$$

where nonlinear loads are present, p can be expressed as the sum of AC and DC components as follows:

$$p = \bar{p} + \tilde{p} \quad (8)$$

The component $\bar{p}$ is the DC component or average of p. It represents the power due to the fundamental voltages and currents and corresponds to the power drawn by the load from the source. The component $\tilde{p}$ is the AC component of p and represents the energy that flows to and from the load and the source. The harmonic reference current is calculated from $\tilde{p}$ and q after $\bar{p}$ has been extracted by a low pass filter.

If the power absorbed by the SAPF to account for losses in the switching devices to keep the capacitor voltage constant is denoted by $\tilde{P}_{loss}$ then the ac component of the instantaneous real power is calculated as follows:

$$\tilde{p} = P - \bar{p} - \tilde{P}_{loss} \quad (9)$$

The reference supply currents in αβ-frame (i^*_α, i^*_β) are then obtained by (10) and are further transformed to the *abc*-frame (i^*_a, i^*_b, i^*_c) through the inverse Clarke's transformation by (11).

$$\begin{bmatrix} i_\alpha^* \\ i_\beta^* \end{bmatrix} = \frac{1}{V_\alpha^2+V_\beta^2} \cdot \begin{bmatrix} v_\alpha & -v_\beta \\ v_\beta & v_\alpha \end{bmatrix} \cdot \begin{bmatrix} \tilde{p} \\ Q \end{bmatrix} \quad (10)$$

$$\begin{bmatrix} i_a^* \\ i_b^* \\ i_c^* \end{bmatrix} = \sqrt{\frac{2}{3}} \cdot \begin{bmatrix} 1 & 0 \\ -1/2 & \sqrt{3}/2 \\ -1/2 & -\sqrt{3}/2 \end{bmatrix} \cdot \begin{bmatrix} i_\alpha^* \\ i_\beta^* \end{bmatrix} \quad (11)$$

Figure 1 is a block diagram showing how reference current is generated using the p-q theory [14].

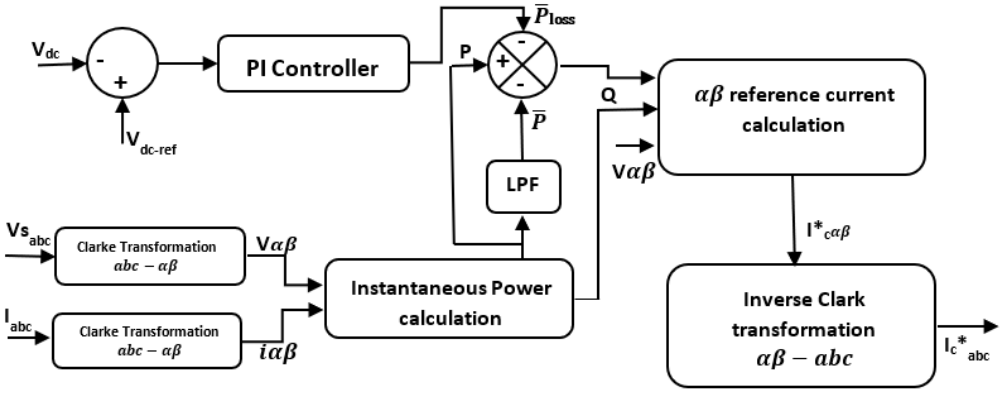

Fig. 1. Block diagram of reference current generation by p-q theory

2.3. Hysteresis Current Control Technique

The hysteresis current control technique is employed to produce the VSI triggering signals in such a way that its output current will have a wave shape identical but opposite in phase to that of the reference current. This paper uses the hysteresis current control technique which is the most widely used technique because of its fast response, accuracy, assured stability and easy implementation [15]. In this technique, the current produced by the inverter I_{fabc} is kept in a hysteresis band around the reference current I_{rabc}. The controller compares the two currents and, based on the error, outputs appropriate switching pulses to the VSI so that the filter current I_{fabc} is maintained inside a hysteresis band [16].

2.4. Algorithm for Regulating dc link Capacitor Voltage

In SAPF, it is important to keep the DC side of the voltage fed inverter constant by controlling the capacitor voltage. Ideally, the capacitor voltage should remain constant and the filter should not draw active power from the power system. This is, however, not the case because conduction and switching losses occur in the VSI during its operation [2]. Most SAPFs use a PI controller to regulate the capacitor voltage because it is simple to implement. The

measured capacitor voltage $v_{dc}$and the desired reference voltage V_{dc_ref} are compared and the corresponding error $e(t)$ is used to feed the PI controller. The PI controller output current is given by:

$$i_{dc} = K_p e(t) + K_i \int_0^t e(t)dt \tag{12}$$

where $e(t)$, the dc-link capacitor voltage error, is defined as

$$e(t) = V_{dc\_ref} - V_{dc} \tag{13}$$

with V_{dc}= the measured capacitor voltage and V_{dc_ref}= the reference capacitor voltage.

This current is used to adjust the reference current so that the right amount of real power will be absorbed by the filter to account for its conduction and switching losses [2].

This paper uses EJSOA to obtain the optimum gain parameters of the PI controller with its fitness or objective function defined as the integral time absolute error (ITAE). The ITAE performance index, the preferred criterion when designing this controller [17], is given by

$$J = \int_0^T t\,|e(t)|dt \tag{14}$$

2.4.1. Enhanced Jumping Spider Optimization Algorithm (EJSOA)

EJSO is a novel and simple meta-heuristic algorithm which mimics the hunting strategies of a jumping spider. A random population of spiders is initially produced to catch a prey in a multidimensional space. The spiders are deemed to use three hunting strategies, namely search for prey, consisting of local search and global search, attack by persecution and attack by jumping on prey[18]. The local search is described by the equation:

$$\vec{x}_i(k+1) = \vec{x}_{best}(k) + walk\left(\frac{1}{2} - \varepsilon\right) \tag{15}$$
$$i = 1, 2, 3, \dots, n.$$

where $\vec{x}_i(k+1)$ = the *i*th spider new position, $\vec{x}_{best}(k)$ = best location of spiders from previous iteration, $walk$ = a uniformly distributed random number generated in the interval [-2, 2] and ε = a randomly generated number in the interval [0,1].

The Lévy flight is applied for the global search. It is given by:

$$\vec{x}_i(k+1) = \vec{x}_{best}(k) + \gamma . L_\alpha(S) \tag{16}$$

where $\vec{x}_i(k+1)$ = the *i*th spider new position and γ ($\gamma > 0$) = the step size, $L_\alpha(S)$ gives a random walk with a random step length *S*. The search ability is most affected by the value of α [19]. A value of 1.5 is usually used.

Attack by persecution represents the situation where a spider is not close enough to the prey and it has to crawl close to the prey before it jumps on it. This walk is represented by:

$$\vec{x}_i(k+1) = \frac{1}{2}\left(\vec{x}_i(k) - \vec{x}_r(k)\right) \tag{17}$$

where $\vec{x}_i(k+1)$ = the *i*th spider new position, $\vec{x}_i(k)$ = the *i*th spider position in the preceding iteration, and $\vec{x}_r(k)$ = the position of spider r ($r \neq i$) randomly selected from the preceding iteration.

In the case of attack by jumping on prey, the spider is close to the prey so it jumps on it. The jump is modelled by:

$$\vec{x}_i(k+1) = \left(\vec{x}_i(k)\, tan(\alpha) - \frac{g\vec{x}_i^2(k)}{2V_0^2 cos^2(\alpha)}\right) * \mu \tag{18.a}$$

$$\alpha = \frac{\varphi\pi}{180} \tag{18.b}$$

where $\vec{x}_i(k+1)$ = the *i*th spider new position and $\vec{x}_i(k)$ = the *i*th spider current position. Both φ (in degress) and μ are random numbers produced in the interval (0, 1). V_o = the speed of the spider projection and g = acceleration duet o gravity. V_o, = 100 mm/sec and g = 9.80665 m/s^2..

The fitness values of search agents are normalized. The normalized value called pheromone is calculated as follows:

$$pheromone(i) = \frac{Fitness_{max} - Fitness(i)}{Fitness_{max} - Fitness_{min}} \tag{19}$$

where *Fitness(i)* = the *i*th spider current fitness value and $Fitness_{max}$ = the best fitness value of the current generation and $Fitness_{min}$ = the worst value of the current generation. The maximum pheromone value, the best value, is 1 and the minimum pheromone value, the worst value, is 0.

If a spider has its pheromone value ≤ 0.3, its position is updated as follows:

$$\vec{x}_i(k) = \vec{x}_{best}(k) + \frac{1}{2}\left(\vec{x}_{r1}(k) - (-1)^\sigma * \vec{x}_{r2}(k)\right) \tag{20}$$

$$r_1 \neq r_2$$

where $\vec{x}_{r1}(k)$ and $\vec{x}_{r2}$ are the positions of spiders r_1 and r_2 which are randomly selected, $\vec{x}_{best}(k)$ is the best position of the spiders in the preceding iteration and σ is a binary number selected at random from 0 and 1.

The EJSO algorithm is represented by the flow chart shown in *fig. 2*.

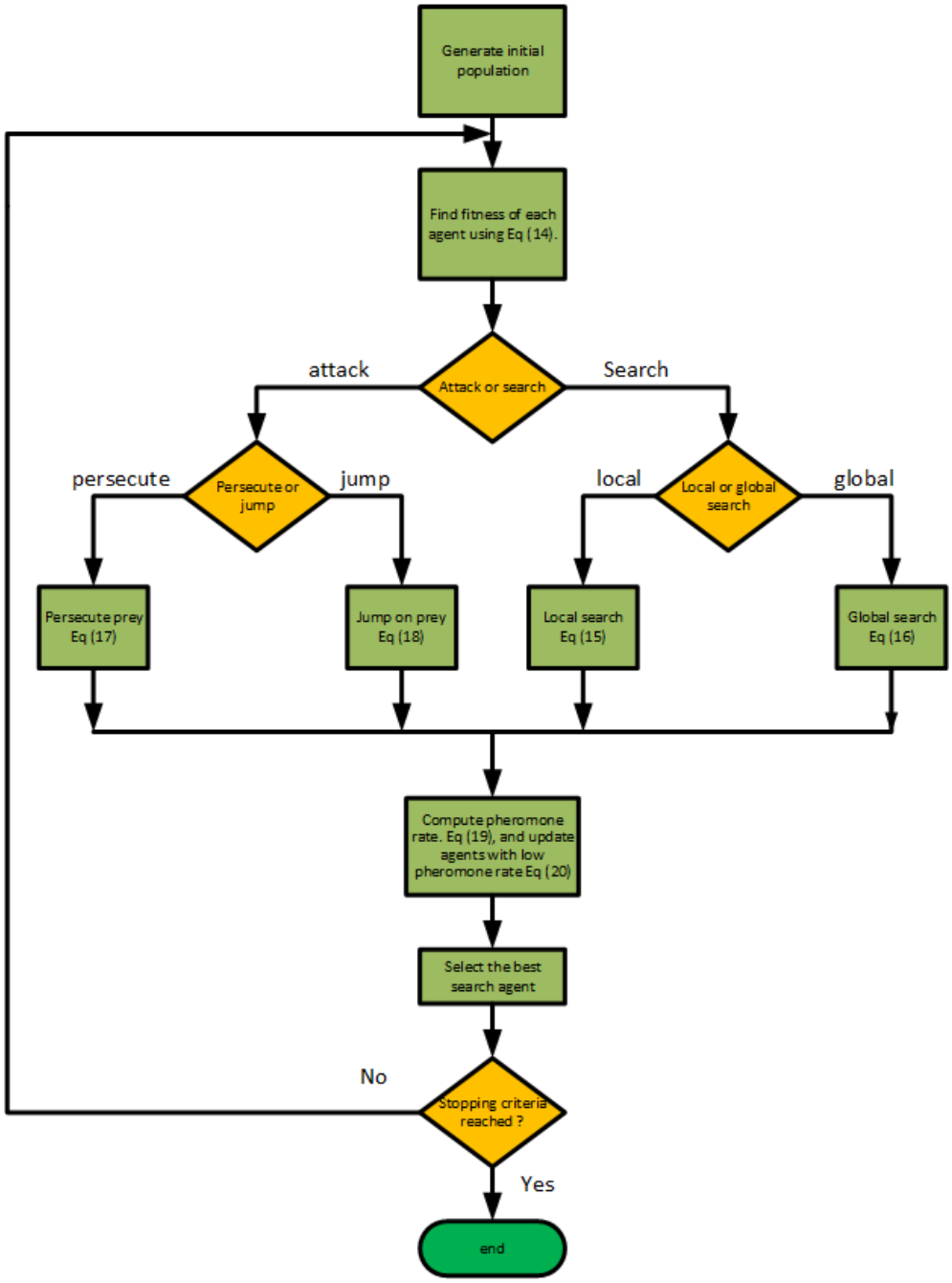

Fig. 2. Flowchart of Jumping Spider Algorithm [18]

2.4.2. Tuning of PI Controller with EJSOA

The following steps are taken to obtain optimum tuning values of the PI controller using EJSOA:

1. Build the SAPF model including the controller algorithms in Simulink.
2. Set parameters of the SAPF.
3. Set initial parameters of EJSOA (i.e., population size (*N*), dimension (*D*), maximum number of iteration)

4. Generate initial random population of spiders ($S_i = 1, 2, \ldots, N$) with dimension $D = 2$ (representing K_p and K_i)
5. Run the SAPF model for a specified nonlinear load using the initial K_p and K_i values and calculate the initial fitness of spiders S_{fit} using (14) for a specified T and sampling rate τ
6. **While** iteration < maximum number of iterations **do**
   if random number generated < 0.5 **then** Attack
   if random number generated < 0.5 **then**
   It is Attack by persecution. Use (17)
   else
   It is Attack by jumping on the prey. Use (18)
   end if
   else Search
   if random number generated < 0.5 **then**
   It is local search for prey. Use (15)
   else
   It is global search for prey. Use (16)
   end if
   end if
7. Calculate pheromone rate using (19)
8. Update search agents' positions (K_p and K_i) that have low pheromone rate using (20)
9. Run the SAPF model and calculate the new fitness of spiders $S_{fit,new}$ using (14)
10. **if** $S_{fit,new} < S_{fit}$ **then**
11. set $S_{fit} = S_{fit,new}$
12. **end if**
13. iteration =iteration + 1
14. **end while**
15. Output the best K_p and K_i values

3. IMPLEMENTATION

MATLAB/Simulink tool has been used to determine how effective the proposed PI controller is in mitigating current harmonics. *Figure 3* shows the complete Simulink models of the power and control blocks. The power blocks comprise the following three components: a three-phase, three-wire voltage source, a nonlinear load consisting of a three-phase uncontrolled rectifier feeding a passive load and a shunt active power filter. The shunt active power filter comprises a dc-bus capacitor, six-IGBT switches with diodes.

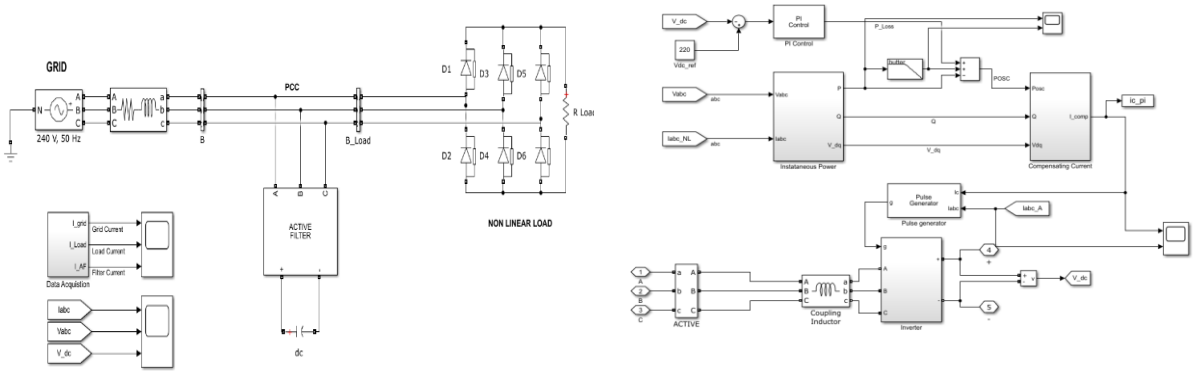

(a) Power Blocks *(b) Control Blocks*

Fig.3. MATLAB/Simulink Model of SAPF

3.1. Optimal tuning of the PI controller

The EJSOA parameters used for finding the optimum tuning values of the PI controller are presented in Table 1. The parameters of the power system, the SAPF and the nonlinear load are given in Table 2 and the complete Simulink model of the control circuit with ITAE block is shown in *fig. 4.*

Table 1. Parameters of EJSOA for optimal tuning

Parameters	**Values**
Population size	50
Number of iterations	30
Sampling period T	1
Sampling rate τ	0.005 ms

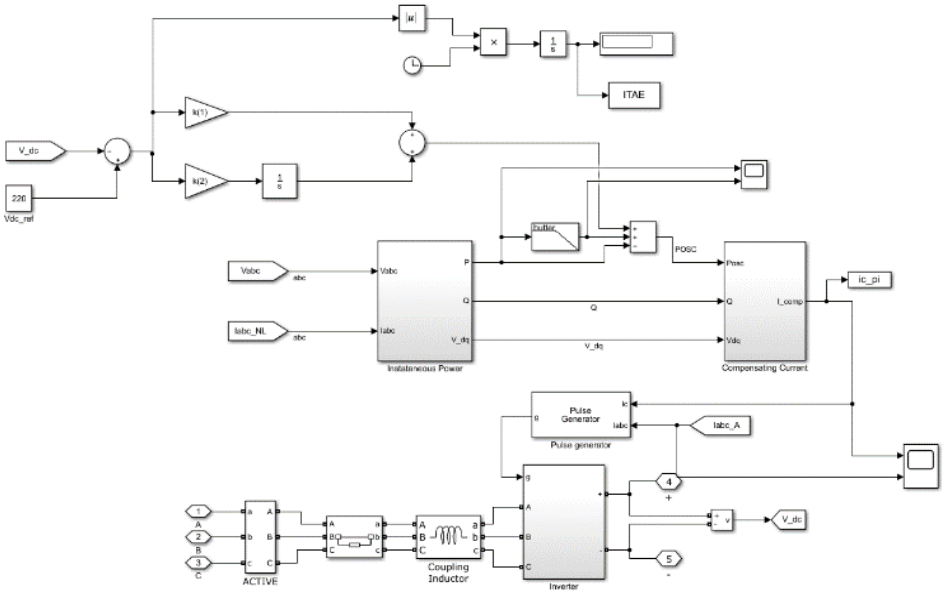

Fig. 4. Simulink model with ITAE block

Table 2. Parameters of overall system for optimal tuning

Parameters	**Values**
Source voltage	380 V
frequency	50 Hz
Line inductor	L_s = 10 mH
Filter inductor	L_f = 0.15 mH
DC-link capacitor	C = 1000 μF
DC load resistance	50 Ω
DC link capacitor voltage	600 V

3.2. Testing

After finding the optimum tuning values of the PI controller, the performance of the proposed SAPF was evaluated using dc load resistances of 50 ohms and 25 ohms. The 50-ohm load resistance is the same as what was used for the optimal tuning of the PI controller. The constants of the power system and the SAPF are as defined in Table 2. The Simulink model of the control blocks used for testing the proposed system is the same as that given in Fig. 4 without the ITAE block.

4. RESULTS AND DISCUSSIONS

4.1. Optimal tuning values of PI controller

The optimal gains obtained were: K_p = 0.057175 and K_i = -1. These gains were then used to verify the effectiveness of the proposed PI controller. Two dc resistances were considered. These two gain values and other system parameters were maintained for the two dc resistance loads.

4.1.1. Source Current Waveform and its Harmonic Spectrum

Case 1: DC resistance = 50 Ω

Figure 5(a) and *fig. 5(b)* show the source current waveform and its harmonic spectrum before connecting the SAPF.

Figures 6(a) and *6(b)* show the corresponding curves when the SAPF is in circuit. From the FFT analysis, the THD reduces from 26.12% to 0.55%.

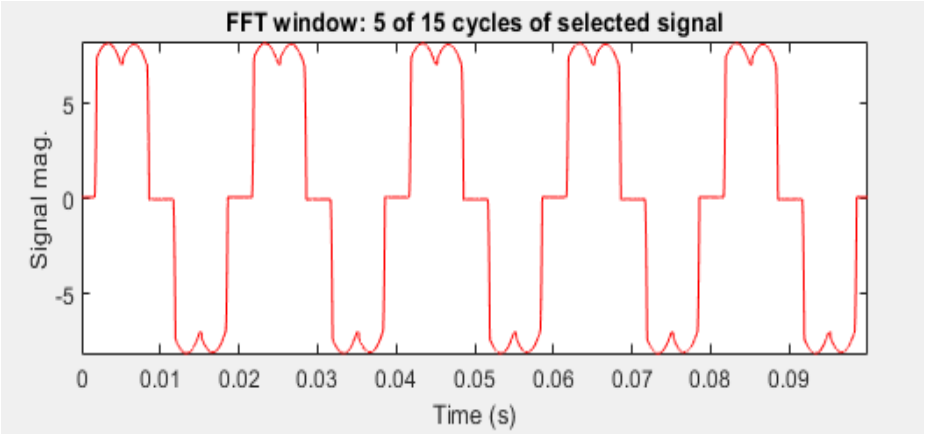

(a) Waveform of source current

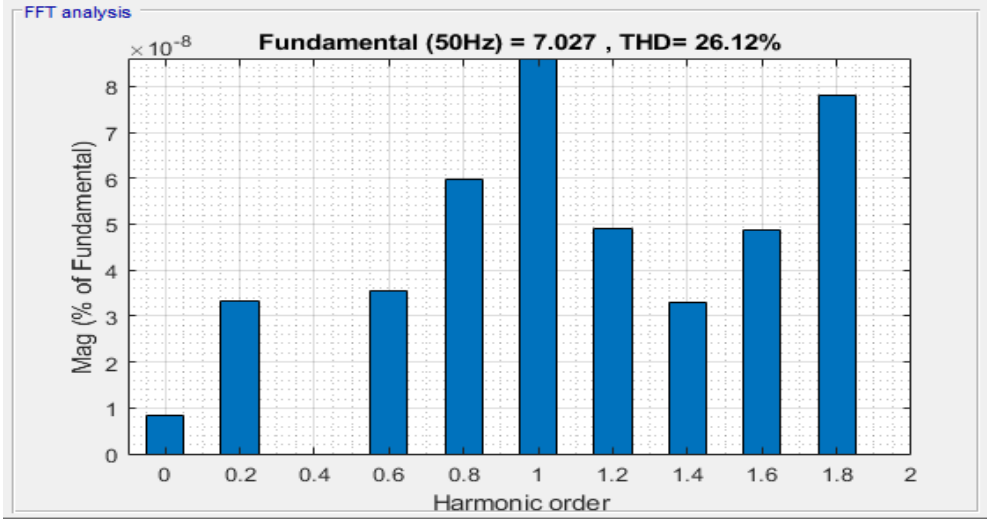

(b) Source current harmonc spectrum

Fig. 5. Source current before compensation

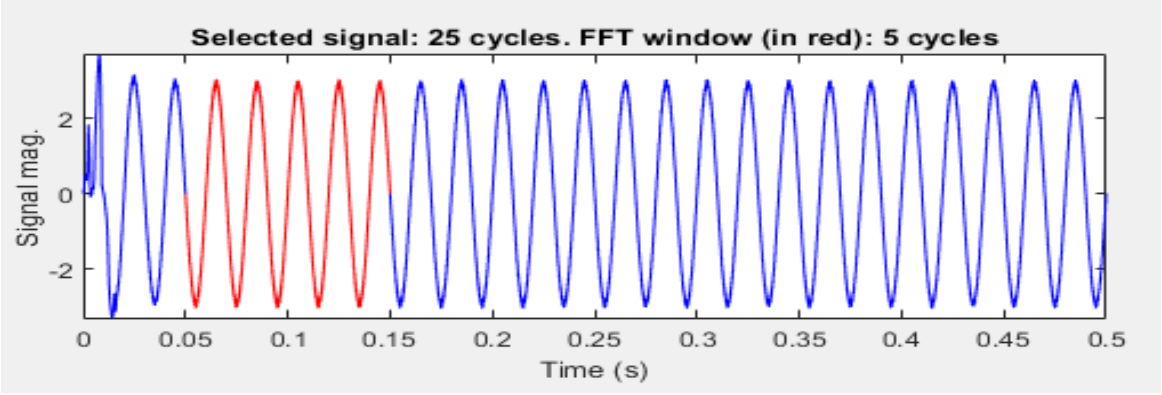

(a) Waveform of source current

Fig. 6. Source current after compensation

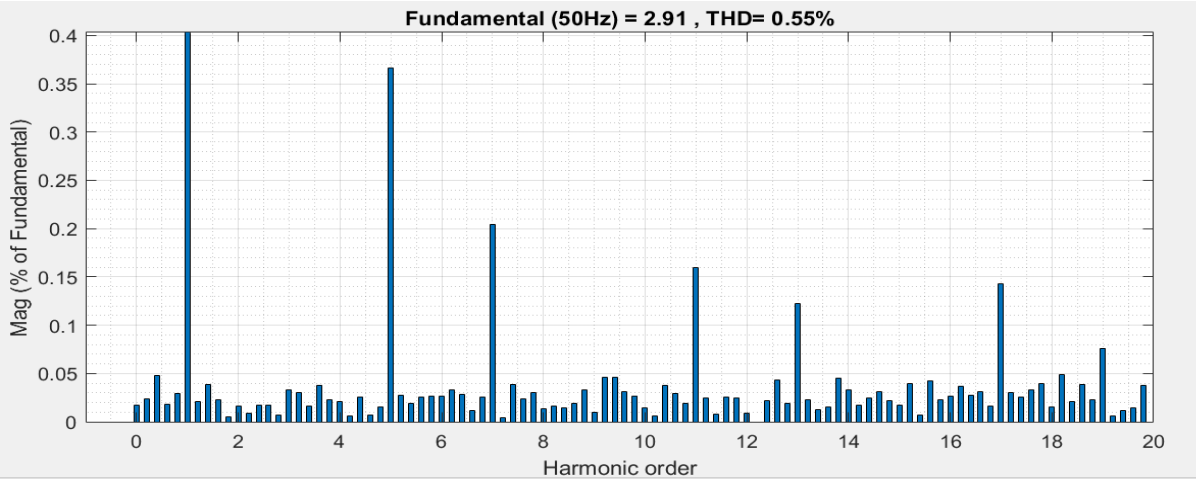

(b) Supply current harmonic spectrum

Fig. 6. Source current after compensation

Case 2: DC resistance = 25 Ω

Figure 7(a) and *fig.7(b*) show the source current waveform and its harmonic spectrum before connecting the SAPF.

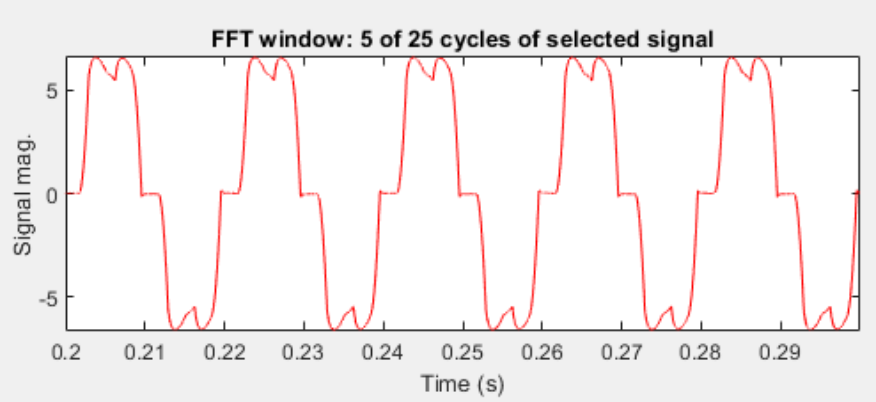

(a) Waveform of source current

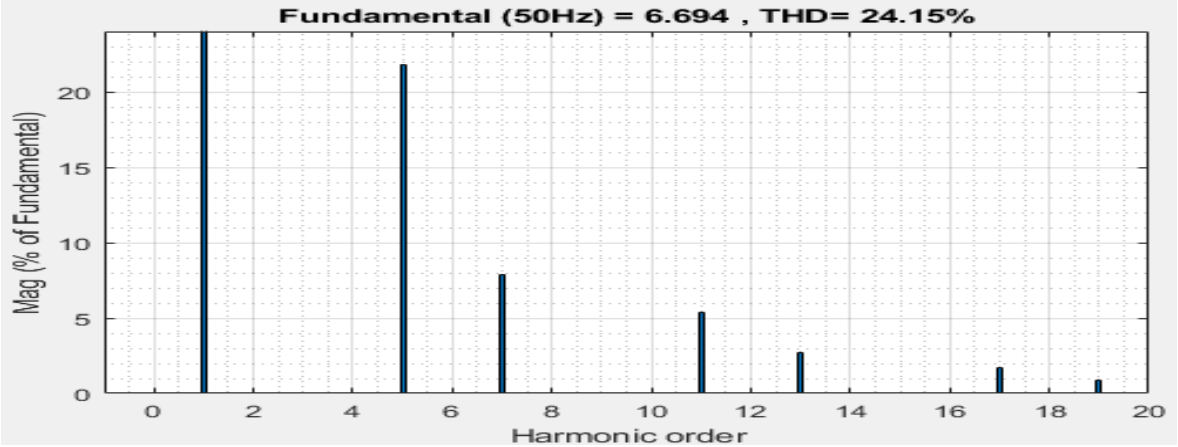

(b) Source current harmonic spectrum

Fig. 7. Source current before compensation

Figures 8(a) and *8(b)* show the corresponding curves when the SAPF is connected. The FFT analysis shows a reduction of the THD from 24.15% to 0.53%.

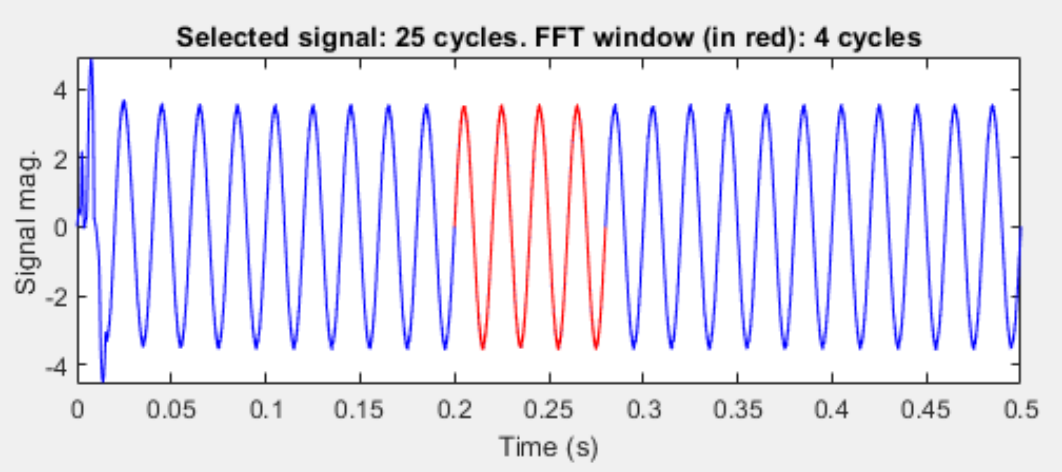

(a) Waveform of source current

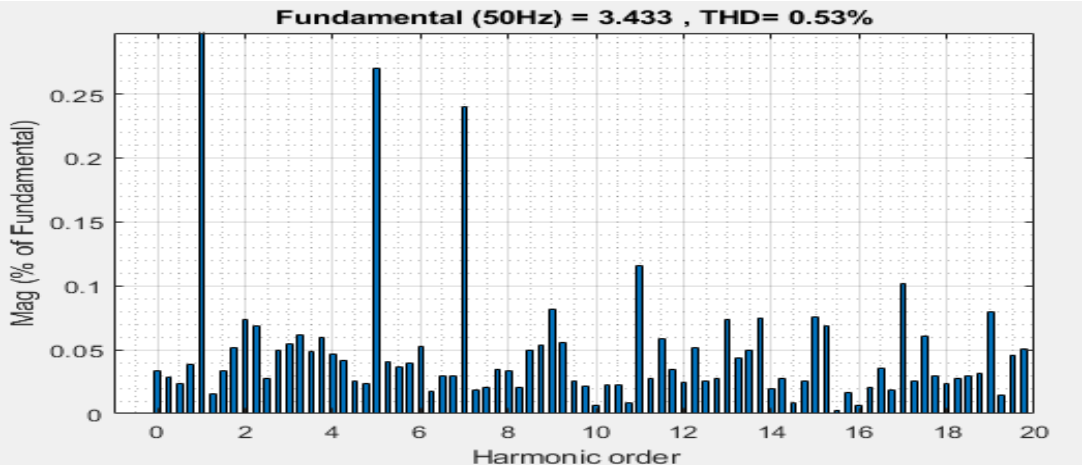

(b) Source current harmonic spectrum

Fig. 8. Source current after compensation

4.2. DC link capacitor voltage response

Figure 9 shows the response of the dc link capacitor voltage regulated by the proposed PI controller for the 50-ohm dc resistance load. The corresponding response for the 25-ohm dc resistance loads is shown in Fig.10. The two waveforms show a fast and stable response with zero steady-state error. Each of the waveforms also has an overshoot of about 17% which makes the response fast. *Figure 11* gives the waveform for the case where the SAPF was run with initial dc resistance load of 50 ohms and at t = 0.25s the dc resistance load was suddenly decreased to 25 ohms to double the load current. As shown by the waveform, the voltage across the capacitor dropped when the current drawn by the load suddenly doubled but it quickly recovered.

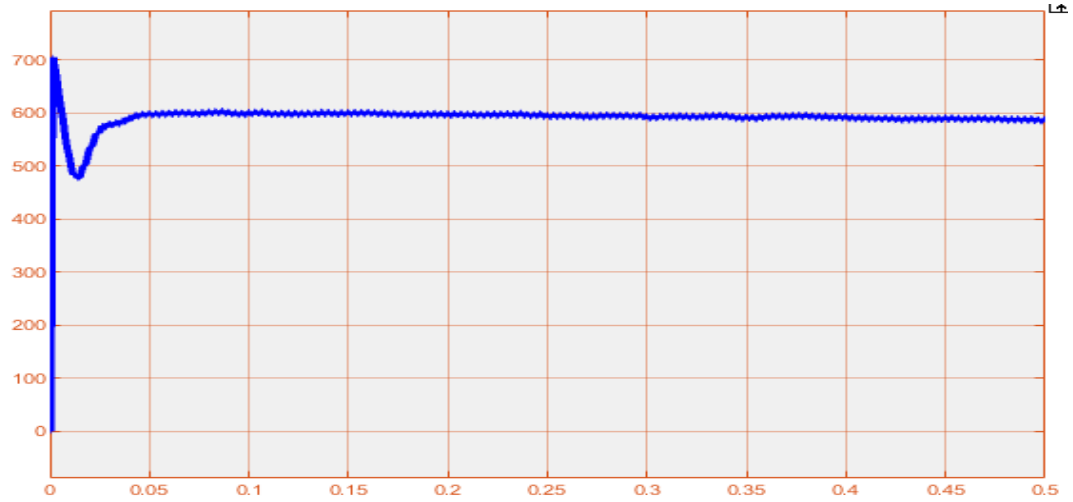

Fig. 9. SAPF capacitor voltage 50-ohm dc load resistance

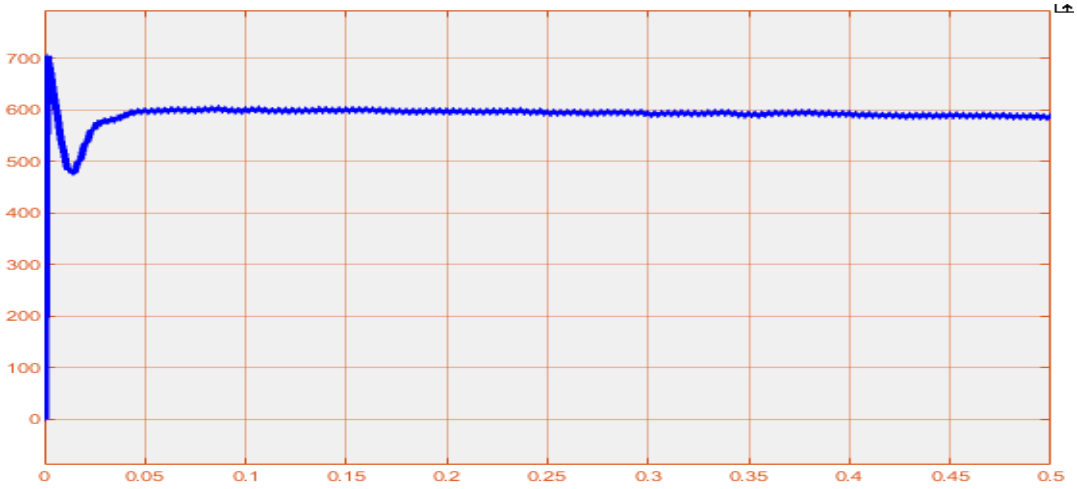

Fig.10. SAPF capacitor voltage for 25-ohm dc resistance

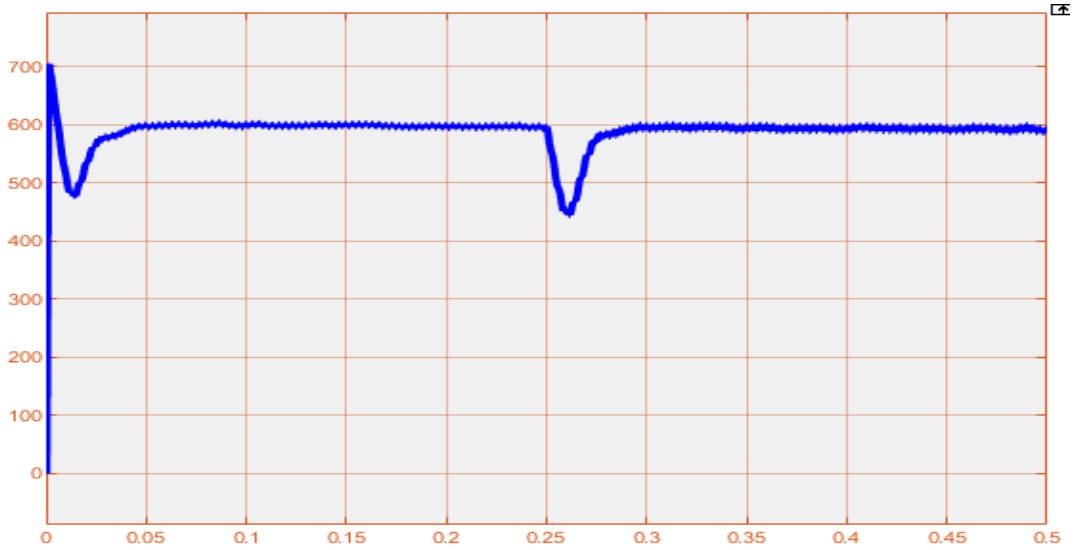

Fig.11. SAPF capacitor voltage when load current doubles.

5. CONCLUSION

The EJSOA has been applied to optimally tune the PI controller of SAPF to mitigate harmonics in power systems. The PI controller has been used for the regulation of the dc link capacitor voltage of the SAPF. The EJSOA has employed the ITAE as the fitness function to determine the optimum gains of the PI Controller. SAPF using this PI controller has been developed and simulated in MATLAB/Simulink environment. The EJSOA-PI controller produced a dc link capacitor voltage response that is fast, stable and steady-state error-free. The capacitor voltage also recovers quickly when it drops in value following a sudden variation in load. The results also showed that the SAPF with the EJSOA-PI controller is capable of reducing the THD of a balanced power system from 26.12% to 0.53%, a figure which is far below the IEEE harmonic standard limit of 5%.

REFERENCES

[1] A. E. S. Salem, O. M. Salim, and S. I. Arafa, *New triple-action controller for inverter power quality improvement*, Comput. Electr. Eng., vol. 81, 2020, doi: 10.1016/j.compeleceng.2019.106543.

[2] Y. Hoon, M. A. M. Radzi, M. K. Hassan, and N. F. Mailah, *Control algorithms of shunt active power filter for harmonics mitigation:* A review, Energies, vol. 10, no. 12, 2017, doi: 10.3390/en10122038.

[3] Y. Hoon, M. A. M. Radzi, M. K. Hassan, N. F. Mailah, and N. I. A. Wahab, *A simplified synchronous reference frame for indirect current controlled three-level inverter-based shunt active power filters*, J. Power Electron., vol. 16, no. 5, pp. 1964–1980, 2016, doi: 10.6113/JPE.2016.16.5.1964.

[4] R. R. Nasyrov, R. I. Aljendy, and A. A. Z. Diab, *Adaptive PI controller of active power filter for compensation of harmonics and voltage fluctuation based on particle swarm optimization (PSO)*, Proc. 2018 IEEE Conf. Russ. Young Res. Electr. Electron. Eng. ElConRus 2018, vol. 2018-Janua, pp. 719–724, 2018, doi: 10.1109/EIConRus.2018.8317194.

[5] A. Fereidouni and M. A. S. Masoum, *Enhancing performance of active power filter with fuzzy logic controller using adaptive hysteresis direct current control*, 2014 Australas. Univ. Power Eng. Conf. AUPEC 2014 - Proc., no. October, pp. 1–6, 2014, doi: 10.1109/AUPEC.2014.6966500.

[6] S. Mahaboob, S. K. Ajithan, and S. Jayaraman, *Optimal design of shunt active power filter for power quality enhancement using predator-prey based firefly optimization*, Swarm Evol. Comput., vol. 44, no. June 2018, pp. 522–533, 2019, doi: 10.1016/j.swevo.2018.06.008.

[7] D. Tian and Z. Shi, MPSO: *Modified particle swarm optimization and its applications*, Swarm Evol. Comput., vol. 41, pp. 49–68, 2018, doi: 10.1016/j.swevo.2018.01.011.

[8] H. Ismkhan, *Effective heuristics for ant colony optimization to handle large-scale problems*, Swarm Evol. Comput., vol. 32, pp. 140–149, 2017, doi: 10.1016/j.swevo.2016.06.006.

[9] Q. Long, *A constraint handling technique for constrained multi-objective genetic algorithm*, Swarm Evol. Comput., vol. 15, pp. 66–79, 2014, doi: 10.1016/j.swevo.2013.12.002.

[10] T. Sudhakar Babu, K. Priya, D. Maheswaran, K. Sathish Kumar, and N. Rajasekar, *Selective voltage harmonic elimination in PWM inverter using bacterial foraging algorithm*, Swarm Evol. Comput., vol. 20, pp. 74–81, 2015, doi: 10.1016/j.swevo.2014.11.002.

[11] R. Akbari, R. Hedayatzadeh, K. Ziarati, and B. Hassanizadeh, *A multi-objective artificial bee colony algorithm*, Swarm Evol. Comput., vol. 2, pp. 39–52, 2012, doi: 10.1016/j.swevo.2011.08.001.

[12] K. Rameshkumar and V. Indragandhi, *Real Time Implementation and Analysis of Enhanced Artificial Bee Colony Algorithm Optimized PI Control algorithm for Single Phase Shunt Active Power Filter*, J. Electr. Eng. Technol., vol. 15, no. 4, pp. 1541–1554, 2020, doi: 10.1007/s42835-020-00437-2.

[13] N. Eskandarian, Y. A. Beromi, and S. Farhangi, *Improvement of Dynamic Behavior of Shunt Active Power Filter Using Fuzzy Instantaneous Power Theory*, vol. 14, no. 6, pp. 1303–1313, 2014.

[14] H. P. Thanh, H. D. Van, A. N. Duy, and C. N. Duy, *Optimizing parameters of the shunt active power filter using Genetic Algorithm*, Proc. - 2017 9th Int. Conf. Knowl. Syst. Eng. KSE 2017, vol. 2017-Janua, pp. 233–238, 2017, doi: 10.1109/KSE.2017.8119464.

[15] C. Lam and M. Wong, *Design and Control of Hybrid Active Power Filters*. 2014. [Online]. Available: http://link.springer.com/10.1007/978-3-642-41323-0

[16] Z. Chelli, R. Toufouti, A. Omeiri, and S. Saad, *Hysteresis control for shunt active power filter under unbalanced three-phase load conditions*, J. Electr. Comput. Eng., vol. 2015, 2015, doi: 10.1155/2015/391040.

[17] A. K. Mishra, S. R. Das, P. K. Ray, R. K. Mallick, A. Mohanty, and D. K. Mishra, *PSO-GWO Optimized Fractional Order PID Based Hybrid Shunt Active Power Filter for Power Quality Improvements*, IEEE Access, vol. 8, pp. 74497–74512, 2020, doi: 10.1109/ACCESS.2020.2988611.

[18] B. N. Atanga, F. B. Effah, and P. Y. Okyere, *An enhanced jumping spider optimization algorithm*, vol. 16, no. 1, pp. 46–61, 2022.

[19] M. Jamil and H. J. Zepernick, *Lévy Flights and Global Optimization*, *Swarm Intell. Bio-Inspired Comput.*, pp. 49–72, 2013, doi: 10.1016/B978-0-12-405163-8.00003-X.

IMPACT OF THE HYDROELECTRIC POWER PLANTS ON THE MOUNTAIN ECOSYSTEMS

Mihaela **ȘTEȚ**, Bogdan **CIORUȚA**
Technical University of Cluj-Napoca,
mihaela.stet@ieec.utcluj.ro,

Keywords: Hydroelectric power generation, mountain ecosystems, environmental impact

Abstract*: In the last decades, there was identified evidence of climate change. These climate changes are associated with various effects on different types of ecosystems and with changes in mountain ecosystems. To respond to these challenges, some states have started the implementation of general and specific measures, among them being the measures taken within the energy sectors*.

1. INTRODUCTION

In the last decades there has been identified evidence of climate changes. These climate changes are associated with various effects on different types of ecosystems and with changes in mountain ecosystems. It can be highlighted a direct and indissoluble relationship between climate change, hydropower plants, and the impact of the latter on the environment.

Mountain regions, complex and diverse in their nature, are central to policies for environmental protection and sustainable development; their problems and difficulties in adapting to climate change require appropriate, rapid, and, above all, permanent measures (sustained continuously). Inhabitable mountain regions usually belong to the geography of the environment, but can also be analyzed from an economic, social, cultural, etc. perspective, their multidisciplinarity being recognized both by the academic-university environment and by decision-makers directly involved in territorial development.

The economic outlook is particularly important at the level of large regional interest groups, and especially at the local and regional level, for the communities directly dependent on the conditions, resources and services offered by the mountain areas.

Increasingly visible, the negative impact of economic activities on upland areas, both high and low, must lead to a shared vision and a sustainable approach to its biodiversity status, as habitat damage can lead to destroying the ecological balance. Based on the above considerations, the article aims to provide an overview of the relationship between mountain biodiversity and the effects of the economic and social development on it (design, construction, operation, and decommissioning of hydroelectric installations), mainly using national documentary sources, but also, international sources, data, and statistical information, which come to complete the global picture of their evolution of the relationship, in time and space. At the time, the relationship between climate change and hydropower plants is considered, the same former bringing a significant contribution to the impact on the environment, with direct cumulative negative effects.

2. METHODOLOGY

The paper is based on research and analysis of scientific papers and research found in international scientific and professional journals, as well as specialty books in the field of environment protection and energy production. Given that the subject of the research is in an area of confluence between the field of energy engineering and the field of environmental protection, studies were investigated in international databases that include papers from the two fields of research. For this reason, there have been analyzed papers from IEEE, Scopus, Elsevier, Wiley databases.

3. ABOUT THE IMPACT ON MOUNTAIN ECOSYSTEMS IN RELATION TO THE SECTORS INVOLVED

Mountain areas are areas of these ecosystems form a relatively populated environment, but increasingly exposed to economic pressures with consequences that accompany zonal economic development: air, water and soil pollution, effects on flora and fauna, hydrological change etc.

The products and services offered by mountain ecosystems are of vital importance to local and regional communities, being an important source of raw materials for agriculture, forestry, tourism, mining, and industrial energy (*Figure 1*). [1]

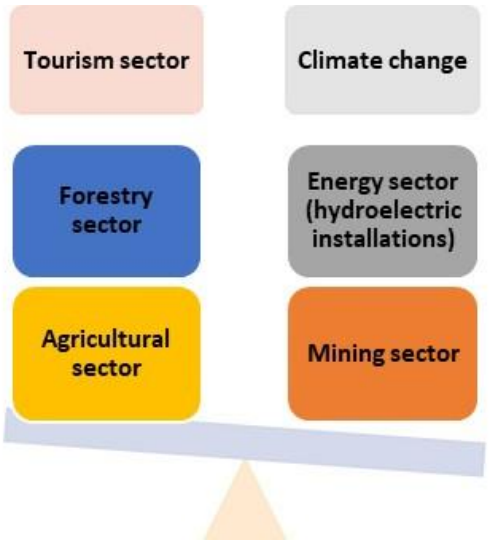

Figure 1. The change in the balance of the impact on mountain ecosystems in relation to the sectors involved

The development of mountain agriculture in different regions of the world is a real threat to some species, local biodiversity.

Uncontrolled deforestation in many mountainous areas around the world has led to a substantial reduction in the forest fund, with sometimes catastrophic effects not only on local flora and fauna, but also on land, not least in situations where the population has been affected by landslides. And even if tree planting activities are undertaken later, they cannot restore the ecosystems impoverished by extinct species.

The expansion of tourism activities in mountain areas, in addition to the economic benefits it brings, affects mountain ecosystems and biodiversity.

The activities of extracting useful mineral resources have many forms of impact, even after their decommissioning: water pollution, soil erosion, negative effects on landscapes, biodiversity, risks of chemical contamination of groundwater. [1]

Climate change in the form of global warming is adversely affecting mountain ecosystems. Some species have experienced declines in their population, and in some cases even their extinction. There are also changes in the precipitation regime, with effects on the flows of watercourses.

Mountain watercourses are often used to generate electricity. But even if they use a renewable energy resource, water, both during construction and in operation, hydroelectric power plants are associated with some form of environmental impact (Table 1).

At the same time, mountain ecosystems are also vulnerable to climate change, which is why it is necessary to monitor the effects these changes have on them. Protecting these ecosystems must be a priority in the design of any development strategies.

To respond to these challenges, some states have started the implementation of general and specific measures, among them being the measures taken within the energy sectors.

Table 1. Different types of activities and impacts associated with energy production and transport (adapted and updated after [2]

Types of activities	Air pollution	Electromagnetic pollution	Impact on biodiversity	Land use and pollution	Noise	Use of hazardous materials	Vibration	Visual pollution	Waste generation	Water use and pollution
Electricity transport	X	X	X	X	X			X		X
Geothermal plants	X			X						X
Hydropower plants*	X		X	X	X		X	X	X	X
Nuclear power plants	X		X	X		X		X	X	X
Solar power plants	X			X		X				
Thermal power plants	X		X	X				X	X	X
Wind power plants			X	X	X			X	X	

*micro-hydropower plants are included in this category

Use of renewable energy sources, like bioenergy, solar, wind, geothermal, hydropower energy, more environmentally friendly, offers an alternative solution to hydrocarbon-based power plants, in the attempt to reduce air pollution and to mitigate GHG emissions. Unfortunately, global climate change could also affect the renewable energy RE sources.

Given the fact that mountain areas are the source of numerous watercourses, the negative effects of climate change are not limited to these areas and their hydrology, but extend to downstream areas, whose hydrology can also be, affected and, consequently, the corresponding ecosystems.

4. THE ENVIRONMENTAL IMPACT OF HYDROPOWER PLANTS ON MOUNTAIN ECOSYSTEMS

First of all, hydropower plants offers a large series of benefits, besides the electricity necessary for economic development. Hydropower plants harness the energy of running water, which is a source of clean and renewable energy. They thus help to reduce consumption of fossil fuels and, consequently, to reduce air pollution. At the same time, water is an internal source of energy, much more accessible and reliable source than fossil fuels.

The formation of accumulation lakes offers the opportunity for complex uses of water. In addition to the main purpose, that of producing electricity, they make it possible to supply drinking water to the region and irrigate local agricultural land. They can also be used for

recreational purposes, such as fishing, water sports and light boating, the storage lakes being genuine tourist attractions.

During periods of heavy rainfall and floods, hydropower facilities, dams, made on rivers, can be used to control floods by regularizing their flows, preventing in this way damages to flora and fauna along the riverbanks. During periods of drought, increased water flow protects aquatic habitats.

In the same time, in the upper part of the dams of the reservoirs of the hydropower plants, communication paths can be built to cross the water courses.

From a technical point of view, the energy generated by hydropower plants can be injected faster into the energy system than from other types of powerplants, allowing the power to be restored quickly after interruptions and maintaining the voltage levels of the system.

In the mountain regions, although hydropower plants offer a wide range of benefits compared to thermal power plants, in terms of impact on the environment, significantly reducing air pollution, they are still not without an impact on the environment. While at the macroecological level it has advantages over other forms of electricity production, at the local and regional levels negative effects on the environment can be highlighted.

Therefore, several forms of impact on the environment of both large power plants and micro-hydropower plants can be identified during the construction phase (noise, waste, negative impacts on soil), but also during operation: in hydrological regime and water quality, effects on soil, flora, fauna (isolation, extinction or emergence of plant or animal species), damage to shores.

Uscătescu et al. [3] classified the forms of the environmental impact of the hydroelectric facilities based on various criteria (*Figure 2*).

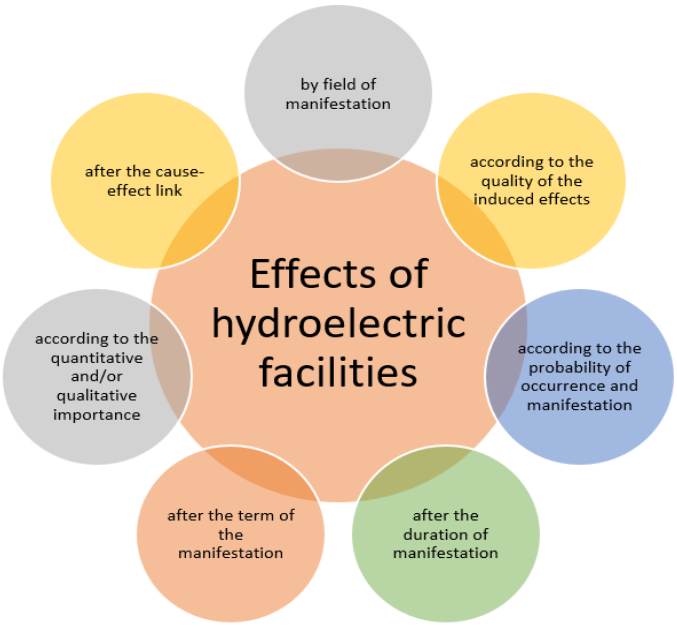

Figure 2. Schematic classification of the effects of hydroelectric facilities on mountain ecosystems (Processed and based on [3])

4.1. Impact on the atmosphere of the hydropower plants

Although in the case of electricity production in hydroelectric power plants we are talking about a renewable source of energy, water, it is not completely free of effects on the air, on the atmosphere.

Thus, different types of noxious substances (NOx, CO, SOx, heavy metals), COV and greenhouse gas emissions can be highlighted during the construction period, through the transport of materials and the operation of equipment and installations. Also, dust emissions are present during the execution of hydroelectric power plants. These emissions are temporary, so their impact on the environment is for a short time.

Flooding the land leads to the appearance of methane, another greenhouse gas, due to the organic materials, covered by water, through the decomposition of vegetation and soil. The amount of emissions depends on the site-specific characteristics, type of the soil, vegetation, temperature of air and water, reservoir management practice, season, the level of water. Also, greenhouse gas emissions depend on the type of hydropower plant HPP, the highest emissions being generated by storage (reservoir) HPP, followed by Run-of-river (RoR) and pumped storage plants [4]. During the operation phase, different activities of maintenance, the operation of cooling and heating systems could generate emissions of greenhouse gases. In the final stage, that of decommissioning of the power plant, the activities performed are also associated with such emissions.

Due to the excess of atmospheric humidity in the area, due to the presence of a large amount of stored water in the case of storage (reservoir) HPP, climatic disturbances occur: the decrease of the average temperature and frequent fog.

4.2. Impact on soil and subsoil

During the construction period, numerous cases of soil degradation are highlighted. The organization of the construction site requires the use of large areas of land. The works carried out to build the dykes change the configuration of the land.

In the case of hydroelectric plants that involve the construction of a dam, especially for the commissioning of large hydroelectric plants, it is necessary to clear forests or flood large areas of land, sometimes even fertile soils. Deforestation, clearing of vegetation can affect soil layers. Changes in texture, cohesion, state of loosening, temperature, etc. can be identified.

There is a risk of waste oil or waste, including hazardous waste, accidental leakage of fuels or lubricants, emissions of pollutants (NOx, SO, SO2, CO), sedimentable powders, heavy metals, which may settle on the ground.

During operation, the banks of the reservoir can be eroded, a phenomenon that also depends on the way the plant is operated.

The existence of a reservoir influences the soil and the subsoil due to the high pressure exerted on the earth's crust by the volume of accumulated water in reservoir and the infiltration of water from the lake into the earth's crust, with inherent intensifications of the action of the groundwater table on the structure of the crust [5].

4.3. Impact on water

Hydroelectric power plants have effects on river ecology through changes in hydro morphological characteristics: hydrological regime, continuity of the river, as well as the morphological conditions.

The changes that can be highlighted are chemical, physical (water temperature), and biological. There can be identified changes of the concentration of nutrients in water. Changes in the characteristics of aquatic and coastal ecosystems are also identifiable. The deviation of certain portions of the watercourses leads to changes of a physical-geographical nature with effects on the biocenoses.

During the construction period, solid particles, accidental leaks of fuels, oils, other chemicals or waste can enter the water. Changes in the movement and accumulation of sediments cause changes in the hydraulic balance and in the morphology of the riverbed, with a negative impact on some habitats.

Below the dams, the oxygen level is low, which has a negative impact on aquatic life. Reducing the flow of water courses causes changes in their thermal level and a decrease in the amount of dissolved oxygen, with long-term influences on the abundance and diversity of species [6]. To reduce this negative impact, aeration turbines can be used, or oxygen injected.

In the case of the construction of micro hydropower plants MHPP, an important problem for both the aquatic ecosystem and the local community is the reduction of water flow. There are also changes in the speed of the water, but also in the turbidity, transparency and chemical composition.

The servitude flow must be maintained at values that do not produce significant changes in the self-purification capacity and thermal regime of the river.

4.4. Impact of hydropower plants on biodiversity

The forms of impact on biodiversity can manifest both directly and indirectly, at the site of the construction of the hydropower plant or at a certain distance from it, immediately or even a few years after the construction or commissioning.

The construction of hydropower plants can lead to the alteration or loss of habitats not only for fish, but also for all other categories of biotic components: plants, terrestrial and aquatic invertebrates, amphibians, reptiles, birds, aquatic and terrestrial mammals. In the case of fish,

invertebrates, reptiles, amphibians and aquatic mammals, habitat fragmentation, disruption or even mortality of species even hundreds of meters from the noise source can occur [6].

Excavation works for the construction of power stations, of intakes and penstocks can have negative effects on riparian phytocenoses. The works of construction of adductions, of the catchment have an impact on the herpetofauna in the area. The negative barrier effect that hydropower plants can have on some mammal species can be highlighted. To reduce the negative impact, the solution of building crossings that have a more natural character, made of rocks, earth and vegetation specific to the respective area, can be practiced.

The flooding of land for the formation of reservoirs leads to the destruction of natural areas that bring together various plant species, but also to the loss of wildlife habitats. Changes in flows can significantly affect the ichthyofauna in the area, but also upstream and downstream.

The construction and operation of small hydropower plants can generate significant impacts on biodiversity when their location and design do not start from compliance with the ecological requirements of habitats and species. The effects of their construction are similar to large dams: modification of hydro-geomorphological parameters of riverbeds [7], interruption of habitat continuity, acceleration of ecosystem succession, rapid eutrophication [6].

The discharge of some sediments into the water course during the construction period of the intake and catchment can affect benthic invertebrates, which are a food source for some fish species, such as trout. For this reason, it is necessary to avoid their discharge into the riverbed.

During the period of operation of the small-hydropower plants, the negative impact on fish and some invertebrates can be highlighted also, determined by the release of sediments and organic matter into the river during the washing of the de-sanding devices of the small hydropower plants.

The diversion of river courses, the blocking of their natural course causes the obstruction of the natural migration routes of fish. Disruption of watercourse connectivity causes the decline of upstream species populations. The solution of building ladders for fish movement is suitable for large fish species, but not useful for small fish species. In the same time, the situation of accidental clogging of the slots of these scales may occur, interrupting the connectivity of the habitats of various species of aquatic life.

According to Romanian legislation, the construction of passageways for migrating aquatic fauna is required only for thresholds higher than 40 cm [8], respectively 50 cm [9], heights that prevent the migration of fish species small and some protected fish species, such as the benthic fish Cottus gobio.

It is therefore necessary to comply with the height, flow and velocity requirements of the water for the protected fish species. Moreover, the study carried out by Utzinger et al. [10] reveal that obstacles larger than 20 cm can stop their upstream movement. In addition to the size of the specimens Ovidio et al. [11] highlights other influencing factors in jump

performances: the type of obstacle, the age of the specimens and the abiotic conditions: depth, temperature and water speed.

The movement of fish and other aquatic organisms in the dam area is determined by the type and size of the hydropower facility. These organisms are vulnerable and can be injured. In order to identify the effects on them at the passing through the turbine the researchers use sensors and acoustic telemetric systems [12]. The ways in which they can be injured are multiple, as Coutant and Whitney [13] point out: blade impact, cavitation, grinding, rapid pressure decreasing, shear stress and turbulence (Table 2).

Table 2. Injuries of fish and aquatic organisms in the dam zone

Type of exposure	Injuries associated with the type of exposure	Source
Shear forces	• bruising, • eye and gill/opercular damage • descaling	Deng et al., 2005 [14]
Fast decreases in pressure	• rupture of the swim bladder, • exopthalmia, • emboli in the fins and gills, • hemorrhaging	Brown et al., 2012 [15]
Cavitation / Elevated total dissolved gas	• gas bubble disease: emboli in the fins, gills, and eyes	Deng et al., 2015 [16]

The rapid decrease in water pressure leads to an increase in the total volume of dissolved gases TDG, which can lead to injury or mortality of fish. Water supersaturated with dissolved nitrogen causes gas bubble trauma (GBT) in fish, a phenomenon that occurs when they pass through the turbine area.

The survival of fish passing through the turbine area is influenced by the speed of the turbine blades, the degree of inclination and the body part of the fish they hit [17], [18]. Depending on how the turbines are built, they can be more or less dangerous. In their report, Franke et al. [19] present the results of a study on reducing the impact on the environment through the design of environmentally hydro turbine systems. Also, Cada [20], Cada et al. [21] present turbines designed to improve fish survival rates.

In the case of large dams Deng et al. [16] identified three main possibilities for their movement downstream: through the turbines, over the spillway or using the bypass facility for juvenile fish. They also add as alternative options to avoid injury to fish such as fish screens to guide fish away from turbines and into bypass or transport facilities, as well as catching and transporting them downstream by water or land transport, using trap-and-haul facilities to collect and move fish. For large dams, also, the accumulation lake could be populated with fish specific to that area. However, the solutions used do not allow massive migrations.

A common solution for ensuring the migration of fish is, especially for small dams, the construction of ladders or windows in the dams that allow the passage of fish. These passages are practiced not only for migratory species, but also to the other species. Their design depends on the configuration of the hydropower, the characteristics of the river and on the fish species in the river [16].

4.5. Other forms of impact

Noise pollution is another form of pollution encountered during the construction period due to the machinery, means of transport used in the construction of dams and other construction and installation elements. Added to this are the vibrations caused by them, as well as the use of explosives, with effects on the population and fauna of the area.

Hazards related to damage to hydrotechnical constructions can affect embankments and dams of water accumulations. Technological accidents such as dam breakages, which can be initiated by natural causes (floods, earthquakes), can cause catastrophic effects both for the flora and fauna, as well as for the population and the surrounding constructions.

But sources of noise and vibrations can also be identified during the exploitation period, caused by turbines and generators, which can cause disturbances of the species in the respective area. There are studies in this regard that reveal that an increase in the noise level compared to the natural background of 3-10 dB can cause a 30-90% reduction in the alerting distances of wild animals [22], in while values higher than 48 dB for birds living in meadows and 42 dB for those living in forests can cause a decline in their numbers [23]. Noise can affect interspecific, intraspecific communications, reproduction, nesting and feeding of various species [16]. Vibration dampers and sound-absorbing panels can be used to limit noise and vibrations.

In addition to the different forms of pollution, visual pollution is also added by changing the visual characteristics of the landscape: constructions and electrical installations, changes in the watercourse bed, changes in the riparian vegetation.

During the construction period, the activities involved in realization of a small hydropower plant has negative effects on the landscape in the area selected for construction due to the specific construction works, the location of the construction site organizations and the intense traffic of machinery. More, a series of waste results, quantities of excavated soil, whose improper management can have effects on the environment.

In Romania, of the more than 430 micro hydropower plants in various stages of planning, authorization and construction, more than a quarter are in protected natural areas [24]. During their exploitation, reductions in the flow rates of water courses have been reported with effects on biodiversity, flora, fauna and landscape being affected [25]. Also, the roads of some localities where these micro hydropower plants were built during their construction were also affected. The negative effects are also felt on the local economy, whose development is based on the agritourism network.

5. CONCLUSIONS

In addition to the many benefits that hydropower plants bring, from economic, social and environmental points of view, there are also some forms of negative impact on the environment associated with them.

Thus, we can speak of a microclimatic impact on the atmosphere associated with the construction of large hydropower plants with storage lakes, to which is added a reduced amount of greenhouse gases, depending on the type of hydropower plant. Added to this is the impact on water courses, through changes in hydro morphological characteristics. Depending on their location, large installations can raise concerns about land degradation, loss of some fertile soils and forests.

Through works for the arrangement of large accumulations that involve deforestation and flooding of land, ecosystem imbalances can occur by modifying the habitats of some animal and fish species. The presence of the dam has influences both on the upstream area, causing the submergence of extensive areas, but also on the downstream areas, destroying the valley forests and pastures. If it is necessary to flood some areas with a special natural, artistic, cultural, historical potential, to the already very high costs of the initial investment will be added substantial additional costs for the displacement of the respective values.

In order to reduce the environmental impact of the hydro power plants a series of solutions have been developed and implemented during the time. Above all. environmental impact assessment is required for each hydropower plant, whether it is new plant projects or existing hydropower plants in operation.

A solution already used in many places around the world is dam removal, in the case of the old dams which need rehabilitation or for the small dams that are no longer used or recorded significant decreases in their reservoir capacity [26].

There are studies that highlight the possibility of reducing the volume of greenhouse gas emissions, the degradation of banks, the phenomenon of erosion, as well as the impact on aquatic and littoral habitats by optimizing the way of managing water from the reservoir in the operation of the hydropower plant.

To ensure the hydrological continuity of the river and not to significantly affect the natural habitat of the various aquatic and coastal species, it is necessary to regulate the minimum flow that must be ensured in the areas where the hydroelectric power station operates.

Petrescu [24] proposes the ecological reconstruction of the affected areas according to European legislation for nature conservation, believing that a solution would consist in renovating the old small hydropower plants, instead of building new ones, which could considerably reduce the impact on the environment.

In this direction, a series of measures can be used: the construction of ladders in the dam, motorized lifts or the implementation of the trap-an-haul solution, for hydropower plants that were not equipped from the beginning with technical solutions to ensure fish migration, removing pollutants from the reservoir, sediment management, design and construction of environmentally friendly turbines, installation of fish screens, implementation of technical solutions for water aeration in the reservoir to ensure water quality, temperature control, design of buildings in a way to integrate into the landscape.

Acknowledgements

This paper was carried out within the project HUSKROUA/1702/6.1/0022 "Regional Center for Training and Monitoring of the Environmental Impact of Electrical Installation" - CRIMIGE, with the financial support of the European Union by Hungary-Slovakia-Romania-Ukraine ENI Cross-border Cooperation Programme 2014-2020.

REFERENCES

[1] D. Antonescu, *Biodiversity of the natural mountains heritage – present challenges and sustainable perspectives*, MPRA Paper No. 84688, posted 20 Feb 2018 06:51 UTC, Online at https://mpra.ub.uni-muenchen.de/84688/, 2018

[2] M. Șteț, *Environmental impact of electricity*, Carpathian Journal of Electrical Engineering (CJEE®), vol. 12, nr. 1, pg. 124-133, 2018. Last accessed on 01.12.2021. Available: http://cee.cunbm.utcluj.ro/wp-content/uploads/carpathian-20189.pdf, 2018

[3] M.R Uscătescu., *Impactul asupra mediului produs de amenajările hidroenergetice de mică putere*, Târgu Jiu. Last accessed on 01.12.2021. Available: www.academia.edu/13308358/impactul_asupra_mediului_produs_de_hidrocentralele_de_mica_putere, 2013

[4] IPCC, *IPCC Special Report on Renewable Energy Sources and Climate Change Mitigation*. Prepared by Working Group III of the Intergovernmental Panel on Climate Change [O. Edenhofer, R. Pichs-Madruga, Y. Sokona, K. Seyboth, P. Matschoss, S. Kadner, T. Zwickel, P. Eickemeier, G. Hansen, S. Schlömer, C. von Stechow (eds)]. Cambridge University Press, Cambridge, United Kingdom and New York, NY, USA, 1075 pp. (Chapter 5 & 9), 2011

[5] M. Istrate, M. Guşă, *Impactul producerii, transportului şi distribuţiei energiei electrice asupra mediului*, Editura AGIR, Bucureşti, 2000

[6] M. Nistorescu, A. Doba, M. Ţîbîrnac, A.A. Nagy, D. Cosmoiu, G.M. Berchi, C. Ilinca, *Ghid de bune practici în vederea planificării şi implementării investiţiilor din sectorul Microhidrocentrale*, Asociaţia ”Grupul Milvus”, 2016

[7] European Anglers Alliance (EAA), *Small scale hydropower - Position paper*, https://www.eaa-europe.org/positions/small-scale-hydropower-2013.html, 2013

[8] Ministerul Mediului și Dezvoltării Durabile MMDD, *Ordin nr. 1.163 din 16 iulie 2007 privind aprobarea unor măsuri pentru îmbunătăţirea soluţiilor tehnice de proiectare şi de realizare a lucrărilor hidrotehnice de amenajare şi reamenajare a cursurilor de apă, pentru atingerea obiectivelor de mediu din domeniul apelor*, Publicat în *Monitorul Oficial* nr. 550 din 13 august 2007

[9] Ministerul Mediului și Pădurilor MMP, *Ordin nr. 799 din 6 februarie 2012 privind aprobarea Normativului de conținut al documentațiilor tehnice de fundamentare necesare obținerii avizului de gospodărire a apelor și a autorizației de gospodărire a apelor*, Publicat în *Monitorul Oficial* nr. 151 din 7 martie 2012

[10] J. Utzinger, C. Roth & A., Peter, *Effects of environmental parameters on the distribution of bullhead Cottus gobio with particular consideration of the effects of obstructions*, Journal of Applied Ecology, 35(6), 882–892, http://doi.org/10.1111/j.1365-2664.1998.tb00006.x, 1998

[11] M. Ovidio, H. Capra, J.C. Philippart, *Field protocol for assessing small obstacles to migration of brown trout Salmo trutta, and European grayling Thymallus thymallus: A contribution to the management of free movement in rivers*, Fisheries Management and Ecology, 14(1), 41–50. http://doi.org/10.1111/j.1365-2400.2006.00522, 2007

[12] Z. Deng, T. J. Carlson, J. P. Duncan, M. C. Richmond, *Six-degree-of-freedom Sensor Fish design and instrumentation*, Sensors, 7:3399–3415, 2007a

[13] C. C. Coutant, R. R. Whitney, *Fish behavior in relation to passage through hydropower turbines: a review*, Transactions of the American Fisheries Society, 129(2):351–380, 2000

[14] Z. Deng, G. R. Guensch, C. A. McKinstry, R. P. Mueller, D. D. Dauble, M. C. Richmond, *Evaluation of fish-injury mechanisms during exposure to turbulent shear flow*. Canadian Journal of Fisheries and Aquatic Sciences, 62(7):1513–1522, 2005

[15] R. S. Brown, B. D. Pflugrath, A. H. Colotelo, C. J. Brauner, T. J. Carlson, Z. D. Deng, A. G. Seaburg, *Pathways of barotrauma in juvenile salmonids exposed to simulated hydroturbine passage: Boyle's law vs. Henry's law*, Fisheries Research, 121: 43–50, 2012

[16] Z.D. Deng, H.A. Colotelo, S.R. Brown, J.T. Carlson, *Environmental issues related to conventional hydropower*, Alternative energy and shale gas encyclopedia / edited by Jay H. Lehr, editor-in-chief ; Jack Keeley, senior editor ; Thomas B Kingery, Information Technology, 2015

[17] S. V. Amaral, S. M. Watson, A. D. Schneider, J. Rackovan, and A. Baumgartner, *Improving survival: injury and mortality of fish struck by blades with slanted, blunt leading edges*, Journal of Ecohydraulics, pp. 1-9, 2020

[18] Z. Deng, T. J. Carlson, G. R. Ploskey, M. C. Richmond and D. D. Dauble, *Evaluation of blade-strike models for estimating the biological performance of Kaplan turbines*, Ecological Modelling 208.2-4 (2007), pp. 165-176, 2007b

[19] G. F. Franke, D. Webb, Jr. R. Fisher., *Development of environmentally advanced hydropower turbine system design concepts*, Tech. rep. Lockheed Idaho Technologies Co., 1997.

[20] G. F. Cada, *The development of advanced hydroelectric turbines to improve fish passage survival*, Fisheries 26.9 (2001), pp. 14-23, 2001

[21] G. F. Cada, L. A. Garrison, R. K. Fisher, *Determining the effect of shear stress on fish mortality during turbine passage*, Hydro Review 26.7 (2007), p. 52, 2007

[22] J.R. Barber, K.R. Crooks, K. Fristrup, *The costs of chronic noise exposure for terrestrial*

organisms, Trends Ecology and Evolution 25(3): 180–189 2010

[23] T.T. Foreman Richard, L.E. Alexander, *Roads and their major ecological effects*, Annual Review of Ecological Systems 29:207-231, 1998

[24] M. Petrescu, *Microhidrocentralele – între foamea de energie și distrugerea mediului*, 17.05.2021, Last accessed on 01.12.2021, Available: www.independentaromana.ro/microhidrocentralele-intre-foamea-de-energie-si-distrugerea-mediului, 2021

[25] M. Şteţ, Y. Adamenko, (coord.), *The environmental impact of the production, transmission, distribution and use of electricity*, Ed. Casa Cărții de Știință, Cluj Napoca, ISBN 978-606-17-1870-2, 226 pg, 2021

[26] M. Mohammed, T. Habtamu, A. Hussein, *Environmental Impacts of Hydropower and Alternative Mitigation Measures*, Curr Inves Agri Curr Res 2(2) - 2018. CIACR.MS.ID.000133. DOI: 10.32474/CIACR.2018.02.000133, 2018

ENHANCEMENT OF THE PREDICTION ACCURACY OF GREY SYSTEM MODEL USING A PARTICLE SWARM OPTIMIZED INITIAL CONDITION

Justice **OHENE-AKOTO**[1], Elvis **TWUMASI** [1], Emmanuel A. **FRIMPONG** [2]

[1] *Department of Electrical and Systems Engineering, University of Pennsylvania, Philadelphia, United States,* [2] *Department of Electrical and Electronic Engineering, Kwame Nkrumah University of Science and Technology Kumasi, Ghana*

justiceakoto8363@gmail.com, etwumasi.coe@knust.edu.gh, eafrimpong.soe@knust.edu.gh

Keywords: Particle, Optimization, Initial condition, prediction, performance.

Abstract*: The grey system model has seen vast application in many fields due to its good accuracy in predicting systems with a limited dataset. In this paper, the prediction accuracy of the traditional grey system model is enhanced using the particle swarm optimization algorithm. The enhancement is mainly the use of PSO to predict an optimum initial condition value based on the input dataset to improve the prediction accuracy of the original grey model that uses the first data of the input dataset as its initial condition. The performance of the enhanced model was tested against the traditional grey model and another model that seeks to enhance the initial condition using the average-minimum-maximum absolute error and the mean absolute percentage error to prove its adaptability. Sample monotonic increasing and decreasing datasets, value of lost load and value of lost load per GDP datasets were used as testing data to prove the accuracy of the proposed model. The proposed model predicted optimum initial condition values of 18.9241, 5.9160, 5.0203 and 3120012789 that resulted in the lowest MAPE OF 0.1798%, 0.1799%, 2.1359% and 11.2813% for the monotonic increasing and decreasing, value of lost load and value of lost load per GDP datasets respectively. It was shown that the proposed model outperforms the traditional grey system model and an improved initial condition model in literature.*

1. INTRODUCTION

In recent years, the grey system model has gained much attention among researchers in performing short-term forecasts because of its efficiency in making accurate inferences from

short-term data [1-3]. The effectiveness of this model has been verified through application to a wide range of real-life problems, including economics, science, and all aspects of engineering [3-7]. The grey system model can understand uncertainties that may arise in a real-life dataset and estimate the future without necessarily modeling each uncertainty. This model has the capability of recognizing, representing, manipulating, interpreting, and utilizing data and information that are vague and lack complete certainty.

Data with few historical variables are primarily challenging to predict [7]. Computational models, statistical models, and fuzzy models always yield high errors when using limited data for prediction because of their dependence on many datasets and the need for the data to satisfy certain assumptions [8-10]. Thus. making meaningful forecasts from imprecise and vague information challenges these models. However, data in real-life systems hardly follow a particular pattern. This puts the grey system model on a level that makes it very important in dealing with grey modeling, grey control, and grey programming [2].

Notwithstanding the advantages of the original grey system model compared to other models, the grey system model suffers from high prediction errors [5,11]. Therefore, many authors have, over the years, tried to overcome these challenges by improving the prediction accuracy of the traditional GM (1,1) by addressing the various parameters that hinder its accuracy in dealing with different data sets. The parameters that affect the prediction precision of the grey model found in the literature are the choice of initial condition value [12], the neglect of the first entry in the prediction [13], and the choice of adjacent neighbor weight [14]. Therefore, many authors have proposed different methodologies to address these challenges. Twumasi et al. [14] used the particle swarm optimization algorithm to choose the optimum adjacent neighbor weight based on the input data to improve the forecasting accuracy of the original grey model. The work in [15] ensured the data utilization efficiency by combining a data grouping technique with modification of the initial condition to establish an optimized grey model. The paper by Tan et al. [16] improved the initial condition for the grey model by using the weighted combination of the latest and oldest components of the original data. Mahdi and Mohamed in [12] have shown that the choice of initial condition value has a high weight in producing accurate forecasts with the grey system model. Their study provided a modified initial condition for the grey system model using a new approach to find the initial condition value. Though these models outperform the original grey model in their prediction, their adaptability on other datasets is low.

This paper seeks to use the particle swarm optimization algorithm to enhance the prediction performance of the traditional grey system model by choosing an optimum initial condition value based on the input dataset to produce accurate predictions. The rest of the paper are arranged in these sections. Section 2 describes the traditional grey system model. Section 3 elaborates the proposed approach in choosing the optimum initial condition and also describes the testing criterion and the type of dataset used. The results and analysis section in section 4 discusses the test results and conclusions are drawn in section 5.

2. GREY SYSTEM MODEL

2.1. The Grey System Model

The Grey system model was developed by Deng Ju-Long in the year 1982 [17]. The model was developed mainly to help improve prediction of limited datasets that come with high level of uncertainty. The model makes prediction by understanding the initial data, and then carry out mathematical modelling on this basis. The mathematical model for the original grey system model is constructed as follows:

Given a non-negative sequence of raw dataset $X^{(0)}(k)$:

$$X^{(0)}(k) = \left(x^{(0)}(1), x^{(0)}(2), \ldots x^{(0)}(n)\right) \tag{1}$$

the accumulated generated sequence, $X^{(1)}(k)$, is given as

$$X^{(1)}(k) = \left(x^{(1)}(1), x^{(1)}(2), \ldots x^{(1)}(n)\right) \tag{2}$$

where:

$$X^{(1)}(k) = \sum_{i=1}^{k} X^{(0)}(k),\ k = 2,3,...,n$$

The background value, $Z^{(1)}(k)$, is calculated using the equation:

$$Z^{(1)}(k) = \left[0.5X^{(1)}(k) + 0.5X^{(1)}(k-1)\right] \quad k = 1,2,3,..., n \tag{3}$$

The basic form of the first-order grey system model GM (1,1) is given by:

$$x^{(1)}(k) + hz^{(1)}(k) = q \tag{4}$$

where h is the development coefficient and q is the grey action quantity.

The whitenization equation 4 is given as:

$$\frac{dX^{(1)}}{dt} + hX^{(1)} = q \tag{5}$$

The coefficients *h* and *q* found using equation 6:

$$[h,q]^T = \left(B^T B\right)^{-1} B^T Y \tag{6}$$

where:

$$Y = \begin{bmatrix} X^{(0)}(1) \\ X^{(0)}(2) \\ . \\ . \\ . \\ X^{(0)}(n) \end{bmatrix} \quad \text{and} \quad B = \begin{bmatrix} -z^{(1)}(2) & 1 \\ -z^{(1)}(3) & 1 \\ . & . \\ . & . \\ . & . \\ -z^{(1)}(n) & 1 \end{bmatrix}.$$

The time response function of the whitenization equation is given by:

$$\hat{X}^{(1)}(t) = \left(x^{(1)}(1) - \tfrac{q}{h}\right)e^{-ht} + \tfrac{q}{h} \tag{7}$$

Therefore, the predicted values of the sequence of the model can be found using equation:

$$\hat{X}^{(0)}(k+1) = \hat{X}^{(1)}(k+1) - \hat{X}^{(1)}(k) \tag{8}$$

Thus,

$$\hat{X}^{(0)}(k+1) = \left(1 - e^{h}\right)\left(C - \tfrac{q}{h}\right)e^{-hk} \tag{9}$$

where C is the initial condition value.

3. PROPOSED ENHANCED GREY SYSTEM MODEL USING PSO OPTIMIZED INITIAL CONDITION

In this study, the particle swarm optimization (PSO) algorithm was used to augment the traditional grey system model, GM(1,1) by choosing an optimum initial condition value to increase its prediction accuracy. The original GM(1,1) takes the first value of the input data set as the initial condition for prediction, however, the proposed model in this work searches for

the optimum value of the initial condition of the response function of the whitezination equation of the classical GM(1,1) based on the given data set using the particle swarm optimization algorithm. The main area this paper contributes to existing knowledge is the unique approach in finding an optimum initial condition for the input historical dataset. The objective function for the selection of the optimum initial condition value was formulated by writing the time response function of the whitenization equation in terms of the initial condition (C). This was done by first multiplying $B^T B$ and $B^T Y$ to get a 2 by 1 matrix shown in equation 10.

$$\left[h,q\right]^T = \left(B^T B\right)^{-1} B^T Y = \begin{bmatrix} \dfrac{\sum_{k=2}^{n} Z^{(1)}(k) \sum_{k=2}^{n} X^{(0)}(k) - (n-1) \sum_{k=2}^{n} Z^{(1)}(k) X^{(0)}(k)}{(n-1) \sum_{k=2}^{n} \left(-Z^{(1)}(k)\right)^2 - \left(\sum_{k=2}^{n} Z^{(1)}(k)\right)^2} \\ \dfrac{\sum_{k=2}^{n} Z^{(1)}(k)^2 \sum_{k=2}^{n} X^{(0)}(k) - \sum_{k=2}^{n} Z^{(1)}(k) X^{(0)}(k) \sum_{k=2}^{n} Z^{(1)}(k)}{(n-1) \sum_{k=2}^{n} \left(Z^{(1)}(k)\right)^2 - \left[\sum_{k=2}^{n} Z^{(1)}(k)\right]^2} \end{bmatrix} \tag{10}$$

Hence, substituting for *h* and *q* into the response function of the whitenization equation (9):

$$\hat{X}^{(0)}\left(k+1\right) = \left(1 - e^{\frac{\sum_{k=2}^{n} Z^{(1)}(k) \sum_{k=2}^{n} X^{(0)}(k) - (n-1) \sum_{k=2}^{n} Z^{(1)}(k) X^{(0)}(k)}{(n-1) \sum_{k=2}^{n} \left(-Z^{(1)}(k)\right)^2 - \left(\sum_{k=2}^{n} Z^{(1)}(k)\right)^2}}\right) \times \left(C - \frac{\frac{\sum_{k=2}^{n} Z^{(1)}(k)^2 \sum_{k=2}^{n} X^{(0)}(k) - \sum_{k=2}^{n} Z^{(1)}(k) X^{(0)}(k) \sum_{k=2}^{n} Z^{(1)}(k)}{(n-1) \sum_{k=2}^{n} \left(Z^{(1)}(k)\right)^2 - \left[\sum_{k=2}^{n} Z^{(1)}(k)\right]^2}}{\frac{\sum_{k=2}^{n} Z^{(1)}(k) \sum_{k=2}^{n} X^{(0)}(k) - (n-1) \sum_{k=2}^{n} Z^{(1)}(k) X^{(0)}(k)}{(n-1) \sum_{k=2}^{n} \left(-Z^{(1)}(k)\right)^2 - \left(\sum_{k=2}^{n} Z^{(1)}(k)\right)^2}}\right) \times e^{-\left(\frac{\sum_{k=2}^{n} Z^{(1)}(k) \sum_{k=2}^{n} X^{(0)}(k) - (n-1) \sum_{k=2}^{n} Z^{(1)}(k) X^{(0)}(k)}{(n-1) \sum_{k=2}^{n} \left(-Z^{(1)}(k)\right)^2 - \left(\sum_{k=2}^{n} Z^{(1)}(k)\right)^2}\right) k} \tag{11}$$

The first value of the input data used as the initial condition value $X^0(1)$ is replaced with a variable C. The objective function, *f(c)* for the PSO optimum search is given by the sum of squared errors shown in (11).

$$f=\sum_{k=1}^{n}\left(\begin{array}{l}\left(X^{(0)}(k)\right)-\left(1-e^{\frac{\sum_{k=2}^{n}Z^{(1)}(k)\sum_{k=2}^{n}X^{(0)}(k)-(n-1)\sum_{k=2}^{n}Z^{(1)}(k)X^{(0)}(k)}{(n-1)\sum_{k=2}^{n}\left(-Z^{(1)}(k)\right)^{2}-\left(\sum_{k=2}^{n}Z^{(1)}(k)\right)^{2}}}\right)\times \\ \left(C-\frac{\frac{\sum_{k=2}^{n}Z^{(1)}(k)^{2}\sum_{k=2}^{n}X^{(0)}(k)-\sum_{k=2}^{n}Z^{(1)}(k)X^{(0)}(k)\sum_{k=2}^{n}Z^{(1)}(k)}{(n-1)\sum_{k=2}^{n}\left(Z^{(1)}(k)\right)^{2}-\left[\sum_{k=2}^{n}Z^{(1)}(k)\right]^{2}}}{\frac{\sum_{k=2}^{n}Z^{(1)}(k)\sum_{k=2}^{n}X^{(0)}(k)-(n-1)\sum_{k=2}^{n}Z^{(1)}(k)X^{(0)}(k)}{(n-1)\sum_{k=2}^{n}\left(-Z^{(1)}(k)\right)^{2}-\left(\sum_{k=2}^{n}Z^{(1)}(k)\right)^{2}}}\right)\times \\ e^{-\left(\frac{\sum_{k=2}^{n}Z^{(1)}(k)\sum_{k=2}^{n}X^{(0)}(k)-(n-1)\sum_{k=2}^{n}Z^{(1)}(k)X^{(0)}(k)}{(n-1)\sum_{k=2}^{n}\left(-Z^{(1)}(k)\right)^{2}-\left(\sum_{k=2}^{n}Z^{(1)}(k)\right)^{2}}\right)k}\end{array}\right)^{2},\quad k=1,2,3,\ldots,n \tag{12}$$

3.1. Testing Criterion

To validate the proposed PSOOIC GM (1,1), sets of randomly generated monotonic increasing and monotonic decreasing data and two actual datasets were used. The monotonic data was used because it is easier to identify outliers or anomalies that may affect the accuracy of any developed prediction model. Sample monotonic sets for testing improved grey system model accuracy are shown in [14]. In this paper, monotonic increasing and decreasing data were generated using equations 13 and 14, respectively.

$$x(t) = 10e^{t} \qquad t = 1, 2, 3\ldots\ldots\ldots\ldots\ldots \text{ n} \tag{13}$$

$$x(t) = 10e^{-t} \qquad t = 1, 2, 3\ldots\ldots\ldots\ldots\ldots \text{ n} \tag{14}$$

Also, two sets of actual data were used because real-life data reflects the real-world conditions under which the model will be used, provides a more accurate assessment of a model's performance, helps to identify weaknesses, proves the model's credibility, and checks its applicability. For the real datasets, the yearly value of lost load (VoLL) (a measure of the economic cost of power outages) and the value of lost load per GDP (VoLL/GDP) from 2016 to 2019 for the Ghana power system using dependency factor, value-added, and electricity consumption data for the residential, commercial, and industrial sectors. The dependency factor was determined using a limited customer survey. The value-added and electricity consumption data were collected from the Ghana statistical service, the technical utility-regulatory company, and the Energy Commission of Ghana [18,19]. The GDP data was collected from the Bank of

Ghana [20]. The composite VoLL used as the input dataset was the sum of the individual sector VoLL and the VoLL per GDP was the ratio of the yearly VoLL to the yearly GDP.

The performance of the improved model to predict the four data sets was assessed using the maximum average percentage error (MAPE) and the average minimum, maximum absolute error chart in excel. The MAPE is shown in equation 15 below

$$MAPE = \frac{1}{2}\sum_{i=1}^{k}\frac{\left|x_p^0(k) - x^0(k)\right|}{x^0(k)} \times 100\% \tag{15}$$

4. RESULTS AND ANALYSIS

From Table 1 the proposed PSOOIC predicted an optimized initial condition value of 18.9241 and this gave the best prediction as compared to the traditional grey system model and an improved initial condition approach model in [12]. The original grey system model would have chosen a value of 16.4872 as the initial condition of the response function of the whitenization equation of the model which represents the first value of the monotonic decreasing data. The fig 1 shows the average, maximum and minimum chart (Average-Max-Min chart) which displays the average, maximum, and minimum absolute error values where the average is plotted with greater importance. From *fig. 1* the predictions from the proposed PSO optimized initial condition (PSOOIC), had the best average absolute error value of 1.0375 as compared to the Original Grey and Improved IC in [12] with values of 5.5011 and 1.0933 respectively. This leverage that the initial condition value is an important parameter in the traditional grey system model. Though the improved IC in [12] had a good minimum and maximum absolute error, the overall performance of the proposed PSOOIC was better on the monotonic decreasing data. Also, the overall mean absolute percentage error (MAPE) in fig 2 revealed that the PSOOIC had the lowest percentage error value compared to the improved IC in [12] and the grey system model. While the proposed model gave an MAPE of 0.1798%, the improved model in [12] and the original grey system model gave MAPE of 0.2108% and 0.8779% respectively.

Table 1. Prediction of monotonic increasing data

Actual Data	Original Grey	Improved IC in [12]	Optimum C	PSOOIC GM(1,1)
16.4872	16.2276	17.3466	18.9241	17.1714
27.1828	26.4843	28.3106		28.0245
44.8169	43.2237	46.2043		45.7375
73.8906	70.5433	75.4078		74.6468
121.8249	115.1302	123.0693		121.8258
200.8554	187.8983	200.8554		198.8259

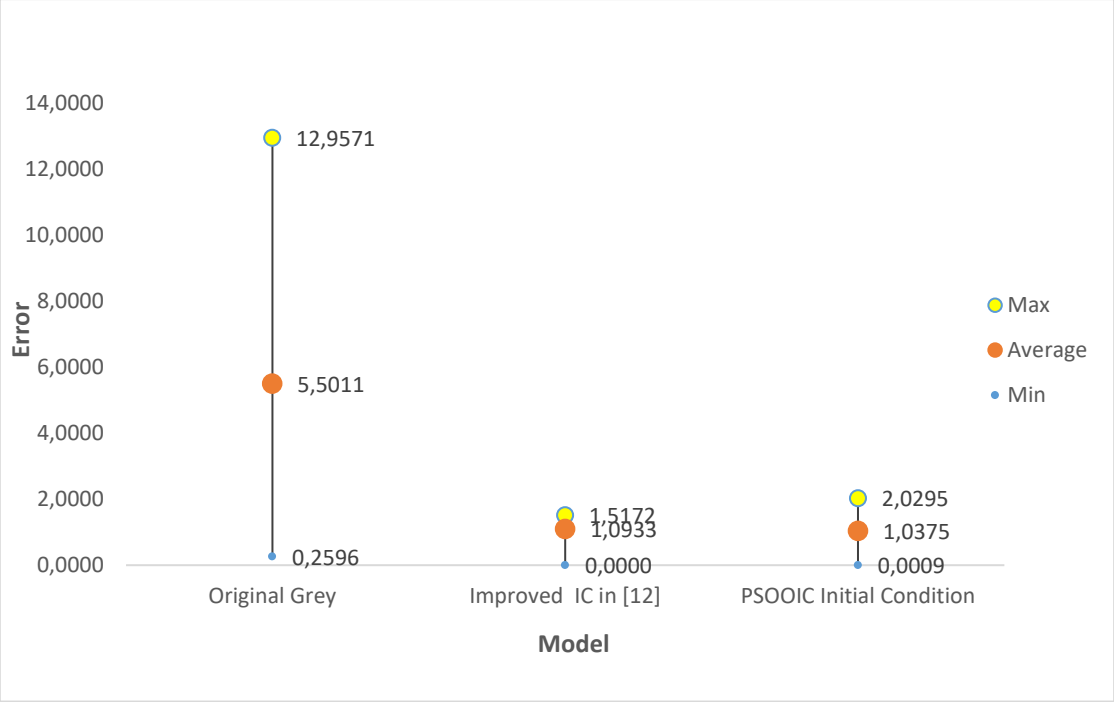

Fig. 1. Average-Max-Min chart of monotonic increasing data

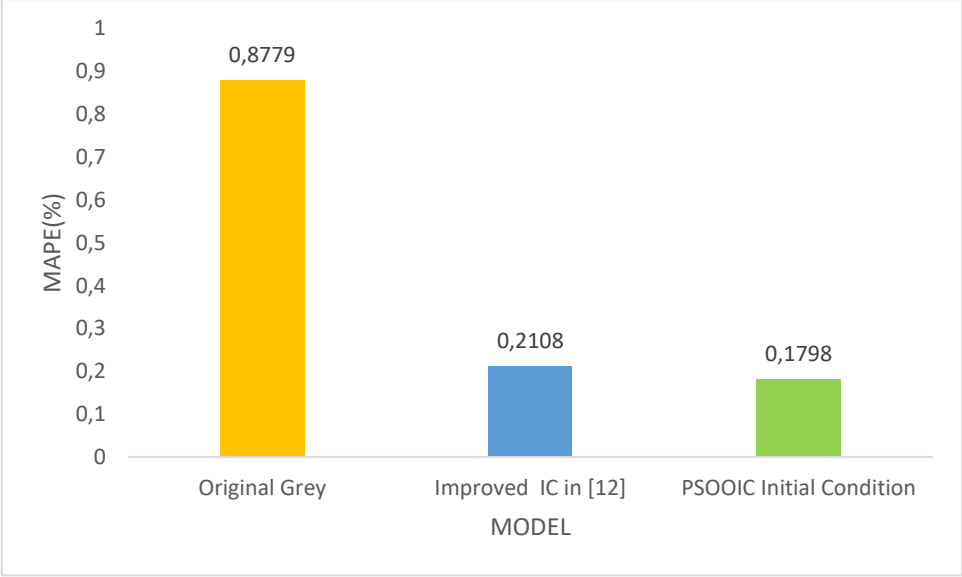

Fig. 2. Mean absolute percentage error of monotonic increasing data

Table 2 shows the prediction of the proposed PSOOIC, improved IC model [12] and the original grey model. The optimum initial condition value of the input data was found to be 5.916. The PSOOIC in *fig. 3* had a lower Maximum and Average Absolute Error of 0.0616 and 0.0263 respectively as compared to the higher values of the Maximum and Average Absolute Error of the original Grey and Improved IC model in [12]. However, the Minimum Absolute Error of the Improved IC in [12] had no forecast error. This notwithstanding the overall performance of the models assessed using the MAPE shown in *figure 4* depicts a better prediction accuracy.

Table 2. Prediction of monotonic decreasing data

Actual Data	Original Grey	Initial Condition	Optimum C	Optimized Initial Condition
6.0653	5.9094	5.7651	5.9160	6.0037
3.6788	3.6209	3.5324		3.6787
2.2313	2.2186	2.1644		2.2540
1.3534	1.3594	1.3262		1.3811
0.8208	0.8329	0.8126		0.8462
0.4979	0.5104	0.4979		0.5185

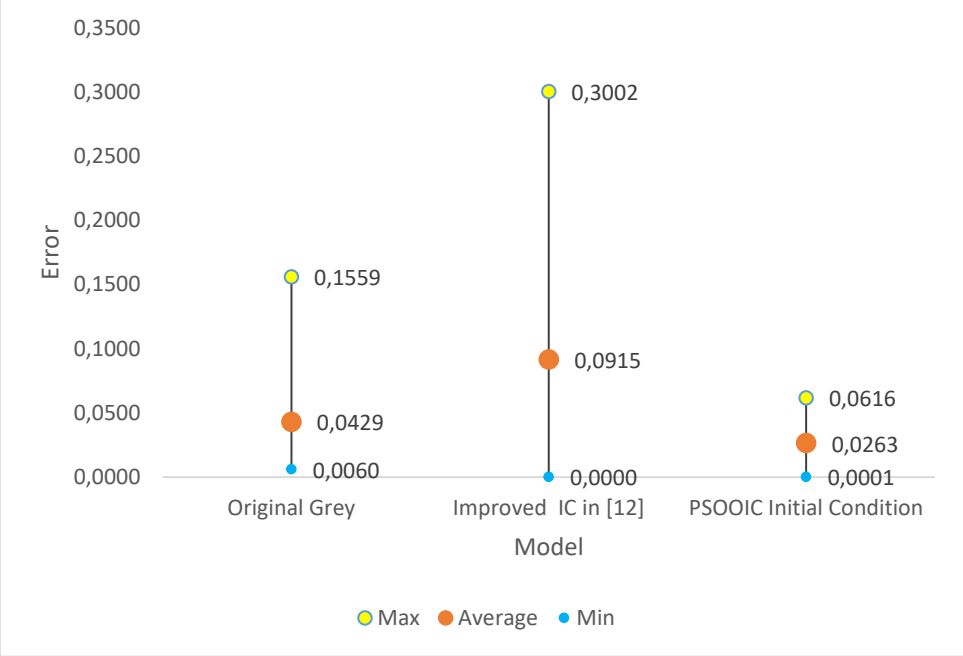

Fig. 3. Average-Max-Min chart of monotonic decreasing data

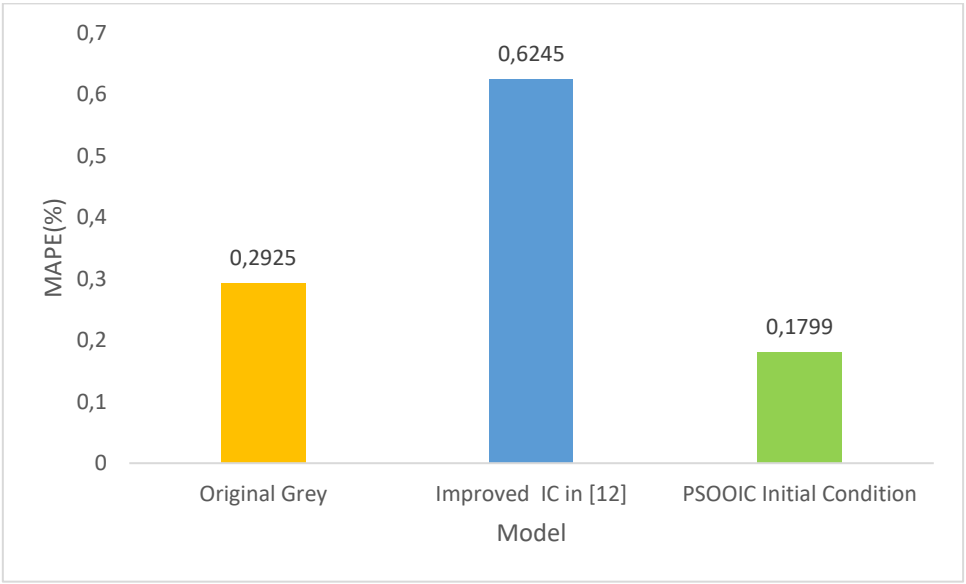

Fig. 4. Mean absolute percentage error of monotonic decreasing data

From table 3 the PSOOIC shows a good prediction when the initial condition value was chosen as 5.0203. This value was realized to be an optimum value that resulted in the wide gap in prediction accuracy between the PSOOIC and the model that tend to improve the initial condition in [12]. The proposed model also outperformed the original grey model; however, the original grey also outperformed the improved model in [12]. It is shown in *figure 5* that the maximum absolute error and the average absolute error of the PSOOIC were 0.4371 and 0.2369 respectively and they were lower than that of the original grey model and improved IC in [12]. The maximum absolute error and the average absolute error of the original grey were 0.6340 and 0.2869 respectively.

From *fig. 6*, it is observed that the degree of deviation of the predicted values of the PSOOIC is smaller than that of the Original Grey and Improved IC in [12] models. The MAPE of PSOOIC was the lowest value of 2.1359%, slightly lower than the Original Grey model with 2.587%, indicating a better forecast. In this VoLL per GDP dataset, the original grey model performed better than the improved IC model in [12] since its MAPE is 4.0876%. This shows that the proposed PSOOIC is a better-improved model for prediction.

Table 3. Value of lost load per GDP

VoLL per GDP	Original Grey	Initial Condition	Optimum C	Optimized Initial Condition
3.9250	4.5590	5.0431	5.0203	4.1041
3.3370	3.2213	3.5634		2.8999
2.0490	2.2761	2.5178		2.0490
1.7790	1.6082	1.7790		1.4478

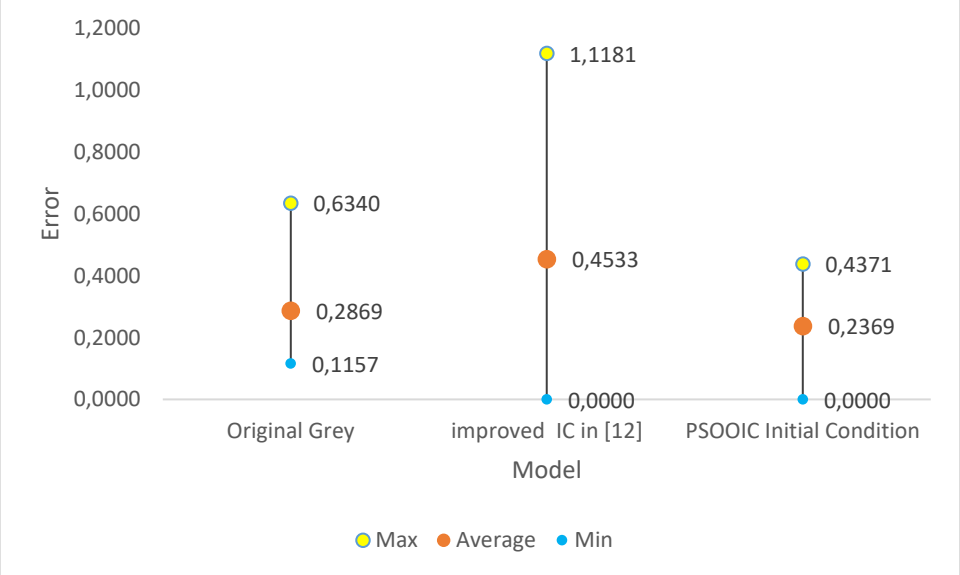

Fig. 5. Average-Max-Min chart of value of lost load per GDP data

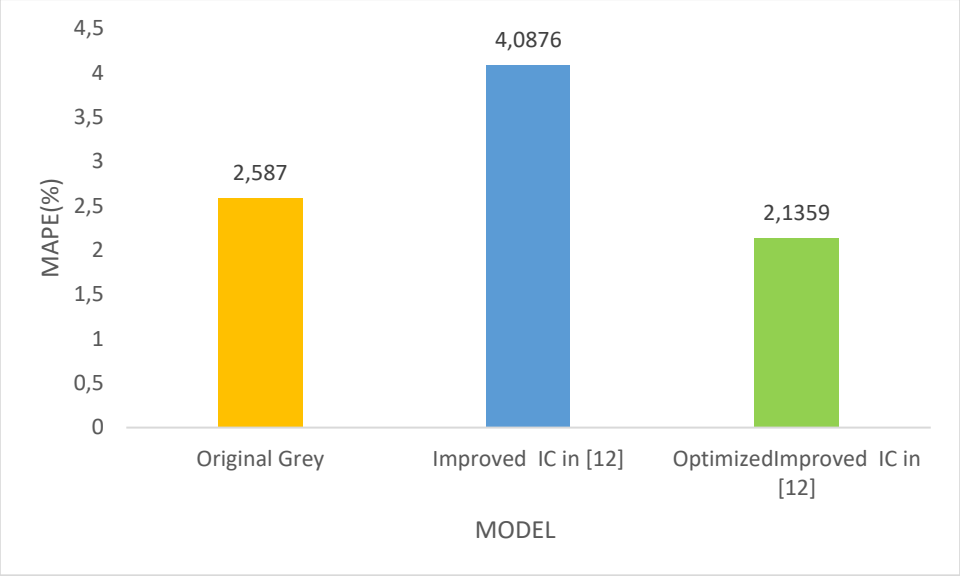

Fig. 6. Mean absolute percentage error of value of lost load per GDP data

It is shown in table 4 that the prediction values provided by the improved model in [12] deviated greatly from the Actual data. This shows that the proposed model and the original grey model performed better than the improved model in [12]. However, the predictions of the proposed PSOIC GM (1,1) that chose an optimum initial condition value outperformed the classical grey model. With a maximum absolute error value of $1.67x10^9$ and an average absolute error of $8.68x10^8$, as shown in fig 7, the performance of the improved initial condition in [12] compared with the original grey system model and the proposed model can be seen to be very poor. Considering the model that sought to improve the initial condition value in [12], a better minimum absolute error was observed in fig 7 compared to the proposed PSOOIC and the traditional grey system model. This depicts that the strength of the improved model in [12] always gives a better minimum absolute error. However, the maximum absolute error and the average absolute error of the PSOOIC give the lowest values of $1.40x10^9$ and $7.50x10^{9,}$ respectively. Moreover, the overall MAPE of the PSOOIC had the smallest value, as shown in fig 8, depicting a better prediction accuracy. From fig 8, the PSOOIC had the smallest value of MAPE (11.2813%) in comparison to Original Grey (12.8168%) and Improved in IC [12] (13.0617%), making the PSOOIC a better model due to its low MAPE that strengthens its predictive precision ability.

Table 4. Prediction of value of lost load

VoLL (Dollars)	Original Grey	Initial Condition	Optimum C	Optimized Initial Condition
2.170×10^9	0.5326×10^9	0.4954×10^9	3120012789	0.7657×10^9
1.981×10^9	0.7058×10^9	0.6565×10^9		1.0148×10^9
1.3445×10^9	0.9354×10^9	0.8700×10^9		1.3449×10^9
1.153×10^9	1.2396×10^9	1.1530×10^9		1.7823×10^9

Fig. 7. Average-Max-Min chart of value of lost load

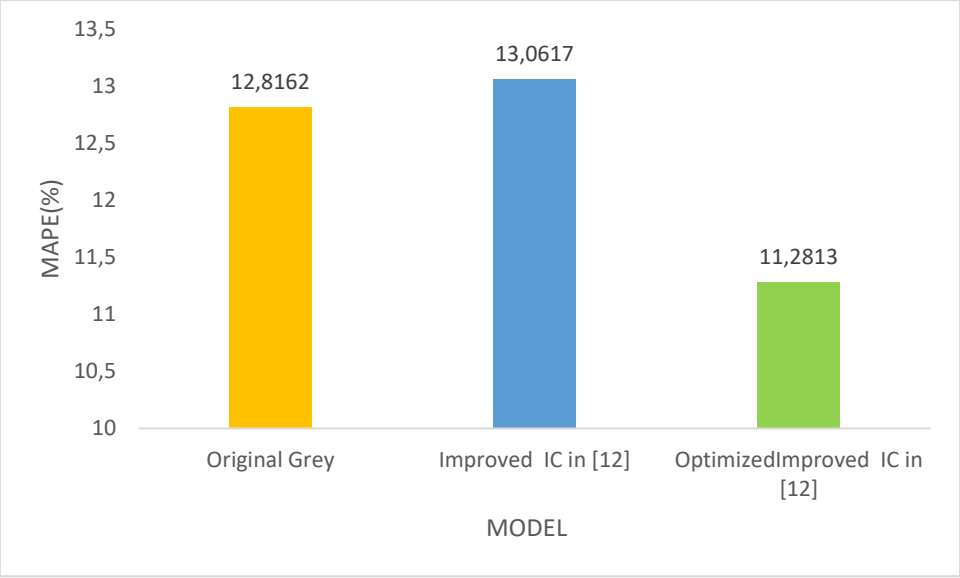

Fig. 8. Mean absolute percentage error of value of loss load data

5. CONCLUSION

In this paper enhanced model of the grey system model has been proposed. This model chooses an optimum initial condition value from the input data using the particle swarm optimization algorithm. The optimum initial condition chosen becomes the initial condition value for the response function of the whitenization equation of the original grey system model which uses the first input of the input data. The accuracy of the proposed model was tested using a generated monotonic increasing and decreasing data, value of lost load and value of lost load per GDP. The proposed PSOOIC had the best performance as compared to the traditional

grey system model and a model that also improved the initial condition. The results showed that the enhanced model using the PSO to choose an optimum initial condition is a better modification of the grey system model.

REFERENCES

[1] B. Zeng, W. Zhou, M. Zhou, *Forecasting the concentration of sulfur dioxide in Beijing using a novel grey interval model with oscillation sequence*, Journal of Cleaner Production, 311, p.127500, 2021.

[2] I. Raheem, N. M. Mubarak, R. R. Karri, T. Manoj, S. M. Ibrahim, S. A. Mazari, S. Nizamuddin, *Forecasting of energy consumption by G20 countries using an adjacent accumulation grey mode*, Scientific Reports, 12(1), pp.1-23, 2022.

[3] S. A. Javed, B. Zhu, S. Liu, *Forecast of biofuel production and consumption in top CO2 emitting countries using a novel grey model*, J. Clean. Prod. 276, 123997, 2020.

[4] B. Li, S. Zhang, W. Li, Y. Zhang, *Application progress of grey model technology in agricultural science*, Grey Systems: Theory and Application, 2022.

[5] K. Li, T. Zhang, *Forecasting electricity consumption using an improved grey prediction model*, Information, 9(8), p.204, 2018.

[6] L. Xuemei, Y. Cao, J. Wang, Y. Dang, Y. Kedong, *A summary of grey forecasting and relational models and its applications in marine economics and management*, Marine economics and management, 2019.

[7] D. Camelia, *Grey systems theory in economics–a historical applications review*, Grey Systems: Theory and Application, 2015.

[8] G. He, K., Mutahir Ahmad, W. Yu, X. Xu, J. Kumar, *A Comparative Analysis of Machine Learning and Grey Models*, arXiv e-prints, pp.arXiv-2104, 2021.

[9] L. Palomero, V. García, J. S. Sánchez, *Fuzzy-Based Time Series Forecasting and Modelling: A Bibliometric Analysis*, Applied Sciences, 12(14), p.6894, 2022.

[10] S. S. Henley, R. M. Golden, T. M. Kashner, *Statistical modeling methods: challenges and strategies*, Biostatistics & Epidemiology, 4(1), pp.105-139, 2020.

[11] E. Twumasi, E. A. Frimpong, D. Kwegire, D. Folits, *Improvement of grey system model using particle swarm optimization*, In: Proceedings of IEEE PES/IAS PowerAfrica, September 2020, pp 1–5, 2020.

[12] M. H. Madhi, N. Mohamed, *An initial condition optimization approach for improving the prediction precision of a GM (1,1) model*, Math Comput Appl 22:21, 2017.

[13] T.L. Tien, *A new grey prediction model FGM (1, 1). Mathematical and Computer Modelling*, 49(7-8), pp.1416-1426, 2009.

[14] E. Twumasi, E. A. Frimpong, D. Kwegyir, D. Folitse, *Improvement of gray system model using particle swarm optimization*, Journal of Electrical Systems and Information Technology, 8(1), pp.1-15, 2021.

[15] V. B. Getanda, P. K. Kihato, P. K. Hinga, H. Oya, *Data grouping and modified initial condition in grey model improvement for short-term traffic flow forecasting*, Automatika, pp.1-11, 2022.

[16] X. Tan, J. Xu, F. Li, M. Wu, D. Chen, Y. Liang, *Improved GM (1, 1) Model by Optimizing Initial Condition to Predict Satellite Clock Bias*, Mathematical Problems in Engineering, 2022.

[17] S. Liu, J. Forrest, Y. Yang, *A brief introduction to grey systems theory*. In Proceedings of 2011 IEEE International Conference on Grey Systems and Intelligent Services (pp. 1-9). IEEE, September 2011.

[18] Ghana Statistical Service, https://www.statsghana.gov.gh/gdpgraph.php?graphindicators=MTE4NzYxMzkxNi45NDI1/gpdgraph/49pp7266p8

[19] Energy Commission of Ghana, '2020 Energy Statistics', 2020

[20] Bank of Ghana, 'www.bog.gov.gh/economic-data/real-sector/'.

INSTRUCTIONS FOR AUTHORS

Name **SURNAME**[1], Name **SURNAME**[2], **...**

[1] *Affiliation of 1st author,* [2] *Affiliation of 2nd author, ...*

Email of 1st author, Email of 2nd author, ...(it is compulsory only for the first author)

Keywords: List 3-4 keywords *(aligned to the left, 10 pt. bold, separated by commas; please choose keywords from IEEE Approved Indexing Keyword List)*

Abstract: *Abstract of max. 200 words, justify, 10 pt. italic.*

1. INTRODUCTION

The paper must be written in English. It shall contain at least the following chapters: introduction, research course (mathematical algorithm); method used; results and conclusions, references.

1.1. Fonts

Use DIN A4 Format (297 x 210 mm) MSWord format. Margins: top, bottom, left and right 2.5 mm each. The text should be written on one side of the page only. Use Times New Roman fonts, line spacing 1.3. The font formats are: paper title: 14 pt, bold, italic, capital letters, author's name(s): 12 pt, regular for name and 12 pt., bold, for surname; Affiliation: 11 pt., italic; key words: 10 pt., bold; Abstract: 10 pt., italic, word Abstract in 10 pt., bold; chapter titles (do not use automatic numbering): 12 pt., bold, capital letters; subtitles: 12 pt., bold, lower case letters; subsubtitles: 12 pt., italic, lower case letters; body text: 12 pt., regular; tables and figures caption: 11 pt.; italic; references: author 11 pt.; regular, title 11 pt. italic, year, pages, ... in regular.

1.1.1. Number of pages

The number of pages is not restricted.

2. FIGURES AND TABLES

Figures have to be made in high quality, which is suitable for reproduction and printing. Don't include photos or color prints if there are not clearly intelligible in gray scale option. Place figures and tables at the top or bottom of a page wherever possible, as close as possible to the first reference to them in the paper. In text, use either *fig. 1* or *figure 1* when necessarily.

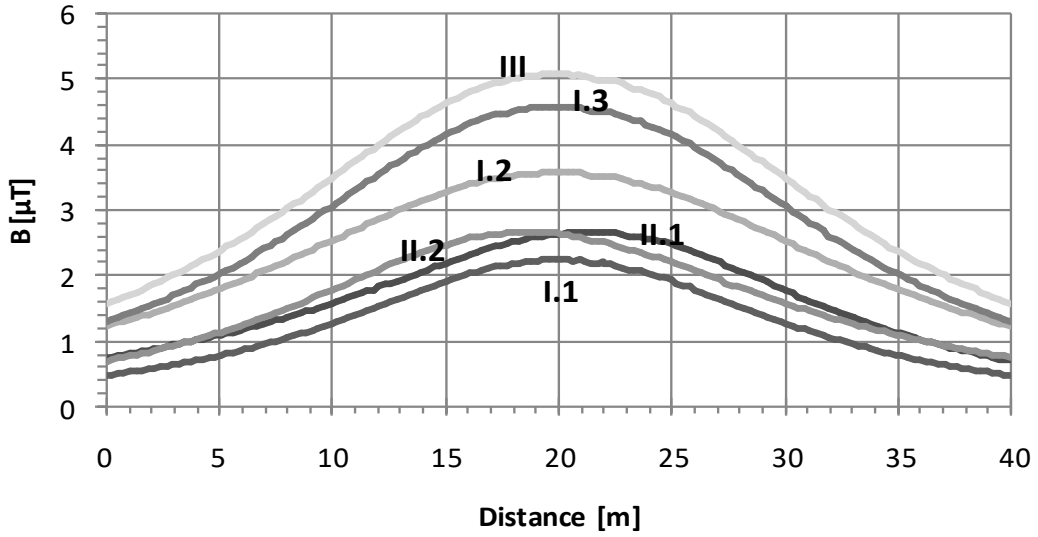

Fig. 1. Magnetic flux density at 1 m above the ground

Table 1. Transposing principle

	Circuit											
	1	*2*	*1*	*2*	*1*	*2*	*1*	*2*	*1*	*2*	***1***	***2***
1/3	*R*	*T*	***R***	***R***	*R*	*S*	*R*	*T*	*R*	*S*	***R***	***R***
line	***S***	***S***	*S*	*T*	*S*	*R*	*S*	*R*	*S*	*T*	***S***	***S***
length	*T*	*R*	*T*	*S*	***T***	***T***	*T*	*S*	*T*	*R*	***T***	***T***
1/3	*T*	*S*	***T***	***T***	*T*	*R*	*T*	*S*	*T*	*R*	***T***	***T***
line	***R***	***R***	*R*	*S*	*R*	*T*	*R*	*T*	*R*	*S*	***R***	***R***
length	*S*	*T*	*S*	*R*	***S***	***S***	*S*	*R*	*S*	*T*	***S***	***S***
1/3	*S*	*R*	***S***	***S***	*S*	*T*	*S*	*R*	*S*	*T*	***S***	***S***
line	***T***	***T***	*T*	*S*	*T*	*S*	*T*	*S*	*T*	*R*	***T***	***T***
length	*R*	*S*	*R*	*T*	***R***	***R***	*R*	*T*	*R*	*S*	***R***	***R***
Name	***I.1***		***I.2***		***I.3***		***II.1***		***II.2***		***III***	

3. EQUATIONS

Equations are centered on page and are numbered in round parentheses, flush to right margin.

$$a = b + c \tag{1}$$

Between equations, not interfered by text, there is only one empty line:

$$a = b + c \tag{2}$$

$$a = b + c \tag{3}$$

In text respect the following rules: all variables are italic, constants are regular; the references are cited in the text between right parentheses [1], the list of references has to be arranged in order of citation.

REFERENCES

[1] International Commission on Non-ionizing Radiation Protection, *Guidelines for limiting exposure to time-varying electric, magnetic and electromagnetic fields (Up to 300 GHz)*, Health Physics, vol. 74, no. 1, pp. 494-522, 1998.

[2] A. Marincu, M. Greconici, *The electromagnetic field around a high voltage 110 KV electrical overhead lines and the influence on the biological systems*, Proceedings of the 5th International Power Systems Conference, pp. 357-362, Timisoara, Romania, 2003.

[3] J. He, R. Zeng, B. Zhang, Methodology and Technology for Power System Grounding, Wiley-IEEE Press, Singapore, 2012.

8th International Conference

INNOVATIVE IDEAS IN SCIENCE 2022

3-4th November 2022, Baia Mare, Romania

Selected papers by the IIS Scientific Committee

Organizer:

Technical University of Cluj Napoca, Romaniamania
Faculty of Engineering, Department of Electrical Engineering, Electronics and Computers

Co-organizer:
Independent University Banja Luka, Bosnia and Herzegovina
University of Applied Sciences Kempten, Germany

Sponsored by:

Academic Organization for Research, Innovation and Professional Development

IIS CONFERENCE COORDINATOR

Cristian BARZ, Technical University of Cluj-Napoca, Romania
Vesna RODIC, Independent University Banja Luka, Bosnia and Herzegovina

IIS ORGANIZING COMMITTEE

Zoltan ERDEI, Technical University of Cluj-Napoca, Romania
Claudiu LUNG, Technical University of Cluj-Napoca, Romania
Mircea HORGOȘ, Technical University of Cluj-Napoca, Romania
Mirela ILIA, SC FDEE Electrica Distributie Transilvania Nord SA, Romania
Olivian CHIVER, Technical University of Cluj-Napoca, Romania
Ramona DEMARCSEK, Tehnical University of Cluj Napoca, Romania
Domide GHERASIM, Technical University of Cluj-Napoca, Romania
Radmila ČOKORILO, Independent University Banja Luka, Bosnia and Herzegovina
Kristina KUZMANOVIĆ, Independent University Banja Luka, Bosnia and Herzegovina
Goran KALINIĆ, Independent University Banja Luka, Bosnia and Herzegovina
Vladan MIHAJLOVIĆ, Independent University Banja Luka, Bosnia and Herzegovina

IIS SCIENTIFIC COMMITTEE COORDINATOR

Zoran KALINIĆ, Independent University Banja Luka, Bosnia and Herzegovina
Vasile TOPA, Technical University of Cluj-Napoca, Romania
Ludovic Dan LEMLE, "Politehnica" University of Timisoara, Romania

IIS SCIENTIFIC COMMITTEE

Petrică POP SITAR, Technical University of Cluj-Napoca, Romania
Gabor SZIEBIG, The Arctic University of Norway, Norway
Luigi VLĂDĂREANU, Romanian Academy - Institute of Solid Mechanics, Romania
Doina PISLA, Technical University of Cluj-Napoca, Romania
Blanusa BRANKO, University in Banja Luka, Bosnia and Herzegovina
Razzaghi MOHSEN, Mississippi State University, USA
Silviu Dan MANDRU, Technical University of Cluj-Napoca, Romania
Nicolae POP, Romanian Academy - Institute of Solid Mechanics, Romania
Radu Adrian TIRNOVAN, Technical University of Cluj-Napoca, Romania
Parimal ACHARJEE, National Institute of Technology Durgapur, India
Lesya SHKITSA, Ivano-Frankivsk National Technical University of Oil and Gas, Ukraine
Dorin Dumitru LUCACHE, "Gheorghe Asachi" Technical University of Iasi, Romania

Predrag Miodrag ŽIVKOVIĆ, University of Niš, Serbia
Vasile NĂSUI, Technical University of Cluj-Napoca, Romania
Rolf JUNG, University of Applied Sciences Kempten, Germany
Marian POBORONIUC, "Gheorghe Asachi" Technical University of Iasi, Romania
Nicolae UNGUREANU, Technical University of Cluj-Napoca, Romania
Sorin DEACONU, "Politehnica" University of Timisoara, Romania
Mihai BĂNICĂ, Technical University of Cluj-Napoca, Romania
Mihai ALBU, "Gheorghe Asachi" Technical University of Iasi, Romania
Mirjana STOJANOVIC-TRIVANOVIC, Independence University Banja Luka, Bosnia and Herzegovina
Cristiana ISTRATE, "Gheorghe Asachi" Technical University of Iasi, Romania
Marius Calin BENEA, “Politehnica” University of Timişoara, Romania
Marius PISLARU, "Gheorghe Asachi" Technical University of Iasi, Romania
Cristian BARZ, Technical University of Cluj-Napoca, Romania
Tihomir Savo LATINOVIC, University in Banja Luka, Bosnia and Herzegovina
Miorita UNGUREANU, Technical University of Cluj-Napoca, Romania
Saša SALAPURA, University of Business Engineering and Management - Banja Luka, Bosnia and Herzegovina
Marijana Žiravac MLADNEOVIĆ, University of Business Engineering and Management - Banja Luka, Bosnia and Herzegovina
Nikola VOJVODIĆ, University of Business Engineering and Management - Banja Luka, Bosnia and Herzegovina
Anamaria DĂSCĂLESCU, Technical University of Cluj-Napoca, Romania
Przemysław SYREK, AGH University of Science and Technology, Krakow, Poland
Ružica ĐERVIDA, Independent University Banja Luka, Bosnia and Herzegovina
Ljubomir ZUBER, Independent University Banja Luka, Bosnia and Herzegovina
Srđan LJUBOJEVIĆ, Independent University Banja Luka, Bosnia and Herzegovina
Borka VUKAJLOVIĆ, Independent University Banja Luka, Bosnia and Herzegovina
Mladen BUBONJIĆ, Independent University Banja Luka, Bosnia and Herzegovina
Nikola VOJVODIĆ, Independent University Banja Luka, Bosnia and Herzegovina
Marius BENEA, Independent University Banja Luka, Bosnia and Herzegovina
Laura BENEA, Independent University Banja Luka, Bosnia and Herzegovina
Dragana PRERADOVIĆ, University of Banja Luka, Bosnia and Herzegovinaf
Dragana DIMITRIJEVIĆ, University of Niš, Serbia
Vesna RODIC, Independent University Banja Luka, Bosnia and Herzegovina
Mihaela POPA, "Politehnica" University of Timisoara, Romania

STUDY OF ELECTRIC VEHICLES WITH ADVISOR

Olivian **CHIVER**, Liviu **NEAMT,** Mircea **HORGOS**
Technical University of Cluj-Napoca, Electrical, Electronic and Computer Engineering Department, Romania
olivian.chiver@ieec.utcluj.ro

Keywords: ADVISOR, simulation, electric, vehicle

Abstract*: The main paper's purpose is to present how students and researchers can use the ADVISOR software in the design and simulation of electric vehicles. Not only electric vehicles but also hybrid, fuel-cell, or internal combustion engine vehicles can be simulated, this paper refers only to the former. Starting with the principal electric vehicle components such as the energy storage system and the electric motor, the user can choose them from the existing ones in the library or can compose/define new others. The software allows imposing different driving cycles (choosing from the library or user-defined) and calculates selected performances of the vehicle based on the simulation. Should emphasize the eloquent way of ADVISOR in presenting the results on the energy consumption of the main components as well as of the entire vehicle. Thus, it is easy to find how certain equipment affects the overall efficiency of the electric vehicle.*

1. INTRODUCTION

In recent years, one of the solutions to reduce the high level of air pollution, especially in large urban agglomerations, consists in vehicles electrification. It is well known that electric vehicles (EV) are not something new, their history starts somewhere in the first third of the 19th century. Much has been written about those who are considered the inventors of the first EV, also about when and who started EVs mass production. One of those accredited as a pioneer in the "large-scale" production of electric cars is William Morrison, a Scottish emigrant who lived in Iowa, a chemist with outstanding achievements in the development of electric batteries [1]. Thanks to his innovations, more powerful and lighter batteries were obtained, so such a battery pack was mounted on a carriage and powered an electric motor

that drove one of its rear wheels. Of course, in this form, the success was quite limited, but the news about the horseless carriage spread quickly, and the development of electric vehicles took off.

In the last years of the 19th century and the first years of the 20th century, famous people like Porsche, Edison, and Ford were interested in the development of EVs. That is when the first hybrid vehicle appeared, produced by Porsche, powered by an electric motor and a gasoline engine. At the beginning of the 20th century, EVs were much more numerous than gasoline ones and almost as many as steam ones (about 40%). The heaviest blow received by EVs was given in 1908 by Henry Ford (who was initially interested in producing a cheap electric car) when he mass-produced a cheap car, the Model T, with a gasoline engine [2]. Because of some realities at that time - electric cars were approximately three times more expensive and had a much shorter range; petrol was cheap; internal combustion engine (ICE) starting was solved by introducing electric starters - EVs entered a dark period, and then they disappeared from the market altogether (the mid-'30s). This period lasted for more than half a century (for personal vehicles), until the beginning of the 70s when the price of oil increased, and the lack of gasoline was felt, the peak being considered the 1973 Arab Oil Embargo. Therefore, the search for alternative solutions began, with hybrid and electric vehicles again enjoying the attention of governments and researchers. The technologies of this period allowed the making of EVs with many disadvantages compared to ICEVs: reduced autonomy, long time for charging, and limited performance (maximum speed around 70 km/h). The research had to continue in an accelerated manner to be able to obtain performances for EVs comparable to those of ICEVs or better. Grants to research labs have increased, and big vehicle manufacturing companies have collaborated with governments to improve technologies. Testing new technologies from the design phase requires proper tools. It is unanimously recognized today that numerical simulations with dedicated software are the basis of the development of new products and technologies. Thus, it is not accidental that in the mid-90s, the Department of Energy (DOE) with the National Renewable Energy Laboratory (NREL) from the U.S.A together with industry partners (Ford, GM, and Chrysler) developed ADVISOR [3]. The software was intended as an analysis tool for the understanding and development of hybrid and electric vehicles.

2. VEHICLE MODEL AND MAIN PERFOMANCES

2.1. Vehicle model

Longitudinal vehicle model assumes only the forces that act longitudinally (*fig. 1*), in the direction of movement, the transverse forces and the internal forces (as the twists of the chassis and the vibrations within it) being neglected. Although it stands for a simplified 2D

model, this is sufficiently correct in appreciating the most important performances of the vehicle including speed, acceleration, gradeability, and braking performance.

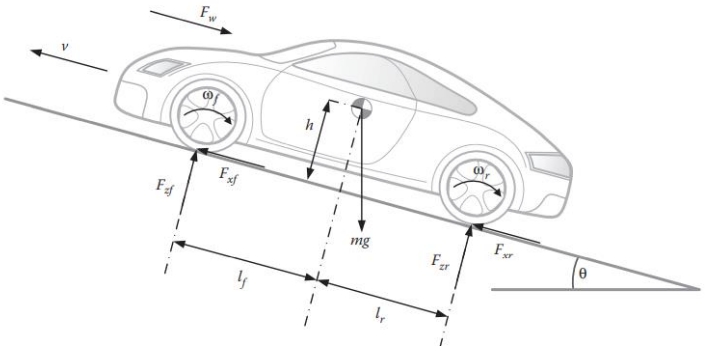

Fig. 1. Longitudinal forces acting on a vehicle [5]

As in every mechanical system, the acceleration force which starts the vehicle or increases the speed, is the difference between tractive force and resistant forces.

$$ma = F_t - F_w - F_g - F_r \tag{1}$$

Were noted: m – vehicle inertial mass, which can be approximated at 5% higher than real mass [6]; a – acceleration; F_t – tractive force; F_w – aerodynamic force or wind force; F_g – gravity force that must be overcome to climb a grade; F_r – rolling resistance force.

The wind force is a function of vehicle shape and size; it is proportional with air density, ρ, frontal area A and relative wind-car velocity, v, through drag coefficient, C_d; relative wind-car velocity represent the sum (when they have opposite sens) or difference (when they have same sens) between car velocity and wind velocity.

$$F_w = \frac{1}{2} C_d \rho A v^2 \tag{2}$$

The gravity force depends by incline angle of the road, θ, vehicle mass, m, and gravity acceleration, g.

$$F_g = mgsin(\theta) \tag{3}$$

The rolling resistance force, which is a friction force, function of vehicle mass, incline road angle and rolling resistance coefficient, C_r, which at its turn depends on tires and road surface.

$$F_r = C_r mgcos(\theta) \tag{4}$$

Another important characteristic that needs to be modeled, specific to hybrid and EVs, is the state of charge of the system battery (*SOC*). *SOC* is determined based of the system capacity (Q_0) [7], usually expressed in *Ah*.

$$SOC = \frac{Q(t)}{Q_0} \tag{5}$$

When simulating EVs, the *SOC* in every moment is in terms of the initial state of charge (SOC_0), coulombic efficiency (η_c) and the battery current [8].

$$SOC(t) = SOC_0 - \int \frac{\eta_c i(t) dt}{Q_0} \tag{6}$$

When the EV is in a regenerative braking regime, the sign of current is minus, and *SOC* increase. If the battery capacity is in *Wh*, there is the relation, *Wh/[Battery voltage]=Ah*.

2.2. Main performances

Among the main vehicle's performances are maximum speed, acceleration performance and gradeability [9]. Maximum electric vehicle speed is the constant cruising speed that the vehicle can develop at the maximum motor power on a flat road. This depends on the highest speed of the motor and total gear ratio of the transmission when the motor is sufficiently powerful.

$$V_m = \frac{\pi n_m r_d}{30 i_g i_0} \tag{7}$$

In (5) is noted: V_m – maximum vehicle speed; n_m – maximum motor speed; r_d – the effective radius of the drive wheel; i_g – gear ratio of transmission; i_0 – final drive gear ratio.

The acceleration performance is given by the acceleration time and the distance covered to increase the speed from zero to a certain high speed (eg. 100 km/h). In the case of EVs the highest acceleration is provided at low speed, and it depends on maximum motor torque (T_m), vehicle mass (m), effective radius of drive wheel (r_d), resultant of resistant forces (F_{tr}) and total gear ratio (i_t).

$$a = f\left(\frac{\frac{T_m i_t}{r_d} - F_r}{m}\right) \tag{8}$$

The gradeability is the largest incline angle of the road that the vehicle can overcome at a certain constant speed while in the case of heavy or off-road vehicles, usually, it is the maximum incline angle that the car can overcome at any speed. Fundamental parameters

which influence the gradeability are the peak motor torque, total gear ratio, radius of drive wheel and friction coefficient (μ) between tires and rolling surface.

$$tg\theta = f\left(T_m, i_t, \frac{1}{r_d}, \mu\right) \tag{9}$$

3. METHODOLOGY

When the vehicle powertrain is analyzed, ADVISOR is focused on power flows among the components. So, to obtain results closer to the experimental measurements, the efficiency of each component in which the power flows must be as accurately estimated as possible, for the entire range of torques and speeds. In this sense, "industry and government experts were consulted to develop estimates of component performance, including "best case" and "conservative" estimates" [3]. Following these consultations, the results of ADVISOR simulations were very realistic, close to those obtained by other laboratories from industry or to measurements.

3.1. ADVISOR software

A simple sketch of an EV is in the top left part while the map of the motor/controller efficiency and rated torque vs speed, is in the bottom left. In the right part are the labels and dialog boxes needed for configuration. Some boxes are active, others are not, this part of the interface being designed in such a way that all types of cars can be configured (electric, series or parallel hybrid, fuel-cell, or ICE).

Fig. 1 shows the main interface of ADVISOR when EV is selected for configuration.

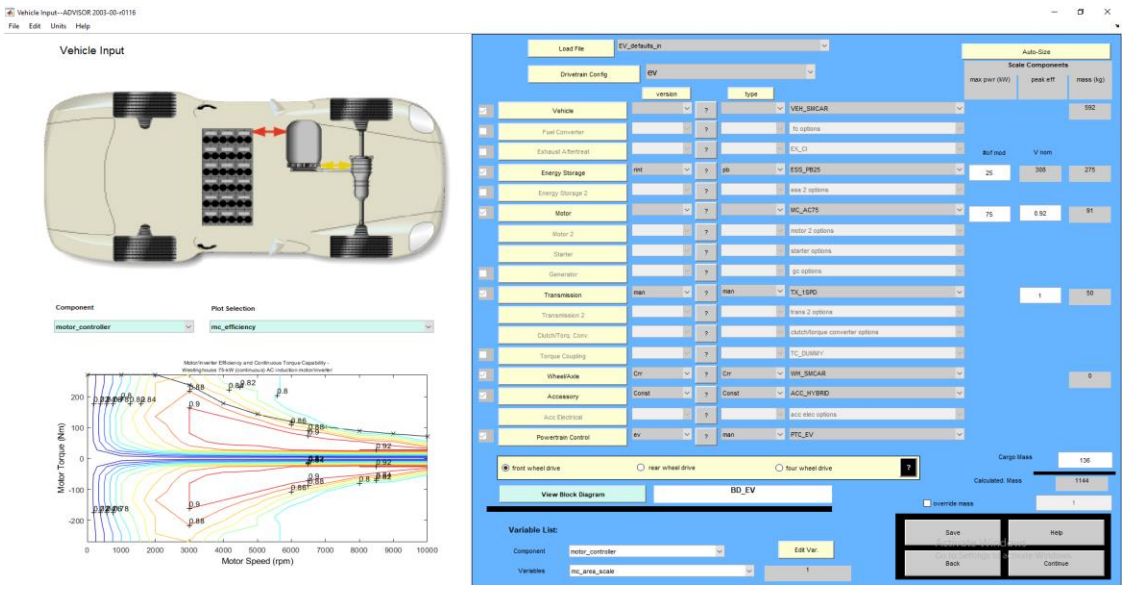

Fig. 1. ADVISOR interface, EV configuration

There is no big difference between the first two boxes, each of them allowing us to define the vehicle type or to choose a certain predefined model and brand. In the *Vehicle* box one can select the vehicle body (common or a certain model/brand, *fig. 2.a*). The next active box is for energy storage system choice (*fig. 2.b*) and the other for the motor (*fig. 2.c*). There are many types of energy storage systems, but the possibility of selection is a function of the selected file in the Load File box.

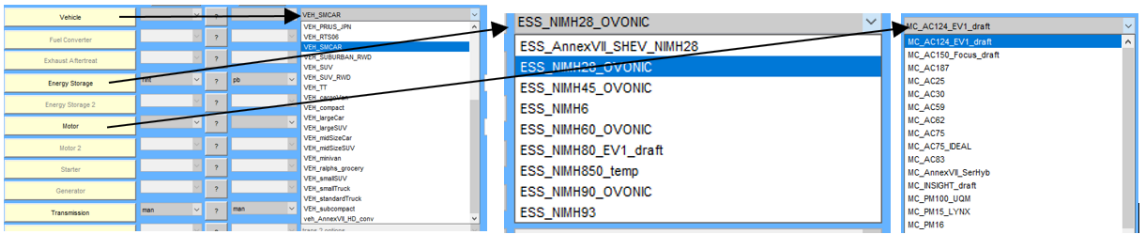

a) Vehicle body; *b) Energy storage system;* *c) Motor.*

Fig. 2. Main components selection

In the *Transmission* box one can select the type of gear box. For EV, usually, 1-speed gear box is predefined, but the user can also select another type of gear box or can define a new one. For EV only manual type is possible. If not 1-speed gear box is selected, the user must alter the file *PTC_EV* which is the only selectable in *Powertrain Control* box. This is necessary because in this file is not defined the change of gear. Wheel/Axle refers to the coefficient of rolling resistance model, wheels, and axle types and in the *Accessory box*, the needed power is accounted. Also in this frame, one can select the driving wheels (front, rear or four).

After one pushed the *Continue* button, the new frame appears (*fig. 3*). In the left part are data about the selected cycling drive, and disponibile measuring units being *US* or *SI*. This stands for the speed-time graph which the car should fulfil during the simulation.

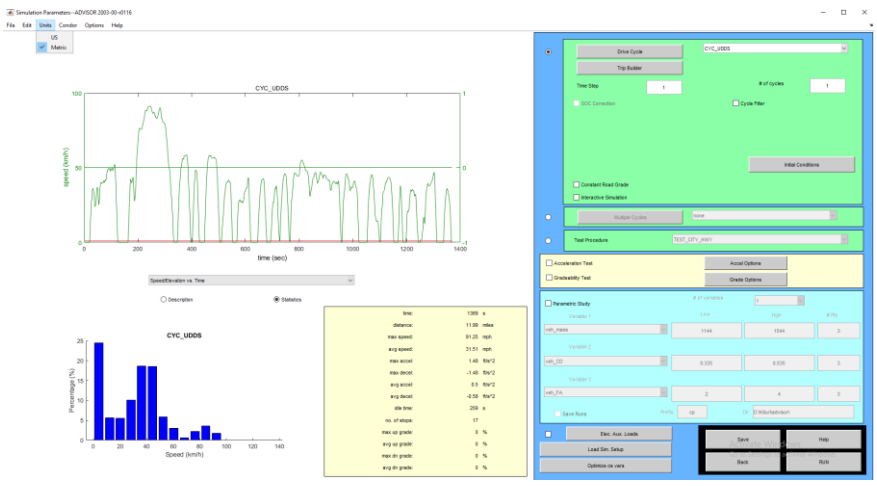

Fig. 3. Advisor second frame

One can choose from the existing many cycles, define a new one, choose a test procedure or an interactive cycle. These cycles are like the used ones in experimental tests. As a main characteristic we can mention the driving specificity, some being for testing driving in city, on highway, combined cycle, and aggressive driving cycle. When a driving cycle (not test procedure) is chosen, one can impose a constant incline road, and defines the initial conditions as: ambient, motor and energy storage system temperature and *SOC*.

In the following, *Acceleration test* and *Gradeability test* (*fig. 4.a, b*) should be set if they are desired. If the *Parametric Study* box is checked, from 1 to 3 parameters (chosen from a large list) can be varied between a minimum and maximum value (fig. 4.c).

After completing these stages, one should press the *Run* button which will start the simulations, and at the end, one can view the results. The possibilities of the presentation of the results will be shown with the case study.

3.2. Case study

The EV model was configurated choosing *EV_defaults_in* file in the *Load File* box and all boxes have been filled in automatically with proper data for EV type. After that, in the *Energy Storage* box, *ESS_PB91* has been chosen instead of *ESS_PB25*. This energy storage system models the *Electrosource Horizon 12N85* lead-acid battery, which has specific energy of 35 Wh/kg and specific power of 240 W/kg, the voltage is 308V and C/5 rate 91Ah. The parameters vary according to *SOC* and temperature. Although the voltage and the number of modules are the same, the amount of energy is almost four times higher than in *ESS_PB25* (while the mass is about 2.3 times). Another change compared to the defaults was the choice of the *MC_AC83* motor instead of the *MC_AC75*. Tis induction motor/inverter can develop 83 KW continuus power, has a 385 A maximum current, 200 V minimum voltage, and has the characteristics (the maximum continuous torque and efficiency vs speed) shown in *fig. 5*. With these changes a total vehicle mass (including 136 kg cargo mass) of 1511 kg resulted.

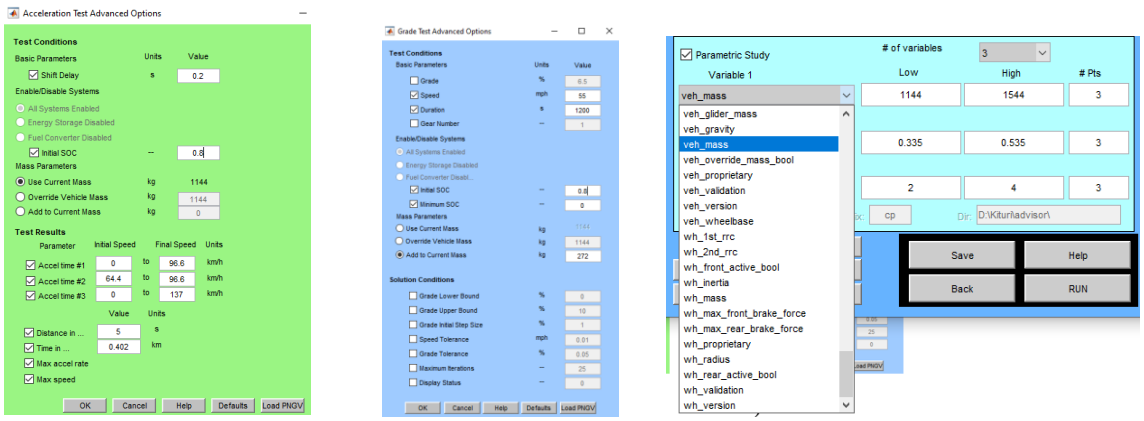

a) Acceleration *b) Gradeability* *c) Parametric study*

Fig. 4. Test options

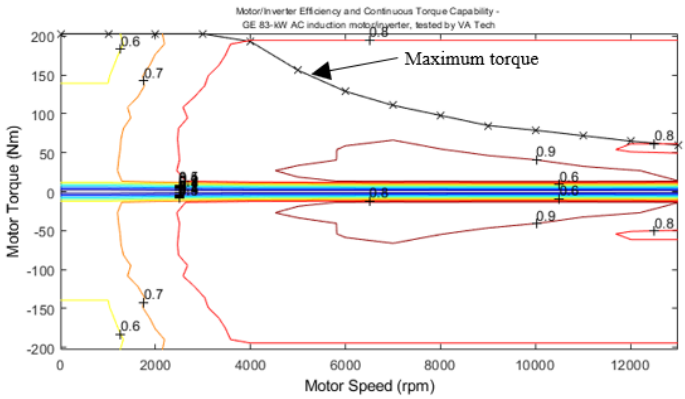

Fig. 5. Motor/inverter characteristics

In the next frame (fig. 3.) *CYC_FTP* drive cycle (federal test procedure in USA) has been chosen and it stands for city driving conditions for light duty vehicle testing having statisc data shown in *fig. 6*. An initial *SOC* of 0.8 was set, and gradeability and acceleration tests was checked. *Parametric study* was ignored in the first simulation.

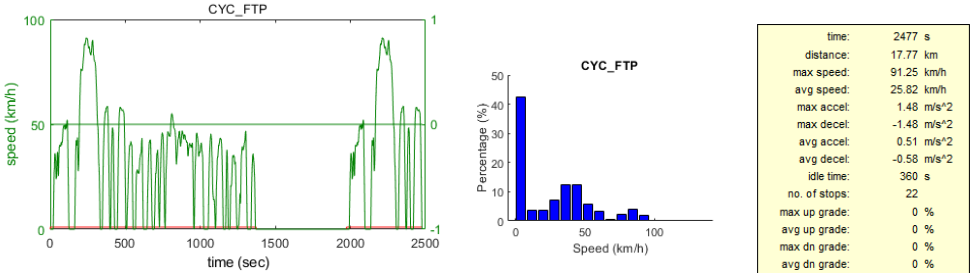

a) Speed vs time *b) Statistic data*

Fig. 6 FTP drive cycle

The second simulation was carried out with the same model, but the *Parametric Study* box was checked, and a single variable was taken into consideration, *gb_spd_scale*, which stands for the multiplication coefficient of the gear ratio in the gearbox. The influence of the gear ratio on the vehicle performance for different driving cycles has been also studied in [10]. Five values were imposed, between 0.8 - 1.2.

In the third simulation, two variables were imposed, adding *mc_spd_scale*, which stands for the multiplication coefficient of the motor speed, and three values were considered: 0.7, 0.85 and 1.

In the last simulation of this model, were imposed three variables: *gb_spd_scale*, *mc_max_crrnt* and *mc_min_volts*. The second stands for the maximum allowed motor current while the last is for the minimum allowed voltage. Three values (minimum, 200 A; the middle value; maximum 385 A, being rated value) were considered for the maximum current and the other three for the minimum voltage (200 V; the middle value, 225 V; 250 V).

The second EV model has been obtained based on the first, changing the *MC_AC83* motor with the *MC_AC62* motor.

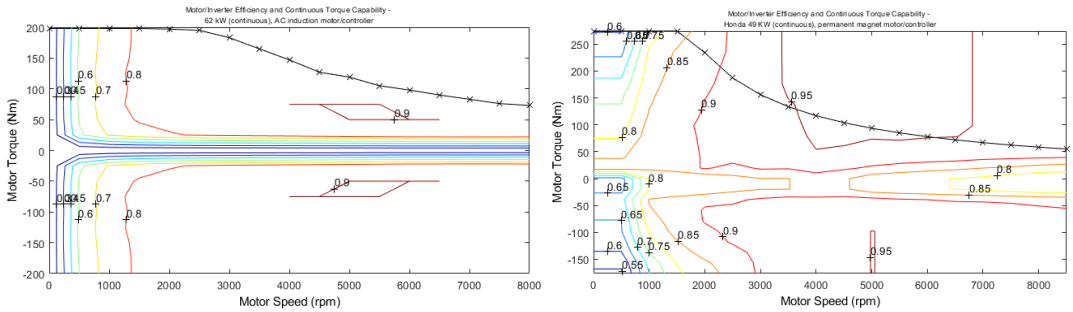

a) AC62 *b) PM49*

Fig.7. Motor/inverter characteristics of the second and third model

The last is also an induction motor and has the same maximum torque, but a reduced speed (and power, 62 kW), the motor characteristics are shown in *fig. 7a*.

The third studied model is also as first, but this time the chosen motor has been *MC_PM49*, which stands for a permanent magnets (PM) motor, having 49 kW continuous power and the characteristics from *fig. 7b*.

4. RESULTS

The simulation of the three models results in the operating points of the motors, shown in fig. 8 (on the *y* axis the measuring unit is *Nm*, and on the *x* axis is *rot/min*). As can be seen, all these motors can easily develop the needed power in this driving cycle. Variations of the *SOC* of the battery in the three cases are shown in *fig. 9*. This is approximately the same in the case of the two induction motors, and it is lower in the case of the PM motor.

Of course, a low *SOC* at the end of the cycle means more consumed energy or less overall efficiency.

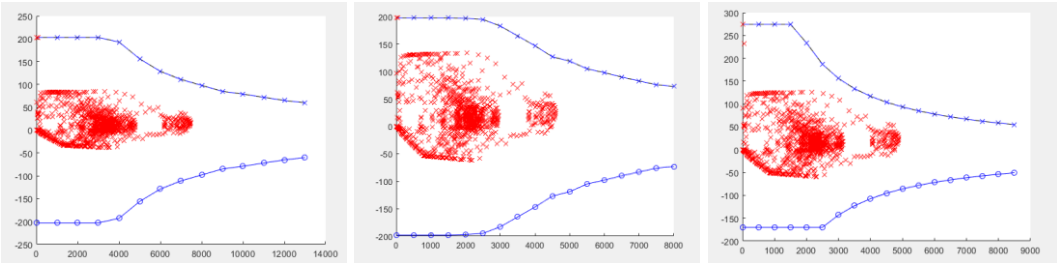

a) AC83 *b) AC62* *c) PM49*

Fig. 8. Operating points of the motors

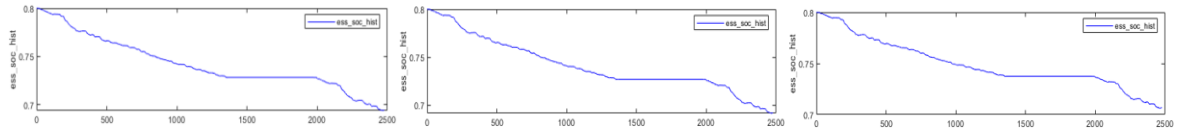

a) AC83 *b) AC62* *c) PM49*

Fig. 9. SOC variation in driving cycle

For the considered driving cycle, with the same energy storage system and the same vehicle (the differences being only given by the different weights of the motors), the overall vehicle efficiency was: 0.368 for the model with *AC_62*; 0.382 for the model with *AC_83*; and 0.425 for the model with *PM_49*. Although the *AC_83* motor is larger than the *AC_62* so the vehicle is heavier, due to the higher performance of the first motor, the total efficiency is also higher. The best motor/controller of the three is the PM_49, which has an average efficiency of 0.88 (as the motor) and 0.85 (as the generator); the next is AC_83 with 0.82 and 0.73 respectively; the last is AC_62 with 0.78 and 0.69 respectively. Regarding the performance of the analyzed models, the results are shown in table 1. Inasmuch for the first simulated model a parametric study was carried out, in the belows figures some of the results are shown.

Table 1. Performances of the models

Motor type / Parameter	AC_83	AC_63	PM_49
Gradeability at 88.5 km/h [%]	18.8	13.4	10.4
Acceleration 0-100 km/h [s]	10.3	15.1	16
Acceleration 65-100 km/h [s]	5.1	6.9	9
Acceleration 0-135 km/h [s]	18.8	27.8	34.3
Maximum acceleration [m/s^2]	3.8	2.3	3.5
Maximum speed [km/h]	157	157.6	157.9

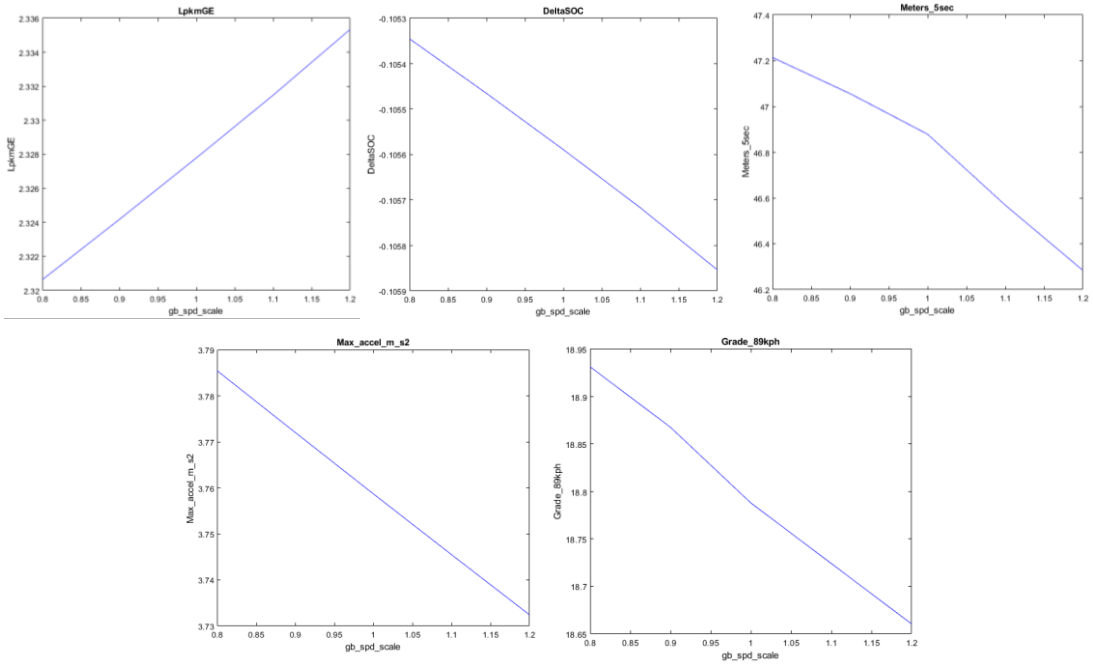

Fig.10 Parametric study considerring a single variable (gb_spd_scale). LpkmGE – gasoline equivalent in liter/km; DeltaSOC- variation of the SOC; Meters_5sec – distance in 5 secons, in meters; Max_accel_m_s2 – maximum acceleration (m/s^2); Grade_89kph – gradeability at 89 km/h

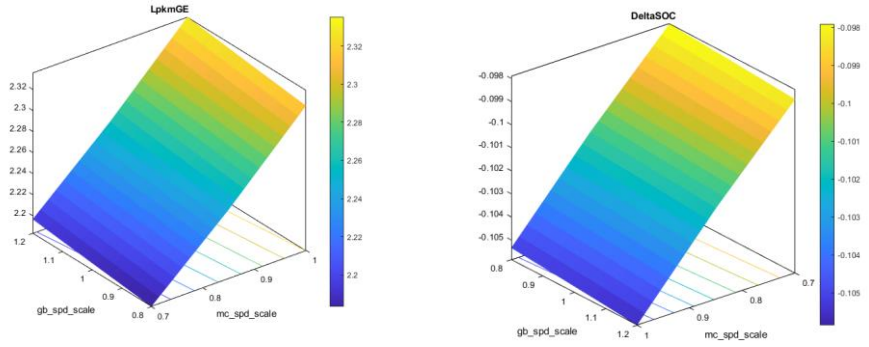

Fig. 11. Parametric study with two variables

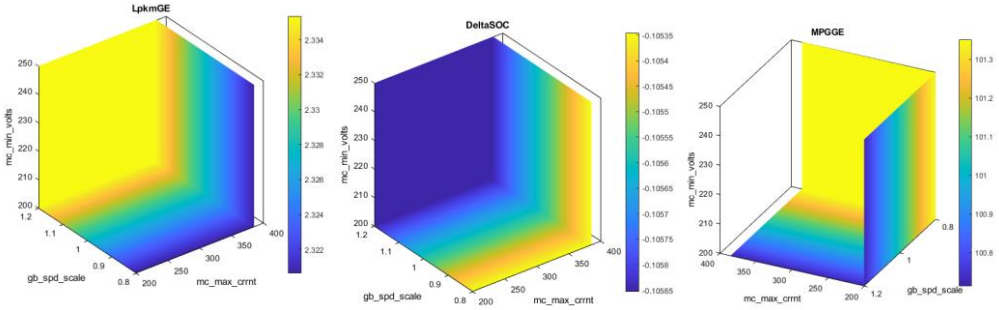

Fig. 12. Parametric study with three variables
(MPGGE - drive cycle miles per gallon gasoline equivalent)

5. CONCLUSION

In this study, the main steps needed to configure the model of an EV and then its simulation in different conditions were presented. For the same vehicle body, cargo mass, and energy storage system, three different motors were considered to find the best solution from the overall efficiency point of view, for a specific driving cycle. The surprise is not that the PMs motor is more efficient in this city-specific driving cycle, but the fact that a high-power induction motor offers higher overall efficiency than a low-power induction motor, even if the first is a less loaded. However, if one looks at the efficiency-speed map, is observable higher efficiency for the AC_83 motor/controller and it is known, the motor is the main consumer of the EV.

The transmission ratio of the gearbox is calculated so that at a slip of 10%, the car can reach a maximum speed of 144.8 km/h (90 miles/h). So, the gear ratio is 8.67 for AC_83, for AC_62 this is 5.34, and for PM_49 it is 5.67. Even though PM_49 has the highest maximum torque and can develop the highest maximum acceleration (table 1), the times in the acceleration test are the highest (low performances). This is caused by the fact that this maximum torque is only available in a limited speed range (the lowest power of the three).

Parametric Study allows one to study the influence of a variable parameter on the vehicle performance. A maximum of three variables can be set at the same time. *Fig. 10*

shows the influence of the gear ratio on the other parameters characteristic of vehicle performance. The influence of the gear ratio and the motor's maximum speed on the same parameters is shown in *fig. 11*. A minimum 2.18 l/km gasoline equivalent is obtained when the two variables are the lowest and increases when any of them increase. The last simulation considered three variables for parametrization (*fig. 12*), but only one of them, *gb_spd_scale*, affects the selected parameters.

REFERENCES

[1] https://iowahistoryjournal.com/an-electrifying-iowan/

[2] https://www.energy.gov/articles/history-electric-car

[3] K. Wipke, M. Cuddy, D. Bharathan, S. Burch, V. Johnson, A. Markel, and S. Sprik, *Advisor 2.0: A Second Generation Advanced Vehicle Simulator for Systems Analysis*, National Renewable Energy Laboratory (NREL), https://www.nrel.gov/docs/fy99osti/25928.pdf.

[4] K.W. Chew, C.K. Koay, Y. R. Yong, *ADVISOR Simulation of electric vehicle performance on various driving cycles,* International Journal of Innovative Science, Engineering & Technology, vol. 1 no. 8, pp. 70-76, 2014.

[5] William Long and Berker Bilgin, *Fundamentals of Conventional Vehicles and Powertrains. In A. Emadi (Ed.), Advanced Electric Drive Vehicles (Chapter 2, pp. 15-25),* CRC Press, 2015.

[6] K. Atamnia, A. Lebaroud, M. Makhlouf, *Traction motor selection based on the performance analysis of pure electric vehicle under different driving scenarios*, Carpathian Journal of Electrical Engineering, vol. 14, no. 1, pp. 57-72, 2020.

[7] Gheorghe Livinţ, Vasile Horga, Marcel Răţoi and Mihai Albu, *Control of Hybrid Electrical Vehicles. In S. Soylu (Ed.), Electric Vehicles - Modelling and Simulations (1 ed., Chapter 3, pp. 41-66)*, Intech Press, Croatia, 2011.

[8] Huertas J.I., Mogro A.E., Jiménez J.P., *Configuration of electric vehicles for specific applications from a holistic perspective*, World Electric Vehicle Journal, vol. 13, no. 2, 2022.

[9] Ehsani M., Gao Y., Gay S.E. & Emadi A, Hybrid Electric, and Fuel Cell Vehicles: Fundamentals, Theory, and Design, CRC Press, 2005.

[10] Olivian Chiver, Nicolae Burnete, Ioan Radu Şugar, Liviu Neamt and Eleonora Pop, *Study on gear ratio of battery electric vehicles*, Ingineria Automobilului, no. 59, pp. 11-16, 2021.

DESIGN AND PERFORMANCE OF A LOW-COST SUBSONIC WIND TUNNEL

Alexander **BARON VON HOHENHAU**
Technical University of Cluj-Napoca
alex@edesign.co.uk

Keywords: Wind Tunnels, Turning Vanes, Diffusers, Flow Uniformity, Pressure Drop, Turbulence

Abstract: *This paper investigates the design and performance of a small-scale inexpensive wind tunnel, with a working cross-section of 305 by 305 mm and a top speed of 56 m/s, powered by an 18.5 kW centrifugal fan. The wind tunnel incorporates a diffuser, a contraction and various flow conditioners. Guidance on the construction and incorporation of each of these components is provided. Their performance was evaluated using a seven-hole probe and the results are compared to findings in literature. Particular attention is paid to flow uniformity and pressure changes. It is demonstrated that wire screens and honeycombs bring about clear improvements in flow quality, although their effect is eclipsed by the outstanding performance of a 4:1 contraction. It is demonstrated that the right design choices allow for the construction of a cost-effective wind tunnel capable of producing excellent flow uniformity with relatively low power requirements.*

1. INTRODUCTION

As part of a larger research effort relating to the design of expansion turning vanes, the author required a suitable aerodynamic testing environment. To this end, a small-scale wind tunnel was constructed. Excellent literature on the construction of wind tunnels already exists, namely publications by Barlow et al. [1] and de Almeida et al. [2]. However, these focus on mid to large-scale facilities and lack detailed flow contours of individual sections.

The open-circuit wind tunnel presented herein consists of five main components: A centrifugal fan, an expansion section, a set of simple turning vanes, a straight settling chamber, and a contraction. The following sections discuss the design and construction of the wind tunnel. This is followed by an analysis of the performance of various component configurations,

in regards to pressure drop and flow uniformity. Where advantageous, additional wire screens and honeycombs have been installed. The main requirements were to attain a minimum flow speed of 35 m/s and a turbulence intensity below 1% downstream of the contraction. The flow downstream of the numerous wind tunnel sections is characterised using a seven-hole probe.

2. WIND TUNNEL DESIGN AND CONSTRUCTION

The layout of the wind tunnel is shown in *Figure 1*, and the dimensions of the individual sections are summarised in Table 1. The sections were constructed from wood procured in the UK, where standard plywood sheets measure 2440 by 1220 mm. By making the typical cross-section of the tunnel 600 by 600 mm, and the length of most sections around 1220 mm, material wastage could be minimised. This reduced cost, while still facilitating a tunnel of adequate size. The rest of this section will discuss the various components of the wind tunnel in greater detail.

Table 1. Geometric characteristics of different wind tunnel components (all lengths are in metres)

Section	Inlet Width	Inlet Height	Outlet Width	Outlet Height	Centreline Length	Area Change (ratio)
Fan	NA	NA	0.394	0.631	NA	NA
Expansion	0.394	0.631	0.600	0.600	0.60	1.45
Curve	0.600	0.600	0.600	0.600	1.20	1.00
Straights	0.600	0.600	0.600	0.600	4.88	1.00
Nozzle	0.600	0.600	0.305	0.305	1.20	0.26

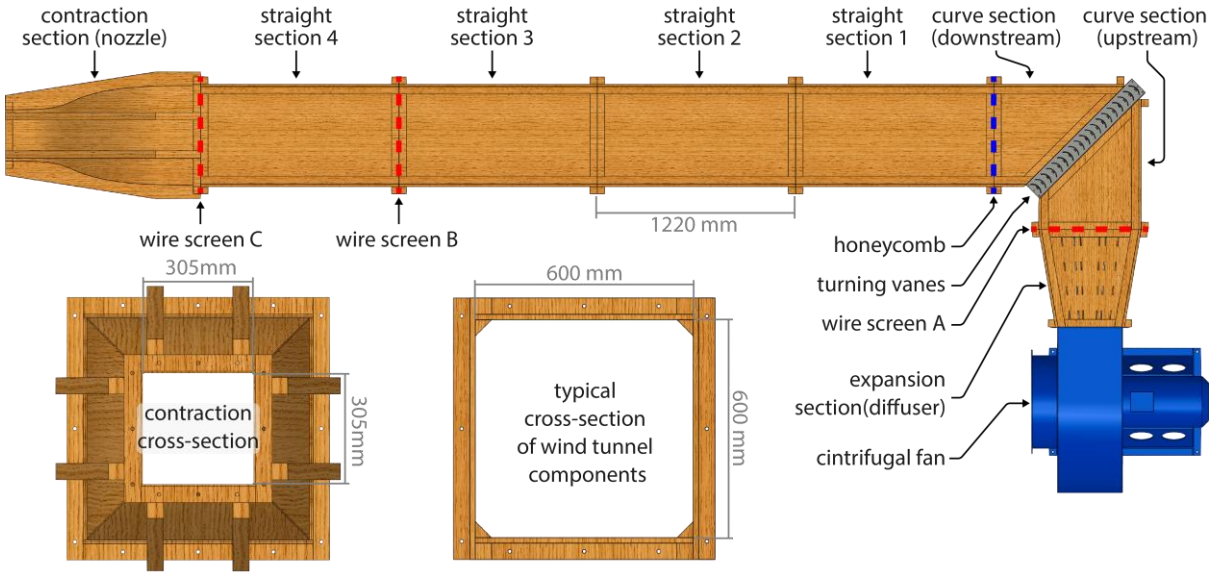

Figure 1. Birds-eye view of the wind tunnel and selected wind tunnel cross-sections. The honeycomb and wire screens are inside the tunnel and their locations are indicated by the dotted lines.

2.1. Constructing the Diffuser

The main purpose of the diffuser is to adapt the 631 by 394 mm cross-section of the fan to the 600 by 600 mm cross-section of the main wind tunnel segments. Due to space restriction, the diffuser length was limited to 598 mm, resulting in an expansion angle (2θ) of 19.48°. The diffuser size is normalised by dividing its length (L = 598 mm) by the inlet width (D_1 = 394) resulting in a ratio of 1.52. According to Smith and Kline, this places the diffuser at the upper limit of the region of no appreciable stall as shown in *Figure 2* [3]. The nearby region of large transitory stall is prone to flow unsteadiness, thereby negatively impacting the data quality of experiments conducted downstream.

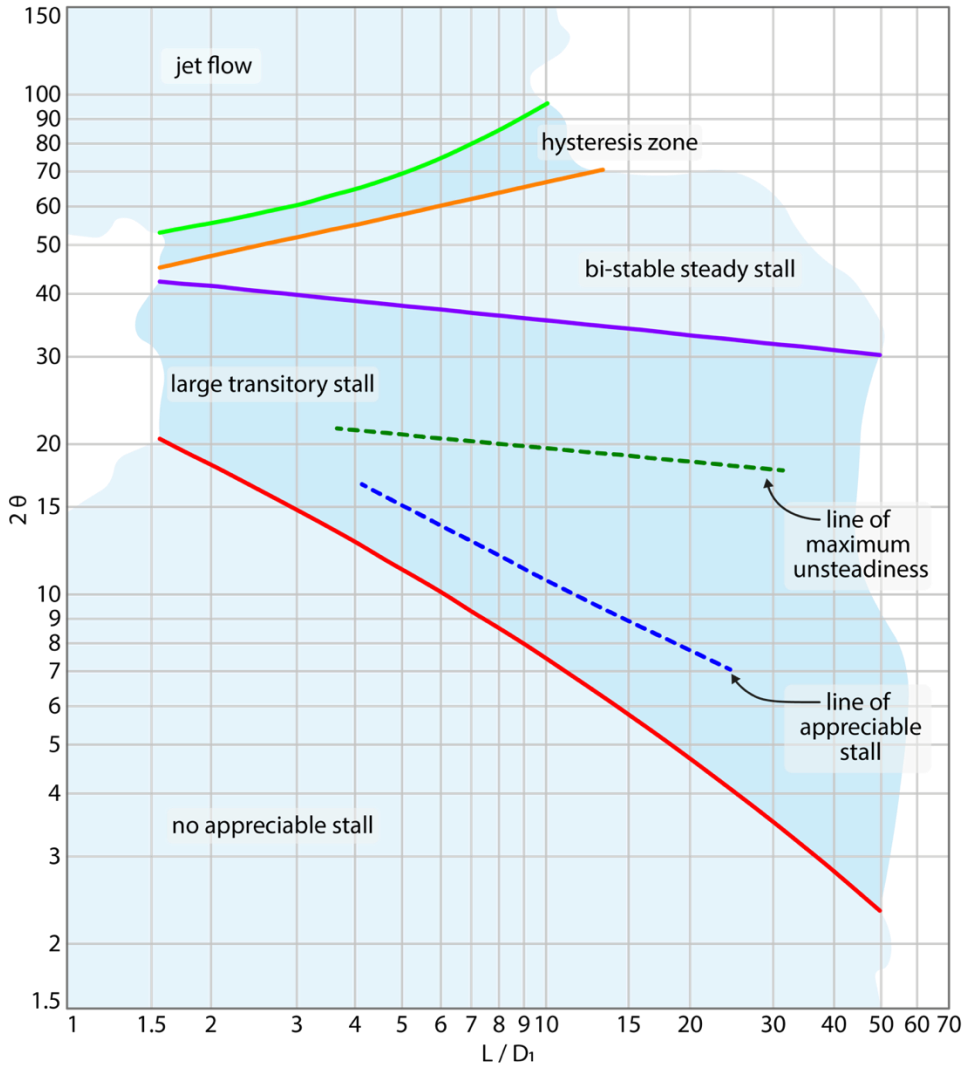

Figure 2. Stall regimes of diffusers with varying normalised diffuser sizes (L/D_1) and total expansion angles (2θ). Adapted from Smith & Kline [3].

Due to the proximity of the expansion geometry to the large transitory stall region, the diffuser was constructed in a manner that allowed for the insertion of dividing walls. This was achieved by placing slots into the floor and ceiling of the diffuser into which the dividers could

be inserted. For this project, the slots were created using a drill and a jig saw, although the author would recommend using a wood router instead, should one be available. The characteristics of the various diffuser configurations are summarised in Table 2.

Table 2: Geometric characteristics of different diffuser configurations

Dividers (QTY)	**Inlet D_1 (m)**	**Outlet D_2 (m)**	**Length (m)**	**2θ (°)**	**Length / D_1 (Ratio)**
0	0.394	0.600	0.600	19.48	1.52
2	0.131	0.200	0.600	6.50	4.58
4	0.079	0.120	0.600	3.90	7.59

The configuration with four dividers is furthest from the region of large transitory stall, though both configurations using dividers are comfortably within the region of no appreciable stall. In addition to the various dividers, the diffuser can also be equipped with a wire screen, to further improve the stall characteristics and smooth the flow profile. Photographs of the different configurations are shown in *Figure 3*. As will be discussed in a subsequent section, the dividers were found to be disadvantageous to flow uniformity. Therefore, they were not used in the final version of the wind tunnel. The slots were sealed using silicone to reduce pressure losses through leakage and increased surface roughness.

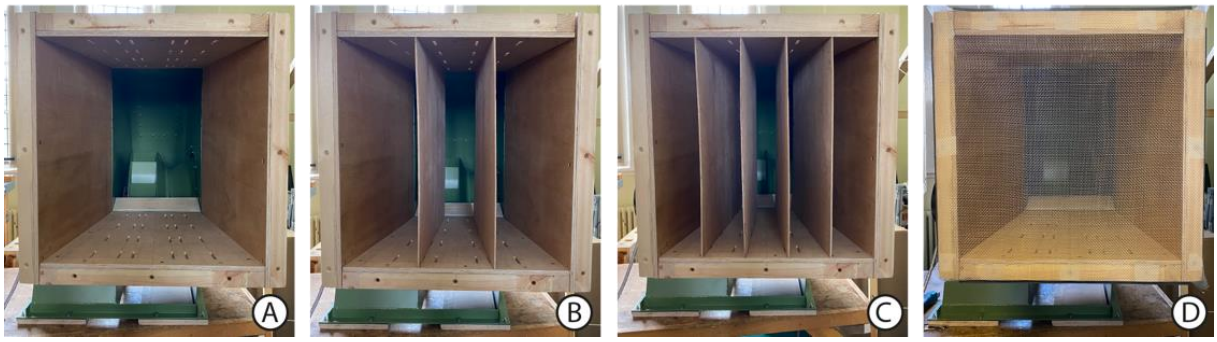

Figure 3. The diffuser with no dividers (A), two dividers (B), four dividers (C), and no dividers but with a wire screen (D). All configurations are shown attached to the fan.

2.2. Constructing the Curved Section

The aforementioned space restrictions also necessitated the use of a curve section within the tunnel. Regrettably, for this wind tunnel segment, there was an insufficient budget for extruding or pultruding complex aerofoil turning vanes. Printing these vanes was also unviable as the 600 mm channel height exceeded the size limit of the available 3D printer. Therefore, the best solution was to rely on the research of de Vega et al. and use circular flat plates that over-turn through 101° [4].

The vanes were manufactured by trimming semi-circular PVC gutter pipe with a thickness of 2 mm. Sharp edges were deburred and the leading edge was sanded smooth. To ensure the correct vane position and spacing, two mild steel plates were laser cut and folded with slots for the vanes and holes for mounting the assembly to the wind tunnel. Correct spacing between the plates was ensured by using M6 threaded bars and nylon-insert nuts. The vanes were secured in their slots using standard silicone. The completed setup is shown in *Figure 4*.

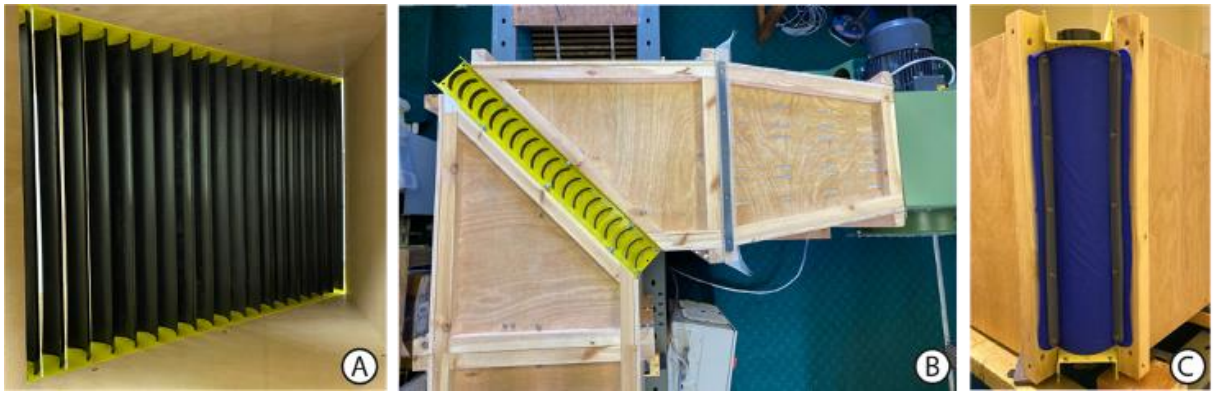

Figure 4. Internal of the curve (A), birds-eye view of the curve (B) and seal between the outer vane and the wind tunnel sections (C).

Unfortunately, this method of constructing the vane section leaves four gaps between the outermost vanes and the wind tunnel. It is required to seal these gaps to prevent the high-pressure flows in the wind tunnel from jetting out at this segment. Failure to do so would lead to energy losses and ultimately a lower maximum flow rate. The gaps were initially sealed using standard masking tape. While this was not an issue at lower speeds, the seal at the outer turning vane tended to rupture when flow velocities and pressures were higher. After several iterations of using more and different tape, it was decided that a sturdier solution was needed. The tape seals were replaced with smooth waterproof plastic fabric, which was rigidly clamped against the wood (see the right of Figure 4). No further sealing issues were observed thereafter.

2.3. Constructing the Straight Sections

The straight tunnel sections are by far the easiest to construct, but they should still be assembled with care as they make up the majority of the wind tunnel and are intended to contribute to a smooth velocity profile at the test section. The sections were constructed in a manner that allowed for the addition of small corner chamfers. These chamfers are said to reduce the level of secondary flow, thereby increasing flow uniformity [4]. The chamfers were cut from lengths of 45 by 45 mm dressed wood using a table saw with a blade angle of 45°. Due to blade kerf, the resulting chamfers are approximately 43 by 43 mm wide. *Figure 5* shows the various stages of construction of the straight sections.

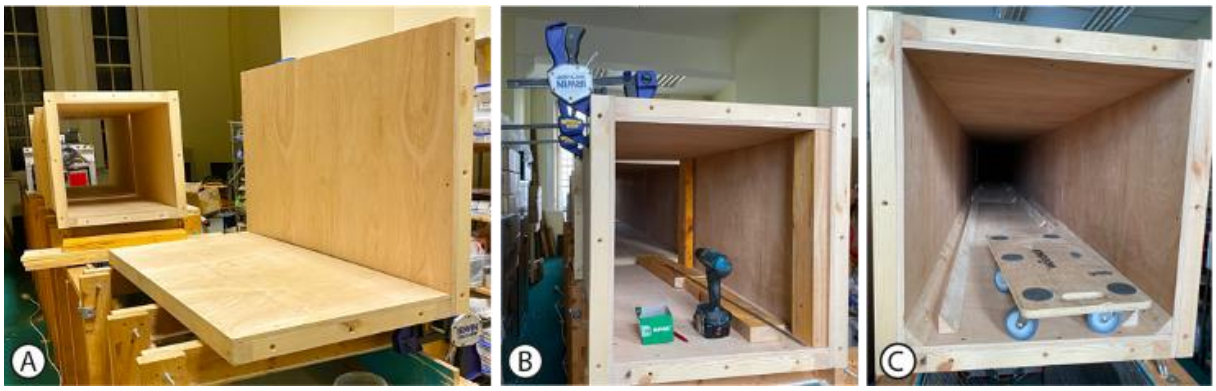

Figure 5. Initial construction of a straight section (A), top panel installation using spacers (B), and chamfer installation with the bottom pieces already fixed in place (C).

The main difficulty in constructing the straight section (and most other sections) lies in the need to accurately assemble the wood. The bottom and top panels were delivered slightly oversized. They were subsequently trimmed to 600 mm using a band saw to give a precise channel width. The panels were assembled using wooden spacers to ensure accurate channel height. Great care was taken to ensure that the flanges on each component, particularly the bolt holes would line up with the other sections. This ensured easy assembly, smooth transitions on the inside of the tunnel, and cross-compatibility between the sections (i.e., it did not matter in which order the straight sections were assembled or how many were actually used). Accurate hole placement was aided through the use of a 3D-printed drilling jig, which indicated the right distance to the end and the correct positioning on the centreline of the timber pieces.

2.4. Constructing the Contraction

Out of all the wind tunnel segments, the construction of the contraction was by far the most challenging. The first problem is posed by the shape. The curve is based on the pressure gradient optimisation conducted by Alfredsson and Sahlin [5]. The underlying function is shown below. Here, L is the contraction total length, x is the variable distance along the contraction, and A, B, C, and D are constants:

$$f = A\left(\sinh\left(B\frac{x}{L}\right) - B\frac{x}{L}\right) \quad when \quad \frac{x}{L} \leq 0.7 \tag{1}$$

$$f = 1.0 - C\left(\sinh\left(D\left(1-\frac{x}{L}\right)\right) - D\left(1-\frac{x}{L}\right)\right) \quad when \quad \frac{x}{L} > 0.7 \tag{2}$$

$$A = 0.205819 \quad B = 3.52918 \quad C = 0.08819 \quad D = 8.23523$$

The actual shape of the contraction is determined using the following equation, where w_{local} is the local width, w_{max} is the maximum width, and R_c is the contraction ratio:

$$w_{local} = \pm w_{min}\left(\frac{R_c}{2}(1-f)+\frac{1}{2}f\right) \tag{3}$$

A diffuser with a length of 1200 mm, an inlet width of 600 mm, and an outlet width of 305 mm has a contraction ratio of approximately 2:1. Graphing the equations outlined herein, the diffuser curves obtained are shown in *Figure 6.*

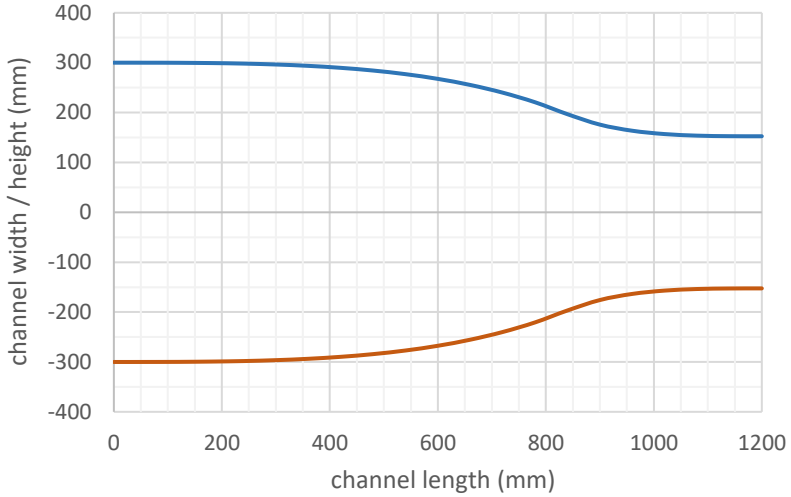

Figure 6. Contraction curves used to define the shoe of the contraction

Equipped with the correct curve equations, the diffuser can be modelled in 3D CAD software, in this case, SolidWorks. The exact dimensions are chosen so that the curve length of the diffuser is 1220 mm, thereby minimising material wastage. The inlet is 600 x 600 mm, while the outlet is 305 x 305 mm. After establishing a shape, the means of constructing the diffuser had to be found. The author thought it would be best to construct the walls of plywood and supporting ribs of dressed timber, as shown in *Figure 7.*

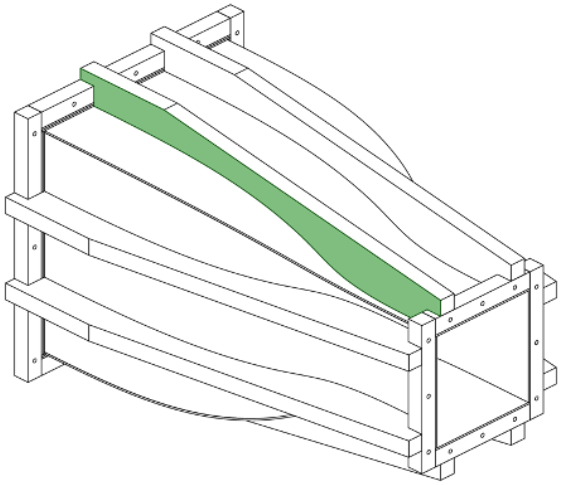

Figure 7: 3D Model of contraction made from 5mm plywood walls and 120 x 45mm timber ribs. The ribs were carefully shaped to provide the correct curvature.

The 3D model of the contraction was turned into a series of manufacturing drawings. A simplified version of one of these drawings is shown in *Figure 8*.

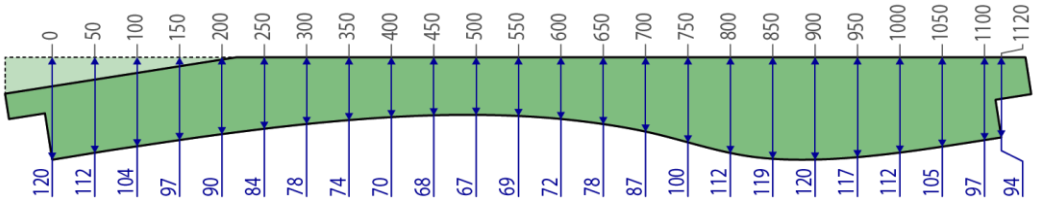

Figure 8. Dimensions (in mm) of the rib curve used for the contraction section. The 0 ordinate marks the beginning of the curve.

The ribs were cut using a band saw and precisely finished using a linisher. Due to the intricate curves of the contraction, a substantial amount of time had to be spent on marking and cutting the wood. The curved walls posed numerous further challenges. They were made from 5mm plywood, which proved difficult to bend sufficiently to fit the ribs. To increase malleability, the plywood was soaked in water for several hours. However, even after this procedure, a lot of pressure was required to force them into the correct shape.

For future endeavours of this kind, the author would recommend using 3mm plywood instead, as it should be more flexible, yet still offer enough strength to cope with the forces exerted by the flow. To cut the plywood to the correct shape, a projection tool within SolidWorks was used to map the curved walls onto a flat surface. Unfortunately, this projection was slightly inaccurate, which led to gaps in the corners, as shown in *Figure 9*.

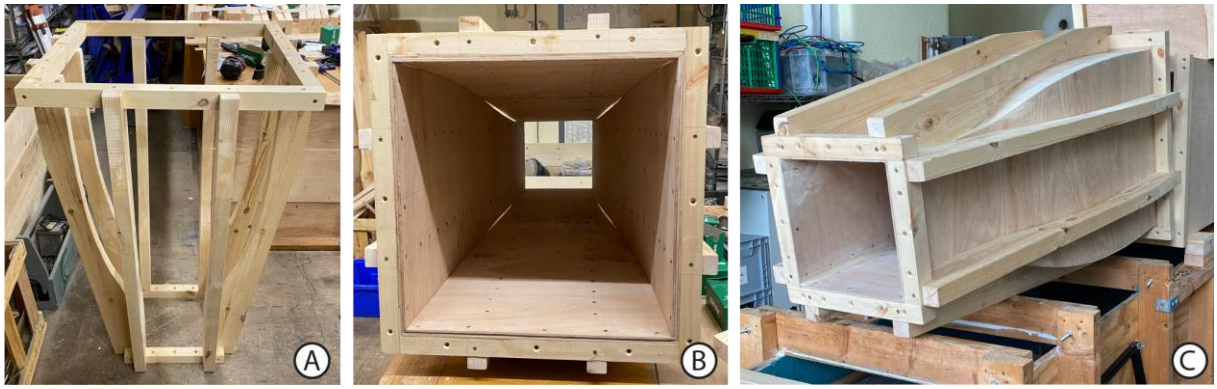

Figure 9. Contraction support structure without walls (A), the interior of contraction with corner gaps (B), and final contraction with gaps sealed using wood filler (C).

3. RESULTS AND DISCUSSION

The main performance criteria for the wind tunnel section are flow uniformity and pressure loss. While there are numerous measures of flow uniformity, this report will use the

coefficient of variation (CV). It is calculated by dividing the standard deviation (σ) of a data set by its average (x_{avg}), as shown in equation (4), where, x_i represents individual data points.

$$CV = \frac{\sigma}{x_{avg}} = \frac{1}{x_{avg}} \sqrt{\frac{1}{n} \sum_{i=1}^{n} \left(x_i - x_{avg}\right)^2} \tag{4}$$

Pressure loss is best represented through the non-dimensional loss factor K as shown in equation (5). The loss factor is simply the ratio of the local pressure loss and the dynamic pressure in the flow.

$$\Delta p = \tfrac{1}{2} K \rho u^2 \tag{5}$$

With many flow conditioners, a higher loss factor is often associated with increased flow uniformity. This is particularly true for wire screens and honeycombs. A good compromise has to be found to ensure that flow conditioners provide sufficiently uniform flow without incurring excessive pressure losses, as these are linearly correlated to power consumption. Unless otherwise indicated, the experiments outlined henceforth were run at a constant fan speed of 2700 RPM, requiring 12.8 kW of power.

The flow was measured using an individually calibrated seven-hole probe and a digital pressure scanner. The latter was equipped with three sets of eight channels, capable of measuring pressure ranges of 160, 1000 and 4000 Pa. The nominal accuracy of each set was ±0.25% of its range, which equates to 0.4, 2.5 and 10 Pa respectively. For a majority of the experiments, the seven-hole probe was connected to the 4000 Pa channels. Both the probe and the scanner were supplied by Surrey Sensors. The outlet of the fan was surveyed in a 13 by 21 point grid, while all the square cross-sections are surveyed using a grid of 21 by 21 points. Each grid point was sampled for 5 seconds and a frequency of 100 Hz. The graphs herein were generated from approximately four million data points. This data set is too large to be included herein but is available from the author upon request. For velocity contours, the individual velocity measurements (u) have been normalised using the local average velocity (u_{avg}).

3.1. Flow conditions at the fan outlet

The flow fan was purchased from Greenmount Fans in England. It was immediately apparent that the volute tongue, was a simple folded piece of sheet metal, creating a sharp step towards the exit of the fan (see *Figure 10*). This design certainly leads to flow separation and flow recirculation in the area immediately downstream of the step.

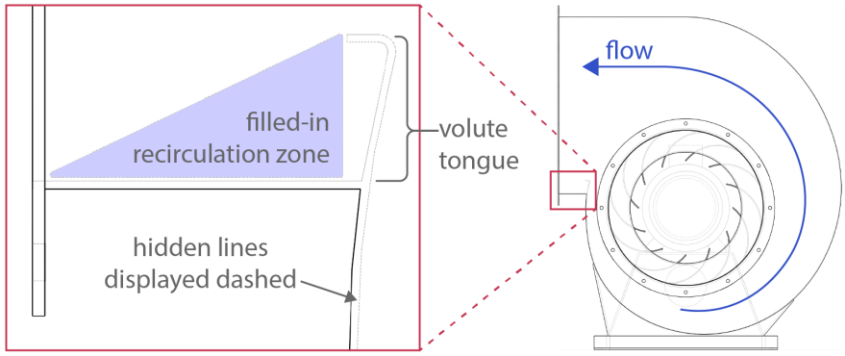

Figure 10: Side section view of the fan with a detailed view showing the wedge's location

Without fundamentally changing the fan design, the contours presented by Wang et al. suggested that filling this zone with a wooden edge would help to improve the quality of the flow [6]. *Figure 11* shows the fan before and after the installation of this wedge. Flow measurements were taken before and after the installation.

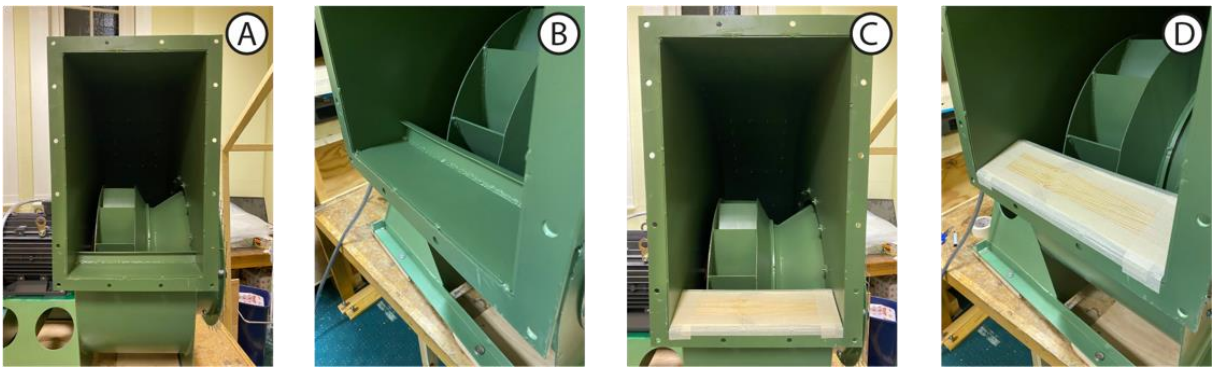

Figure 11: Flow fan without modifications (A and B) & with a wedge installed at the exit (C and D).

From the velocity profiles shown in *figure 12*, it is clear that the flow is highly three-dimensional. The magnitude of the secondary flow (indicated by arrows) is up to 60% as large as the primary flow (indicated by the colours in the contour).

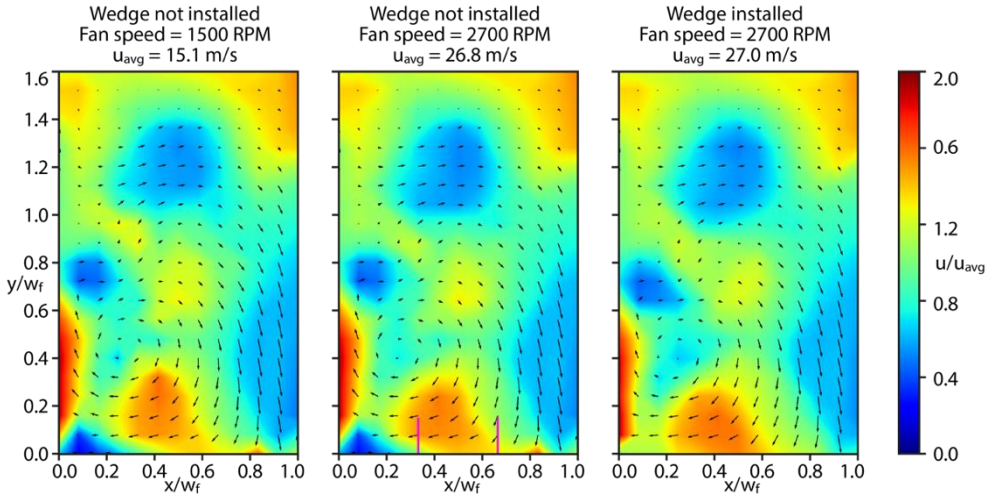

Figure 12. Velocity contours at the fan outlet, before and after the installation of the wedge.

The rotation of the blades and the fan geometry form a strong clockwise vortex, which is present in all trials. Varying the RPM across normal testing ranges has little effect on the velocity distribution. The installation of the wooden wedge facilitates the movement of flow toward the bottom-left corner. Additionally, the general flow uniformity is increased as the coefficient of variance is decreased from 0.235 to 0.230.

3.2. Performance of the Diffuser

It is generally favourable to have diffusers with lower expansion angles. However, the diffuser for this wind tunnel had to be fairly short, resulting in a relatively large expansion angle. To lower the expansion angle, dividing walls could be installed within the diffuser. *Figure 13* compares using zero, two and four dividing walls. Due to the highly three-dimensional nature of the flow, the dividing walls are disadvantageous. Instead of aiding the expansion, they isolate areas of flow. This means that high and low-velocity flows cannot mix, thereby reducing flow uniformity. The coefficient of variation with zero, two and four dividing walls is 0.276, 0.365, and 0.334 respectively.

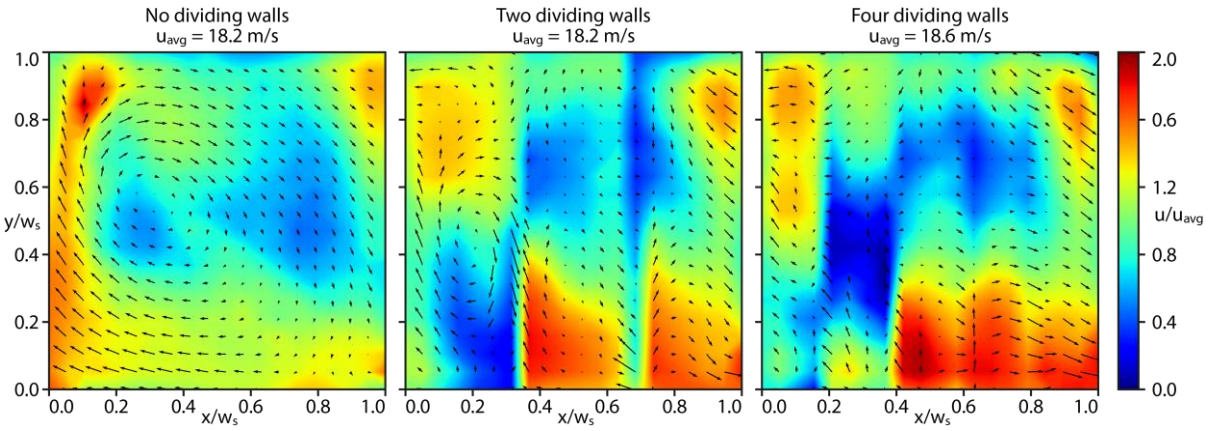

Figure 13: Velocity contours at the expansion outlet with a varying number of dividing walls

Instead of incorporating dividing walls, the diffuser can also be fitted with a wire screen. Unfortunately, as the flow passes the wire screen, small jets are created by the individual holes in the screen. These jets can disturb the velocity probe measurements, as shown in the centre of *Figure 14*. To avoid such disturbances, the measurements can be taken further downstream, where the jets have dissipated, as shown on the right of Figure 14. Here, it is apparent that the wire screen smoothed the flow contour and the CV is reduced from 0.262 to 0.159.

Conservatively evaluating the pressure losses at the wire screen downstream of the expansion, the loss factor K is found to be 1.193 ± 0.090. This is slightly below the value of 1.333 predicted based on the works of Wu et al. [8].

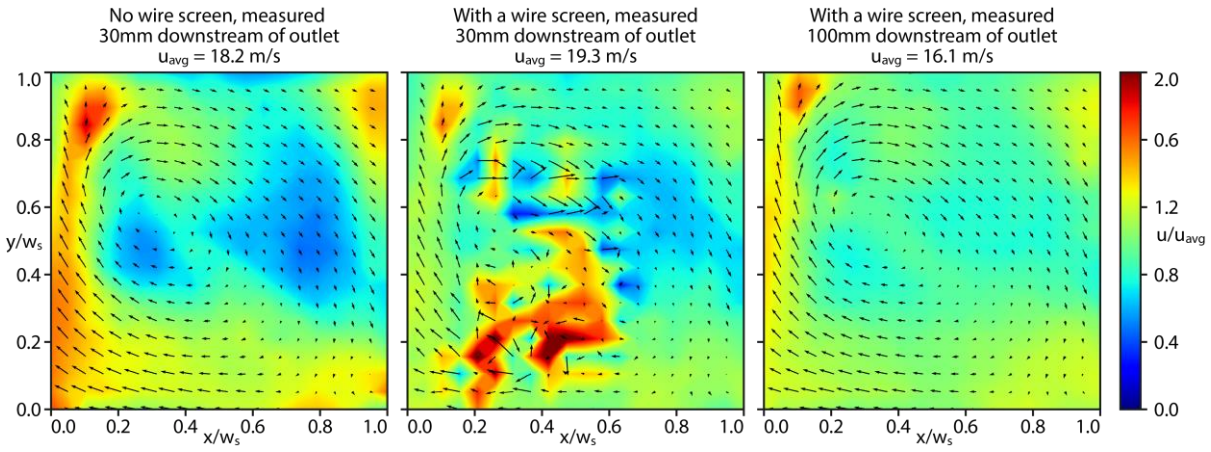

Figure 14: Velocity contours of the expansion before and after installing a wire screen

Based on flow rate measurements taken at the wind tunnel outlet, the dynamic pressures can be calculated for each wind tunnel section. This allows for an estimation of the total pressure drop through the diffuser. Based on the inlet velocity, the diffuser has a loss factor K of 0.410 ± 0.019.

In this location, some of the error can be attributed to regular vortices caused by the centrifugal blades of the fan and the random noise within the pressure measurements themselves. The theoretical loss factor prediction based on a publication by Eckert et al. is merely 0.05 [7]. Despite the loss factor in this section being substantially higher than the literature-based prediction, it is still small enough to reach satisfactory speeds in the wind tunnel.

3.3. Performance of the Turning Vanes and Honeycomb

Due to the structure of the curved section containing the turning vanes, the velocity could not be measured in the proximity of the vane cascade. Instead, the velocity was sampled 230 to 300 mm downstream of the inner vane and 830 to 900 mm downstream of the outer vane, as shown in *Figure 15*.

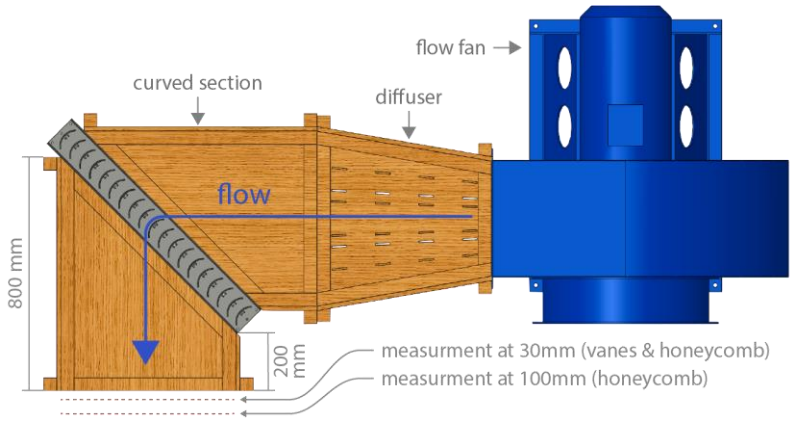

Figure 15. Birds-eye view of measurement planes used to generate the primary velocity contours shown in Figure 16

Experiments were carried out with and without the honeycomb and the resulting primary velocity contours are shown in *Figure 16*. Once again, the central contour reveals measurements that were taken too close to the flow conditioner. Where the probe aligns with a honeycomb tube it reads unreasonably high velocity and where it aligns with a tube wall it returns excessively low velocity. Thus, the resulting data seem somewhat nonsensical. As with the wire screen, this can be mitigated by taking measurements further downstream.

Upon inspecting the size and direction of the velocity vectors it becomes apparent that the secondary flow is almost entirely eliminated. Unfortunately, the honeycomb also seems to slightly increase the size of the boundary layer, as indicated by the areas of slow flow around the perimeter of the right-most contour. This means that the coefficient of variance is increased slightly from 0.125 to 0.152. Despite this increase, the honeycomb was kept in place for most further experiments, as it was deemed worthy to sacrifice a little flow uniformity for the elimination of secondary flow.

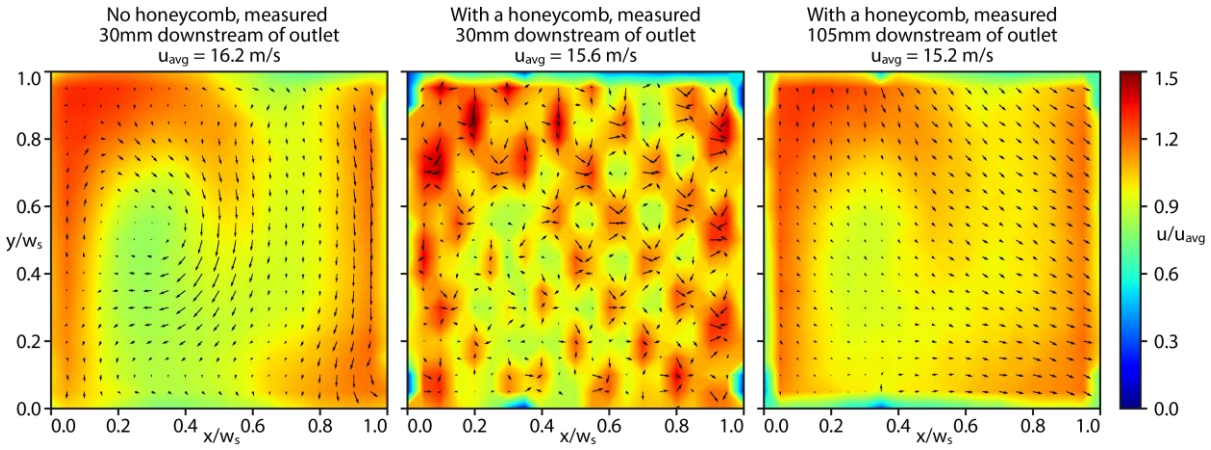

Figure 16. Velocity contours before and after installing a honeycomb downstream of the vanes

It was found that the vanes have a loss factor K of 0.258 ± 0.028, which is roughly in line with the 0.300 predicted by Vega et al. [4]. The honeycomb has a loss factor K of 0.813 ± 0.475 which is significantly higher than the literary value of 0.380, which is based on the works of Innocentini et al. [9]. The higher standard deviation is caused by the loss factor of the honeycomb not scaling with the square of the velocity. While the loss factor is around 1.96 at 1.27 m/s, it drops to 0.42 at 12.71 m/s, which is considerably closer to the value suggested in literature. As power requirements only become an issue at higher flow velocities, this discrepancy will not prevent reaching the desired wind tunnel speeds.

3.4. Effect of adding corner chamfers

The installation of the corner chamfers slightly lowered the CV in the straight sections from 0.133 to 0.127. However, this corresponds to a mere 0.07m/s reduction in the standard

deviation, which is negligible when compared to the average primary flow velocity of 16 m/s. Vega et al. suggest that the chamfers would increase the CV by reducing secondary flow, but this cannot be independently verified here [4]. Potentially the corner chamfers are too small, as their base size is only 43 mm compared to the 600 mm channel width. Nevertheless, the chamfers clearly do not have any substantial negative impacts on the flow either. Therefore, they were left in place for the majority of further experiments.

3.5. Performance of the Contraction

Measuring the flow downstream of the contraction is challenging, as the boundary layer in this section is very thin and the flow velocity is rapid. Without any flow conditioners installed, the wind tunnel can achieve speeds up to 56 m/s, which corresponds to 203 km/h or 126 mph. For reference, the highest-level wind speed ("hurricane force") on the Beaufort scale is 12, measuring a meagre 33 m/s (118 km/h or 73 mph).

When considering these speeds, it is clear that the rate of change of velocity in the boundary layer is very high. Consequently, the measurements are very sensitive to the location of the seven-hole probe. Even deviations of a single millimetre can change the readings substantially. Great care was taken to set the probe's positions correctly, but a tolerance of ±1 mm is to be expected.

Table 3. Overview of various coefficients of variance for different flow conditioner configurations

	before contraction (all points)	**after contraction (all points)**	**after contraction (no edge points)**
CV (no conditioners)	0.133	0.0442	0.00410
CV (all conditioners)	0.103	0.0499	0.00516

As shown in Table 3, the wire screens and honeycomb reduce the coefficient of variance upstream of the contraction by 23% (from 0.133 to 0.103). Interestingly, this effect does not translate downstream of the contraction. Before installing the flow conditioners, the contraction reduces the CV by 77% (from 0.133 to 0.0442), but only by 52% (from 0.103 to 0.0499) thereafter. Even when discounting the measurements on the circumference of the grid, the most sensitive to the positioning of the probe, the CV is still lower in the flow without flow conditioners.

The most probable explanation is that the measurement technique has reached an accuracy limit, as the difference between a CV of 0.0442 and 0.0499 is merely 0.0077. This approximately corresponds to a difference in the standard deviation of 0.0302 m/s. Here it is worth noting that the sensor card used for this set of trials had a measurement range of 4000 Pa and a tolerance of ±0.25% (or 10 Pa). The pressure tolerance can be expressed in terms of

velocity by using equation (6), where P is pressure, ρ is the fluid density and u is the fluid velocity:

$$u = \sqrt{2\,P/\rho} \tag{6}$$

The 10 Pa tolerance is equivalent to a speed of roughly 4 m/s for a single measurement. However, a lower standard error is produced by sampling the pressure at a rate of 100 Hz over several seconds at each point. Thus, the average standard deviation across time after all flow conditioners have been installed is 0.219 m/s. This is not to be confused with the standard deviation of the flow field across space, which is the deviation of the time-averaged velocities between measurement points and equates to 0.232 m/s. Both values significantly exceed the 0.0302 m/s increase in deviation encountered after installing the flow conditioners.

In summary, the contraction works exceptionally well. As shown in *Figure 17*, it produces a very smooth velocity contour, regardless of the use of flow conditioners. Should it not be possible to incorporate a contraction into a testing facility, wire screens can be used to increase flow uniformity by reducing peaks in the velocity profile. Honeycombs can be used to reduce the magnitude of the secondary flows, an improvement visible even downstream of the contraction. Nevertheless, the impact of these types of conditioners is far inferior to that of the 4:1 contraction.

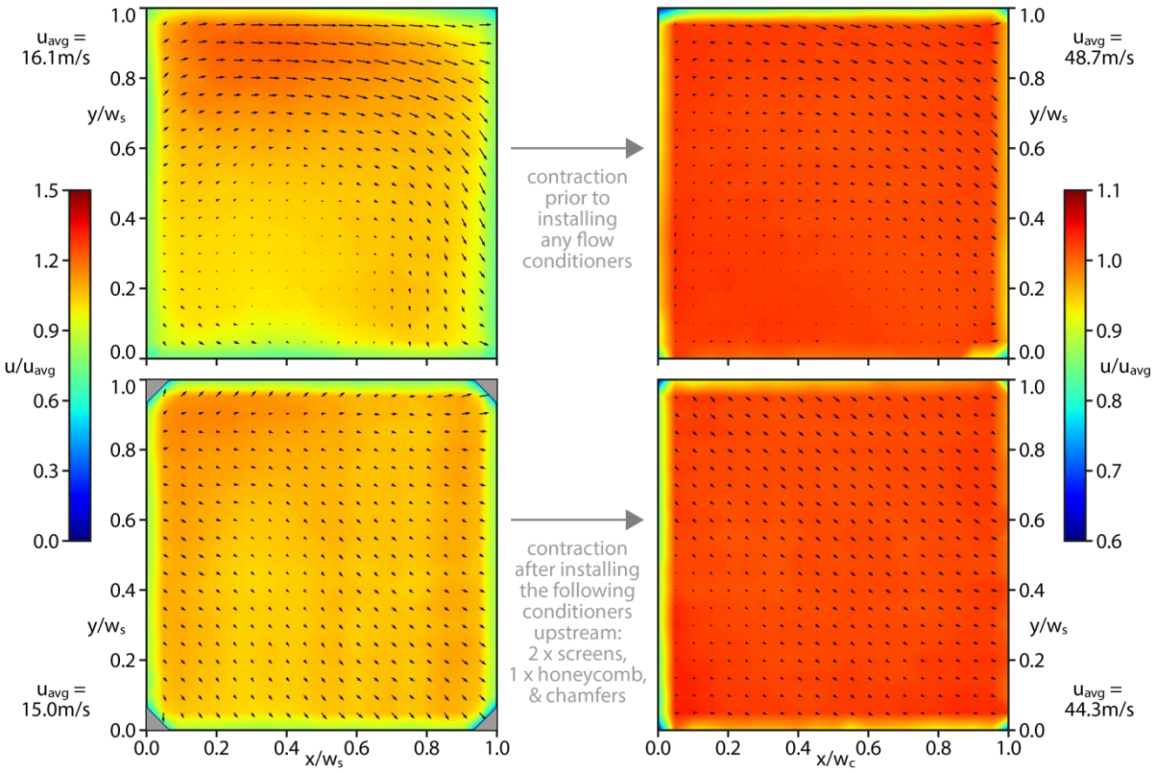

Figure 17. Comparison of velocity contours before (left) and after (right) passing through the flow contraction, with (top) and without (bottom) flow conditioners.

The experiments that have been described over the previous pages have been essential in validating that an adequate environment, for testing expansion turning vanes, has been provided. As can be seen from *Figure 17*, the contours have a slight secondary flow to the right. This is likely to do with the location of the flow fan, encouraging the flow to take the path of least resistance when leaving the tunnel, which coincidentally is towards the right.

For a majority of the flow field downstream of the contraction, the magnitude of this secondary velocity is approximately 1.2 m/s. This is equivalent to merely 2.5% of the primary velocity magnitude and, therefore, should have a negligible impact on the flow results and analysis. The turbulence intensity downstream of the contraction is 0.5% and is comfortably below the required upper limit of 1%. As shown in the contours, even with the flow conditioners installed, the wind tunnel is more than capable of reaching an average flow speed of 35 m/s downstream of the contraction. As such, all flow quality requirements have been met.

4. SUMMARY OF PRESSURE DROP PERFORMANCE

The theoretical loss factor for the straight section has been calculated using the Darcy-Weisbach equation, based on the friction factor f. Note that this factor is often determined using the Moody Chart or iterative calculations [10]. The author has found it useful to use the Sonnad-Goudar correlation instead, a non-iterative equivalent to the Colebrook-White equation [11]. Using this theoretical approach, the loss factor is predicted to be 0.017. This is in stark contrast to the experimental loss coefficient of 0.102 (see *Figure 18*).

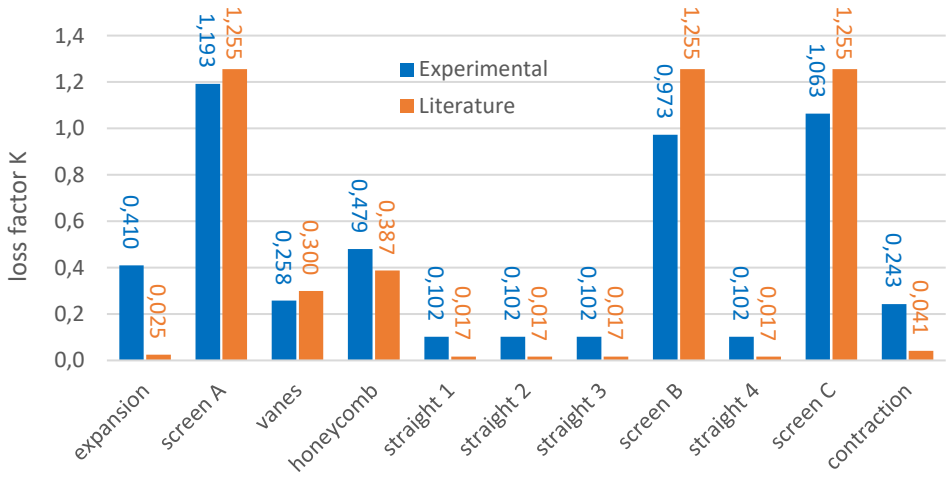

Figure 18. Theoretical versus measured pressure drops in the wind tunnel.

The difference is likely caused by the seam between the sections. While great care was taken to make the transitions as smooth as possible, small mismatches remain. However, the loss factor of the straight section becomes negligible when compared to the loss factor of the

screens. The screens clearly lead to the largest pressure drop in the system and the experimental loss being smaller than the prediction is to be taken as a clear positive.

5. CONCLUDING REMARKS

The flow characterisations demonstrate that it is possible to construct a small-scale wind tunnel with a relatively modest budget without having to sacrifice flow quality. However, building such a facility in-house is time intensive. It took approximately four months of full-time work to carry out the necessary steps (design, quotation, installation, commissioning, etc.) and another six weeks to complete the characterisation. Other key findings are summarised below:

- Conditioning the flow immediately downstream of a fan should be done with care. The flow in this area tends to be highly three-dimensional. Conditioners that segment the flow, such as dividing walls or coarse honeycombs, have the potential to decrease flow uniformity.
- Should it not be possible to include a contraction, it is possible to achieve significant improvements in the flow using honeycombs and wire screens. The former help to suppress secondary flows while the latter increases flow uniformity.
- A good contraction is key to ensuring high flow quality in the test section. The geometry used in this particular wind tunnel works so well, that it almost completely overshadows the effect of the wire screens and honeycomb.
- When incorporating wire screens, the designer should expect these flow conditioners to require a significant portion of the available power. In this system, more than half of the total pressure losses can be attributed to the three screens.

REFERENCES

[1] J. B. Barlow, §W. H. Rae and A. Pope, *Low-Speed Wind Tunnel Testing*, New York: John Wiley & Sons Inc., 1999.

[2] O. de Almeida, F. C. de Miranda, O. F. Neto and F. G. Saad, *Low Subsonic Wind Tunnel-Design and Construction*, Journal of Aerospace Technology and Management, vol. 10, 2018.

[3] C. R. Smith and S. J. Kline, *An Experimental Investigation of the Transitory Stall Regime in Two-Dimensional Diffusers*, Journal of Fluids Engineering, pp. 11-15, 1974.

[4] L. L. de Vega, F. J. M. Fernández and P. M. Botas, *Optimisation of a Low-Speed Wind Tunnel - Analysis and Redesign of Corner Vanes*, pp. 1-152, 2014.

[5] B. Lindgren and A. V. Johansson, *Design and Evaluation of a Low-Speed Wind-Tunnel with Expanding Corners*, Royal Institute of Technology, Stockholm, 2002.

[6] K. Wang, J. Yaping and C. Zhang, *Aerodynamic optimization of forward-curved blade centrifugal fan characterized by inclining bionic volute tongue*, Structural and Multidisciplinary Optimization, vol. 63, p. 2493–2507, 2021.

[7] W. T. Eckert, K. W. Mort and J. Jeau, *Aerodynamic Design Guidelines and Computer Program for Estimation of Subsonic Wind Tunnel Performance*, National Aeronautics and Space Administration (NASA), Washington DC., 1976.

[8] W. T. Wu, J. F. Liu and W. H. Hsieh, *Measurement and correlation of hydraulic resistance of flow through woven metal screens*, International Journal of Heat and Mass Transfer, vol. 48, no. 14, pp. 3008-3017, 2005.

[9] M. D. M. Innocentini, V. R. Salvini, A. Macedo and V. C. Pandolfelli, *Prediction of Ceramic Foams Permeability Using Ergun's Equation*, Materials Research, vol. 2, no. 4, pp. 283-289, 1999.

[10] L. F. Moody, *Friction factor for pipe flow*, Transactions of the A.S.M.E., pp. 671-684, 1944.

[11] J. R. Sonnad and C. T. Goudar, *Turbulent Flow Friction Factor Calculation Using a Mathematically Exact Alternative to the Colebrook–White Equation*, Journal of Hydraulic Engineering, pp. 863-867, 2006.

[12] *Employee earnings in the UK*: 2020, Office for National Statistics, London, 2021.

COMPONENTS OF TECHNICAL EDUCATION FROM THE POINT OF VIEW OF MODERN SOCIAL REQUESTS

Vitalii **PANCHUK**[1], Cristian **BARZ**[2], Volodymyr **KOPEI**[1], Oleh **ONYSKO**[1], Iuliia **MEDVID**[1], Anatolii **PANCHUK**[1], Tetiana **LUKAN**[1]

[1] *Ivano-Frankivsk National Technical University of Oil and Gas,*

[2] *Technical University of Cluj-Napoca, North University Center of Baia Mare*

onysko.oleg@gmail.com

Keywords: educational programs, educational services, professional education

Abstract*: Modern technical universities are obliged to show flexibility in the provision of educational services, since the modernization of modern enterprises is ongoing and professional employment additionally requires the rhythmic improvement of skills, skills and educational level of the employee, the permanent acquisition of other additional knowledge and skills that increase the value of the employee in the event of a corresponding need for them applying, as well as obtaining, another profession, if the employee foresees the application of his knowledge at the intersection of different fields of activity. And all this requires enabling the optimization of the provision of educational services by unifying their certain components in order to save its time and financial resources.*

1. INTRODUCTION

Increasingly, the abundance race of the humankind life by using of various technological devices is evidently put requests, in order to encourage the development of sufficient competencies in a number of completely different domains. It is no secret that the great prospects for the fullest application of personal computers and information resources are in themselves a motivational official for those who want to take a different level of enlightenment services. At modern, learning about the educational professional program, having the right to choose a number of primary subjects, often show the lust of other

disciplines of the educational propositions, which are not included in the chosen program. International educational cooperation and scientific research can gratly increase the possibility of educational qulity.

2. MOTTO "NEVER TOO LATE TO LEARN"

In the Ivano-Frankivsk National Technical University of Oil and Gas (IFNTUNG), an educational and scientific center for professional training and practice, where you can get educational services for a labor profession, such as a welder or a machine operator, has been established and is actively operating. The training of these professions takes place according to an optimized schedule, that is, it enables the provision of educational services in a convenient way for students. To master the second higher education within the university, there is a corresponding educational unit, which naturally ensures the coordination of previously achieved educational elements with the chosen one willing to study under the new educational program. The educational complex of the university includes colleges, graduates of which can continue their studies and obtain a bachelor's degree in a shortened period of 2 years. To provide an opportunity to implement own creative developments on the territory of the university, there is an Innovation Development Center [1], which became possible thanks to the international grant project 2SOFT/1.2/86 "Ro-Ua Cross-border academic development for research and innovation", which is implemented within the framework of the Joint Operational Program Romania-Ukraine 2014-2020 [1, 2].

2.1. An example of the provision of educational services, including two higher educations and two working professions

Ihor Kostyuk studied at the Department of Computerized Mechanical Engineering (KMV) of the Mechanical and Technological Faculty during 2001-2006, receiving a specialist diploma (equivalent to a master's degree).

Since 2007, Igor has been working on seismic vessels in various regions of the world. He has job at FUGRO and CGG companies as a pneumatic device mechanic (source mechanic). The work of a mechanic- engineer on pneumatic devices consists in servicing, repairing, lowering and raising all types of seismic equipment, hydraulic and pneumatic devices, compressors and compressor control systems used when working on seismic vessels (*Fig. 1*). Permanent work in repair work and a limited number of employees motivated Ihor to obtain a welder's degree within his native university. After that, he also acquired the profession of electrocar operator, which optimized the staffing schedule on the ship.

Fig. 1. Ihor Kostyuk on the background of a seismic vessel

Since his life motto is "It's never too late to learn", and at the same time the company's management gladly accepted such a motto, therefore Ihor received a second higher education within the walls of the University of Oil and Gas at the Faculty of Geophysics during 2006-2008.

2.2. An example of a college graduate who obtained a bachelor's degree in 2 years, and then entered a master's degree and completed it, receiving a diploma with honors

Andrii Bukhalo is a graduate of the mechanical college of VPTU-21, which is part of the educational complex of the University of Oil and Gas, and currently holds a master's degree in "Computerized and robotic engineering technologies". Since 2018, Andriy has been an employee of one of the most famous companies in Ukraine that produces children's toys. His current occupation is designing toys based on 3D modeling, using application software packages, which he was trained to use in the university environment (*Fig. 2*). Students of the Department of Computerized Mechanical Engineering get acquainted with 3D graphics application starting from the first year and continue to intensively apply and improve their skills throughout the entire bachelor's and master's courses.

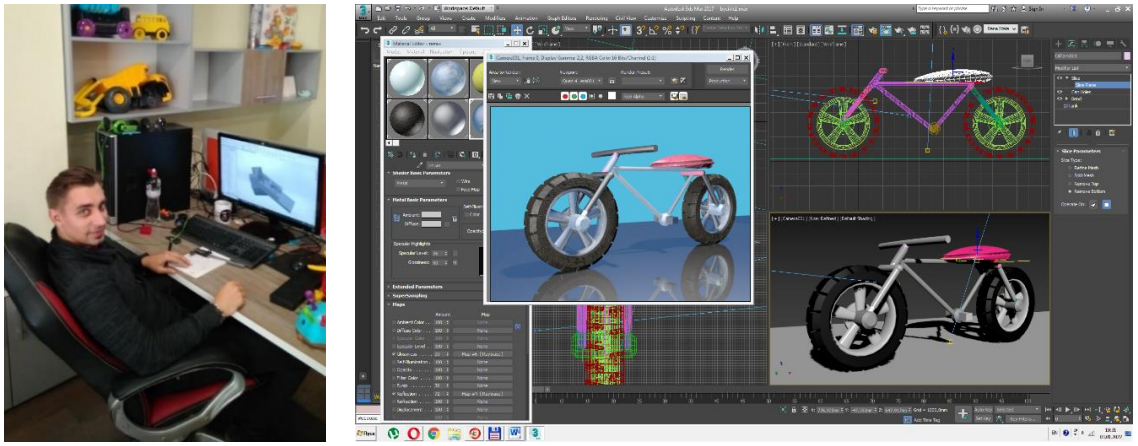

Fig. 2. Andrii Bukhalo at his workplace (2020), on the right is a screenshot from one of the educational laboratory works, which were performed in the environment of 3-dimensional graphics

2.3. An example of using the capabilities of the RoUa Innovation Development Center

One of the examples of the implementation of creative technical ideas is the active use of 3-dimensional graphics, with the subsequent implementation of the completed project using the equipment of the Center for Innovative Development (*Fig. 3*) [1], [3].

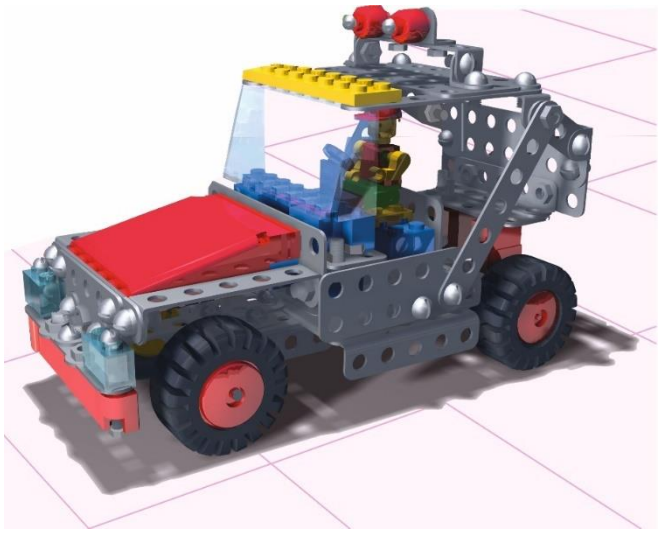

Fig. 3. A model of an innovative children's constructor, which is proposed to be developed using the equipment of the Center for Innovative

2.4. An example of receiving higher technical education in parallel under two educational and professional programs

In 2021, Bohdan Wynnychuk received a master's degree in "Computerized and robotic engineering technologies" from the University of Oil and Gas and a diploma from the Faculty of Mechanics and Robotics issued by the Krakow Academy of Mining and Metallurgy. A bilateral study agreement between two educational institutions makes it possible to receive double master's level educational services in 1.5 years (*Fig. 4*).

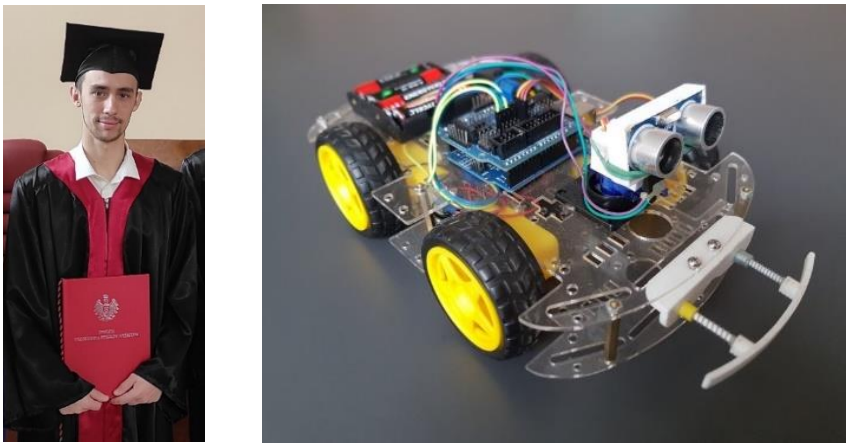

Fig. 4. Bohdan Vinnychuk with a master's degree from AGH, on the right is a robot cart designed by him and manufactured at IFNTUNG. (photo 2021)

2.5. An example of obtaining a master's degree from the Institute of Engineering Mechanics as a second higher education diploma and an internship university sertificate

Iuliia Medvid - received a master's degree in the specialty "Computerized and robotic technologies of engineering technologies " in 2020, having a previous master's degree in the specialty "Finance". The duration of study was 2.5 years. In 2022, the 1st category engineer of the Department of Computerized Mechanical Engineering Iuliia Medvid completed a 180-hour internship at the Technical University of Cluj-Napoca, North University Center of Baia Mare (*Fig. 5*).

UNIVERSITATEA TEHNICĂ DIN CLUJ-NAPOCA

Facultatea de Inginerie

CERTIFICATE

this is to certify that

Iuliia MEDVID

Engineer of
Department of Computerized Engineering,
Ivano-Frankivsk National Technical University
of Oil and Gas

passed a scientific and pedagogical internship from October 10 to November 21, 2022, at the Department of Electrical Engineering, Electronic and Computers from Technical University of Cluj-Napoca, North University Center of Baia Mare, in the amount of 6 credits (180 hours)

Internship Supervisor

Assoc. Prof. Eng. Cristian BARZ PhD

Cluj-Napoca 21.11. 2022

UNIVERSITATEA TEHNICĂ DIN CLUJ-NAPOCA

Facultatea de Inginerie

Internship program

1	Application of CAD and CAM systems for research and improvement of electro mechanics and automatic systems	30 hours
2	Acquaintance with the work programs of the disciplines: industrial automation, automation of robotic technological complexes, design, development and use of electrical, mechanical, electronic components, computer control of production processes, design, implementation and programming of specialized systems with microprocessors, microcontrollers and programmable logic circuits	40 hours
3	Gaining experience in CN controlling application	20 hours
4	Study of methods of collection, processing and transmission of signals/information in mechatronic systems	30 hours
5	Gaining experience in drawing up applications for participation in joint international research projects	20 hours
6	Preparation of an article for publication in a journal indexed in the scientific metric database Scopus and/or WoS	40 hours

Total: 180 study/work hours (6 ECTS credits)

Fig. 5. Certificate given to Iuliia Medvid that she completed an internship at the Technical University of Cluj-Napoca, North University Center of Baia Mare

3. INDUSTRIAL PRACTICE AND PROFESSIONAL TRAINING

Production of projects "in iron" is an optional but desirable element of the educational technical program. It indicates the level of engineering training and is a certain marker of professional implementation. To solve such issues, the means of subtractive and additive machining technology are available in the center of innovative development, as well as directly in the scientific and educational laboratory base of the department of Computerized Mecanical Engineering [1, 4]. An example of a combination of the design and manufacturing process is the robot arm (*Fig. 6*). It should be noted that the educational professional program "Engineering of mechatronic systems" is actually an additional bonus provided by the department of computerized mechanical engineering, in addition to the Educational Professional Programm "Applied Mechanics".

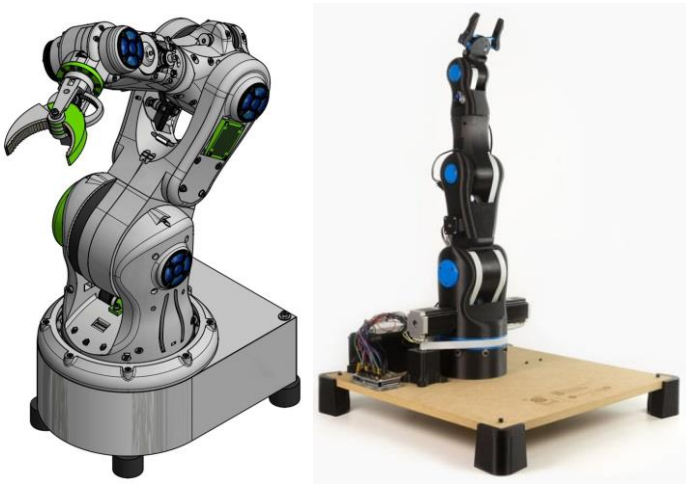

Fig. 6. 3D printed robot arm (3D model and real robot)

Important is not only the practical implementation of student projects, but also their design and research novelty. Indicative from this point of view is the thesis of the graduate of 2021 - master's student Mark Penderetskyi, which presents the development of an ultra-light cycloidal gearbox for a four-legged mini-robot [5].

4.AN EXAMPLE OF PROMOTING THE OPPORTUNITIES OF THE EDUCATIONAL AND SCIENTIFIC CENTER FOR PROFESSIONAL TRAINING AND PRACTICE

This center includes a metalworking workshop, i.e. it has metal cutting machines, welding equipment and plasma cutting machines at its disposal (*Fig.7*).

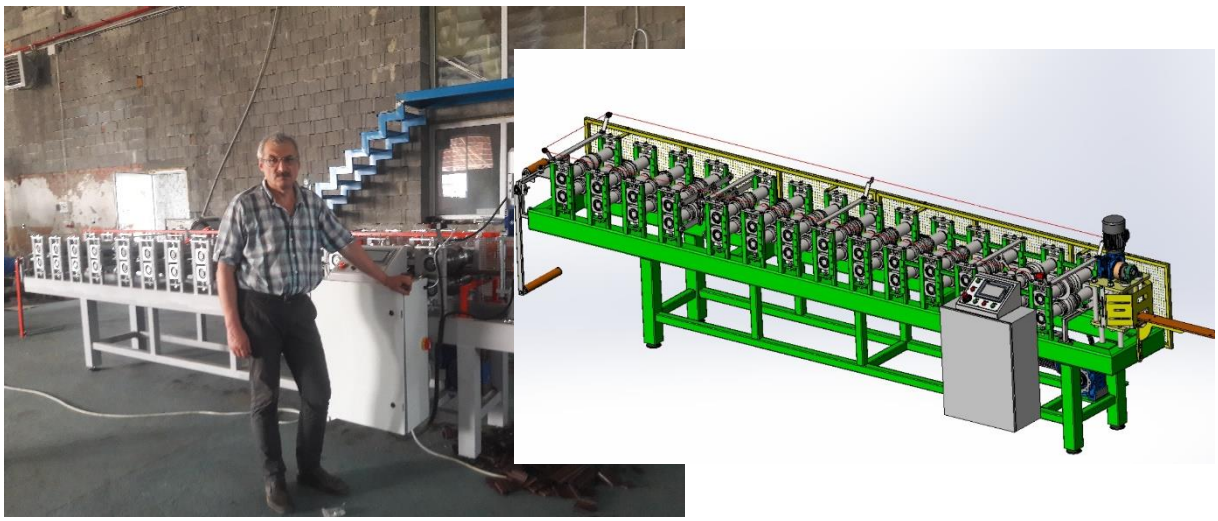

Fig. 7. Director of the center, Professor Anatoriy Panchuk of the KMV against the background of the designed and manufactured automatic line (right a computer model of the line)

The KMV department (students, graduates and teachers) participates in the development and production of modern industrial equipment. In particular, in 2021, a project was developed and its production started on the basis of the Educational and Scientific Center of Professional Training and Practice IFNTUNG - a batch of automatic lines for the production of a rack profile (*Fig. 7*).

5. CONCLUSIONS

In modern technical education, specialized software applications, specialized algorithmic languages, familiarization, production and pre-diploma practices are widely used, which are included in educational programs, but real professional employment additionally requires:

- ✓ rhythmic improvement of skills, skills and educational level of the employee;
- ✓ from time to timeacquisition of other additional knowledge and skills that increase the value of the employee in the event of the corresponding need for their application;
- ✓ obtaining another profession, if the employee foresees the application of his knowledge at the intersection of different fields of activity;
- ✓ enabling the optimization of the provision of educational services by unifying their certain components in order to save its time and financial resources;
- ✓ effective practical training in real production conditions.

REFERENCES

[1] V. Panchuk, O. Onysko, V. Nasui, R. Tirnovean, *Guide On Innovation In Mechanical Domain*, Ivano-Frankivsk, 2021.

[2] L. Shkitsa, V. Panchuk, V. Kornuta, *Innovative methods of popularizing technical education*. IOP Conference Series: Materials Science and Engineering, vol. 200, no. 1, 012023, 2017. doi: 10.1088/1757-899X/200/1/012023

[3] D. Kato, K. Hattori, S. Iwai, M. Morita, *Effects of collaborative expression using LEGO® blocks, on social skills and trust*. Social Behavior and Personality, vol. 40, no. 7, pp. 1195–1200, 2012. doi:10.2224/sbp.2012.40.7.1195

[4] *Completely new 3D printing technology on the 2nd of March at a virtual event*. URL: https://www.bcn3d.com/ sigma-source-files/ (last appeal: 10.01.2023)

[5] O. Onysko, M. Penderetsky, C. Barz, V. Panchuk, V. Kopei, L. Pitulei, T. Lukan, *Geometrical and force model of the mini cycloidal gearbox for 4-leggs robotic platform.* Innovative mechanical engineering. University of Niš, Faculty of Mechanical Engineering. vol. 1, no. 3, pp. 109 – 114, 2022.

ANALYSING THE PERFORMANCE OF PHOTOVOLTAIC SYSTEMS IN THE MARAMURES REGION

Cristian **BARZ**[1], Zoltan **ERDEI**[1], Oleh **ONYSKO**[2], Predrag **ŽIVKOVIĆ**[3], Iuliia **MEDVID**[2], Vitalii **PANCHUK**[2], Vesna **RODIC**[4], Alexander **BARON VON HOHENHAU**[1]

[1] *Technical University of Cluj-Napoca, Department of Electrical, Electronic and Computer Engineering*

[2] *Ivano-Frankivsk National Technical University of Oil and Gas, Department of the Computerized Machine Building, Ukraine*

[3] *University of Niš, Faculty of Mechanical Engineering, Niš, Serbia Independent*

[4] *University Banja Luka, Republic of Srpska, Bosnia and Herzegovina*

cristian.barz@ieec.utcluj.ro,

Keywords: Photovoltaic system, inverter, Fronius, productivity analysis, PVGIS;

Abstract: *This paper presents the performance of several types of inverters and the data they collected in the MARAMURES region of Romania. They were run in various different environments, angles of inclination and geographical positions. Each type of inverter is equipped with an application which helps the operator keep a record of daily production, track instant production and even check the monthly and annual power output. The last part compares the real energy production with a forecast generated by the PVGIS platform. This shows the differences in efficiency between two photovoltaic installations of the same type and size, due to different angles of elevation and azimuth.*

1. INTRODUCTION

Green energy is one of the key requirements for a sustainable future. The global push to promote the transition to green energy has increased rapidly in recent years. This has led to a sharp fall in prices, making renewable energy much more accessible. Iceland, for example, has extensive geothermal resources, while places such as the Scottish Highlands are

suitable for wind energy. While the United States has invested in hydropower, in other areas, solar power is best. Each type of renewable energy comes with advantages and disadvantages, often related to supply. Therefore, the best solution often uses a combination of different energy sources.

The development of solar energy is not new. It started more than a hundred years ago, in the midst of the industrial revolution, when Henry Becquerel discovered the photovoltaic effect. This allows for the production of electricity directly from the sun's rays. For many consecutive years, photovoltaics remained just a curiosity, as the transformation of solar radiation into electricity was too inefficient. Due to the advent of the transistor and the continuing advancements in semiconductor technology, the efficiency of photovoltaic panels has increased significantly. Over the years, efforts have been made to increase the efficiency of photovoltaic energy, making it more and more practical [1].

One of the most promising types of unconventional energy sources in the world is photovoltaic energy. Compared to traditional fossil fuels, such as coal, oil, and gas, or even nuclear energy, the advantages are quite clear. Solar energy does not emit greenhouse gases, does not require the use of radioactive elements, and requires low levels of maintenance. Furthermore, photovoltaic systems require comparatively few components, and the contained photovoltaic cells have a lifespan of several decades.

Thanks to modern power generators, which can easily be installed in every house, individual users can generate their own energy, quietly and without any fear. In contrast, wind and hydropower often require complex turbines to drive generators and produce electricity. These turbines and generators are noisy and contain moving parts which wear and break down over time, thereby necessitating more frequent maintenance [2-7].

EU legislation on the promotion of renewable sources has evolved significantly over the last 15 years. In 2009, EU leaders set a target for 20% of EU energy consumption to come from renewable energy sources by 2020. In 2018, the target was adjusted to 32% of EU energy consumption to come from renewables by 2030.

In July 2021, in view of the EU's new climate ambitions, the co-legislators received a proposal to revise the target to 40% by 2030. Debates are currently taking place on the future policy framework for the period after 2030 [8].

In this study, we try to determine the level of investment required for solar power plants and estimate the required time period for the return on our investment. All the calculations are based on statistical data gathered over the years from various web platforms.

2. PHOTOVOLTAIC SYSTEMS

The basic component of a photovoltaic system is the photovoltaic cell which is made of semiconducting materials, their properties being used to capture solar radiation. Through

the inverter in the photovoltaic system, solar radiation is transformed into a direct current, which in turn is transformed into alternating current [9-10].

In more than half of Romania, the annual solar irradiance ranges from 1000 to 1300 kWh/m^2/year. The most important regions of Romania with high solar potential are the Black Sea coast, Dobrogea, and a great portion of the Romanian plain, with an average irradiance of 1600 kWh/m^2/year [11]. This climate allows for the efficient operation of solar panels from March until October.

Romania's experience in solar energy represents a competitive advantage for the future development of this area, as the country is a pioneer in the field. Between 1970 and 1980 around 800,000 m^2 (0.8 km^2) of solar collectors were installed, placing the country third worldwide in the total surface of photovoltaic cells. These research efforts generated an important human and infrastructure potential. Between 1984 and 1985 the peak of solar installations was achieved but after 1990 unfavourable macroeconomic developments led to the abandonment of production and investments in the solar energy field. Today about 10% of the former installed collector area is still in operation [12].

3. INVERTERS

An inverter is a device that converts direct current (DC 12V) into alternating current (AC 240V). Most household appliances are powered by an alternating current of 240V. When the energy is taken from a direct current source, a generator, or a battery, the inverter has the important role of transforming this energy into alternating current. In conclusion, the inverter can be thought of as a *bridge*, connecting the direct current power source and the alternating current device.

Over the years, the technology used in common inverters has advanced enormously, and modern appliances are equipped with numerous refined functions. This allows the inverter to operate at a heightened level of performance (depending on the number of volts required to power the device), thus facilitating electricity savings and easing installation and transport.

The quality of an electrical signal transmitted by a pure sine wave inverter is essential to power most electrical devices, as they are highly sensitive to the nature of the electrical signals they receive.

3.1. Single-phase inverters

Single-phase inverters are predominantly used by residential consumers and are mainly found in apartments. Therefore, the power of such a connection cannot exceed 9.9 kW. The

advantage of these devices is the reduced cost when compared to a three-phase inverter, and the compatibility with single-phase electrical networks.

The Fronius Primo without a transformer (*Fig. 1*), is an ideal compact single-phase inverter for homes and small businesses, applications with power categories from 3.8 to 8.2 kW, in accordance with the ESA rules for residential applications.

Fig. 1. Fronius Primo Inverter

There are many inverters on the market (*Fig. 2.*) (Fronius, Huawei, Goodwe, Solis, etc.). All of them have an online platform for monitoring and some can even be controlled remotely.

Fig. 2. Different inverters types (Huawei and Solis)

A conventional single-phase inverter is based on four insulated-gate bipolar transistors (IGBTs) each containing an anti-parallel diode to provide bidirectional current. This is controlled through Pulse-width modulation (PWM) which helps to achieve the desired voltage. Finding the desired voltage is usually done through an external adjustment loop at the upper level, which then enables PWM generation.

Among other things, the external control loop must be able to supply the required sinusoidal frequency and the correct amplitude in relation to the bus voltage.

3.2. Three-phase inverters

Three-phase systems are usually used for industrial applications or for buildings containing large consumers. They convert direct current to three-phase mains current. This allows for a greater distribution of electricity, as it allows a DC voltage to be converted into a balanced three-phase sinusoidal voltage. Compared with single-phase inverters, three-phase inverters can support more switches to increase the accuracy of the proposed voltage while also reducing harmonics.

The Fronius Primo can operate efficiently at a maximum input voltage of 600 V. For increased efficiency and extra cost savings in commercial applications, the Fronius Primo can operate at a maximum input voltage of 1000 V. The industry's top features now come as a standard with the Fronius Primo, including dual maximum power point tracking, spring failure protection, and integrated wireless monitoring. The integrated SunSpec Modbus interface enables uninterrupted data monitoring and recording via the Fronius online and mobile platform, Fronius Solar-Web, which displays current data and a wide range of settings.

Inverters connect regularly to their own smart meters (*Fig. 3*), through which they can control the power supplied to the grid. This is especially useful to maintain a value of 0 Wh if no energy is to be supplied to the electrical grid and production is only intended for in-house consumption. The smart meters are placed in the main electrical panel monitoring the entire electrical network. They display the amount of energy produced by the solar panels, as well as the power consumed within the system, with the help of inverter communication.

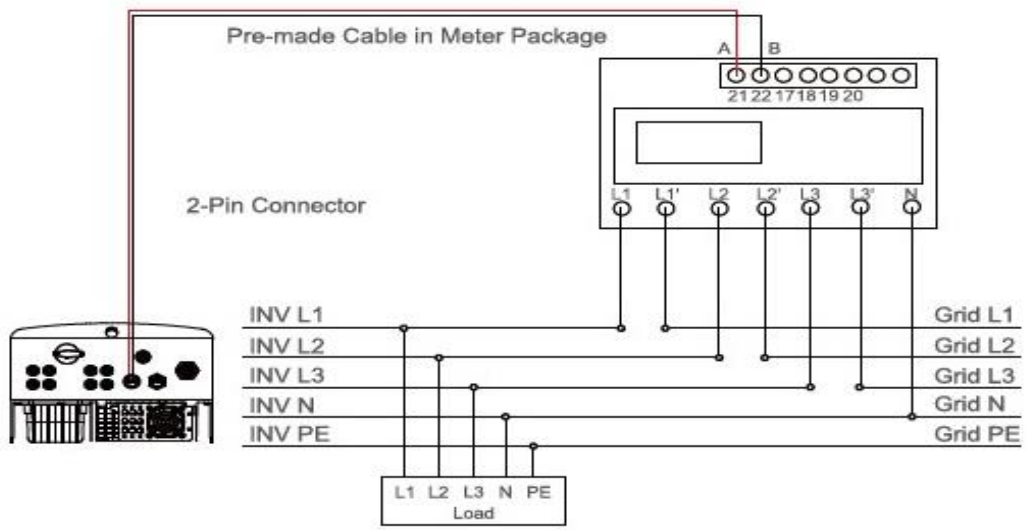

Fig. 3. Connection diagram of a three-Phase with a smart meter

4. ANALYSIS OF THE PERFORMANCE

This application of inverters comes for helping the installers with the role of configuring the appropriate settings depending on the installation locations of the photovoltaic systems. The application for the operators of the photovoltaic system allows them to visualize the data production in real-time and a history of the energy production for months and years.

With this, the operators can approximate the energy production and optimise energy consumption by operating the most power-hungry appliances when the photovoltaic system has the maximum output.

This paper analyses different characteristics of photovoltaic systems (type, angle position, azimuth, etc.) in comparison with the predicted quantity of energy provided by the statistical data on the PVGIS (Photovoltaic Geographic Information System) platform. All these characteristics influence the daily energy generated by solar power plants, which is crucial information needed to calculate the investment efficiency of solar systems.

We analyse systems placed in the same region, to ensure constant weather conditions. However, the structural orientation varies. The first solar system is mounted on a tin roof with an elevation of 25° and azimuth of -16.60°. The second system is also mounted on a roof with an elevation of 35° and azimuth of -85° (*Fig. 4*).

Fig. 4. Comparing positions of both solar systems

These two particular solar systems were chosen for comparison as they are located in the same region in Lapus County, have the same installed power of 3kW, and have the same type of Fronius Primo inverter for better accuracy of the measured results.

All inverter platforms are password protected and can only be accessed by the installation company or the owner of the system. The platforms provide information related to the daily, weekly, monthly and annual energy production, the internal energy consumed, the

amount of money earned from generation, the prevented carbon dioxide emissions and much more. All these functions allow for better monitoring of the solar system and its efficiency.

Analysing the daily production between the two systems, there is a clear difference of a few hundred watthours per day on the 22 of June 2022 (*Fig. 5*).

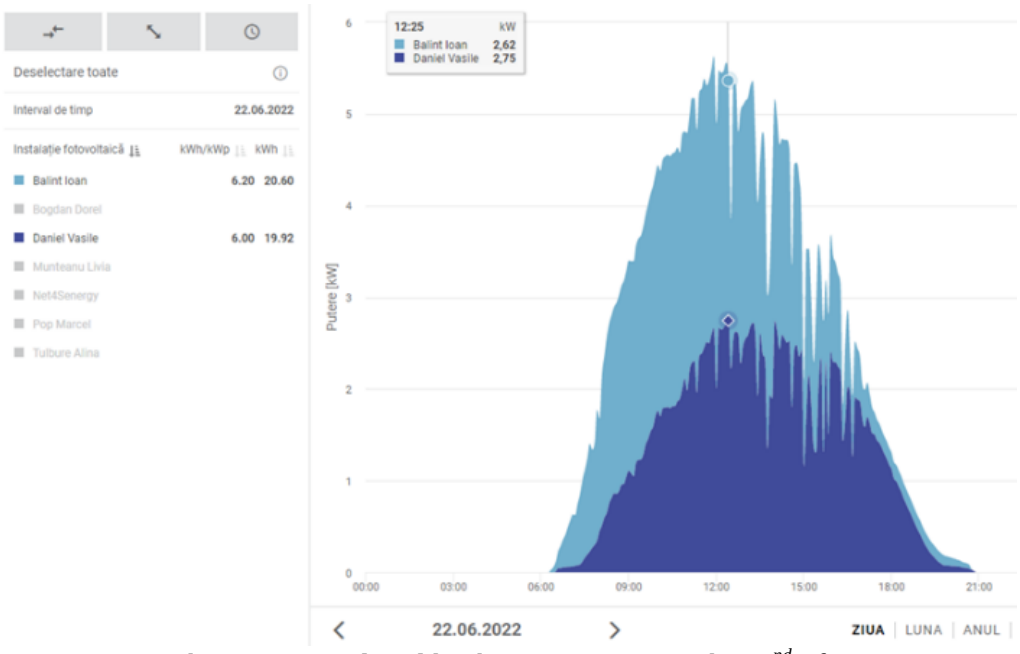

Fig. 5. The energy produced by the two systems on the 22nd of June 2022

For the whole month of June, the difference amounts to approximately 15 kWh, which equates to 3% more energy against a monthly reference output of 500 kWh (*Fig. 6*).

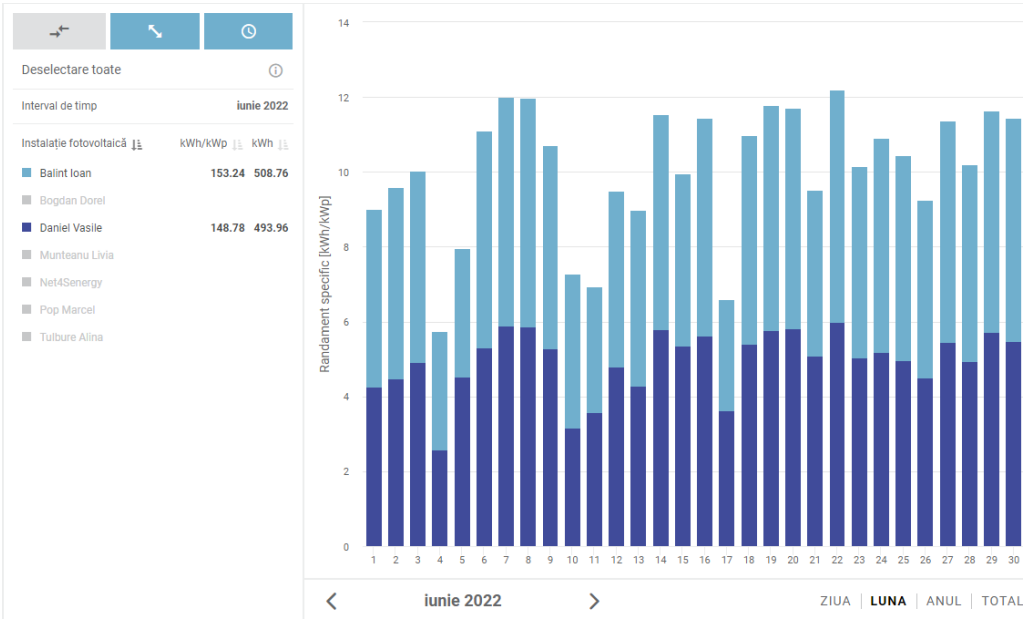

Fig. 6. The energy produced in June 2022 by the two systems

Based on this information the amount of energy produced at these locations can be forecasted. The values from the forecast (*Fig. 7*) can then be compared to the real output achieved after the system was installed (*Fig. 8*). In October 2021, the real value of 311 kWh was substantially higher than the 280 kWh forecasted by the PVGIS platform. Of course, the PVGIS platform provides an approximative value based on statistical data collected over the years and it is obvious that the weather can be different from year to year.

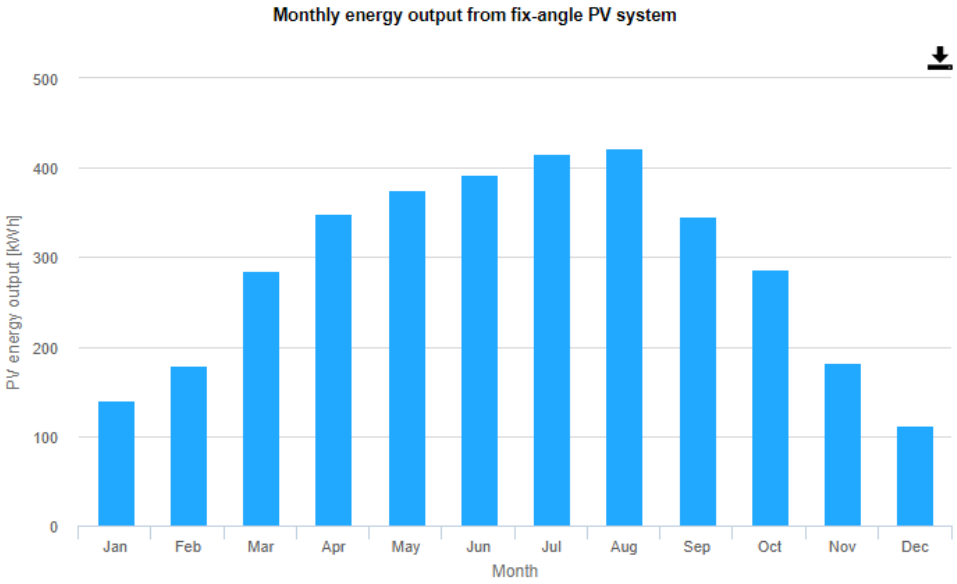

Fig. 7. Monthly forecasted energy in Lapus Country

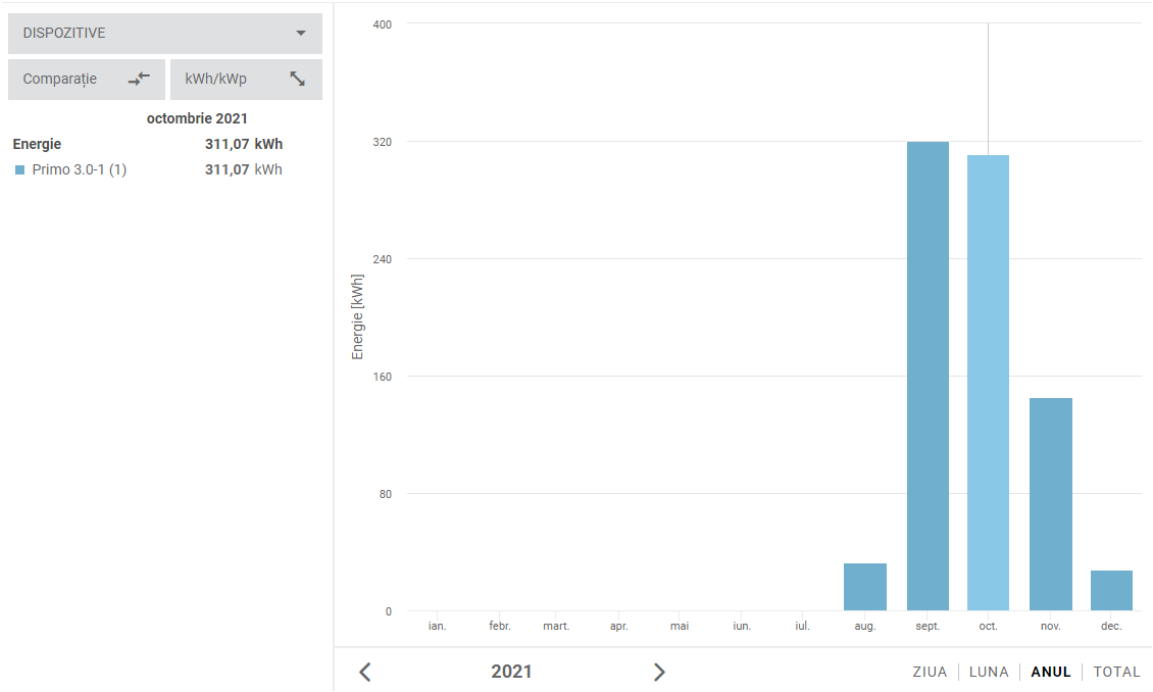

Fig. 8. Energy produced monthly in 2021 by the first system

We compare another month with PVGIS platform (*Fig. 9*), now from June 22 when we have generated energy by 494 kWh in comparison with 285 kWh from statistical, comparison is important because with statistical data we have a value of start for calculating the period of recover our investment in the solar system.

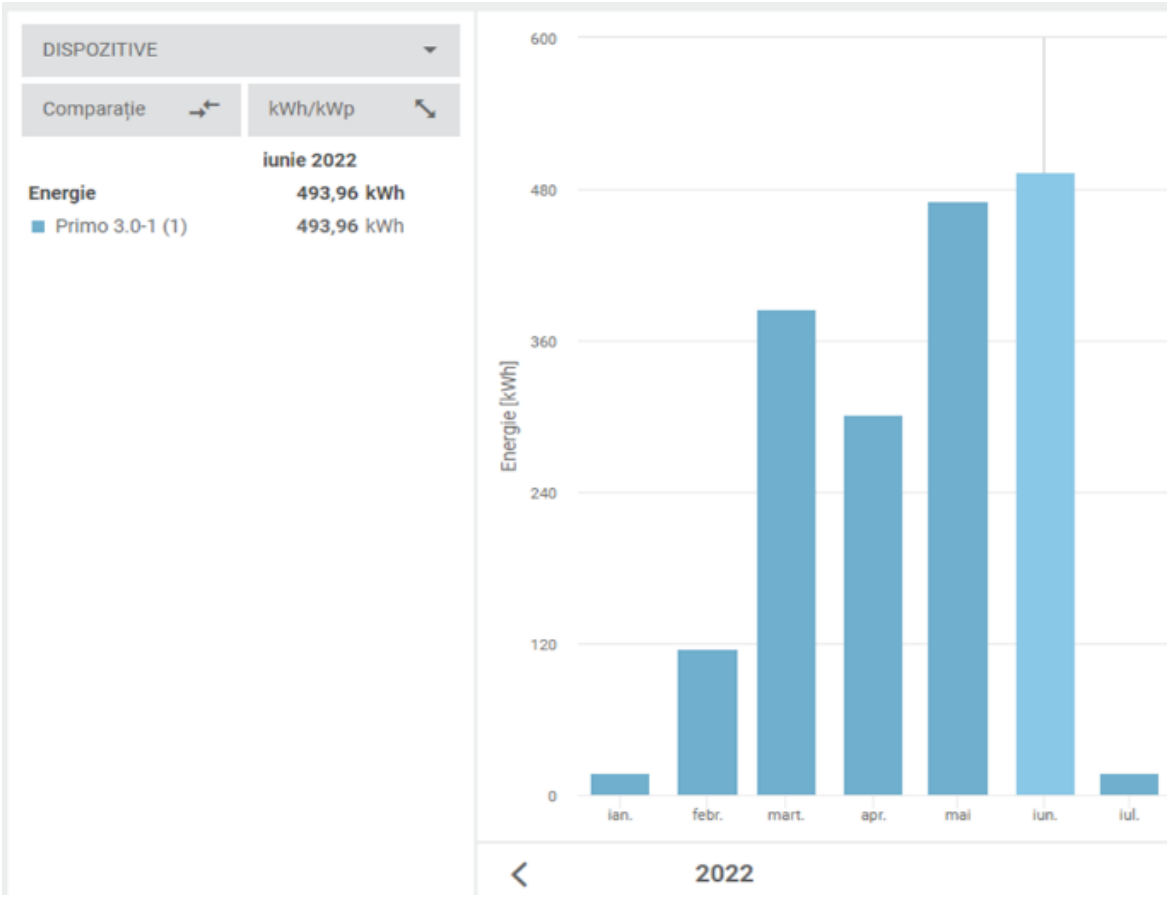

Fig. 9. Energy produced in June 2022 by the first system

5. CONCLUSIONS

Considering that both systems operated in the same weather conditions, the additional energy generated by the second system may be the result of the different angles of elevation, azimuth and inclination of the solar panels.

It has been shown that the monthly energy produced by the system was higher than the forecast for all months of the year, which indicates that the investment in the solar system will be recovered more quickly than anticipated (around one year less).

Nowadays, it is important that all the aspects of renewable energy are considered. Solar panels are easily available for everyone, but these systems are not cheap. Investments can often be recovered within 10 years and with new legislature and subsidies in Romania, investments can be recovered in as little as 6 years for on-grid systems.

REFERENCES

[1] Wati D. A. R., *Maximum power point tracking of photovoltaic systems using simple interval type-2 fuzzy logic controller based on hill climbing algorithm*, 2016 International Seminar on Intelligent Technology and Its Applications (ISITIA), pp. 687-692, 2016.

[2] Sias, QA and Robandi, I, Recurrence Perturb and Observe Algorithm for MPPT Optimization under Shaded Condition, 2016 International Seminar on Intelligent Technology and Its Applications (ISITIA), Lombok, Indonesia, pp. 533-538, 2016.

[3] Joy M. C., Chaithanya V. and Jayanand B., *Three-phase Infinite Level Inverter*, 2016 IEEE 1st International Conference on Power Electronics, Intelligent Control and Energy Systems (ICPEICES), pp. 1-6, 2016.

[4] Islam M. and Czarnecki L., *Design and simulation of a single phase grid connected photovoltaic CukZeta inverter*, 2013 IEEE 39th Photovoltaic Specialists Conference (PVSC), pp. 2896-2901, 2013.

[5] Patrao I., Figueres E., Gonzalez-Espin F. and Garcera G., *Transformerless topologies for grid-connected single-phase photovoltaic inverters*, Volume15, Issue7, pp. 3423-3431, 2011.

[6] Jaen-Cuellar A. Y., Elvira-Ortiz D. A., Osornio-Rios R. A. and Romero-Troncoso R. J., *Efficiency monitoring of photovoltaic inverters considering weather conditions*, 2018 IEEE International Autumn Meeting on Power, Electronics and Computing (ROPEC), pp. 1-6, 2018.

[7] Gong Y., T. Lv, Duan Y., Wang H. and Li Q., *Controllable power output research for single phase photovoltaic inverter*, 2009 International Conference on Sustainable Power Generation and Supply, pp. 1-4, 2009.

[8] Parlamentul și Consiliului European, *Directiva 2009/28/CE privind promovarea utilizării energiei din surse regenerabile, de modificare și ulterior de abrogare a Directivelor 2001/77/CE și 2003/30/CE*, 23 aprilie 2009.

[9] Duong M.Q., Le K., Sen D., Mussetta M., Sava G., Effects of bypass diode configurations on solar photovoltaic modules suffering from shading phenomenon, 2017 10th International Symposium on Advanced Topics in Electrical Engineering (ATEE), pp. 731-735, 2017.

[10] Wardhana A. S., Suryoatmojo H. and Ashari M., *Design of parabolic solar concentrator to improve the optical efficiency for thermal engine generator using dual reflector Gregorian method*, 2016 International Seminar on Intelligent Technology and Its Applications (ISITIA), pp. 457-464, 2016.

[11] European Bank for Reconstruction and Development (EBRD). *Renewable Energy Resource Assessment. Romania. Country Profile*; 2010

[12] Vac C., Sana S., Arion F., *Renewable Energy Market in Romania*, Bulletin UASVM Horticulture, 68(2), pp. 237–40, 2011.

Acknowledgements

This article was produced under the project HUSKROUA/1702/6.1/0075 "Cross-border network of energy sustainable universities" – Net4Senergy, as part of the ENI CBC Hungary-Slovakia-Romania-Ukraine 2014-2020.

ANALYSIS OF ELECTRICITY USE IN THE TOURISM SECTOR OF IVANO-FRANKIVSK REGION

Iryna **SMYK**, Liudmyla **ARKHYPOVA**

Department of Tourism, Institute of Natural Sciences and Tourism, Ivano-Frankivsk National Technical University of Oil and Gas, Ivano-Frankivsk, Ukraine

iryna.smyk-a10122@nung.edu.ua, konsevich@ukr.net

Keywords: ecological safety, tourism industry, electricity consumption, renewable energy sources.

Abstract: *The article presents an analysis of electricity use in the tourism sector of Ivano-Frankivsk region. The territorial structure of electricity consumption distribution in the tourism sector across the regions of Ivano-Frankivsk region has been studied, and quantitative indicators of electricity use by the tourism sector over the last five years have been modeled. It has been demonstrated that as the number of tourists increases, the proportion of electricity consumed from the overall energy network also increases, as the share of electricity generated from renewable sources for self-sufficiency of the tourism sector is currently negligible. Analysis of global experience allows us to assert that the use of renewable energy sources is environmentally friendly, modern, safe, and resource-efficient, and is the path chosen by all developed countries. A review of information sources suggests that modern tourism development includes several aspects: reducing carbon footprint, reducing the impact on local ecosystems, and increasing economic benefits for local communities. It is important to understand that expenditures on ecology and nature conservation measures are not just unavoidable costs, but also investments in business. Such an attitude allows for benefits and profits. Investments in green technologies always pay off, as today's modern tourists are willing to pay for comfort and ecology. The necessity of referring to global experience in using renewable energy sources in tourism is emphasized, and trends in implementing global experience in the practice of tourism industry in Ivano-Frankivsk region are analyzed.*

1. INTRODUCTION

In the modern world, the development of research on environmental safety is becoming increasingly relevant, especially when it comes to sustainable development and ways of

preventing negative impacts on the environment through the use of alternative sources [1]. Additionally, the tourism industry is gradually recovering after experiencing catastrophic consequences during the pandemic. The latest UNWTO data indicate that tourism is slowly returning to pre-pandemic levels starting from 2021. However, this positive trend also brings about a number of negative impacts on the environment, as the share of electricity use, water supply, and pollution in recreational areas increases. Today, it is extremely important for Ukraine to address the issue of rational use of electricity, as the energy infrastructure has suffered catastrophic consequences from military actions on its territory [2]. Analysts estimate that the full restoration of the energy infrastructure could take from two to five years, and restrictions on electricity use may last until the end of the war. Since the tourism industry is directly dependent on the energy system and requires round-the-clock electricity supply, it is necessary to study electricity usage trends in the largest tourist areas of Ukraine [3].

Since February 2022, the number of internally displaced persons in the Ivano-Frankivsk region has reached almost 140,409 people, according to the head of the regional military administration. In the first months of the war, the hotel industry in the Ivano-Frankivsk region reached 100% occupancy rate, which negatively affected the level of environmental impact of accommodation facilities, as the use of electricity increased several times, leading to an increase in PM10, SO2, and NOx emissions. Therefore, we consider research on the use of electricity in the tourism industry to be relevant and will lead to further addressing the issue of increasing the level of ecological safety of the territory. It also stimulates the search for new energy supply systems for the tourism industry in order to reduce environmental damage.

2. RESEARCH COURSE

Based on the above analysis of the problem and the accumulated scientific and practical experience, the following tasks have arisen before us:

- to study the ecological problems and negative consequences caused by irrational use of energy resources;
- to investigate the current state of tourism development in the Ivano-Frankivsk region;
- to analyze the use of electricity in the Ivano-Frankivsk region and to investigate the share that falls on the tourism industry;
- to study the prospect of widespread use of renewable energy sources (RES) in the tourism sector.

The article employs general scientific methods, including dialectical method and systemic approach. Additionally, analysis and synthesis methods, as well as statistical analysis, were used to investigate the use of electricity by the tourism sector.

3. RESULTS

Ecological safety during the exacerbation of threats associated with the negative impact of war on the environment is the most important component of overall safety. Situations related to natural and man-made safety are considered at meetings of the National Security and Defense Council of Ukraine. The materials of such discussions form the basis of decrees of the President of Ukraine. Decrees coordinate the efforts of executive authorities aimed at preventing emergencies, disasters, and other extraordinary situations, as well as aimed at improving the system of regulation and improving the state of natural and man-made safety [3].

According to energy expert V. Vidzyhovskyi, in the conditions of war, it is necessary to have prepared solutions to maintain reliable operation of Ukraine's energy security. In addition, the director of energy programs at the Razumkov Center, Volodymyr Omelchenko, believes that the risks of Russian missile strikes on Ukraine's energy infrastructure are directly proportional to the de-occupation of Ukrainian territories [3]. Therefore, the destruction of thermal power plants (TPPs) and combined heat and power plants (CHPPs) is a significant problem for ecological security, as it leads to uncontrolled air pollution, which is assessed by three indicators of emissions: PM10 - solid micro-particles of ash dust with a size of up to 10 microns, which can cause respiratory diseases; SO2 - sulfur dioxide, which in high concentrations can cause life-threatening fluid accumulation in the lungs; NOx - nitrogen oxides - gases that cause inflammation of the respiratory tract and disrupt cellular mechanisms [4].

Furthermore, thermal power plants (TPPs) are one of the main sources of environmental pollution, causing acid rain that drastically reduces soil fertility and crop yields, and leads to forest destruction. Just one coal-fired TPP with a capacity of 1000 MW emits about 90 tons of arsenic, 300 tons of barium, 20 tons of mercury, and other toxic elements into the environment annually. Even the emissions of radioactive substances from coal-fired TPPs are 2-5 times higher than those from nuclear power plants. Therefore, the issue of reducing the ecological footprint of the energy system remains relevant.

In particular, the Cabinet of Ministers of Ukraine's Order No. 907-r dated August 4, 2021, approving the Energy Security Strategy, states that the country's energy infrastructure is worn out and characterized by high energy losses during production, transportation, and consumption, a lack of energy-efficient changes, and the structure and characteristics of generating capacities do not meet the needs. Furthermore, the generating capacities that operate using coal are among the largest polluters of the environment, are on the brink of a critical resource limit and physical deterioration, and require replacement with more sustainable and environmentally friendly energy production. [5]

To analyze the use of electricity in the tourism sector, it is advisable to analyze the latest official statistical indicators of the development of the tourism industry in the Ivano-Frankivsk region.

Starting from 2015 to 2018, the tourism industry in Ivano-Frankivsk region had a positive trend of increasing the number of tourists. In 2017, the region was visited by 2.1 million tourists, while in 2018 the number increased to 2.2 million. Since 2019, there has been a slight decline in the number of tourists, with 2 million visitors recorded that year. In 2020, the figure was 1.8 million, a 10% decrease from the previous year. In 2021, the number of visitors returned to the 2019 level and amounted to 2.0 million tourists. *Figure 1* shows the number of tourists who visited the region from 2017 to 2021.

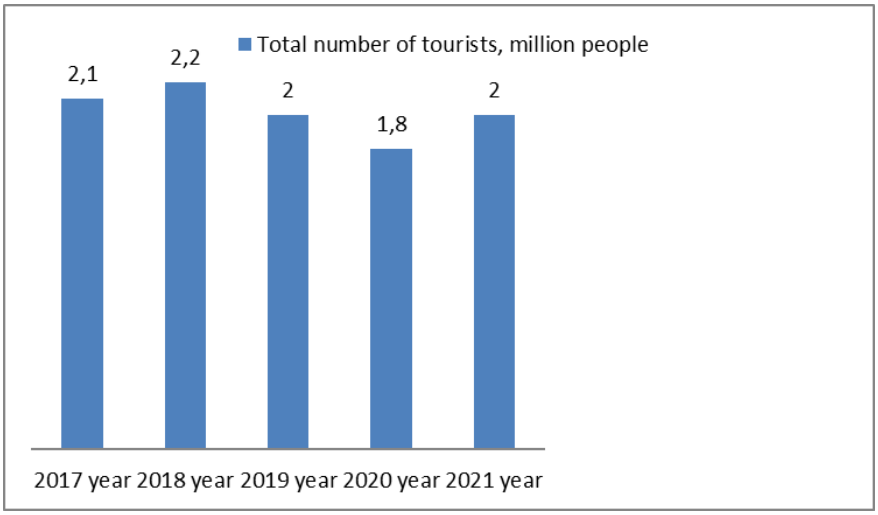

Figure 1. The total number of tourists who visited the Ivano-Frankivsk region in 2017-2021 [6]

The website of the Ivano-Frankivsk Regional State Administration does not provide data on the consumption of natural gas and electricity in the Ivano-Frankivsk region, so we can model the calculation of one-time electricity usage by tourists.

According to energy experts, on average, one person consumes approximately 11.47 kWh of electricity per day [7]. Accordingly, the daily electricity consumption by tourists over the past five years is as follows:

- In 2017 - 24 million kWh;
- In 2018 - 25.23 million kWh;
- In 2019 - 22.9 million kWh;
- In 2020 - 20.64 million kWh;
- In 2021 - 22.9 million kWh.

According to the results of a monitoring sociological study of the tourism industry in the Ivano-Frankivsk region [8], the average stay of tourists in the region is 3 days, so we can obtain an approximate indicator of electricity consumption by the tourism sector per year. The graphical representation is shown in *Figure 2*.

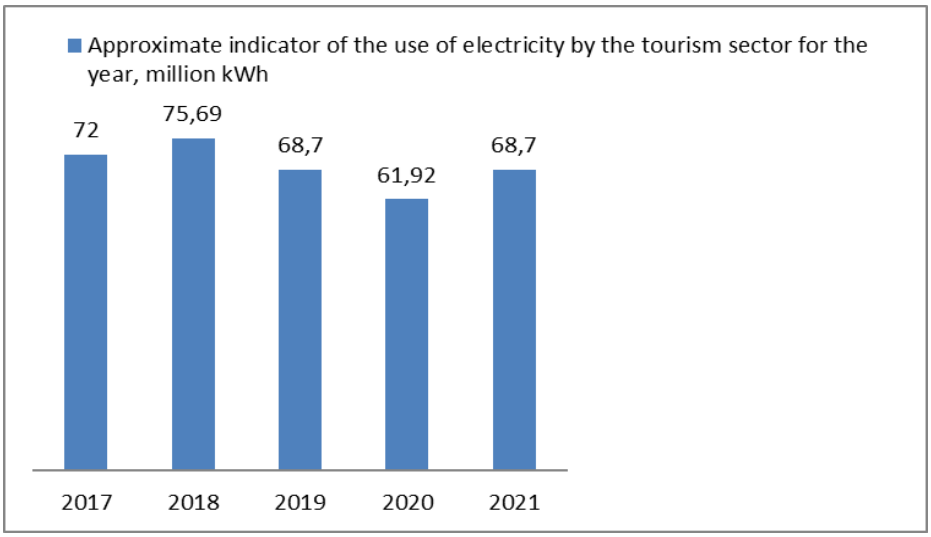

Figure 2. Estimated indicators of electricity use (million kWh) by the tourism sector of the Ivano-Frankivsk region over the past five years

Thus, as the number of tourists increases, the share of electricity consumption also increases. The geography of the visited regions in Ivano-Frankivsk region is as follows: the largest number of tourists were concentrated in the territories of Polianytska local community, Yaremchanska local community, Ivano-Frankivsk city, and Vorokhtianska local community.

In the report by the Chief of the Tourism Department of the Department of International Cooperation, European Integration, Tourism, and Investments of the Ivano-Frankivsk Regional State Administration, Vitaliy Perederko, it was noted that the tourist tax of Ivano-Frankivsk region for 12 months of 2022 amounted to 17.96 million UAH. The largest territorial revenues were recorded in the following communities: Polianytska - 9,813.02 thousand UAH (54.65% share of the total volume of revenues in the region), Yaremchanska - 3,274.08 thousand UAH, Ivano-Frankivska - 2,428.72 thousand UAH, Vorokhtyanska - 975.15 thousand UAH, Kosivska - 306.23 thousand UAH, Vygodska - 187.75 thousand UAH, Kolomyiska - 166.95 thousand UAH, Verkhovynska - 156.98 thousand UAH, Delyatynska - 81.34 thousand UAH, Bohorodchanska - 80.32 thousand UAH [8].

Therefore, based on this data, we can model the territorial structure of the distribution of electricity consumption by the tourism sector in Ivano-Frankivsk region, *fig. 3*.

So, the most energy-intensive area in the tourism sector is Polyanitska tourist group, which accounts for approximately 56% of the total electricity consumption in the tourism sector of Ivano-Frankivsk region. Therefore, the most relevant area for the development and implementation of alternative sources of electricity production is Polyanitska tourist group.

Currently, the tourism sector in Ivano-Frankivsk region almost does not use renewable energy sources in its activities. We believe that in this case, there is a need to turn to the world experience of using renewable energy sources in tourism and implement it in the practice of the tourism industry in Ivano-Frankivsk region.

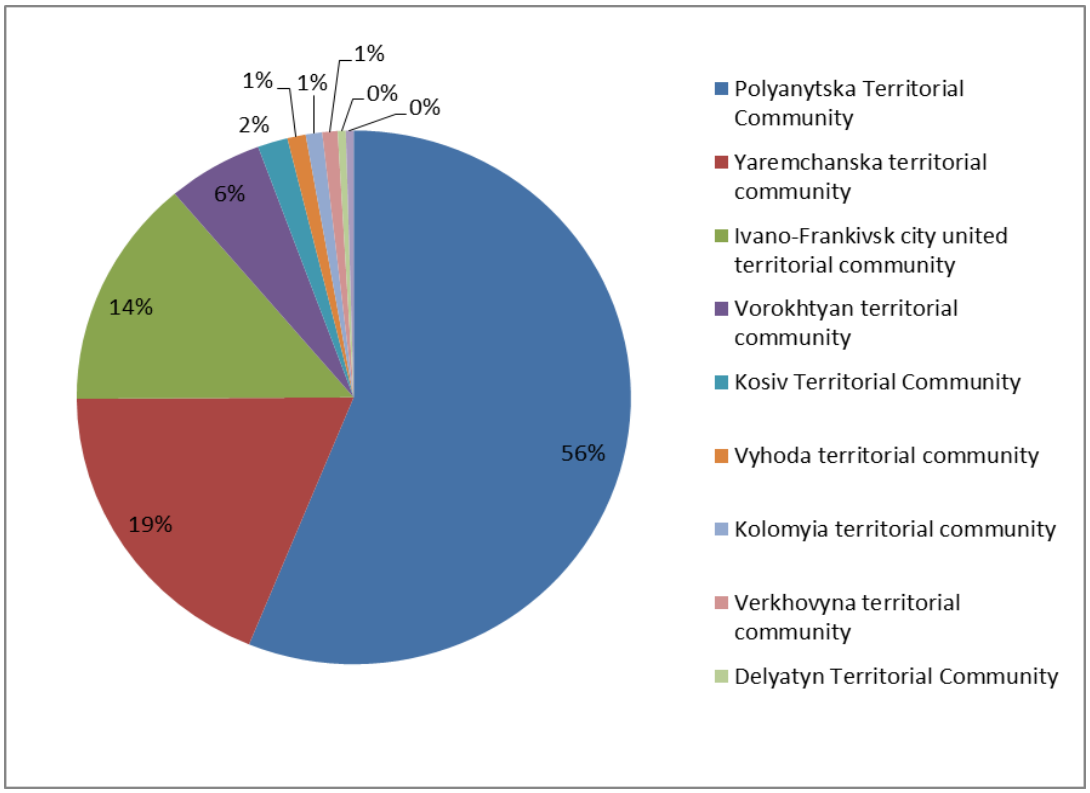

Figure 3. Territorial structure of distribution of electricity consumption by the tourist sector of Ivano-Frankivsk region

In recent years, due to a significant decrease in the cost of photovoltaic panels and, consequently, the production of electricity on them (up to 0.05-0.10 USD per kWh), their use in providing energy for tourist and hotel facilities is becoming increasingly economically effective. Generating electricity on solar installations located on the roofs of hotels, parking lots, and tourist facilities allows owners to reduce the amount of network electricity consumption, not only reducing costs but also attracting tourists with "green energy supply." For tourist facilities connected to power grids, the trend of creating duplicating capacities on renewable energy sources together with diesel generators to provide uninterrupted tourist services during wartime is particularly promising [9].

Alternative energy sources are not considered a niche product. First of all, providers of transport services - one of the pillars of the travel industry - see a perspective in eco-innovations.

Translate this text into English. Today, customers of the German railway company Deutsche Bahn on domestic IC and ICE routes use exclusively environmentally friendly electricity; by 2030, 80% of the group's energy needs will be met from renewable sources. And together with the Siemens Mobility division, trains with hydrogen fuel cells are being developed, which will be tested from 2024 with the prospect of replacing diesel locomotives still used on some non-electrified routes.

With a greenhouse gas emission level of 31 grams per passenger-kilometer, the bus sector in Germany can already claim to be the cleanest type of transport in the tourism industry.

The total environmental costs of a bus, which in addition to CO2 emissions also include construction, maintenance, disposal, and fuel supply, are exceptionally low, not least thanks to ongoing innovations [10, p.139].

As hotels are the second-largest energy consumer in the tourism industry, it is crucial that accommodation providers reduce their emissions and use renewable energy. There are compelling economic arguments in favor of reducing emissions in the hotel industry: transitioning to low-carbon models will ensure cost-effectiveness while simultaneously boosting competitiveness.

There are energy-efficient technologies that facilitate such transformations, as well as advanced methods of hotel design and operation. However, to achieve full success, the market must provide favorable conditions for low-carbon growth, including financial, structural, institutional, and regulatory mechanisms.

At the same time, small and medium-sized hotels, which make up 90% of the hospitality sector in Europe, need access to adequate and easily accessible information about low-carbon business models, as well as independent technical consultations and financial support. Measures to increase awareness involving consumers and utilizing digital technologies will allow for necessary changes in behavior and attitudes towards this issue [11].

The founder and chairman of Jetwing (Sri Lanka) has always believed that people and nature cannot exist in isolation from each other. Accordingly, Jetwing Hotels has always demonstrated its commitment to environmental conservation, which has been embodied in the company's Sustainability Strategy. To reduce emissions associated with hotel activities, Jetwing Hotels first reduced its dependence on the grid by reducing energy consumption through innovative energy-efficient solutions, and secondly invested in solutions related to renewable energy.

More than 50% of the energy needs of Jetwing Hotels are met through renewable energy sources such as fuelwood from sustainable primary sources, solar electricity (photovoltaic panels), solar thermal energy, and biogas. To achieve this, absorption refrigerators, centralized hot water supply systems, solar photovoltaic panels on roofs, and biogas reactors are installed in all hotels. Reducing dependence on the national grid is strategically important and allows this network of hotels to actively use its own methods to ensure energy and ecological sustainability [12].

Another good example: a number of tourist attractions in Egypt have started transitioning to the use of clean or renewable sources of energy in an effort to conserve the environment and attract "green tourism." The transition to renewable sources of energy is taking place within the framework of the "Green Energy Protocol," signed in December 2013 by the Ministries of Ecology, Tourism, and Electricity. The protocol encourages the use of wind, solar, or water power in electricity production, as electricity production in Egyptian tourist facilities generally produces emissions of about 35 million tons of carbon dioxide per year into the atmosphere.

Egypt has initiated a series of projects related to the application of various target indicators related to "green" and renewable energy, which aim to generate over 50% of the necessary energy using non-fossil fuel sources by 2030.

By implementing the existing action plan and adhering to ecological principles, the Egyptian government is taking a number of actions in three main directions.

The first direction involves encouraging and supporting cities with developed tourism and corresponding infrastructure in reducing carbon emissions and transitioning to clean and renewable energy. The local administration of such cities as Sharm El-Sheikh or Hurghada has developed policy measures at the city level to ensure sustainability, which includes setting targets for achieving the status of carbon-free cities. These measures rely on initiatives to increase awareness, including a comprehensive media campaign aimed at conserving Egypt's natural resources, promoting individual use of clean energy, and supporting and popularizing "green" tourism [13]. In addition, numerous seminars, training courses, and conferences have been organized for key stakeholders aimed at increasing awareness. European countries that have succeeded in using clean energy in the tourism industry, including Belgium, Germany, and Italy [14], provide assistance in implementing Egypt's protocol.

Today, during the war, we can observe a widespread use of generators in the work of tourism companies in the Ivano-Frankivsk region. On the one hand, this allows tourism establishments to continue their activities uninterrupted during power outages, but such activity entails a number of negative impacts on the environment.

In particular, according to the curator of the social project LUN, Anna Denysenko, who studies air quality in cities using her own tracking system, the use of generators causes pollution with a mixture of carbon monoxide, fine particulate matter, nitrogen oxides, and so on. The use of poor quality filters results in the appearance of fine particulate matter (PM1, PM2.5, PM10) in the air. They can enter the bloodstream, lungs, and affect the nervous system, heart, brain, and cause a range of chronic diseases. Additionally, generators emit carbon monoxide, nitrogen oxides, and other hazardous compounds into the air [15].

Therefore, the most promising direction for the development of the tourism sector is the widespread use of renewable energy sources.

In Ivano-Frankivsk region, there are currently 45 industrial solar power plants with a total capacity of 128 MW, built with private investor funds, of which 17 began operating in 2019. In addition, 1,100 private households have connected to the electric grid of "Prykarpatteoblenergo" (4th place among regions in terms of the number of installed solar energy systems and 3rd place in terms of installed solar energy capacity). Their total capacity is approximately 27 MW, and the electricity generated covers the own needs of more than 7,000 households. Renewable energy sources account for about 2.0% of the total electricity generated in the region. In early 2018, the first stage of a wind power plant with a capacity of 0.6 MW was launched in Shevchenkove village, Dolyna district. There are five small hydropower plants with a capacity of 3.6 MW on the rivers of the region. The biogas plant of LLC "Goodwell

Ukraine" with a capacity of 1.2 MW has produced 3 million kWh of electricity and 3,207 Gcal of thermal energy. There are two biogas plants of LLC "Clear Energy" with a total capacity of 0.7 MW operating on the landfill of TPV in the territory of Rybnenska village council.

It should be noted that the main destructive factor affecting the modernization of the tourism industry in Ivano-Frankivsk region is the military aggression from Russia, which has a negative impact on the restoration of international tourism due to flight bans, rising oil prices, and disruptions in food supply chains. In the future, this will result in a decrease in population income and job opportunities, ultimately leading to a decline in tourist flow. Rising oil prices require a shift towards renewable energy sources and the implementation of energy-saving technologies. This emphasizes the need for ecologization of the tourism industry and requires increased investments, as well as a comprehensive policy aimed at increasing the number of international tourists and expanding the use of environmentally friendly energy sources.

4. CONCLUSIONS

Thus, the use of renewable energy sources is environmentally friendly, modern, safe, resource-efficient, and is the path chosen by all developed countries.

Today, modern tourism development includes several aspects: reducing carbon footprint, minimizing impact on local ecosystems, and increasing economic benefits for local communities. It is important to understand that expenses on ecology and nature conservation measures are not just inevitable costs but investments in business. Such an approach allows for benefits and profits. Investments in green technologies always pay off, and today's modern tourist is willing to pay for comfort and ecology.

The article analyzes the use of electricity in the tourism sector in the Ivano-Frankivsk region. The territorial structure of electricity consumption by the tourism sector in the regions of the Ivano-Frankivsk region was studied, and quantitative indicators of electricity consumption by the tourism sector for the last five years were modeled. It has been proven that as the number of tourists increases, the share of electricity consumed from the general energy grid also increases since the share of electricity generated from renewable sources for self-sufficiency of the tourism sector is negligible at the moment.

The article states that tourism plays a leading role in some of the most innovative initiatives in sustainable energy in the world. Technological solutions for hotel energy supply are analyzed, as well as a myriad of other initiatives that indicate that tourism is at the forefront of transformations aimed at ensuring environmentally friendly energy.

REFERENCES

[1] Arkhypova, L.M.; Mandryk, O.M.; Moskalchuk, N.M.; Prykhodko, M.M.; Radlovska, *Renewable energy resources in the system of sustainable development of Carpathian region of Ukraine*, J. Phys. Conf. Ser. 2021, 1781, 012010.

[2] *State policy of ensuring national security of Ukraine: main directions and features of implementation*, monograph / Kryshtanovych M.F., Pushak Y.Ya., Flejchuk M.I., Franchuk V.I. - Lviv: Spolom, 2020.

[3] Arkhypova, L., Vinnychenko, I., Kinash I., Horoshkova, L., Khlobystov, Ie. , *Theoretical Substantiation of Modeling of Recreational Systems*, Ecological Engineering & Environmental Technology, 23(5), pp. 99–108, 2022.

[4] *Ukrainian coal-fired power plants are among the biggest air polluters in Europe – report*, URL: https://mind.ua/news/20226512-ukrayinski-vugilni-elektrostanciyi-e-odnimi-z-najbilshih-zabrudnyuvachiv-povitrya-u-evropi - zvit

[5] *On the approval of the Energy Security Strategy*, URL: https://zakon.rada.gov.ua/laws/show/907-2021-%D1%80#Text

[6] Main Department of Statistics in Ivano-Frankivsk Region, URL: https://ifstat.gov.ua/

[7] Mandryk O., Moskalchuk N., Arkhypova L., Pryhodko M., Pobigun O., *Research quantitative indicators of the potential of solar energy in the Carpathian region of Ukraine*. IOP Conf. Series: Materials Science and Engineering, 749, pp. 1–9, 2020.

[8] Tourism of the Ivano-Frankivsk region'2022.pdf URL: https://speakerdeck.com/iftourism/turizm-ivano-frankivskoyi-oblasti2022?slide=11, 2022.

[9] Kravchynskyi R, Korchemlyuk M, Khilchevskyi V, Arkhypova L, Mykhailyuk I and Mykhailyuk J, *Spatial-factorial analysis of background status of the Danube River basin state on the northeastern slops of the Ukrainian Carpathians*, Journal of Physics: Conference Series 1781(1) 012011, 2021.

[10] *Cherep A. V. Voronkova V. G. Cherep O. G. The influence of creative innovative technologies on the sustainable development of the tourism industry in Europe after the COVID-19 pandemic*, Humanities Studies, Issue 8 (85), pp. 134-146, 2021.

[11] Carbon Footprint of Tourism. URL : https://sustainabletravel.org/issues/carbon-footprint-tourism/

[12] World Tourism Organization, "World Conference Tourism and Future Energy - Reducing CO2 Emissions, EXPO-2017, Astana, Kazakhstan, June 26-27, 2017, https://www.e-unwto.org/doi/pdf/10.18111/9789284419517

[13] Electricity and Renewable Energy, https://www.trade.gov/country-commercial-guides/egypt-electricity-and-renewable-energy

[14] The EU and Egypt intensify cooperation in the field of climate, energy and ecological transition. URL: https://ec.europa.eu/commission/presscorner/detail/uk/IP_22_3662

[15] Emissions into the air and negative impact on the lungs: the expert explained the danger of generators, https://tsn.ua/ukrayina/vikidi-v-povitrya-i-negativniy-vpliv-na-legeni-ekspertka-rozpovila- v-chomu-nebezpeka-generatoriv-2226244.html

[16] Development Strategy of Ivano-Frankivsk Region for 2021-2027, https://www.minregion.gov.ua/wp-content/uploads/2020/04/ivano-frankivska-strategiya-rozvytku-ivano-frankivskoyi-oblasti -na-2021-2027-roky.pdf

PRESSURES ON ENVIRONMENT AND HUMAN HEALTH GENERATED BY BIO-WASTE MANAGEMENT IN MARAMUREȘ COUNTY, ROMANIA

Irina **SMICAL**[1], Adina **POP-VĂDEAN**[2]

[1)]*Technical University of Cluj Napoca, North University Center of Baia Mare, Department of Mineral Resources, Materials and Environment Engineering, Romania .*

[2)]*Technical University of Cluj Napoca, Department of Mechatronics and Machine Dynamics, Romania*

Irina.SMICAL@irmmm.utcluj.ro, adinaluciapopvadean@yahoo.com

Keywords: bio-waste, pollution, waste management, recycling

Abstract: *Bio-waste represents the largest and most problematic category of municipal waste. Their particularity of decomposition and generation of leachate, respectively of greenhouse gases, imposed finding solutions to reduce and even stop the landfilling of this waste, encouraging the application of recycling measures. Like other developing countries, Romania has no unitary system for the separate collection of bio-waste. This leads to a very low rate of their recovery, on average 10.35% of the total biodegradable waste collected, the majority being disposed of by landfilling with an average annual rate of approx. 72.17%. The lack of a separate bio-waste collection infrastructure in Maramures County means that more than 50,000 tons of organic waste to end up in landfill dumps every year posing risks for environment factors and human health.*

1. INTRODUCTION

In Europe, bio-waste represents 30-40% of municipal waste. Between 118 and 138 million tonnes of bio-waste are generated annually [1], [2]. Bio-waste poses a risk for environmental factors, especially when landfilling, because of the leachate and methane released during the decomposition processes [3].

The European Directive 2008/98/EC set a recycling target of 65% till 2035 for municipal waste and bio-waste, implicit [4]. However, in the absence of certain legislative

obligations regarding the selective collection and valorization of bio-waste, some European countries, including Romania, have not yet created a functional infrastructure for selective collection, treatment, and valorization. Thus, a large part of the bio-waste ends up together with the residual waste in the municipal waste dumps where it generates leachate and landfill gases. This is predominantly in Europe, although there are countries such as Austria, Germany, Belgium, Holland, Italy, Slovenia, Estonia, and France that practice the selective collection and recovery of bio-waste for many years [1], [5]. The degree of valorization through composting or anaerobic digestion of bio-waste for the period 2018-2021 means an average for Europe of 92 kg/capita, and 103.75 kg/capita for France, 151.25 kg/capita for the Netherlands, 105.5 kg/capita for Lithuania, 129 kg/capita. Germany and Denmark recorded an average of 157.75 kg/capita [6]. There are some countries for which data of the year 2021 are not yet available so for the period 2018-2020, Austria had an average of 185 kg/capita, and Italy 109.33 kg/capita for the same period. Romania has fully registered an average for the period 2018-2021 of 13.25 kg/capita, while Bulgaria, for the period 2018-2020, had an average of 15.33 kg/capita. Compared to Romania, Bulgaria recorded a slightly higher amount of recovered bio-waste than Romania for the period 2018-2020 [6].

The non-existence of a unitary action in all member states for the separate collection of bio-waste entails the inability to achieve a statistical representation in line with reality.

In order to protect the environment, some countries banned the storage of bio-waste many years ago without waiting for this measure to be legally imposed at the European level. In this sense, the following can be mentioned: Austria, which banned the storage of bio-waste starting in 2009, respectively Belgium [5].

The recovery of bio-waste, either through composting or through anaerobic digestion, has a significant contribution to the circular economy, since organic waste could return to the soil as a nutrient material, respectively it could provide biogas favoring the saving of natural resources and the protection of the atmosphere.

In Romania, of the total collected biodegradable waste, most of it is disposed of on landfill dumps, registering an average of 72.17% in the period 2016-2020, the highest share being in 2017 of 74.70% [7]. Not all the amount of bio-waste is eliminated, part of it is recovered through composting. In this sense, it can be mentioned an average for the period 2016-2020 of 10.35% with the highest valorization rate of 13.37% in 2016 and the lowest in 2018 of 6.42% [7]. According to statistical data, the bio-waste recovery trend is decreasing, therefore a unitary strategy for a selective collection and recovery infrastructure throughout the country is necessary [7]. Unlike the the data presented publicly in the national environmental report, for Maramures county there is no public report for reflecting the way bio-waste is managed, the achievement of the objectives established by the County Waste Management Plan or the achievement of the objectives provided by the specific legislation [8-12].

The objective of this study is the analysis of the current bio-waste management in Maramures county and the highlighting of its pressures on the environment and human health.

2. MATERIALS AND METHOD

The method of carrying out the study is based on the collection, processing, and statistical interpretation of data and information regarding the national and county management of bio-waste and the correlation of the got data and those provided by the legislation and specialized literature.

In the previous context, data and information were requested from the national and county authorities responsible for bio-waste management and public information.

Bio-waste management in Maramureș County is the responsibility of local public authorities and the intercommunity development association, regulatory authorities, sanitation operators, etc. In this respect, based on the legislative provisions and the history of specific activities, action plans, and strategies are made, and reports containing data about the management process, attributions, and results are issued.

3. RESULTS AND DISCUSSION

According to GEO 92/2021 [13], which transposes Directive 2008/98/EC [4], bio-waste is "biodegradable waste from gardens and parks, food and kitchen waste from households, offices, restaurants, wholesale warehouses, canteens, catering companies or shops retail and comparable waste from food processing plants" (*fig. 1*); This bio-waste is part of the municipal waste category.

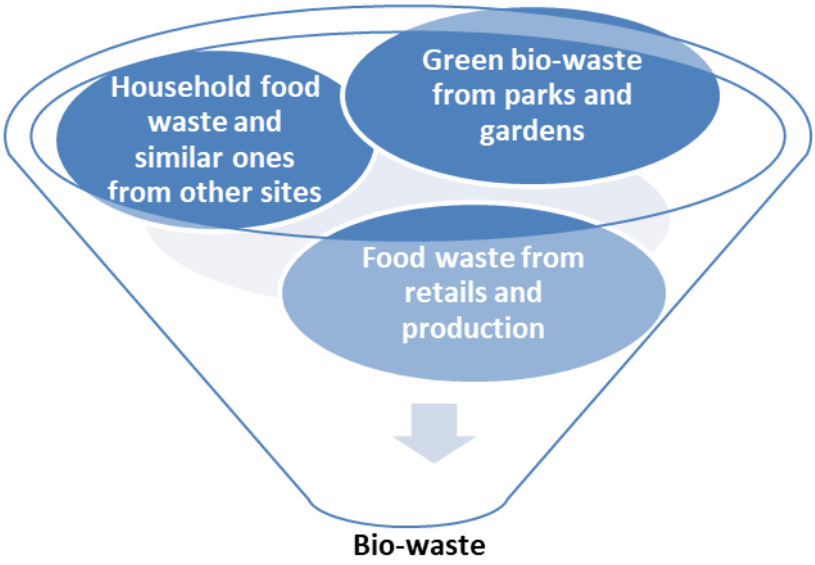

Fig. 1 Bio-waste components (according to GEO no. 92/2021 [13])

Starting in 2018, the amount of individually composted biodegradable waste was no longer considered recycled [14]. However, the data presented in the 2021 national environmental report indicate for the period 2017-2020 a decrease in biodegradable waste disposed of from 74.7% in 2017 to 69.3% in 2020. This indicates an emphasis on the recovery of this category of waste [14].

According to the National Waste Management Plan for 2020 the objective of reducing the amount of municipal biodegradable waste stored was set up to 35% of the total amount expressed gravimetrically to that one generated in 1995 [15], [16]. At the national level, this objective was not reached for the year 2020, being 43.3% [14]. To meet the target of 35% compared to 1995, Romania obtained a derogation setting the limit in 2024 [15], [17].

In Maramureș County, the data reported by the environmental protection authority do not refer to the achievement of the objective of reducing the amount of landfilled bio-waste compared to 1995, nor do they offer information on the degree of recovery or disposal thereof. Reference is made only to the quantities of bio-waste from municipal waste [8]. The graph in figure 2 expresses the dynamics of bio-waste content in municipal waste including bio-waste from household waste, and bio-waste from gardens, parks, green spaces, markets, and streets. To calculate the weight of bio-waste from gardens, parks, green spaces, and markets, respectively the streets, the quantities reported by the county authority for environmental protection were correlated with the percentages provided in PJGD MM [17].

As can be seen in *fig. 2* there is a tendency to increase the share of bio-waste in municipal waste. According to the projection from the PJGD, an 11% reduction in the amount of bio-waste generated in 2025 compared to 2020 is expected [17].

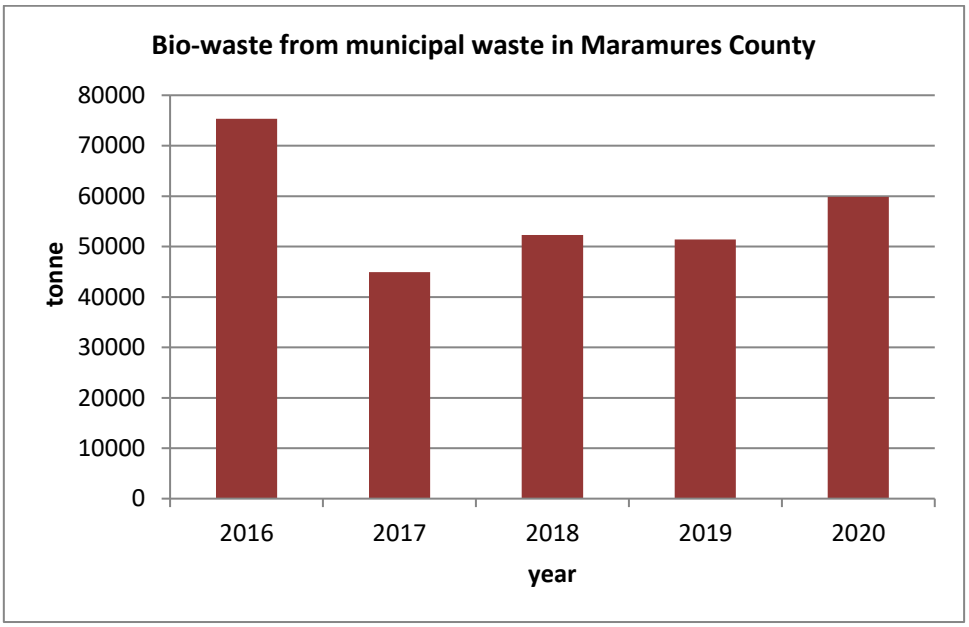

Fig. 2 Bio-waste from municipal waste in Maramures County [8])

From the data provided by CWMP MM [17], as well as by IDAIHWM MM [11], since 2010, several 82,785 composters with a volume of 400 liters each have been distributed to rural households. Thus, support is provided for the composting of bio-waste in households and implicitly a reduction in the quantities of bio-waste collected is expected. Biocomposting in households has both the advantage of reducing organic waste and obtaining compost which is a material rich in nutrients for the soil.

In Maramureș county, bio-waste is collected mixed with household waste, except in the municipality of Baia Mare where a special service belonging to City Hall collects and uses green bio-waste for composting [11] [8]. The rest of the bio-waste is collected and mixed with household waste by the sanitation operator.

Following the answers received from the authorities responsible for recording and management of bio-waste in Maramures county, some strengths, weaknesses, opportunities, and threats can be highlighted according to table 1. [7], [9-12].

Table 1 The SWOT analysis of bio-waste management in Maramures county

Strengths
• Legislative acts, strategies, and plans for waste (bio-waste) management; • Authorities and bodies responsible for the application of legislative provisions and waste (bio-waste) management; • The Integrated Waste Management System project;
Weaknesses
• Insufficient public information regarding the generation of bio-waste, the degree of its valorization or elimination, applied technologies, the achievement of performance objectives, and the reduction of the amount of landfilled bio-waste, etc; • Deficient collaboration between the authorities and responsible factors and fractured traceability of data; • Non-existence of a common, interactive, digital platform of the habilitated entities with attributions in the implementation of legislation and bio-waste management for storage information, and data reporting; • Non-existence of infrastructure for the selective collection of bio-waste from households and economic operators; the non-existence of a record of the generated bio-waste; • Collection of bio-waste mixed with residual household waste; • Non-existence of technical norms and a functional infrastructure for bio-waste recovery (composting platforms, anaerobic digestion facilities, mechanical-biological treatment facilities, etc.); • Lack of results on the efficiency of equipping households with biocomposters correlated with the situation before the application of this measure; • Non-existence of incentives for households composting;

• Non-functionality of the Integrated Waste Management Center in the Sîrbi area and implicitly of the mechano-biological waste treatment line.
Opportunities
• Financing of some projects for the infrastructure of valorization of the collected bio-waste (composting platforms, mechanical-biological treatment stations, biogas facilities, etc); • Supplementing the endowments with bio-composters for individual households in the urban areas; • Carrying out programs to educate and raise awareness among the population regarding the importance of bio-waste recycling and reducing the quantities that would be disposed of in landfills.
Threats
• Cumbersome and inefficient connections between waste generators, operators of sanitation services, and the County responsible authorities; • Lack of a common digital data platform that can serve in real-time the authorities with duties to monitor bio-waste management and the implementation of the provisions of the law; • Superficiality in providing information of public interest to citizens; • The failure of the infrastructure of separate collection and valorization of bio-waste implicitly could attract sanctions from European bodies.

3.1 Effects on the environment generated by bio-waste management

The management of bio-waste is an activity that includes several stages starting from its generation and up to its valorization or disposal. Currently, the infrastructure for the separate collection, treatment, and valorization of bio-waste is negatively affected by the lack of technical regulations [18].

According to directive 2008/98/EC [4], bio-waste must be collected separately from other categories of waste. For this, distinctly colored and labeled containers and a high frequency of picking them up are necessary because this waste decomposes easily and generates leachate and a bad smell.

As it appears both from the response received from the authorities and the environmental reports, in Maramureș county there is no infrastructure for the separate collection of bio-waste, and also not for its treatment and recovery [9-12]. A partial exception is the municipality of Baia Mare, which collects green bio-waste and uses it through composting on its platform [8], [19].

Bio-waste creates a certain discomfort right from the collection stage, because in a short time, they decompose, generating leachate and a bad smell. The same is true for final landfilling.

According to the data published in the EPA MM Environmental Report [8] corroborated with those from CWMP MM [17], over 50,000 tons of bio-waste are generated annually in Maramures county. Together with residual waste, they end up in municipal landfills where they generate leachate and greenhouse gases. The serious problem faced by Maramures county is both the non-existence of a separate bio-waste collection infrastructure and the lack of a landfill dump for storing the residual waste. This involves the temporary storage of bio-waste mixed with residual waste up to their transfer to landfilling dumps. Besides the olfactory discomfort, these bio-wastes can attract rodents, decomposing insects, or birds. By leachate, they can transfer into the aquatic environment organic matter and ammonia nitrogen compounds, and also compounds with heavy metals because leachate can constitute a corrosive and decomposition environment for certain materials with toxic contents [20]. On the other hand, landfill gas represented in particular by methane contributes to increasing the greenhouse effect and, implicitly, to climate change.

4. CONCLUSIONS

Bio-waste constitutes the largest part of the municipal waste category. It poses a risk to environmental factors and human health through its ability to decompose and generate leachate and greenhouse gases such as methane and carbon dioxide. Moreover, the presence of these organic wastes in municipal landfilling can create an environment conducive to the corrosion or decomposition of certain materials with toxic elements, facilitating their transfer into water, air, or soil deteriorating their quality, also biodiversity, and even human health.

In Maramureș County, a separate collection of bio-waste is not carried out. Only small fractions of the green bio-waste category are collected in Baia Mare city where they are composted. At the county level, there is no infrastructure for treating and valorizing bio-waste, although this had to be started given the deadline of 31st December 2023. The infrastructure involves not only the separate collection of this waste, but also recycling facilities, either through composting or anaerobic digestion. The measure proposed by the directive 2008/98/EC leads to an increase in the recovery rate of bio-waste and, implicitly, to a reduction in the amount of bio-waste that would be disposed of by landfilling. Moreover, these quantities must be lower than 35% since 2020 (2024) compared to the amount of bio-waste generated in 1995 [4]. Unfortunately, for Maramureș County, there is no database with the quantities of bio-waste generated and collected, nor with regard to the amounts of bio-waste recovered, or disposed of. There was only the mention that selective collection is not done and this waste is collected together with residual waste [8], [17]. In this case, in Maramures County, over 50,000 tons of bio-waste are disposed of yearly by landfilling with all the negative consequences for the environment and health that arise from this operation.

REFERENCES

[1] European Union, *The Bio-waste Management Challenge*, Interreg Europe, 2021.

[2] https://www.interregeurope.eu/sites/default/files/2022-04/Bio-waste%20challenge.pdf

[3] European Union (Maarten Dubois, Edward Sims, Tim Moerman, David Watson, Bjorn Bauer, Jean-Benoît Bel, Georg Mehlhart), *Guidance for separate collection of municipal waste*, 2020, EY, PlanMiljØ, ACR+, RWA and Öko-Institut

[4] https://op.europa.eu/en/publication-detail/-/publication/bb444830-94bf-11ea-aac4-01aa75ed71a1

[5] Victor Hugo Argentino de Morais Vieira and Dácio Roberto Matheus, *Environmental assessments of biological treatments of bio-waste in life cycle perspective: A critical review*, *2019*, Waste Management & Research, Vol. 37(12), pp. 1183–1198, 2019.

[6] Directive 2008/98/EC of the European Parliament and of the Council of 19 November 2008 *on waste and repealing certain Directives*, OJ L 312 22.11.2008, p. 3, 2008.

[7] Enzo Favoino & Michele Giavini, Scuola Agraria del Parco di Monza, *Bio-waste generation in the EU: Current capture levels and future potential, Bio-based Industries Consortium (BIC)*, 2020.

[8] https://zerowasteeurope.eu/wp-content/uploads/2020/07/2020_07_06_bic_zwe_report_bio_waste.pdf

[9] Eurostat, *Municipal waste by waste management operations, Recycling composting and digestion*, 2023.

[10] https://ec.europa.eu/eurostat/databrowser/view/ENV_WASMUN__custom_4805919/default/table?lang=en

[11] National Environment Protection Agency (NEPA), *Answer information no. 1/332/LAP/03.02.2023*, 2023.

[12] Environment Protection Agency of Maramures County (EPA MM), *Environmental Register for 2021*, 2022.

[13] Environment Protection Agency of Maramures County (EPA MM), *Answer information no. 12018/05.12.2022*, 2022.

[14] Maramures County Council (CC MM), *Answer information no. 27034/19.12.2022*, 2022.

[15] Intercommunity Development Association for Integrated Household Waste Management in Maramureș County (IDAIHWM MM), *Answer information no. 1965/20.12.2022*, 2022.

[16] Environment Protection Agency of Maramures County (APM MM), *Answer information no. 183/16.01.2023*, 2023.

[17] Government Emergency Ordinance (GEO) no. 92 of 19 August 2021 regarding the waste regime, M.Of. nr. 820/26 aug. 2021.

[18] National Environment Protection Agency (NEPA), *National Environment Report for 2021*, 2022.

[19] Government Decision no. 942 of 20 December 2017 regarding the approval of the National Waste Management Plan, (M.Of. no. 11/5 Jan. 2018.

[20] Government Ordinance no. 2 of 11 August 2021 on the landfill of waste, M.Of. no. 794/18 August 2021.

[21] Council Decision of Maramures County no. 119 of 29 June 2021 regarding the approval of the County Waste Management Plan of Maramureș.

[22] Law no. 181 of 19 August 2020 regarding the management of compostable non-hazardous waste, M.Of. no. 762/20 Aug. 2020.

[23] Council Decision of Baia Mare City. no. 95/2022 (Annex 3), *Regulation of the Organization and Operation of the Urban Environment Public Service, Baia Mare City*.

[24] https://www.baiamare.ro/Baiamare/Hotarari/2022/9%20martie/hot95_22_Anexa_3_2SPAU_ROF_2022_ACTUALIZAT.pdf

[25] Zhao Youcai, *Pollution Control Technology for Leachate from Municipal Solid Waste*, 2018.

ENERGY AND GREENHOUSE GAS REDUCTION ASSESSMENT IN MANUFACTURING ENVIRONMENT

Zoltan **ERDEI**, Cristian **BARZ**, Alexandru **GRIB,** Cristina **TAMASAN**
Technical University of Cluj-Napoca, Department of Electrical, Electronic and Computer Engineering
Zoltan.ERDEI@ieec.utcluj.ro

Keywords: energy efficiency, energy saving, sustainability, energy management, energy audit

Abstract*: This paper aims to identify, analyze, and conclude on solutions to improve the energy performance of an economic agent, by carrying out an energy audit to satisfy part of the energy needs of the organization. The respective economic agent operates in the field of the production of devices for the control and distribution of electricity. The objectives of the paper refer to the identification of the way of using electricity, to the identification and analysis of alternative solutions, such as photovoltaic panels, which could substantially reduce energy costs, to the performance of an economic analysis regarding these alternative solutions to determine which are economically efficient for the economic agent in question. The site energy audit was carried out during the week commencing 10th February 2023 and consisted of a health and safety site induction, followed by a kick-off meeting with key site personnel, followed by data gathering and surveys of the factory operation and processes. The objective of the energy survey is to provide a compliant audit for the ESOS submission for the organisation. The energy audit covers all energy consumption applicable to the site in order to establish an energy use map for the major consumers and identify potential energy saving opportunities.The energy savings identified in this study are based on the findings of the site visits and are considered viable opportunities that will require further work to develop them into investment grade business cases.*

1. INTRODUCTION

There has been a growing realization that earth and its climate are being pressured by human activities. Based on a better understanding of climate change and other scientific and

societal factors, expectations have changed to require that more be done – and quickly. If we are to address the threats of a changing climate, all of us need to be actively involved in optimizing energy consumption.

Active stewardship starts in our own backyard, making sure operations are clean and safe, and reducing environmental footprint. Managing our use of energy will help lower the amount of fuel used in manufacturing, heating and cooling, resulting in fewer greenhouse gas emissions, while lowering operating costs.

With growing work demands, a need for accelerated energy reductions, and fewer resources to get work done, this study can assist with existing energy management plans or administer entire energy management programs for an organization from start to finish.

Effective energy management plans and strategies will reduce operating costs, include processes that sustain the improvements, and protect the environment. Most importantly, a well-developed Energy Management Plan will support the energy vision and translate it into actionable, sustainable processes and initiatives. It will include a continual improvement process that examines real-time energy consumption and measures, analyzes, and implements programs to reduce usage.

The value realized from energy audits and the Energy Conservation Opportunities are optimized when linked back to business, or organizational energy objectives.

This study can assist with the development of an energy policy or an energy management strategy and to prepare a roadmap that will guide your sustainable "Energy Culture" into the future.

An energy management roadmap can ensure sustained energy management success.

These can include regulatory requirements, business objectives, facility certifications, specific energy reduction targets, renewable energy integration, and more.

An energy audit is then performed to identify all the possible energy improvement opportunities.

Once these improvement recommendations are implemented, it will be establishe how to verify and measure the effects. The right metering and monitoring equipment will assist in the implementation of an energy management program and help ensure that these improvements are realized and sustained.

The typical energy management plan systematically addresses behavioral, operational, and technological aspects of an operation.

Organization-wide energy management training is conducted, and Key Performance Indicators (KPI) are established. These KPIs are visible at all levels of the organization with the expressed support of senior management.

These energy goals and performance would be systematically reviewed and the energy plan updated as part of a refinement/improvement strategy for long-term sustainability.

A well-defined and deployed energy management plan can be expected to result in:

- An organization that is empowered at all levels to pursue and act on energy-related initiatives.
- Optimized energy and cost reductions.
- Optimized utilization of resources applied to energy initiatives.
- Sustainability: continued success of initiatives and a thriving energy culture within the organization.

2. METHOD USED

It was conducted an energy/greenhouse gas (GHG) reduction assessment for the organisation in February 2023. The assessment was conducted using QUEST methodology (Quick Environmental Savings Technique).

This methodology relies on three pillars, People – Data – Equipment, to identify no- and low-cost improvements for energy (and thus GHG emissions). These opportunities can be implemented quickly for immediate cost savings.

The QUEST approach is different than "traditional" resource efficiency services, which typically focus on capital improvements (i.e., equipment, building technologies). No-cost / low-cost operational improvements are often missed by these approach.

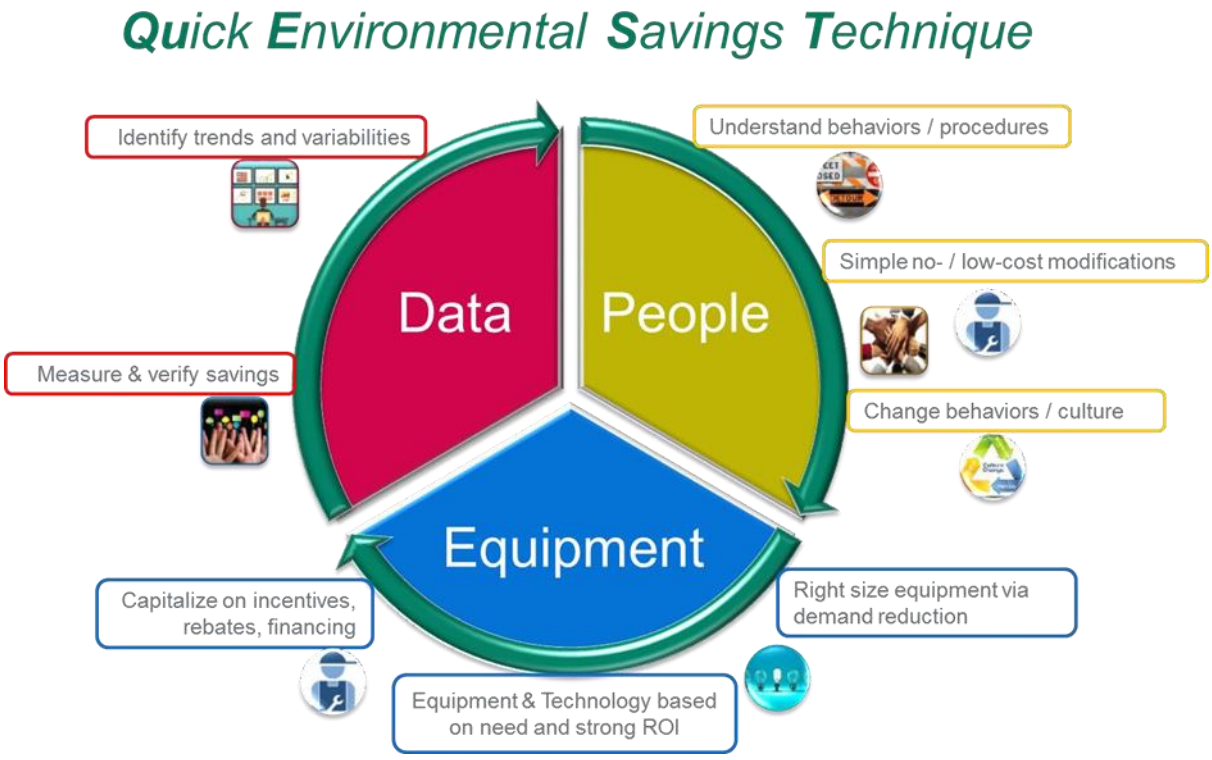

Fig. 1. QUEST methodology (Quick Environmental Savings Technique)

Using QUEST methodology, it was undertook the following:

- Reviewed and analyzed provided energy/emissions data in order to:
  - (1) understand current state, including performance variabilities
  - (2) identify focus areas for the on-site assessment
- Conducted a two-day on-site assessment to identify energy/emissions reduction opportunities, with a focus on no- and low-cost opportunities
- Developed and, where possible, quantified reduction opportunities, leveraging the provided data and the information/observations from the on-site assessment
- Prepared this report to communicate identified opportunities. The full QUEST report includes:

– This summary report, providing an overview of the facility performance and the identified opportunities

– The QUEST workbook, providing the underpinning data for the summary report

The energy audit consists of three main stages:

- Measurement of energy use across the organisation, and identification of areas of significant energy consumption.
- Identification of energy saving opportunities associated with improvement to energy efficiency or operational and behavioural change.
- Evaluation and reporting on the cost-effectiveness of opportunities identified, including setting out the costs and benefits of each energy efficiency opportunity.

Energy use comprises of a period of 12 consecutive months, using data from invoices and meter readings for the calendar year 2022.

Energy consumption units (kWh) will be used to determine the total energy consumption for the site and also identify areas of significant energy use within the facility. The ranking of the energy saving measures are based on a simple payback period (SPP) that is calculated from the capital cost estimate and the savings that will result from the implementation of the measure. Measures that will incur additional on-going costs for operation and maintenance will include those costs as part of the evaluation.

3. FACILITY ENERGY DATA AND ANALYSIS

The following data has been used to collate the energy information for the calendar year 2022:

Electricity Invoices

The site has a single point of supply for all electricity used on site which is measured by a fiscal billing meter for the MPAN 190014428734.

Copies of invoices for each month during 2022 have been obtained for the site.

Gas Invoices

The site has a single point of supply for all gas used on site which is measured and recorded by a fiscal billing meter for the MPRN 835602.

Copies of invoices for each month during 2022 have been obtained for the site.

Energy Metering on Site

In addition to the main billing meters there are a small number of sub-meters installed on the site to measure downstream energy use mostly concerned with electricity consumption.

Not all the meters are recorded by the site but there is a weekly meter reading taken for the main electricity meter, the main gas meter and for a few of the sub-meters.

The manual readings are checked and entered onto a spreadsheet that is used for monitoring the energy use metrics and is useful for checking the invoices if required to challenge any dispute.

The Building Energy Management System (BEMS) records some of the energy information but the system is old and almost obsolete, it is not used at the maximum energy monitoring potential.

Total site energy consumption has been obtained from the energy invoices for the fiscal meters for the calendar year 2022. This data was used to set the general site wide energy consumption figures and benchmark unit costs.

Sub metering data was then used to break down the overall energy consumption into different energy users to start the energy mapping of the site.

The following table provides the overall site level energy consumption data used for this audit.

Table 1. Facility Consumption Data

Resource	**Unit**	**Latest 12 Months**	**Latest 12 Months Cost (EUR)**	**Unit Costs (EUR/Unit)**
Electricity	kWh	3,279,562	€ 514,891	€ 0.16
Natural Gas	kWh	1,214,759	€ 75,315	€ 0.06

The following tables provide a breakdown of the electricity consumed on the site.

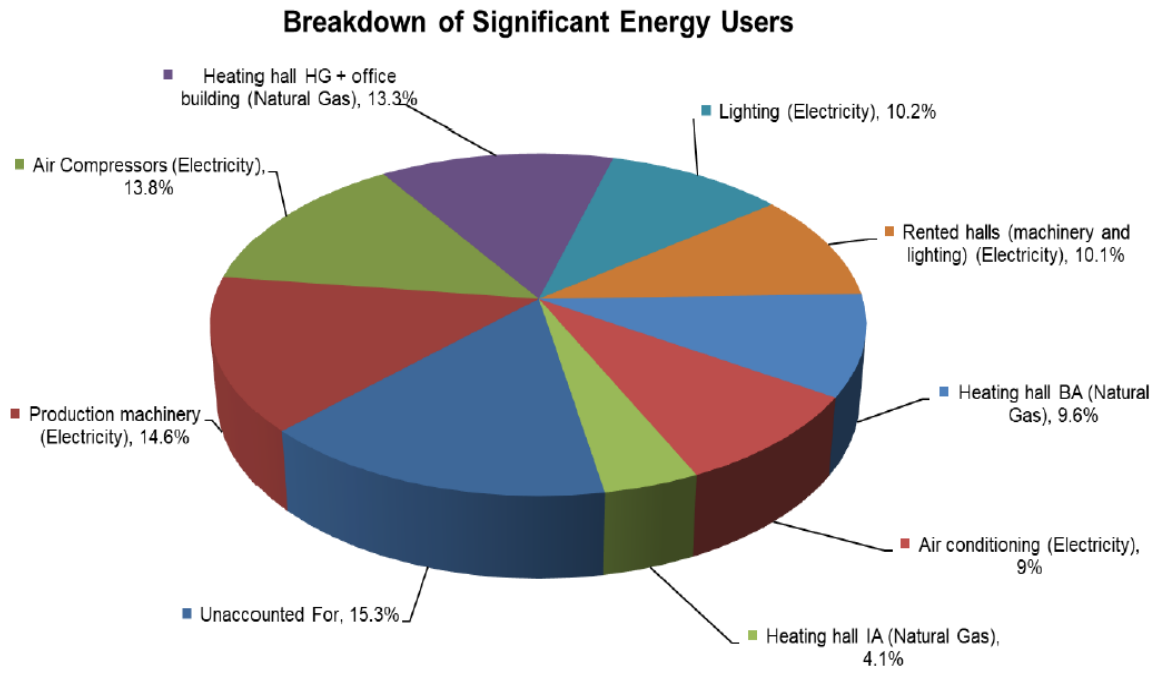

Fig. 2. Facility energy consumption

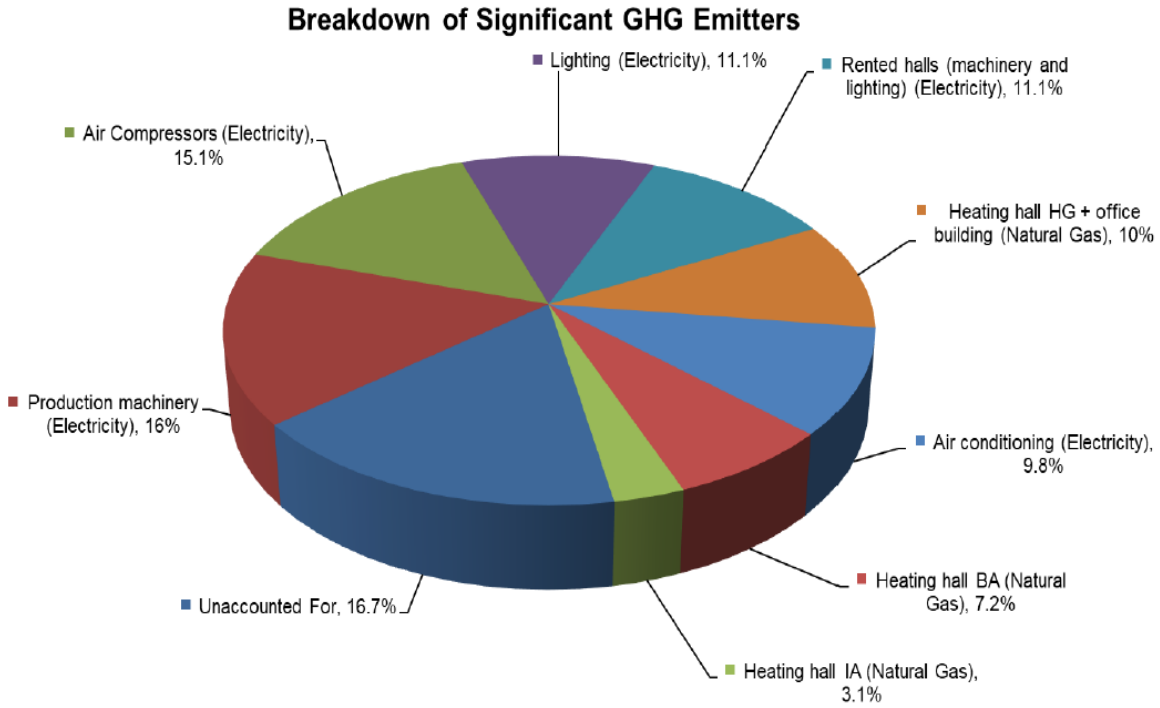

Fig. 3. Facility GHG emissions

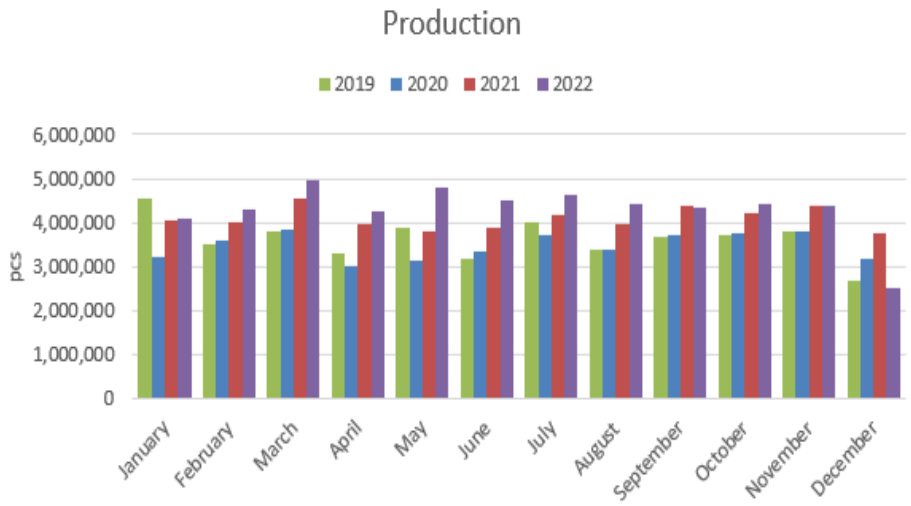

Fig. 4. Production Trend Data

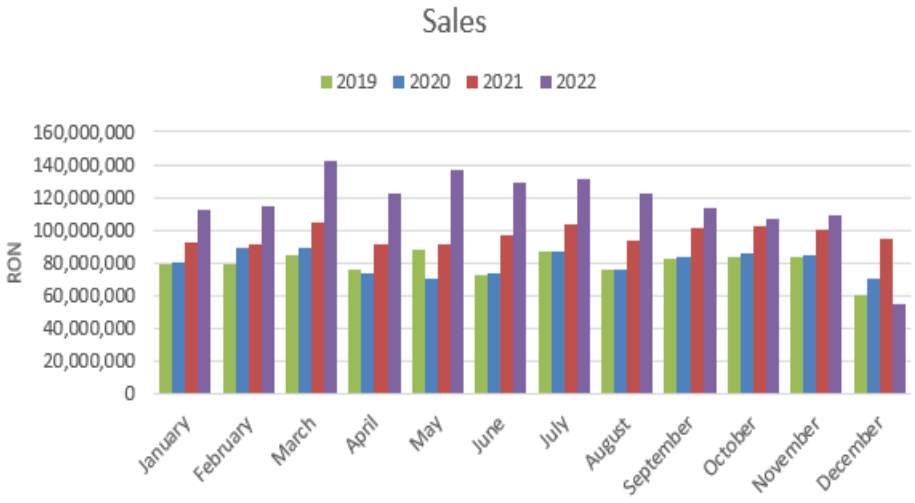

Fig. 5. Sales trend data

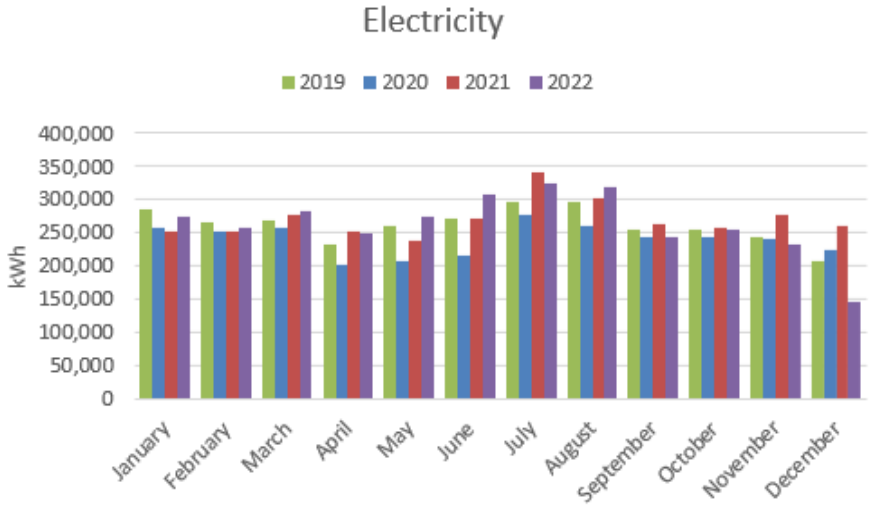

Fig. 6. Electricity trend data

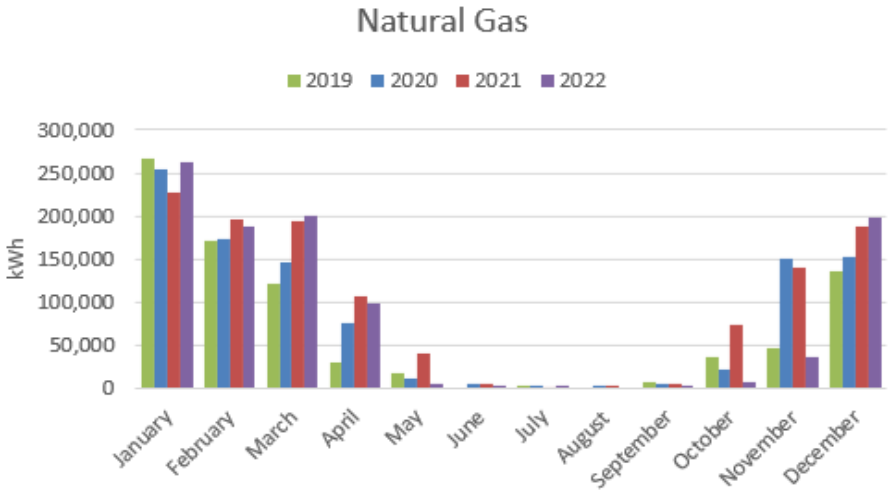

Fig. 7. Natural gas trend data

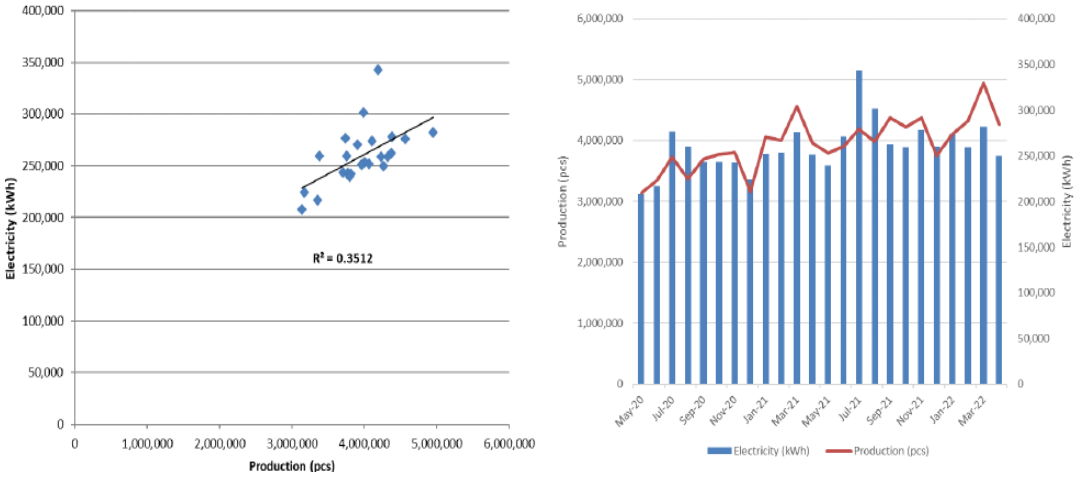

Fig. 8. Regression Observations: Electricity vs. Production

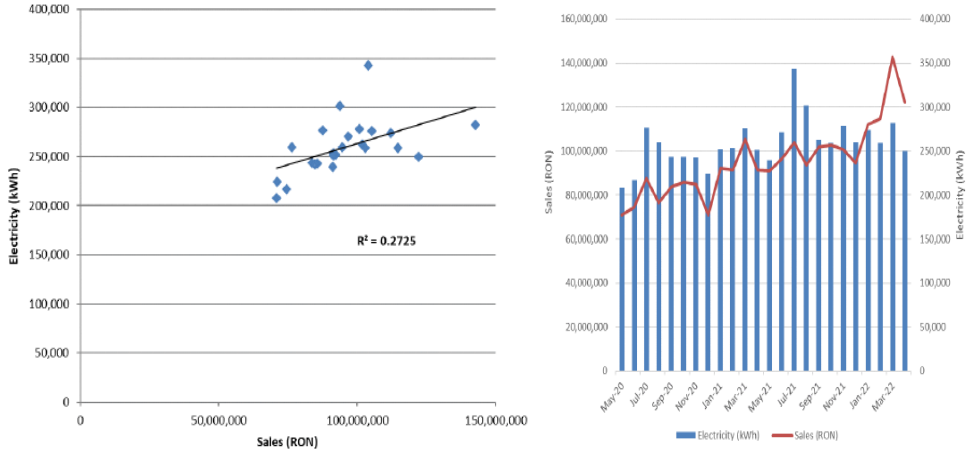

Fig. 9. Regression Observations: Electricity vs. Sales

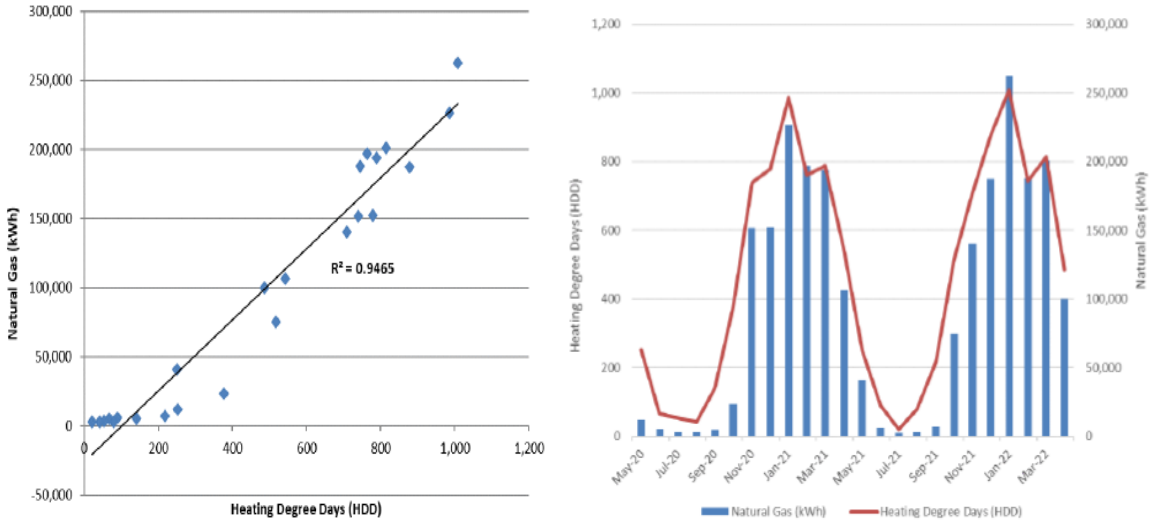

Fig. 10. Regression Observations: Natural Gas vs. Heating Degree Days

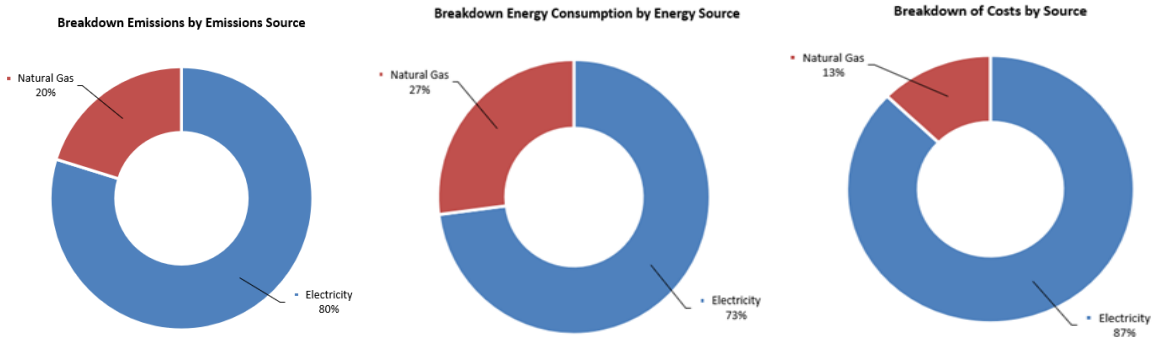

Fig. 11. Baseline emissions, energy and cost by souce

4. RESULTS. ENERGY REDUCTION OPPORTUNITIES

The energy saving opportunities identified at the organisation have been summarised in the table below.

The site survey identified energy saving opportunities relating to the consumption and cost of electricity and gas used on the site. Each of the opportunities will be described in this section of the paper with budget estimates for the cost of implementation of the measure and the time it will take to recover the cost based on the energy savings and the simple payback period. The energy savings will result in a reduction in carbon dioxide emissions that will also be included in the benefits.

The identified reduction opportunities have been sorted into 3 separate “buckets”, as follows:

Table 2. Bucket: < 2 years

Opportunity Title	Capital Cost (EUR)	Financial Savings (EUR/year)	Payback (years)	Energy Reduction (kWh/year)	Carbon Emissions Reduction (MT CO2e/year)
Close Gates and Windows in Air Conditioned Areas	€ 0	€ 19,023	0.0	121,166	32
Compressed Air Leak Survey and Repair	€ 10,000	€ 14,576	0.7	92,844	25
Lighting-Level Optimization	€ 7,000	€ 14,224	0.5	90,600	24
Process Water Heat Recovery	€ 2,000	€ 4,553	0.4	73,440	13
Replace Natural Gas Water Heaters with Electric Heaters	€ 840	€ 602	1.4	12,860	2

Table 3. Bucket: > 2 years

Opportunity Title	Capital Cost (EUR)	Financial Savings (EUR/year)	Payback (years)	Energy Reduction (kWh/year)	Carbon Emissions Reduction (MT CO2e/year)
Upgrade HVAC Systems in Production Halls	€ 603,000	€ 62,786	9.6	1,134,957	199
Building Management System	€ 710,417	€ 59,021	12.0	449,432	109
Upgrade Compressors to VSD Compressors	€ 200,000	€ 38,496	5.2	245,200	65
Air Compressor Heat Recovery	€ 80,000	€ 19,188	4.2	309,478	56
Monitoring and Targeting - Utilities	€ 95,000	€ 11,804	8.0	89,886	22
Sahara Units Water Flow Control	€ 18,000	€ 6,026	3.0	97,200	18
Install Additional Pipe Insulation	€ 10,000	€ 3,766	2.7	60,738	11
Utilize Outdoor Air for Air Compressors	€ 12,000	€ 3,297	3.6	21,000	6

Table 4. Bucket: Futher study needed

Opportunity Title	Capital Cost (EUR)	Financial Savings (EUR/year)	Payback (years)	Energy Reduction (kWh/year)	Carbon Emissions Reduction (MT CO2e/year)
Solar PV	€ 1,250,000	€ 272,333	4.6	0	460

Reduction Opportunities Detail

Close Gates and Windows in Air Conditioned Areas

Gates and windows in air conditioned areas are being left open, closing them will reduce energy consumption for cooling. Note that although automated doors and windows

may be a pathway toward achieving this goal, a more cost effective option which is proposed is to encourage behavioural change from workers.

Compressed Air Leak Survey and Repair

Implement a regular leak survey program and repair leaks as soon as practical. Savings are based on estimated compressor system leakage of 15% of total load. Capital costs are mainly maintenance costs and possibly some engineering costs to reduce "air bleeding."

Lighting-Level Optimization

The site has done good progress in LED replacement and will continue to do so until all fluorescent lighting is replaced. However, there is further potential as lighting is generally lit on all floors during production times. It could be switched off in lines close to the windows as well as based on actual lighting need. Lighting can be reduced to safe levels (~500 lux) in production areas, especially during day/afternoon shifts, and lighting can be increased locally (~1000 lux) by means of task lighting, which is not consistently available in all areas.

Process Water Heat Recovery

Recover waste heat from process cooling water unit that is closest to the production hall to provide heat during winter months.

Replace Natural Gas Water Heaters with Electric Heaters

Replace natural gas water heaters with electric instaflow tankless water heaters at each sink in the office building.

Upgrade HVAC Systems in Production Halls

Equip each production hall with sensor-controlled cooling / heating variable refrigerant flow (VRF) systems and air handling units with heat recovery, this solution will eliminate natural gas consumption for heating and cooling and eliminate air handler rental fees.

Building Management System

A building management system, otherwise known as a building automation system, is a computer-based control system installed in buildings that controls and monitors the building's mechanical and electrical equipment such as ventilation, lighting, power systems, fire systems, and security systems. Automated building systems can be programmed to operate and adapt to changing conditions in a manner which can significantly reduce building energy consumption.

Upgrade Compressors to VSD Compressors

Replacement of fixed speed compressors with variable speed drive (VSD) compressors.

During DRAFT review, the site expressed that SIGMA Air Manager (by Kaeser) is currently installed, however the paper maintains that compressors equipped with variable speed drive will offer savings over the current system arrangement.

Air Compressor Heat Recovery

Installing oil/water heat exchangers and a hot water accumulation tank will allow the recovery waste heat from 8 air compressors on-site, thereby reducing boiler natural gas consumption.

Monitoring and Targeting – Utilities

Relate energy consumption data to the weather and/or production figures or other measures in such a way to obtain a better understanding of how energy is being used. In particular, make the energy consumption visible to enable operations personnel to compare consumption in real time with a target to prompt looking for signs of avoidable waste or other opportunities to reduce consumption.

Sahara Units Water Flow Control

Install temperature sensors in every heater zone and equip Sahara water air heaters with 3 way mixing valves and programmable setback controllers.

Install Additional Pipe Insulation

Install additional pipe insulation where it is not present on heated pipes, especially in the boiler rooms and other supporting facilities.

Utilize Outdoor Air for Air Compressors

Utilize outdoor air for air compressor input to reduce air compressor energy consumption.

Solar PV

Use available roof area (and other areas if able) to add solar photovoltaic (PV) panels for on-site renewable electricity production.

5. CONCLUSION

From the analyzes carried out, it emerges that the organisation has an efficient energy management system, which is also validated by the ISO 50001 certification (standard for the energy management system).

I will further present the conclusions and energy efficiency improvements obtained for the respective economic agent.

Regarding the consumption of electricity, it can be seen that it is used at appropriate yields, the quality parameters are in accordance with the regulations in force and also there is a degree of ensuring the continuity of supply of almost 100%, considering the existence of the electric generator , AAR automation and the existence of UPS uninterruptible power supplies.

The energy saving opportunity is equivalent to 529,696 euro per annum, which is 48% of expenditure on electricity and gas in 2022. The investment required to realise these savings is estimated at approximately 2,998,257 euro. However, it is to be noted that there is a wide spread of payback periods, with a number of opportunities paying back within a few months, and a number of opportunities having paybacks significantly longer than currently acceptable thresholds. Should the site wish to proceed with any of the projects identified, then those opportunities would require further development to provide a full engineering solution and verifiable savings.

By implementing these energy optimization solutions, the following results were obtained:

Table 5. Opportunities summary table

Bucket	Capital Cost (EUR)	Financial Savings (EUR/year)	Payback (years)	Energy Reduction (kWh/year)	Percent Site Energy Reduction	Carbon Emissions Reduction (MT CO2e/year)	Percent Site Carbon Emissions Reduction
≤ 2 years	€ 19,840	€ 52,979	0.4	390,909	9%	96	9%
> 2 years	€ 1,728,417	€ 204,384	8.5	2,407,892	54%	485	45%
Further Study Needed	€ 1,250,000	€ 272,333	4.6	0	0%	460	42%
Grand Total	€ 2,998,257	€ 529,696	5.7	2,798,801	62%	1,041	96%

REFERENCES

[1] Allouhi, A.; El Fouih, Y.; Kousksou, T.; Jamil, A.; Zeraouli, Y.; Mourad, Y. *Energy consumption and efficiency in buildings: Current status and future trends*. J. Clean. Prod, 109, pp. 118–130, 2015.

[2] Pérez-Lombard, L.; Ortiz, J.; Pout, C. *A review on buildings energy consumption information.* Energy Build., 40, pp. 394–398, 2008.

[3] Poel, B.; van Cruchten, G.; Balaras, C. *Energy performance assessment of existing buildings*. Energy Build., 39, pp. 393–403, 2007.

[4] Batey, M.; Mourik, R. *From calculated to real energy savings performance evaluation: An ICT-based methodology to enable meaningful do-it-yourself data collection*. Energy Effic., 9, pp. 939–950, 2016.

[5] Bonan J., Cattaneo C., d'Adda G., Tavoni M. *Combining information on others' energy usage and their approval of energy conservation promotes energy saving behaviour*, Nature Energy, 5(11), pp. 832-833, 2020.

[6] Cagno E., Worrell E., Trianni A., Pugliese G. *A novel approach for barriers to industrial energy efficiency*, Renewable and Sustainable Energy Reviews, 19, pp. 290-308, 2013.

[7] Fawzy, S.; Osman, A.I., Doran, J.; Rooney, D.W. *Strategies for mitigation of climate change: a review*, Environmental Chemistry Letters, 18: pp. 2069–2094, 2020.

[8] Moriarty, P.; Honnery, D. *Energy Efficiency or Conservation for Mitigating Climate Change?*, Energies, 12(18):3543, 2019.

[9] Gary P. Moynihan and Frank L. Barringer *Energy Efficiency in Manufacturing Facilities: Assessment, Analysis and Implementation*. Published: January 18th 2017.

[10] Jensen R. John, Prentice –Hall, Inc,: Upper Saddle River, N.J, 2007 xvl, and 592, pp. *Remote Sensing of the Environment : An earth Resource*, 2007.